University of Southampton
Faculty of Engineering, Science and Mathematics
School of Electronics and Computer Science

COMPUTATIONALLY EFFICIENT EQUALISATION OF BROADBAND MULTIPLE-INPUT MULTIPLE-OUTPUT SYSTEMS

A final thesis submitted in partial fulfilment of the requirements for the award of Doctor of Philosophy at the University of Southampton

Viktor Bale (MEng)

Communications Research Group
School of Electronics and Computer Science
University of Southampton
Southampton SO17 1BJ
UNITED KINGDOM

31th December 2006

Supervised by:

Dr. Stephan Weiss
Reader

dedicated to my parents, Zuzana and Philip

ABSTRACT

UNIVERSITY OF SOUTHAMPTON

A Final Thesis for PhD by Viktor Bale (MEng)

Computationally Efficient Equalisation of Broadband Multiple-Input Multiple-Output Systems

Multiple-input multiple-output (MIMO) systems are encountered for example in communications, if several transmit and receive antennas are employed, such that a separate transmit channel exists between every possible pairing of transmitter and receiver antennas. As a result of this spatial diversity, the channel capacity is dramatically increased over the single-input single-output (SISO) case. While this increase is desired, the use of high data rates requires sophisticated equalisation and/or detection schemes in the receiver to compensate for spatial and temporal dispersion in broadband MIMO channels, since a time-dispersive, in addition to spatially-dispersive channel, must be assumed. The estimation of the broadband MIMO channel or its inverse in general are difficult and call for training sequences that reduce the slot time for the transmission of actual data, which may counteract the promised gain in channel capacity. Another problem can be the computational cost since in many systems this will be at least linearly proportional to the added spatial diversity.

This thesis is concerned with the application of techniques that find the best broadband MIMO equaliser in terms of MSE or BER performance while keeping the computational cost as realistically low as possible. It examines established adaptive and analytic methods of doing this and then moves on to the application of subband adaptive filtering techniques to perform MIMO channel equalisation and detection, since this technique has been found to give considerable advantages with respect to computational complexity and convergence rate for related SISO applications. For many slow-converging low-cost adaptive algorithms applied to the inversion of channels, the convergence rate can be increased by use of subband processing, where, in independent frequency bands, separate smaller-scale adaptive algorithms are operated at a reduced update rate. We will apply such methods to the identification and inversion of MIMO channels. Fractionally spaced systems also are known to outperform their symbol-spaced counterparts hence these are factored into the subband MIMO systems developed.

Many simulation results demonstrating the benefits of MIMO systems with respect to the channel capacity, the performance of various adaptive and analytic MIMO inversion techniques and the potential complexity and convergence rate improvements of the subband approach in the MIMO context are presented. Adaptation to MIMO systems generally take much longer than for SISO systems. For adaptive identification the time increases by an amount approximately equal to dimensions of the MIMO system. A frequency-domain inversion method shows the best performance compromise between MSE and BER performance and the requirement to minimise computational complexity, though it suffers from inaccuracies at high SNR values. The subband approach shows benefits for highly time-dispersive channels, and its potential improvement in tracking ability for dynamic channels means it can be beneficial in time-varying fading environments. Finally, fractionally-spaced equalisation often show considerable benefits and is even capable of equalising channels that are not possible to equalise using standard symbol-spaced methods.

Acknowledgements

First and foremost I would like to express my greatest appreciation to my supervisor Dr. Stephan Weiss. His excellent guidance and exceptional support for when the going got tough at times during both my research and my personal life was greatly appreciated and highly valued. The Head of the Communications Research Group, Prof. Lajos Hanzo, has also provided me with helpful guidance and motivation, and has created an excellent research environment. This guidance in addition to generous financial support during my studies is gratefully acknowledged. Additionally, I would like to thank the effort of Simon Armour, my external examiner, in his thorough coverage of my thesis and his helpful comments and advice to improve it.

The assistance in administrative work of Denise Harvey is appreciated. I would like to take this opportunity to thank my friends and colleagues, past and present, within the Communications Research Group at the University of Southampton for contributing to a pleasant research environment; in no particular order Choo Leng Koh, Charles Tibenderana, Hubert Dietl, Noor Sham Othman, Mahmoud Hadef, Wei Liu, Hafizal Mohamad, Ahmad Samingan, Bee Leong Yeap, Jin Yee Chung, Jin Wang, Ronald Tee, Rob Maunder, Nurul Nadia Ahmad, Soon Xin Ng, Feng Guo, Andy Wolfgang, Jos Akhtman and Sohail Ahmad.

Outside the research group, I have cherished the good friendship of Andy Chapman, Kosy Amarasinghe, Petros Oikonomakos, Andy Rushton, Dan Milton, Alan Williams and John Warren, without whom I would have found it hard to maintain seven mostly happy years in Southampton. I would also like to express my gratitude to colleagues at my new place of work, PA Consulting Group, for the moral support and motivation they have given to spur me on to complete this thesis; particularly to Tim Lunn and Stephen Chan.

Finally I would like to express my gratitude to my parents for their unconditional love and financial support to reach this point in my education.

List of Publications

1. **V. Bale and S. Weiss**, "An Optimum Linear Frequency-Selective MIMO Equaliser using Time-Domain Analytic Inversion", PREP2004 Conference on Electronics, Photonics, Communications & Networks, and Computing Science, pp. 24-35, University of Hertfordshire, UK, April 2004, vol. Oral Presentations.

2. **V. Bale and S. Weiss**, "A Low Complexity Subband Adaptive MIMO Equaliser for Highly Frequency-Selective Channels", Proceeding of 2004 International Workshop on Spectral Methods and Multirate Signal Processing, pp. 61-68, September 2004, Vienna, Austria.

3. **V. Bale and S. Weiss**, "Comparison of Analytic Inversion Techniques for Equalisation of Highly Frequency-Selective MIMO Systems", Proceedings of 2nd International Workshop on Signal Processing for Wireless Communications, pp. 150-155, June 2004, Kings College London, UK.

4. **V. Bale and S. Weiss**, "Equalisation of Broadband MIMO Channels by Subband Adaptive Identification and Analytic Inversion", Proceedings of International ITG/IEEE Workshop on Smart Antennas, April 2005, Duisberg, Germany.

5. **V. Bale and S. Weiss**, "Subband Adaptive Equaliser Tracking for Fractionally-Sampled Fading Broadband MIMO Channels", Proceedings of European Signal Processing Conference (EUSIPCO), September 2005, Antalya, Turkey.

Contents

1 Introduction 1

1.1 Research Motivation 1

1.2 Overview 4

1.3 Thesis Contribution 6

2 MIMO Channels 8

2.1 MIMO Background 8

2.2 Channel Description 12

2.3 Channel Capacity 13

2.3.1 Uncorrelated Sub-Channels 14

2.3.2 Correlated Sub-Channels 19

2.4 Channel Models 21

2.4.1 Spectral Dynamics 21

2.4.1.1 Narrowband Channel 21

2.4.1.2 Measured Channels 23

2.4.1.3 Standardised Channels 26

2.4.1.4 Band-limiting 30

2.4.2 Temporal Dynamics 33

2.4.2.1 Static Channel 34

2.4.2.2 The Rayleigh Process 35

2.4.2.3 Quasi-Static Channel 36

2.4.2.4 Doppler Fading Channel 36

2.4.3 Spatial Dynamics 37

2.5 Wideband MIMO Communication Problem 38

2.6 Summary 38

3 Multi-Channel System Identification **40**

3.1 MIMO Linear Filtering Problem 41

3.2 Adaptive MIMO Filtering 43

3.2.1 Mean Squared Error 43

3.2.2 Wiener-Hopf Solution 45

3.2.3 Gradient Descent Adaptation Techniques 46

3.3 Multi-Channel Least Mean Squares Algorithm 47

3.3.1 Algorithm Description 47

3.3.2 Properties of the M-LMS algorithm 48

3.3.2.1 Computational Complexity 48

3.3.2.2 Stability Analysis 48

3.3.2.3 Convergence Speed 50

3.3.2.4 Bias 51

3.4 Multi-channel Normalised LMS Algorithm 52

3.4.1 Algorithm Description 52

3.4.2 Convergence Characteristics 53

3.5 Other Adaptive Algorithms 53

3.5.1 Recursive Least Squares 53

3.5.2 Frequency-Domain Adaptation 55

3.6 Simulations and Discussion 57

3.6.1 System Identification 57

3.6.2 System Tracking 60

3.7 Summary 65

4 System Equalisation **67**

4.1 Inversion Methods and Criteria 68

4.1.1 Capacity of Equalised Channels 70

4.1.2 Regularised Inversion and the MMSE Solution 70

4.1.3 Equalisation versus Predistortion 73

4.1.4 Fractionally-Spaced Equalisation 74

4.2 Analytic System Inversion 75

4.2.1 z-Domain Inversion 76

4.2.2 Time-Domain Inversion 79

4.2.3 Frequency-Domain Inversion 84

4.2.4 FIR Equaliser Length 87
4.2.5 Channel Estimation Errors 88
4.2.6 Noisy Adaptation 90
4.3 Adaptive System Inversion 92
4.3.1 System Architecture 92
4.3.2 Convergence Characteristics 94
4.4 Adaptive Equaliser Tracking 95
4.5 Other Adaptive Equalisation Techniques 95
4.6 Simulations and Discussion 97
4.6.1 Analytic System Inversion 97
4.6.2 Channel Estimation Errors 104
4.6.3 Adaptive System Inversion 104
4.6.4 Adaptive Equaliser Tracking 106
4.6.5 System BER Performance 109
4.7 Summary 113

5 Subband MIMO Equalisation **115**
5.1 Subband Concepts 116
5.1.1 Multi-Rate Systems 116
5.1.2 Modulated Filter Banks 118
5.1.3 Polyphase Representation 120
5.1.4 Critically Decimated versus Oversampled Subbands 123
5.2 Performance of Subband Systems 124
5.2.1 Computational Complexity 124
5.2.2 Convergence Speed 125
5.2.3 Final MSE 126
5.2.4 Modelling Accuracy 126
5.3 Subband MIMO Inversion 128
5.3.1 Subband Adaptive System Identification 128
5.3.2 Subband Analytic System Inversion 130
5.3.2.1 Subband Time-Domain Inversion 130
5.3.2.2 Subband Frequency-Domain Inversion 133
5.3.3 Subband Adaptive System Inversion 136
5.3.4 Subband Adaptive Equaliser Tracking 139

5.4 Simulations and Discussion 140
5.4.1 Subband Adaptive System Identification 141
5.4.2 Subband Analytic System Inversion 144
5.4.3 Subband Adaptive System Inversion 149
5.4.4 Subband Adaptive Equaliser Tracking 152
5.4.5 Subband System BER Performance 154
5.5 Summary 158

6 Fractionally-Spaced Equalisation **161**
6.1 Phase Behaviour 161
6.2 Polyphase Representation 163
6.3 Zero-Forcing Equalisation 166
6.3.1 FIR Equalisability 167
6.3.2 Frequency-Domain Equalisability 169
6.3.3 Noise-Enhancement 172
6.4 MMSE Equalisation 173
6.5 Rank-Deficient MIMO Equalisation 174
6.6 Subband Fractionally-Spaced Equalisation 176
6.7 Simulation Results 180
6.7.1 Adaptive Identification and Analytic Inversion 180
6.7.2 Adaptive Inversion 180
6.7.3 Adaptive Equaliser Tracking 182
6.7.4 Rank-Deficient MIMO Equalisation 185
6.8 Summary 186

7 Conclusions **188**
7.1 Summary 188
7.2 Outlook 194

A Fading Channel Model **196**
A.1 Rayleigh Faded Doppler Fading Channel 196

B MIMO Capacity Derivations **202**
B.1 Linear MIMO Capacity Increase 202
B.2 Limiting MIMO Capacity 203

C Multi-channel MMSE Solution **204**

C.1 Multi-Channel MMSE Equaliser - Regularised Pseudo-Inverse Equivalence 204

Mathematical Notation **206**

References **208**

Chapter 1

Introduction

1.1 Research Motivation

In recent years, theoretical and practical investigations [1–4] have shown that it is possible to realise enormous channel capacities, far in excess of the single-input single-output (SISO) capacity given by the Shannon, or Shannon-Hartley law [5]. The transmission rate can be increased by a rich multipath scattering environment if the environment is exploited correctly [1]. This in itself is a novel concept as, in the past, a highly scattering environment has often been perceived as a problem. With multiple-input multiple-output (MIMO) systems it is this very nature of the environment that makes high capacities possible, as several channels can be realised in the same time, space and frequency if the environment makes the response of each of the SISO sub-channels comprising the MIMO channel sufficiently different. Initial pioneering work employed this capacity in the form of space-time coding to improve the reliability of the link [6,7], and later information-theoretic results proved that using MIMO systems can indeed increase the capacity beyond that of the Shannon law [1, 2]. More recently, practical MIMO systems have been designed and created, which have confirmed through experimentation the theoretical results previously shown [3, 4]. Although the concept of MIMO systems has many applications, such as acoustics [8], this work will deal with radio communications channels.

A MIMO system has more than one transmission point and reception point, with the transmitted signals travelling through the same medium at the same time, and in the case of modulated radio communications, in the same frequency band. As a result, the transmitted signals are superimposed at the receivers. The receiver is required to separate the signals from these multiple antennas and to de-correlate them to recover the transmitted data streams. Figure 1.1 shows a high

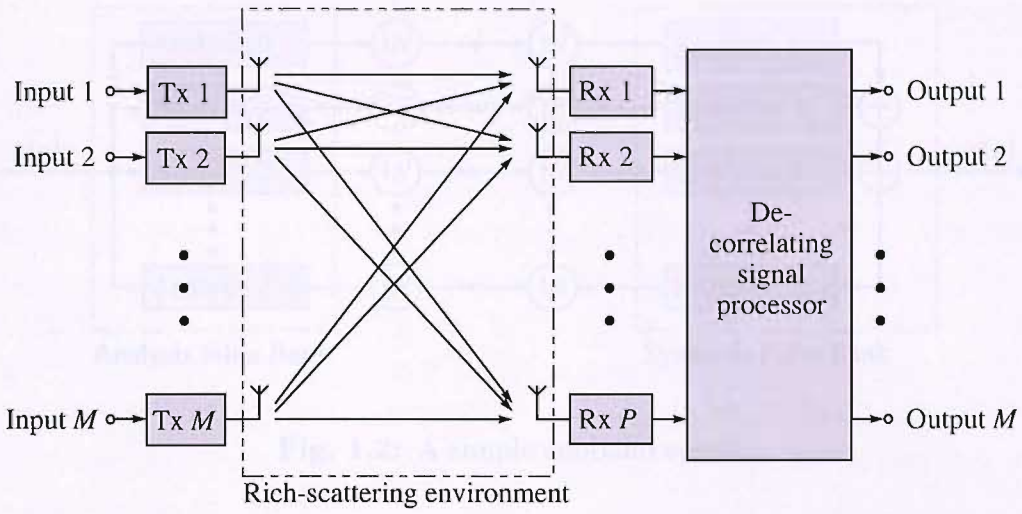

Fig. 1.1: A high level schematic of a MIMO system used for radio communications.

level schematic of a MIMO system used for radio communication. The task of separating multiple signals is not particularly difficult if the sub-channels are flat in the frequency-domain, and a large portion of previous work into MIMO systems only considers this case. Although the transmission environment is required to be highly scattering for MIMO systems to reach their full potential, if the symbol transmission period is long relative to the delay spread, then the sub-channels will indeed be flat. One of the primary goals of MIMO systems however is to increase as much as possible the transmission rate, and hence it would be more realistic to consider high date rate systems where the channel is broadband and frequency-selective. In this case the inversion of the MIMO system which is a required step towards finding the MIMO channel equaliser can become a very complicated task. Hence we have two layers of complexity- that that the channel is MIMO, but also that the channel will introduce inter-symbol interference (ISI). The choice of the modulation scheme is unaffected by the fact that the system is MIMO.

The multiple inputs to the MIMO system in Figure 1.1 can have a number of sources. Firstly, a single user signal could be de-multiplexed into the multiple inputs. In this way the extra capacity provided by the MIMO system is used for this one user, resulting in a large potential increase in the data rate [3, 4]. This simplicity at the transmitter is one of the reasons why MIMO systems can be so appealing, and this is the application upon which this thesis will mainly focus. Another possibility is to have a multi-user system with one user on each antenna, meaning that although each user still has the same data rate as with a SISO system, the total spectrum required to support all these users is no greater

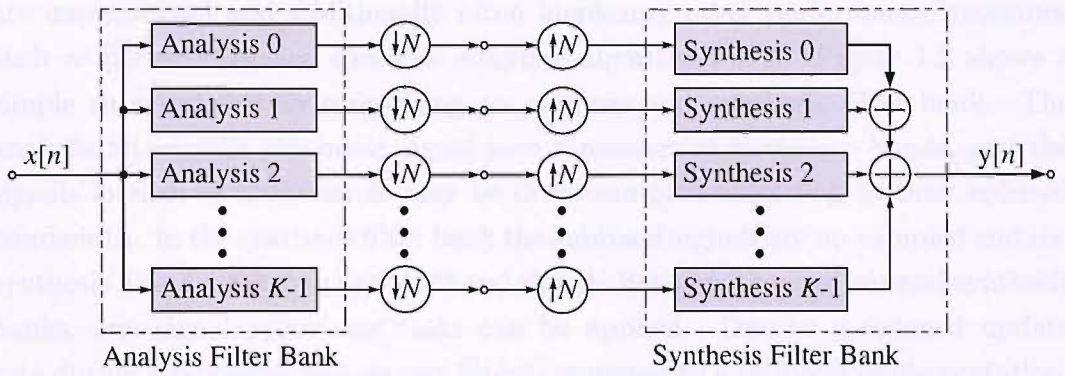

Fig. 1.2: A simple subband system.

than that required to support a single user. A third possibility is to have a space-time coded system operating over the multiple antennas, where the capacity of the MIMO system is employed to improve the quality and robustness of the link, thereby reducing the bit error rate (BER) for the same data rate [9–11].

The field of MIMO systems adds a new dimension to the complexity of signal processing algorithms. In general, any existing signal processing algorithm that operates on a SISO system can be applied, in a modified form, to MIMO systems. For example, an adaptive algorithm that converges an adaptive filter to the inverse of an unknown SISO channel can be modified to work for a MIMO channel. However, with this not only does a signal processor have to deal with the adaptation algorithm, the individual data streams must be equalised and decorrelated as well. Therefore, whatever the complexity of a SISO signal processing algorithm, an equivalent algorithm implemented for MIMO systems will always be more complex due to the multitude of sub-channels and the additional task of MIMO detection. As MIMO systems rely on a rich multi-path environment, complicated sub-systems are required to process the signals passing through these sub-channels. The problems are further exacerbated when each SISO sub-channel comprising the MIMO system may be wideband or broadband, where each channel has a long impulse response. When identifying the channels, the convergence speed of an adaptive system is also an issue as the algorithm may converge slowly for complicated systems. Considering all these factors, it is evident that complexity may be a problem.

Despite the continual increase in processing power available on digital signal processors, the emergence of new processing algorithms such as required for MIMO systems places ever-increasing demands on these processors. Subband techniques have emerged as an interesting and efficient method for digital signal processing, lowering the computational requirements of the processors on which algorithms

are implemented and additionally often increasing other performance measures, such as the convergence speed of adaptive algorithms [12]. Figure 1.2 shows a simple subband system comprising an analysis and synthesis filter bank. The analysis filters split the input signal into a number of frequency bands, and the signals in each of these bands may be down-sampled according to their reduced bandwidth. In the synthesis filter bank the subband signals are up-sampled and the synthesis filters reconstruct the fullband signal. Between the analysis and synthesis banks, any signal processing tasks can be applied. Due to a reduced update rate during adaptation and shorter filters compared to a fullband implementation, computational savings arise when using this subband approach. In addition, the parallel structure and the characteristics of the subband spectra can be beneficial for processing.

As subband processing has had excellent results for very complex SISO systems, it may provide a solution to the problems caused by the complexities introduced by MIMO systems. There is likely to be advantage in fusing the two areas of MIMO systems and subband processing in an attempt to be able to implement complicated MIMO algorithms on modestly powered signal processors. It is the aim of this study to create and evaluate the performance of a subband broadband MIMO channel equaliser at the receiver.

Finally, fractionally-spaced equalisers are known to outperform their symbol-spaced counterparts. Where final achievable performance is limited by additional sources of error inherent in the subband approach, sampling the input at fractions of a symbol period can improve the performance. Hence performing fractionally-spaced sampling in a subband MIMO equaliser is an interesting topic, especially since both subband systems and fractionally sampled equalisers can be expressed in polyphase form.

1.2 Overview

Chapter 2 sets the scene for the rest of the thesis. It starts by giving a background overview of the history and recent developments in MIMO systems. It formally introduces MIMO channels, reviews their possible capacity and explains different categories of MIMO channel which have an effect of the capacity, namely uncorrelated high-rank, uncorrelated low-rank and correlated low-rank sub-channels. Several suitable channel models are developed which are characterised by their behaviour in the frequency, time and spatial domains and these are used in simulations throughout this thesis. Finally we summarise this chapter and motivate the development of multi-channel adaptive systems.

Chapter 3 formulates the theory behind optimum and adaptive multi-channel filters. One way of creating an equaliser for an unknown broadband MIMO channel is to identify the channel or its inverse in some manner, and an adaptive algorithm will be used for this purpose. The chapter progresses to describe the multi-channel least mean square (M-LMS) adaptation algorithm, which can be used to adapt to unknown MIMO systems, before giving an overview of various convergence properties. A modified version of the M-LMS, the normalised M-LMS (M-NLMS) algorithm, will then be introduced and its advantage over the M-LMS explained. The NLMS algorithm will be used as the adaptation algorithm of choice in this thesis. The chapter moves on to giving a brief overview of other candidate adaptation algorithms that could be used. Finally, adaptation and dynamic channel tracking simulation results are shown before drawing conclusions.

Chapter 4 starts by covering the basics of MIMO channel inversion, and explains inversions methods and criteria. The pseudo-inverse is introduced as a method of inverting rectangular and rank-deficient matrices and the method of regularisation is shown as a powerful tool in solving ill-posed problems that can arise when inverting MIMO systems. Although throughout this thesis we assume that the MIMO channel will be equalised at the receiver, we briefly discuss the alternative possibility of using pre-distortion at the transmitter. We also briefly formally introduce fractionally-spaced equalisers. The chapter moves on to developing in some detail three analytic inversion techniques, namely z, time or frequency-domain, that can be used to calculate an equaliser to a known broadband MIMO channel, which has been previously adaptively identified for example. It then explains how to choose the length of an FIR equaliser and mathematically explains the effects of channel estimation errors, where the adaptive channel identification has not been executed until convergence and of noisy channel estimation, where noise limits the attainable adaptation accuracy. A fully adaptive technique of finding the channel equaliser is then shown and convergence characteristics explained. Finally, we give a brief overview of other adaptive equaliser methods before showing extensive simulation results and drawing conclusions in a summary.

Chapter 5 introduces the concept of subband processing and reviews its advantages over the standard method of fullband processing. It starts by introducing multi-rate signal processing operations and modulated filter banks which are the building blocks of subband processing and explains the relative advantages and disadvantages of critically-sampled versus oversampled subbands. We briefly cover the properties of subband systems, before building up and explaining adaptive MIMO channel identification systems and analytic inversion methods in subbands. In each case we state or calculate the computational cost of the processes as the reduction of this is one of the often-quoted advantages of performing signal pro-

cessing operations in subbands. We also show the subband implementation of fully adaptive MIMO system inversion and explain potential advantages over the fullband method in terms of convergence speed and computational cost. Finally we show extensive simulation results and compare performances to the equivalent fullband system results in Chapter 4, before summarising the chapter.

Chapter 6 begins by covering the principle behind fractionally-spaced equalisation (FSE) and how it can outperform symbol-spaced equalisers (SSE). It explains that FSE can perform both the task of matched filtering and SSE. It then develops a polyphase representation of FSE, before developing zero-forcing FSE. Equalisability is calculated in the frequency domain and noise-enhancement effects are shown. Next, the minimum mean squared error (MMSE) FSE is calculated, and we see that MMSE FSE outperforms MMSE zero-forcing FSE — with FSE there are an infinite number of zero-forcing equalisers, one of which gives the MMSE solution. The chapter explains how FSE can be used to equalise MIMO systems that are rank-deficient, and hence unequalisable, when sampled at the symbol period. It also shows that the FSE performance of rank-deficient MIMO systems depends on the band-limiting of the channel. Next, the chapter shows how FSE may be applied to subband systems, creating a subband adaptive MIMO FSE, before finally showing and explaining the results of numerous simulations.

Chapter 7 summarises the main findings of this thesis and puts forward ideas for future work.

1.3 Thesis Contribution

The novel contributions of this thesis are:

- Linear adaptive filters have been extended to the multi-channel case for use with MIMO systems. Their performance has been analysed and compared to the SISO case for both static and time-varying environments.
- Three analytic and one adaptive MIMO inversion methods — the z-domain, time-domain and frequency-domain — have been developed and analysed. The relative advantages and disadvantages of these techniques have been shown in terms of performance and computational cost [13, 14].
- In a noisy environment, the pseudo-inverse of a MIMO channel regularised by the noise-to-signal ratio has been shown to be equivalent to the MMSE Wiener-Hopf MIMO equalisation solution.

- The limitations of the computationally efficient frequency-domain analytic MIMO inversion method in high SNR conditions have been shown. A solution to this problem has been examined and performance shown.

- Subband processing techniques have been proposed and for MIMO channels with a long delay-spread we have shown that the method can lead to significant computational reduction [15, 16]. For time-varying channels the subband method can result in superior tracking performance and this has been shown in simulations.

- By harnessing fractionally-spaced signal processing, improvements to MIMO equaliser tracking performance for dynamic channels have been shown using both fullband and subband processing technique with the subband method performing better in some cases [17].

- The analysis of MIMO FSE in Chapter 6 is novel work.

- Showing how FSE MIMO systems can be used to equalise systems that would be rank-deficient when sampled at the symbol rate.

Chapter 2

MIMO Channels

This chapter will provide an overview of the recent research activity relating to MIMO systems. It will formally describe the MIMO system and outline a number of models that may be used to characterise typical MIMO channels. Further, it will state and explain the MIMO capacity equation and discuss various issues that may affect this. The chapter ends with a summary of the main issues.

2.1 MIMO Background

Although research in the field of MIMO systems is now maturing, it is still a fairly new topic that was popularised by ground-breaking papers by Foshini *et al.* [6] in 1996 on a MIMO detection algorithm and information-theoretic results again by Foschini in 1998 [1] and Telatar in 1999 [2]. An interesting historical note is that although Telatar first made the breakthroughs in 1995, they were circulated in the form of an internal memo at Bell Labs and were published only in 1999.

Although the above authors popularised this area for research, there were a few research papers on MIMO systems in radio communications prior to this. Possibly the earliest paper on MIMO systems was published in 1977 by Nichols *et al.* [18]. Their work was intended to counteract the cross-channel interference (CCI) in dual-polarised radio communications and cross-talk in multi-wire systems, and is therefore directly relevant to our work. It investigated the detection of two signals passed through a 2×2 non-time-dispersive MIMO channel and received by two antennas, based on the mean square error (MSE) and maximum likelihood (ML) criterion. The minimum mean squared error (MMSE) solution was found by a gradient-descent adaptive process and required no knowledge of the channel, whereas the ML detection (MLD) method required channel knowledge. The work showed favourable results when compared with no cross-talk cancellation.

One other early work was performed by Salz in 1985 [19], which was similar to that of Nichols *et al.* except that he dealt with a $N \times N$ MIMO system and the intended application was again dual-polarised radio systems as well as negating the cross-talk and CCI in frequency/time-division multiplexing, cordless private branch exchanges (PBX), spread-spectrum multi-user systems and multi-sensor radar/sonar systems. His work gave a mathematical treatment of the equalisation and detection, using transmit and receive filters, of the data streams passed through a MIMO channel that introduces CCI and ISI.

Multi-channel and MIMO systems in acoustics have been actively researched for about two decades in the form of multi-channel adaptive algorithms and the application of reproducing sound fields at a required point using multiple loudspeakers [20,21]. For example, Nelson *et al.* [21] showed how it was possible to use stereophonic sound reproduction to obtain a required sound field at two microphones using two loudspeakers in a room with a known acoustic impulse response. Gänsler and Benesty [22] gave a thorough mathematical treatment of two-channel adaptive acoustic echo-cancellation. This work in the field of acoustics is of interest here as, although the problem is slightly differently formulated to that of radio communication MIMO equalisation at the receiver, it is also fundamentally a MIMO inversion problem. As such we may draw on the research performed in this field in addition to the existing research in radio MIMO systems to further our own work.

The majority of the new work since Foschini and Telatar broadly falls into two categories, the first of which involves using the extra capacity of MIMO systems for spatial multiplexing (SM), where a user enjoys an increased data rate at a slightly worsened bit error rate (BER). The worsening is due to the possibility that the MIMO channel may be ill-conditioned. The second category is to employ the capacity to provide extra diversity through the use of space-time codes to provide the same data rate as a SISO system but at a much improved BER. We shall now discuss developments in each of these categories in turn, starting with the SM approach.

One of the most popular ways to detect the transmitted data streams is to use a linear MIMO equaliser at the receiver. This involves finding a matrix that will cancel out the effect of the cross-channel terms in the MIMO channel (i.e. the elements off the main diagonal) and if we assume a normalised system, then the terms on the main diagonal should be equal to one. This can be achieved by calculating the inverse matrix of the MIMO channel, also known as the zero-forcing (ZF) solution. When the MIMO channel and the ZF inverse are combined, an identity matrix results. The main problem with this approach is that it only

counteracts the spatial dispersion or co-channel interference effects of the channel but takes no account of the noise introduced. If the channel is ill-conditioned in the presence of noise, a poor solution will result. An approach that gives a better BER performance in a noisy environment is to find the MMSE solution. Either way, the process performed is the linear combinatorial manipulation to minimise the undesired cross-terms, and both these techniques are well known in both the area of equalisation [23] and multiuser detection [24].

An improvement to this simple method is to employ ordered successive interference cancellation (OSIC), which is again a technique well-known in the multiuser community. The first application of this to MIMO systems was by Foschini *et al.* [3, 4, 25], to create a system they called the Vertical- Bell Labs Space-Time (V-BLAST) architecture. They adapted this from an earlier architecture called Diagonal BLAST (D-BLAST) [6] which falls into the second category of space-time diversity described later. The system uses iterative linear combinatorial nulling based on either the ZF or MMSE criterion, and the OSIC is applied after each iteration to improve the post-detection BER.

Since this initial work, the technique has been adapted by Bjerke and Proakis [26, 27] to perform MLD, Decision-Directed Maximal Ratio Combining (DD-MRC), Maximum Likelihood Sequence Estimation (MLSE) and a MIMO Decision Feedback Equaliser (DFE) instead of using the ZF or MMSE criterion, and Bhargave *et al.* [28] created another MIMO MLD system, with improved results over the original V-BLAST. Hassell-Sweatman *et al.* [29, 30] showed by simulation interesting performance comparisons between the ZF, MMSE, V-BLAST and unordered V-BLAST types of MIMO detection systems, which demonstrated that of these the V-BLAST algorithm has the superior performance. Boubaker *et al.* [31] created a sub-optimal low complexity multi-carrier BLAST architecture by combining it with Orthogonal Frequency Division Multiplexing (OFDM) over time-dispersive channels. OFDM is another recent active research area, and the technique can be very useful due to its inherent robustness against time-dispersion (equivalently frequency-selectivity) [32].

The original V-BLAST algorithm was only designed to work with narrowband and therefore flat channels, and so has no intrinsic ability to counter-act the effect of systems that introduce inter-symbol interference (ISI). Since one of the aims of MIMO technology is to increase the information throughput, this assumption seems unrealistic as the ability to work with wideband channels is required to achieve high data rates. These channels are frequency-selective, or time-dispersive, i.e. the bandwidth of the data signal will exceed the coherence bandwidth of the channel, and taking no account of this will result in an irreducible BER, as was

shown by Boubaker *et al.* [33] in simulations with a Global System for Mobile communications (GSM) typical urban channel [34,35]. A number of recent works have been published that modify the V-BLAST algorithm to function properly with frequency-selective channels, starting with Lozano and Papadias [36] who created MIMO equalisers for frequency-selective channels based on DFE and two different OSIC-DFE techniques, showing that significant gains could be made using the OSIC system. So and Cheung [37,38] used an interesting model using *imaginary antennas* to represent the time-dispersiveness of a frequency-selective channel and went on to create systems capable of counteracting the dispersive effects of the channel. The channel is represented by the same number of imaginary antennas as the impulse response length of the channel and each imaginary antenna transmits a signal delayed by an appropriate amount through a flat channel weighted by the coefficient corresponding to that delay in the channel impulse response. Based on this, they used OFDM to create a V-BLAST OFDM system [38] and also created V-BLAST systems based on the ZF and MLD criteria [37].

We now move on to the second category of using the extra capacity of the MIMO system to provide space-time diversity and hence superior error rate performance at the same data rate. A comprehensive article by Paulraj and Papadias [39] shows the state of research shortly before pioneering MIMO research by Tarokh *et al.* [10, 11, 40] and Alamouti [9]. Before this, all space-time systems where either SIMO or MISO and used signal processing rather than coding techniques. Since then MIMO space-time coding has been developed which actually codes the input data streams across space and time to exploit the spatial diversity of MIMO channels. These codes broadly fall into two categories which are Space-Time Block Codes (STBC) as proposed by Alamouti [9] and Space-Time Trellis Codes (STTC) by Tarokh *et al.* [10,11,40]. The codes differ in the same way that standard SISO block and trellis codes differ, that is that block codes encode the data into discrete blocks, while trellis codes encode the data using convolutional techniques. As this thesis is more concerned with the techniques that employ the capacity of MIMO system to provide higher data rates through spatial multiplexing, little more will be said about space-time codes, however the interested reader may find a good recent overview of STBCs and STTCs in a paper giving a brief survey of MIMO research to 2003 by Gesbert *et al.* [41].

Recently, researchers have been examining the relationship between using MIMO capacity for SM and diversity. One of the first works that draws from the strengths of both categories is by Hassibi and Hochwald [42]. They develop coding techniques that provide the spatial multiplexing for high data rates used in such systems as V-BLAST but also has some of the spatial diversity inherent in space-time coding techniques. The system subsumes as special cases both V-BLAST and STBCs

and generally outperforms both but as the codes are linear they remain simple to encode. Information-theoretic work by Catreux *et al.* [43] compares via analysis and simulations results the gain performance of the SM and diversity approaches. Finally, Zheng and Tse [44] mathematically examined the trade-off between the two approaches.

Many experimental systems have been built over the years to demonstrate the performance of MIMO systems [3, 4, 45–48].

MIMO system deconvolution suffers from computational complexity problems. The dual task of combating ISI from the time-dispersiveness and CCI from the spatial-dispersiveness of a MIMO channel make the task much more difficult than either one alone. This is further exacerbated by the fact that we are assuming no channel knowledge, so this must either be obtained adaptively using trained or blind techniques, and in this thesis we will in general use the former. The literature review suggested that there has been little or no research into complexity reduction of creating equalisers for frequency-selective MIMO systems. This thesis will suggest, examine and assess the performance of various solutions to the problem that lower the complexity of the deconvolution and sometimes improve the convergence behaviour of adaptive algorithms used to invert the channel. Possible solutions to these problems covered in this thesis are improved adaptive algorithms, analytic channel inversion using time, frequency and z-domain approaches, subband processing methods and fractionally-spaced equalisation techniques.

2.2 Channel Description

In this section the MIMO channel and some associated mathematical notation will be formally introduced. This will be used throughout this thesis.

A MIMO channel is a system that has multiple inputs (e.g. multiple transmitters) and multiple outputs (e.g. multiple receivers), as is shown in Figure 1.1. It can be thought of as a collection of point-to-point, or single-input single-output (SISO), sub-channels between each pair of transmitters and receivers. As a result the responses of the individual SISO sub-channels forming a MIMO channel can be denoted as the elements of a so-called MIMO channel matrix. The system transfer equation therefore is

$$\begin{bmatrix} y_1[n] \\ y_2[n] \\ \vdots \\ y_P[n] \end{bmatrix} = \begin{bmatrix} h_{11}[l] & h_{21}[l] & \cdots & h_{M1}[l] \\ h_{12}[l] & h_{22}[l] & \cdots & h_{M2}[l] \\ \vdots & \vdots & \ddots & \vdots \\ h_{1P}[l] & h_{2P}[l] & \cdots & h_{MP}[l] \end{bmatrix} * \begin{bmatrix} x_1[n] \\ x_2[n] \\ \vdots \\ x_M[n] \end{bmatrix}, \tag{2.1}$$

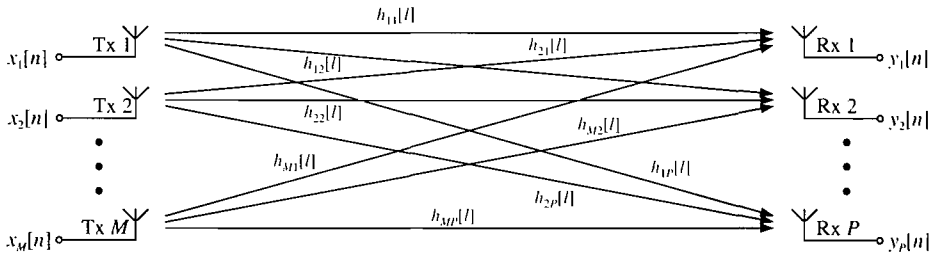

Fig. 2.1: A block diagram representation of a MIMO channel.

where "$*$" represents matrix convolution, $h_{mp}[l]$ is the SISO channel impulse response between transmitter m and receiver p, $x_m[n]$ is the input data to transmitter m and $y_p[n]$ is the output data at receiver p. Further, P is the number of receivers and M is the number of transmitters. Equation (2.1) is expressed pictorially in Figure 2.1. If $h_{mp}[n]$ are linear time-invariant (LTI) systems, (2.1) can be expressed in the z-domain as

$$\mathbf{y}(z) = \mathbf{H}(z) \cdot \mathbf{x}(z), \tag{2.2}$$

where

$$\mathbf{H}(z) = \begin{bmatrix} h_{11}(z) & h_{21}(z) & \cdots & h_{M1}(z) \\ h_{12}(z) & h_{22}(z) & \cdots & h_{M2}(z) \\ \vdots & \vdots & \ddots & \vdots \\ h_{1P}(z) & h_{2P}(z) & \cdots & h_{MP}(z) \end{bmatrix} \tag{2.3}$$

with z-transform pairs $h_{mp}(z) \bullet\!\!-\!\!\circ\, h_{mp}[n]$, and $\mathbf{x}(z)$ and $\mathbf{y}(z)$ being vectors containing the z-transforms of the corresponding vectors in (2.1). Note that (2.2) and (2.3) can be used to represent both flat and frequency-selective channels.

2.3 Channel Capacity

The main driving force behind the recent explosion in MIMO research was a few information-theoretic papers, now famous amongst the MIMO research community, by Foschini and Gans [1,6], Telatar [2], and Raleigh and Cioffi [7,49], which promised huge gains in the capacity of radio communication system over the Shannon capacity if MIMO channels could be exploited properly. Since these papers started the great recent interest in research of MIMO systems, this section covers the results of this work, and outlines the new MIMO capacity equations for independent uncorrelated sub-channels as well as more recent work showing how this ideal capacity is affected if the sub-channels are not completely uncorrelated. It also briefly discusses some work to model realistic MIMO channels, based on the physical properties of the environment, and how this would affect the capacity.

2.3.1 Uncorrelated Sub-Channels

Here we discuss the ideal case of uncorrelated MIMO channels. We start by stating the original SISO Shannon capacity equation normalised by the bandwidth for a flat fading channel,

$$C = \log_2\left(1 + \rho|h|^2\right) \text{ bps/Hz}, \tag{2.4}$$

where ρ is the average signal-to-noise ratio (SNR) and $|h|^2$ is the normalised instantaneous channel power transfer characteristic which varies due to Rayleigh fading. Assuming that h is a Rayleigh fading channel normalised so that the expectation of its power gain is unity we can obtain both the mean capacity and the outage probability plots by calculating the capacity for a suitable large sample set of h.

Telatar, and Foschini and Gans showed that assuming $M \leq P$ the instantaneous capacity for flat MIMO systems is [1,2]

$$C = \log_2 \det\left[\mathbf{I}_P + \frac{\rho}{M}\mathbf{H}\mathbf{H}^H\right] \text{ bps/Hz}, \tag{2.5}$$

where $\det[\cdot]$ is the determinant, $\mathbf{I}_p$ is the $P \times P$ identity matrix and P is the number of receivers, M is the number of transmitters, $\mathbf{H}$ is the instantaneous MIMO channel matrix and $(\cdot)^H$ is the hermitian transpose. The SNR now is the mean of the total SNR at all transmit antennas. This equation can be rewritten in an equivalent form [2,41]

$$C = \sum_{i=1}^{M} \log_2\left(1 + \frac{\rho}{M}\lambda_i\right) \text{ bps/Hz} \tag{2.6}$$

assuming that $M \leq P$, where λ_i are the non-zero eigenvalues of $\mathbf{H}^H\mathbf{H}$. A third equivalent representation of (2.5) is given by [50]

$$C = \log_2 \frac{\det\left[\mathbf{R}_\nu + \mathbf{H}\mathbf{R}_x\mathbf{H}^H\right]}{M\det\left[\mathbf{R}_\nu\right]}, \tag{2.7}$$

where $\mathbf{R}_x$ and $\mathbf{R}_\nu$ are the co-variance matrices of the input to the transmitters and noise at the receivers, respectively. Co-variance matrices are further explained in Chapter 3. It is easy to see that this is equal to (2.5) when the inputs and noise powers are equal and the signals uncorrelated. This representation will be useful when deriving an expression for the capacity of a channel-equaliser system in Chapter 4.

It can be shown that for MIMO systems with uncorrelated sub-channels and assuming $M \leq P$, the capacity increases nearly linearly with the number of transmitters,

$$\mathcal{E}\{C\} = M\log_2\left(1 + \frac{\rho}{M}\right) \tag{2.8}$$

$$\approx M\log_2\rho \qquad \text{for } \rho \gg M \tag{2.9}$$

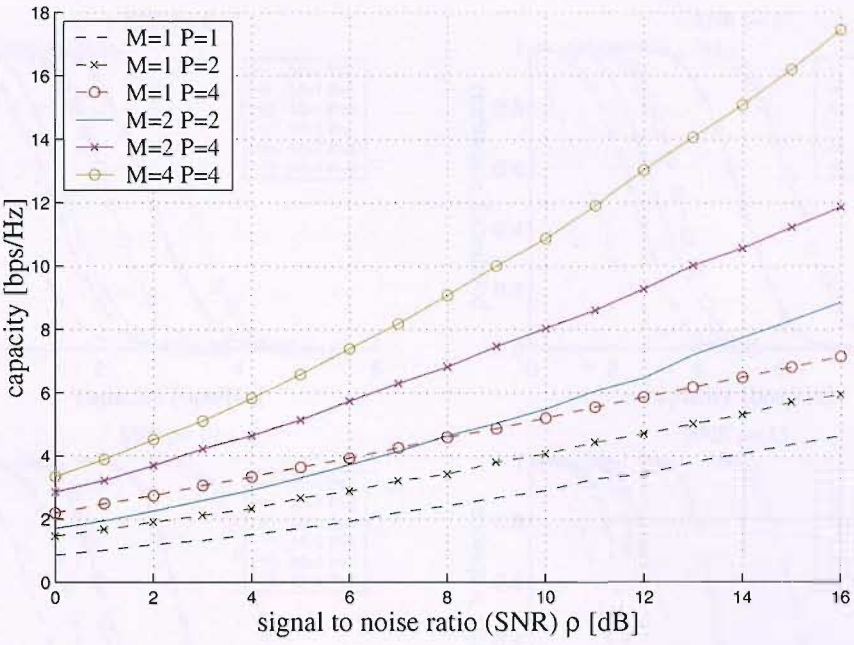

Fig. 2.2: The mean MIMO capacity for independent Rayleigh sub-channels and a range of MIMO system sizes, according to (2.5).

where $\mathcal{E}\{\cdot\}$ is the expectation operator and the derivation for this case be found in Appendix B. However, the capacity does not increase without bound with M and there is a limiting capacity as M tends to infinity, the derivation for which can again be found in Appendix B,

$$\lim_{n\to\infty} \mathcal{E}\{C\} = \frac{\rho}{\ln 2}. \tag{2.10}$$

Figure 2.2 shows the mean capacity of a MIMO channel with independent sub-channels for varying numbers of transmitters and receivers. The most basic case is the SISO channel which is, of course, the same as the original Rayleigh channel capacity as stated by the Shannon law. There are two single-input multiple-output (SIMO) cases, where there is one transmitter and 2 or 4 receivers. We see that the gradient for these cases is the same as for the SISO case but with a constant capacity offset of about 1.1 and 2.2 bps/Hz for 2 and 4 receivers respectively, which arises from the extra diversity provided the multiple receive antennas. This means that, fundamentally, the channel cannot transfer more information; it is simply the case that the receiver is more effective at extracting it from the radio signals in space. This is in contrast to the 2×2 and 4×4 cases where the gradients are steeper than for the SISO system. The 2×2 system is capable of transferring almost twice as much information, and the 4×4 system almost four times as much. This is in agreement with (2.9) which showed that we expect an almost linear increase in capacity with the number of transmit antenna, for a high

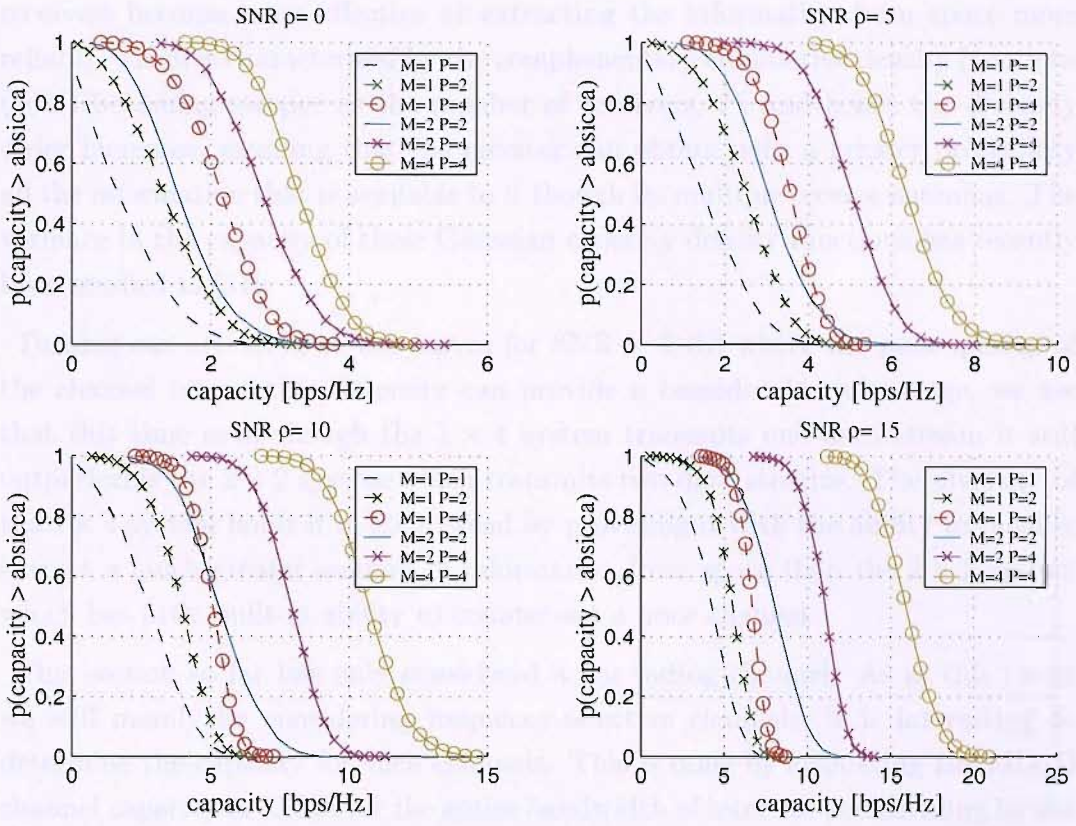

Fig. 2.3: The MIMO capacity ccdf for independent Rayleigh sub-channels and a range of MIMO system sizes and SNR=0, 5, 10 and 15 dB.

SNR. This means that if harnessed properly, MIMO systems can fundamentally increase the amount of information transmitted through space using radio signals. Diversity is still a desirable feature however, at low SNRs. Notice that below an SNR of 8 dB the 1×4 system outperforms the 2×2 system.

Using (2.5) we may also obtain the complementary cumulative density functions in Figure 2.3, which show the probability of a MIMO system exceeding a particular capacity for a range of MIMO system sizes and SNRs of 0, 5, 10 and 15 dB. At the highest SNR of 15 dB, where the received signal has a good strength, and therefore diversity is of limited benefit, we see all the MIMO systems outperform the SISO and SIMO systems. Comparing the two systems that have four sub-channels, namely the 1×4 and 2×2 systems, we see that the 2×2 system which use the additional capacity for multiplexing but little diversity outperforms the 1×4 system which has plenty of spatial diversity but only transmits a single data stream. The 2×4 system which has more diversity, and 4×4 system which transmits more data streams than the 2×2 system both outperform. Finally, looking at the SIMO systems we see that the diversity does not fundamentally increase the data transmission capability over the SISO system, more that the

receivers become more effective at extracting the information from space more reliably, which is characterised by the complementary cumulative density functions (ccdf) becoming steeper as the number of receivers, P, and hence the diversity order increases, meaning that the receiver can obtain with a greater probability all the information that is available to it though its multiple receive antennas. The variance in the capacity of these Gaussian capacity density functions has recently been studied in [51].

Turning our attention to the curves for SNR = 0 dB where the poor quality of the channel means that diversity can provide a considerable advantage, we see that this time even though the 1×4 system transmits one data stream it still outperforms the 2×2 system which transmits two data streams. The diversity of the 1×4 system holds it in good stead by providing it with the ability to reliably extract a much greater amount of information from space than the 2×2 system which has little built-in ability to counter-act a poor channel.

This section so far has only considered a flat fading channel. As in this thesis we will mainly be considering frequency-selective channels, it is interesting to determine the capacity for such channels. This is done by evaluating the MIMO channel capacity in (2.5) over the entire bandwidth of interest, and dividing by the bandwidth to obtain a normalised equation directly comparable to (2.5), yielding [52]

$$C = \frac{1}{B} \int_B \log_2 \det \left(\mathbf{I} + \frac{\rho}{M} \mathbf{H}(f) \mathbf{H}^H(f) \right) df \qquad \text{bps/Hz}, \tag{2.11}$$

where $\mathbf{H}(f) = \mathbf{H}(z)|_{z=e^{j2\pi f}}$ is the spectral representation of the MIMO channel matrix. This equation may be used in the same way as (2.5) but the resulting capacity depends on the spectral characteristics of the system.

There is a common misconception in the MIMO research community that uncorrelated MIMO sub-channels means that the MIMO channel matrix will be high rank and therefore will result in the capacity predicted by the capacity plots of Figures 2.2 and 2.3. However, research has shown that this is not the case [53, 54], leading to the discovery of so-called *pin-hole* channels. This section has so far assumed that the uncorrelated sub-channels will result in a high rank MIMO matrix- we term these uncorrelated high rank (UHR)- but it can be shown that although correlated sub-channels will cause the MIMO matrix to be low rank, the converse is not true with the proof being in the existence of uncorrelated low rank (ULR), or pin-hole channels. The case of correlated low rank (CLR) channels will be discussed in the next section, but now we will cover ULR channels.

Pin-hole channels occur when the signal at the transmitter and receiver are subject to highly localised scattering, but the distance between these local scattering

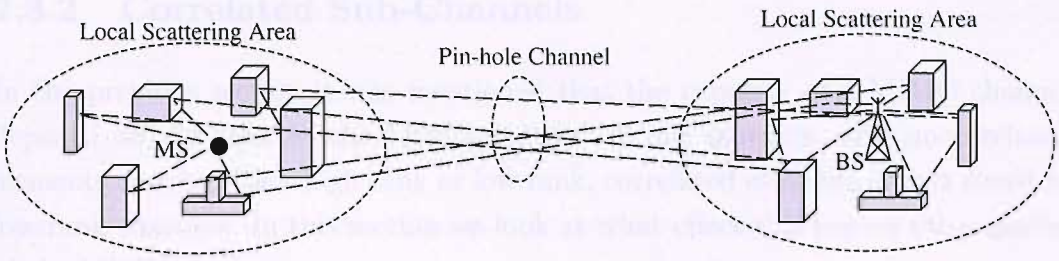

Fig. 2.4: A pin-hole channel with uncorrelated sub-channel but causing a low rank MIMO matrix channel.

areas is relatively high or the space between them physically narrow, meaning that the signals must all travel though the same path in space between these two local scattering areas, as shown in Figure 2.4. Whereas for the Rayleigh faded UHR MIMO channel the elements of $\mathbf{H}$ are given by i.i.d. complex-valued Gaussian variates, the model for a ULR channel results in $\mathbf{H} = \mathbf{a}_{rx}\mathbf{a}_{tx}^H$ where $\mathbf{a}_{rx}$ and $\mathbf{a}_{tx}$ are independent receiver and transmitters fading column vectors with i.i.d. complex-valued Gaussian elements [53]. Therefore every realisation of $\mathbf{H}$ is rank one even though the elements are uncorrelated. In this extreme case no multiplexing gain is possible and the system, and therefore capacity, collapses to that of a SIMO system (because the system can still benefit from spatial diversity at the receiver). Therefore it is the rank of $\mathbf{H}$ we should be interested in, and not merely whether the sub-channels are uncorrelated or not, as this is what affects the capacity, and can do so significantly as shown in [53, 54]. In reality most MIMO channels are between these two extremes of a full-rank and rank one system, and if there is a good level of scattering over the *whole* area between Mobile Station (MS) and Base Station (BS), as is usually the case in urban microcells and picocells, for example, we may assume that the true rank of $\mathbf{H}$ is nearer the upper end of the scale.

Finally, another area of work has been to explicitly model the multipath components of the MIMO system in an attempt to determine more realistic capacity equations based on more realistic scattering models [7,49,55,56] and most recently a geometric correlated channel model [57]. All this work invariably shows that the curves of Figures 2.2 and 2.3 represent ideal upper limits and depending on the actual channel the true capacities are generally lower than this but still much greater than those of SISO or SIMO systems.

2.3.2 Correlated Sub-Channels

In the previous section it was mentioned that the capacity of a MIMO channel depends on the rank of the MIMO matrix. While matrices with uncorrelated elements may be either high rank or low rank, correlated elements always result in low rank channels. In this section we look at what effect this has on the capacity of the MIMO channel.

It can be shown that assuming that the transmitted signals are uncorrelated and the MIMO channel introduces cross-correlation between the data streams, the capacity of a MIMO system with correlated sub-channels depends on the correlation coefficients, r, between various pairs of the received signals [58]. If we consider a 2×2 system, the correlation coefficient between the two received signals is given by [59]

$$r = \frac{h_{11}h_{12}^* + h_{21}h_{22}^*}{\sqrt{(|h_{11}|^2 + |h_{21}|^2)(|h_{12}|^2 + |h_{22}|^2)}} \tag{2.12}$$

where $(\cdot)^*$ denotes the complex conjugate. If we assume equal received powers then this reduces to

$$r = h_{11}h_{12}^* + h_{21}h_{22}^* \tag{2.13}$$

and after some mathematical development [59] we obtain a MIMO capacity equation

$$C = \log_2\left(1 + \rho + \left(1 - |r|^2\right)(\rho/2)^2\right). \tag{2.14}$$

Notice that when the sub-channels are independent then $r = 0$ then this equation reduces to (2.8), and that when the channels are completely correlated and the MIMO matrix has rank one then $r = 1$ and the equation reduces to a SIMO system, benefiting only from spatial diversity but no multiplexing gain. In the case that the received powers are not equal, the capacity becomes

$$C = \log_2\left(1 + \rho + 4\alpha(1-\alpha)(1 - |r|^2)(\rho/2)^2\right) \tag{2.15}$$

where

$$\alpha = \frac{|h_{11}|^2 + |h_{21}|^2}{|h_{11}|^2 + |h_{21}|^2 + |h_{12}|^2 + |h_{22}|^2} \tag{2.16}$$

The more general case of a $M \times P$ with $M = P$ MIMO system is somewhat more complicated since we must calculate the correlation coefficients between every pair of received signals and incorporate this into the capacity equation. The correlation coefficient between receivers p_1 and p_2 is given by [58]

$$r_{p_1,p_2} = \frac{\sum_k h_{p_1,k}h_{p_2,k}}{\sqrt{\sum_k |h_{p_1,k}|^2 \sum_k |h_{p_2,k}|^2}}, \tag{2.17}$$

but to gain some insight we may simplify the problem by assuming that all the received powers are equal, $r_{p_1,p_2} = r$, in which case the MIMO capacity is

$$C = M \log_2 \left(1 + \frac{\rho}{M}(1-r)\right) + \log_2 \left(1 + \rho r \left(1 + \frac{\rho}{M}(1-r)\right)^{-1}\right). \quad (2.18)$$

This gives the worst case estimation of the capacity as in reality physically more distant antennas will have a lower correlation coefficient than close ones, meaning that the capacity will be greater than that suggested by (2.18). The true capacity will be in between the worst case extreme of (2.18) and the best case extreme of (2.5). Notice that in (2.18) if $n = 2$ or $r = 0$ or $r = 1$ the equation reduces to (2.14) or (2.5) or a SIMO system arising from the spatial diversity from the multiple receive antenna, respectively. Now we discuss the implications of these results. Plots of how the correlation coefficients affect the MIMO capacity can be found in [58, 59] and they show that the effect is dependent on the size of the MIMO system. For 'small' systems where $M = P < \sim 10$ then the capacity remains at about 90% of its maximum value, about 50 bps/Hz for $\rho = 30$ dB, for a correlation coefficient of up to 0.8. This means that a substantial fraction of the capacity promised by (2.5) can be realised for even modestly scattering channels, and this has been confirmed experimentally [48]. For a larger system, $M = P \approx 50$ the drop off is worse with the capacity falling below 90% its maximum value by the time the correlation coefficient reaches 0.2. However, the capacity is about 200 bps/Hz for $\rho = 30$ dB, which is still considerable above that of the smaller system simply by virtue of the fact that many more antennas are being used.

The interested reader may further like to look at a paper by Shiu *et al.* [60] which gives an mathematical analysis with simulations to demonstrate the findings of the effect of fading correlation of the capacity of MIMO systems. They develop a physical "one-ring" scattering model, similar to the scattering areas of pin-hole channels explained in the previous section, but where the scattering occurs only at one side of the communication link and use this model to determine the correlation and subsequently the effect on MIMO capacity when using various antenna configurations, for example in-line, broadside or hexagonal arrangements. Finally, there has been a great amount of interest very recently in capacity limits for realistic correlated MIMO channels, and many analyses have been performed in [61–66]. Additionally, the effect of sub-channel correlation when using adaptive frequency-domain equalisation, mentioned in 3.5.2, has been studied in [67].

2.4 Channel Models

This section will introduce various MIMO channel models that will be used in future simulations throughout this thesis. It will give an overview of arbitrary, measured and standardised channel models and their characteristics and behaviour both over frequency, time and space. The measured and standardised channel models are typically valid for a particular stated bandwidth. We will see examples of such channels, and these will be the channels that will be used in the simulations performed in future chapters. All channel models are assumed to be normalised with respect to the large-scale path loss between transmitters and receivers.

2.4.1 Spectral Dynamics

This section will explain two kinds of channel— narrowband and wideband— which can be characterised by their frequency domain behaviour and impulse response delay spread. The channels shown can be considered to be samples from an underlying statistical process which characterises the long-term behaviour of the channels. Later, in Section 2.4.2 we will see the temporal dynamic behaviour of the channels when many samples can be taken from the statistical process and vary over time according to some underlying rules.

2.4.1.1 Narrowband Channel

A narrowband channel has a frequency response that is near flat across the frequency band of interest. The delay spread [23] of these channels is much shorter than the symbol period and as a result these channels introduce no or little significant ISI. Equivalently, the coherence bandwidth [23] of the channel is much greater than the signal bandwidth.

The length of the impulse response, L_h, of such a channel is usually very small, one or two symbol periods for example. Hence the impulse responses of the sub-channels, $h_{mp}[l]$, in (2.1) are only a few symbol-spaced taps long. If $L_h = 1$ for all sub-channels then they are spectrally flat with a phase rotation and magnitude equal to that of each complex coefficient. Such a MIMO channel would be very easy to invert by finding the scalar matrix inverse. Since flat channels present no particular problem in inversion especially as MIMO systems are only likely to be implemented using small numbers of antenna, e.g. 4×4 and the process can be performed quickly, we shall not consider them further, and use them for no future simulations.

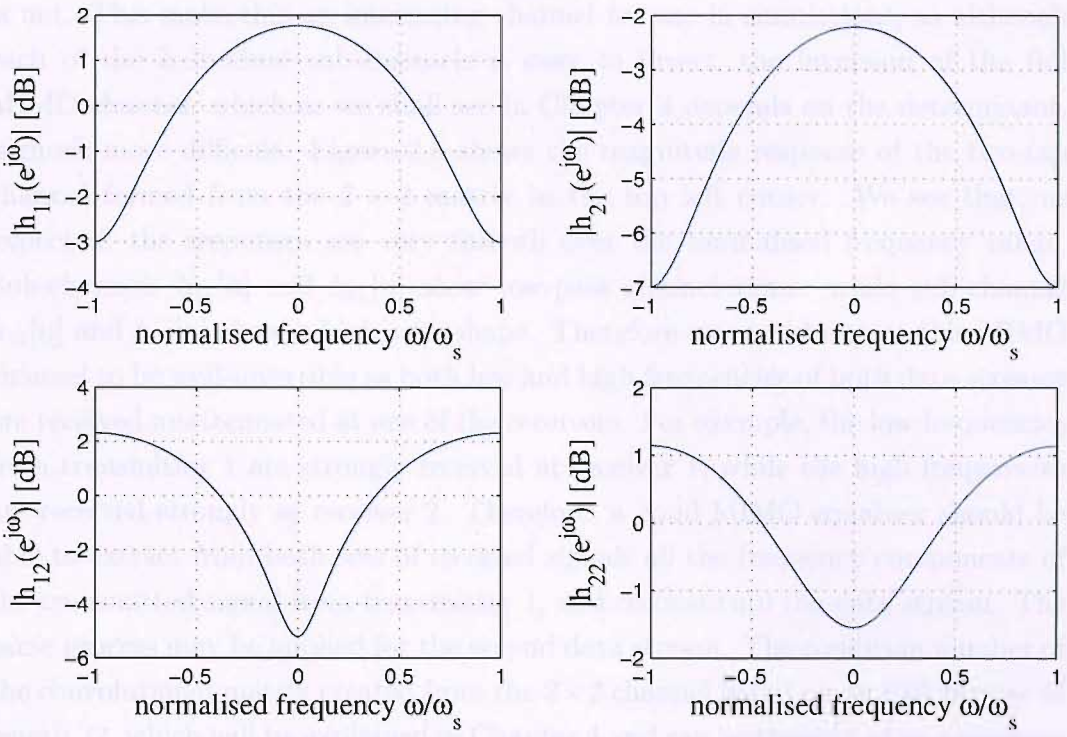

Fig. 2.5: Magnitude responses of two-tap sub-channels.

A channel that we also consider to be narrowband has $L_h = 2$, hence we call this a two-tap channel. Whether the channel is truly narrowband depends on the impulse response, but for convenience be assume that we may place it in this category. A two-tap channel is mildly time-dispersive and has frequency-selective spectral characteristics, although the dynamics are quite smooth over the band of interest. This channel will introduce a small amount of ISI, the delay spread and coherence bandwidth will be of a similar order of magnitude to the symbol period and bandwidth, respectively. As this is a theoretical channel that we use for testing our future equaliser systems, the time between the two taps is arbitrary, however to relate this channel to the real world we can choose a delay of about $2\mu s$ to make it similar to a COST 207 Typical Urban channel [68].

The channel will contain first-order polynomials in z in each of the elements of $\mathbf{H}$ in (2.3). A single realisation of such a channel is given by

$$\mathbf{H}(z) = \begin{bmatrix} 1+0.5z^{-1} & 1-0.7z^{-1} & 0.7+0.1z^{-1} & 0.7+0.5z^{-1} \\ 0.4+0.2z^{-1} & 1-0.3z^{-1} & -0.3+0.6z^{-1} & 0.9-0.1z^{-1} \\ 0.5-0.1z^{-1} & -0.7+0.8z^{-1} & -1+0.2z^{-1} & 0.8+0.3z^{-1} \\ 0.7+0.1z^{-1} & -0.7-1.0z^{-1} & -0.2-0.8z^{-1} & 0.4+1.0z^{-1} \end{bmatrix}. \quad (2.19)$$

To keep simulation time reasonable when this channel is used in simulations, it will be static. The sub-channels are all minimum phase but the matrix determinant

is not. This make this an interesting channel for use in simulations, as although each of the individual sub-channels is easy to invert, the inversion of the full MIMO channel, which as we shall see in Chapter 4 depends on the determinant, is much more difficult. Figure 2.5 shows the magnitude response of the two-tap channel formed from the 2×2 matrix in the top left corner. We see that, as expected, the responses are very smooth over the normalised frequency range. Sub-channels $h_{11}[n]$ and $h_{21}[n]$ show low-pass characteristics while sub-channel $h_{12}[n]$ and $h_{22}[n]$ show a high-pass shape. Therefore we would expect this MIMO channel to be well-invertible as both low and high frequencies of both data streams are received unattenuated at one of the receivers. For example, the low frequencies from transmitter 1 are strongly received at receiver 1, while the high frequencies are received strongly at receiver 2. Therefore, a good MIMO equaliser should be able to extract from both sets of received signals all the frequency components of the transmitted signal from transmitter 1, and reconstitute the data stream. The same process may be applied for the second data stream. The condition number of the convolutional matrix created from the 2×2 channel based on an FIR inverse of length 32, which will be explained in Chapter 4 and can be thought of as a measure of the difficulty involved in inverting the channel, is about 20. Occasionally we will need a 4×4 two-tap channel which is the full matrix shown above.

2.4.1.2 Measured Channels

Now we consider highly time-dispersive channels, which introduce ISI of several tens, hundreds or even thousands of symbol periods and have a significant RMS delay spread [23, 69]. The RMS delay spread of this channel will be much greater than the symbol period, or equivalently the coherence bandwidth will be much less that the symbol bandwidth and for this reason we shall term these wideband channels.

Non-Minimum Phase. Complex-valued non-minimum phase channels were taken from microwave measurements at the Signal Processing Information Base (SPIB) located at Rice University [70], which are fractionally-sampled at twice the baud rate of 30 MSybmols/s and approximately 300 coefficients long. The RMS delay spread of the channels range from 30 ns to 120 ns. Due to their response length and the non-minimum phase property, a MIMO channel constructed from these responses will generally be difficult to invert.

Figure 2.6(a) shows the channel impulse responses (CIR) and Figure 2.6(b) the magnitude responses of the four channels. Since they are fractionally-sampled we see a low pass characteristic in all channels, due to the receiver filter. Often we

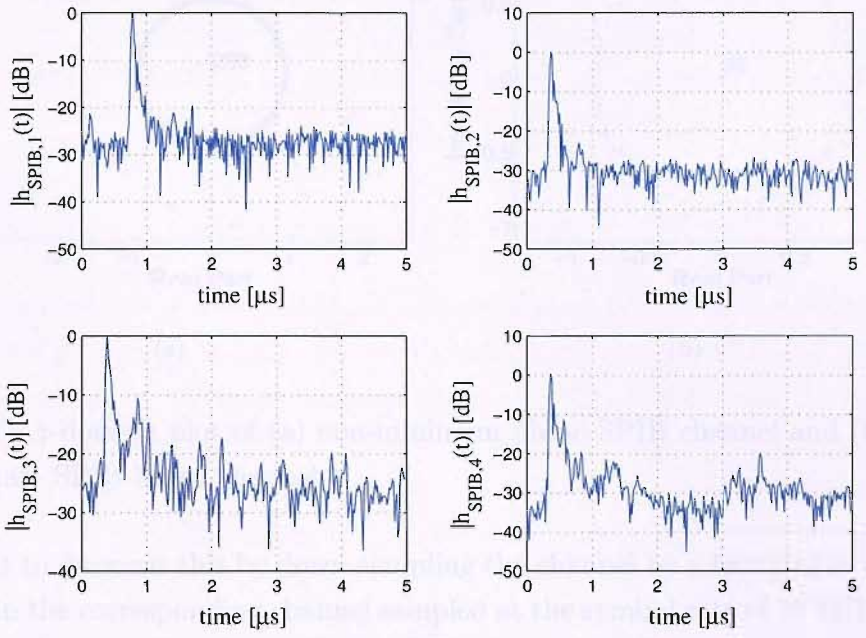

(a)

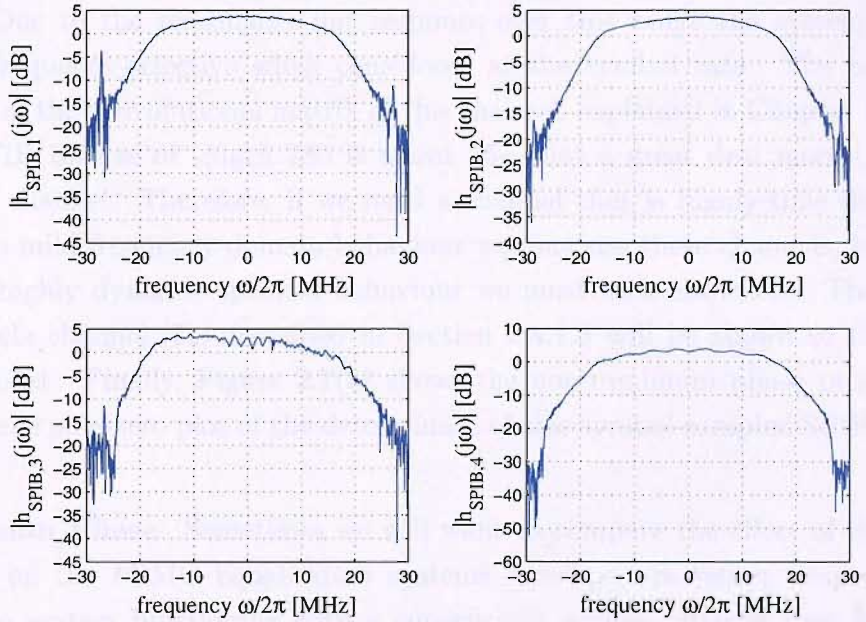

(b)

Fig. 2.6: SPIB sub-channels (a) Impulse responses (b) Magnitude responses

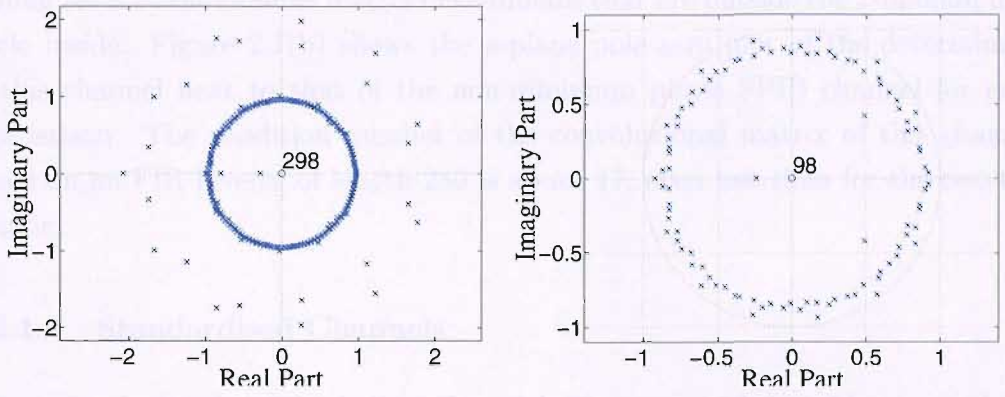

(a) (b)

Fig. 2.7: z-domain plot of (a) non-minimum phase SPIB channel and (b) minimum phase SPIB-based channel

will want to discount this by down-sampling the channel by a factor of two, hence we obtain the corresponding channel sampled at the symbol rate of 30 MHz. Since the channel is attenuated outside ± 15 MHz these aliased components should not affect the response inside ± 15 MHz a great deal, hence we assume the magnitude response is the same as in Figure 2.6(b) but only for the range -15 MHz to 15 MHz. Due to the reasonably flat response over this range the system is only mildly frequency-selective when considered at the symbol rate. The condition number of the convolutional matrix of this channel, explained in Chapter 4, based on an FIR inverse of length 280 is about 35— not a great deal more than the two tap channel. Therefore, if we need a channel that is highly-time dispersive but with mild frequency-domain behaviour we may use these channels, but if we require highly dynamic spectral behaviour we must look elsewhere. The Saleh-Valenzuela channel [71] described in Section 2.4.1.3 will be shown to fulfil this requirement. Finally, Figure 2.7(a) shows the non-minimum phase property in the z-plane pole-zero plot of the determinant of this symbol-sampled SPIB MIMO channel.

Minimum Phase. Sometimes we will want to compare the effect of the SPIB channel on the MIMO equalisation systems developed in future chapters with the same system functioning with a superficially similar channel that has been modified to become minimum phase. This will show us what effect the phase behaviour has on the system. For this we will use a channel that is based on the SPIB channels but where the coefficients before the main peak in the impulse response have been removed and the channels have been truncated to length 50 for simplicity. Further, one of the cross-channels is attenuated which has the effect of

pulling zeros of the channel matrix determinant that are outside the z-domain unit circle inside. Figure 2.7(b) shows the z-plane pole-zero plot of the determinant of this channel next to that of the non-minimum phase SPIB channel for easy comparison. The condition number of the convolutional matrix of this channel based on an FIR inverse of length 280 is about 17, even less than for the two-tap channel.

2.4.1.3 Standardised Channels

There are plenty of standard channel models in existence for a wide range of circumstances and environments, often created by standards institutions. Two channel models of interest to us are the typical urban (TU) channel from the European Cooperation in the field of Scientific and Technical Research (COST) Action 207 project (COST-207) [68] which was developed to define a time-dispersive test channel for use with GSM equaliser performance evaluation, and the Saleh-Valenzuela channel [71, 72].

COST-207. One of the channels defined in the COST-207 research project was for a TU environment. Figure 2.8 show the impulse response and spectral behaviour for a channel that conforms to the TU specification. The model actually specifies a time-varying channel but here we consider a stationary "snap-shot" of the channel. The maximum path delay $\tau_{\max} = 2.692\mu s$, and the RMS delay spread $\tau_{\text{rms}} = 0.904\mu s$. Other channels defined by COST-207 are bad urban (BU), rural area (RA) and hilly terrain (HT) [68].

Saleh-Valenzuela Statistical Model. The Saleh-Valenzuela (SV) [71, 72] channel model enables us to create a highly-time dispersive and frequency-selective channel, which we may consider to be wideband, and as it is a statistical model we may run the generation algorithm as many times as required to create as many channel realisations as we require. In this respect it is better than the SPIB channels which are single measured samples of a channel. The model assumes that the channel impulse response consists of a number of exponentially decaying clusters of rays, and within each cluster the rays also decay exponentially. Further, the time between each cluster and also each ray within each cluster are taken from two different random Poisson distributions. The phase of each ray is taken from an independent random variable distributed over $[-\pi, \pi)$.

Describing the model mathematically, let the arrival of the l^{th} cluster of rays be denoted $T_l, l = 0, 1, 2, \cdots$, and let the arrival time of the k^{th} ray measured relative to the beginning of its cluster be denoted $\tau_{kl}, k = 0, 1, 2, \cdots$. We defined $T_0 = 0$ for the first cluster and $\tau_{0l} = 0$ for the first ray within the l^{th} cluster. The model

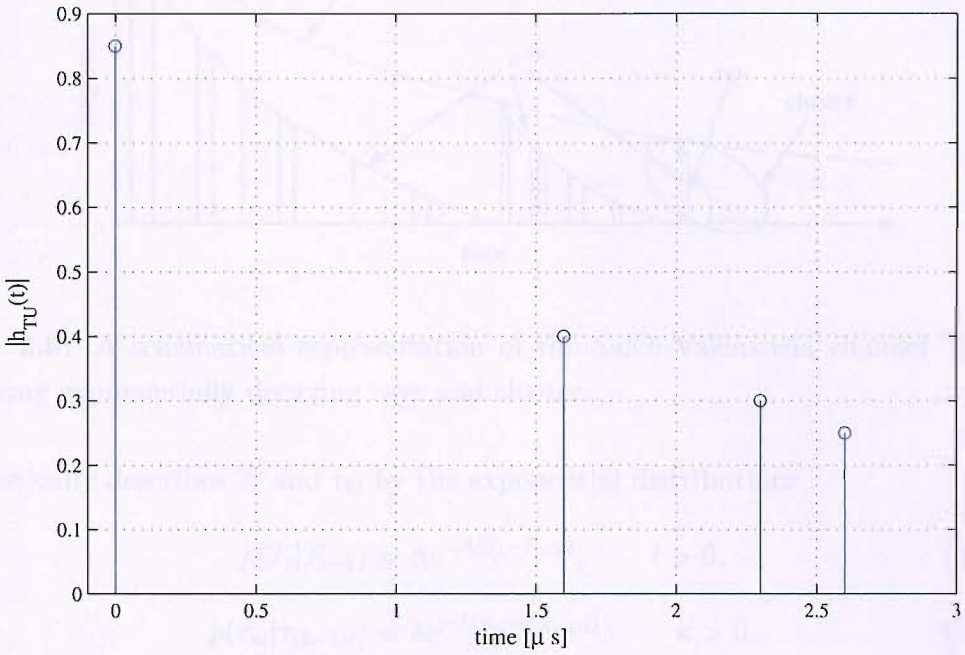

(a)

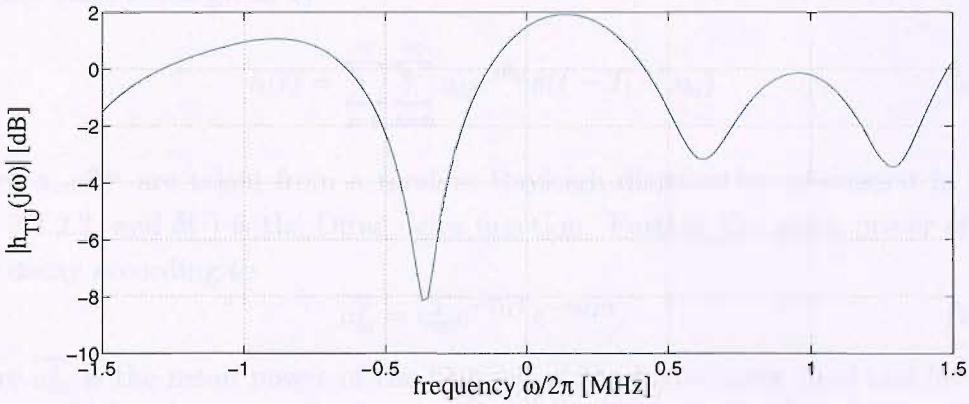

(b)

Fig. 2.8: COST-207 Typical Urban channel model (a) impulse response (b) spectral behaviour

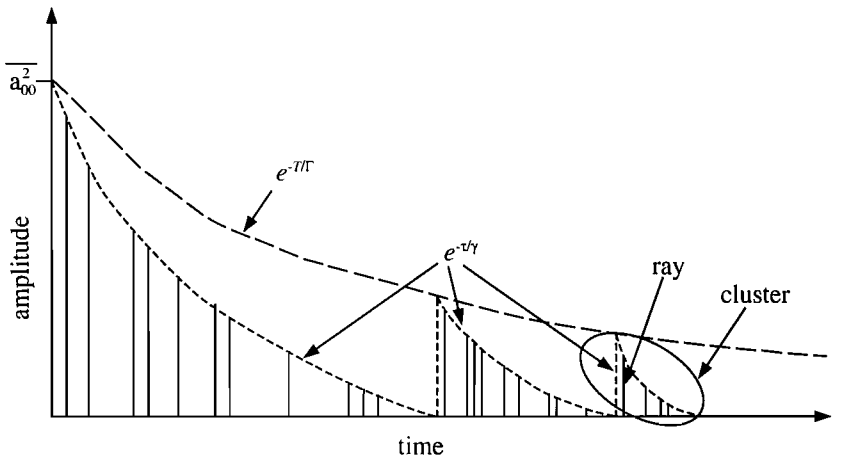

Fig. 2.9: A schematical representation of the Saleh-Valenzuela channel model showing exponentially decaying rays and cluster.

statistically describes T_l and τ_{kl} by the exponential distributions

$$p(T_l|T_{l-1}) = \Lambda e^{-\Lambda(T_l - T_{l-1})}, \qquad l > 0, \tag{2.20}$$

$$p(\tau_{kl}|\tau_{(k-1)l}) = \lambda e^{-\lambda(\tau_{kl} - \tau_{(k-1)l})}, \qquad k > 0, \tag{2.21}$$

where Λ is the cluster arrival rate and λ is the ray arrival rate. Let the gain of the k^{th} ray in the l^{th} cluster be denoted a_{kl} and its phase by θ_{kl}, the the channel impulse response is given by

$$h(t) = \sum_{l=0}^{\infty} \sum_{k=0}^{\infty} a_{kl} e^{j\theta_{kl}} \delta(t - T_l - \tau_{kl}) \tag{2.22}$$

where $a_{kl}e^{j\theta_{kl}}$ are taken from a random Rayleigh distribution, discussed in Section 2.4.2.2, and $\delta(\cdot)$ is the Dirac delta function. Further the mean power of the rays decay according to

$$\overline{a_{kl}^2} = \overline{a_{00}^2} e^{-T_l/\Gamma} e^{-\tau_{kl}/\gamma}, \tag{2.23}$$

where $\overline{a_{00}^2}$ is the mean power of the first ray in the first cluster (and can be normalised to one), and Γ and γ are the power decay time constants for clusters and rays, respectively. For clarification the model is shown with three clusters and several rays in each cluster in Figure 2.9.

Saleh and Valenzuela evaluated the accuracy of their model by comparing it to measurements they had obtained in two storey high medium-sized office building with dimension 115m by 14m. The external walls were made of steel and glass while the internal walls were made from wooden studs and plaster board, and the office contained typical office furniture and lab equipment. The measurement

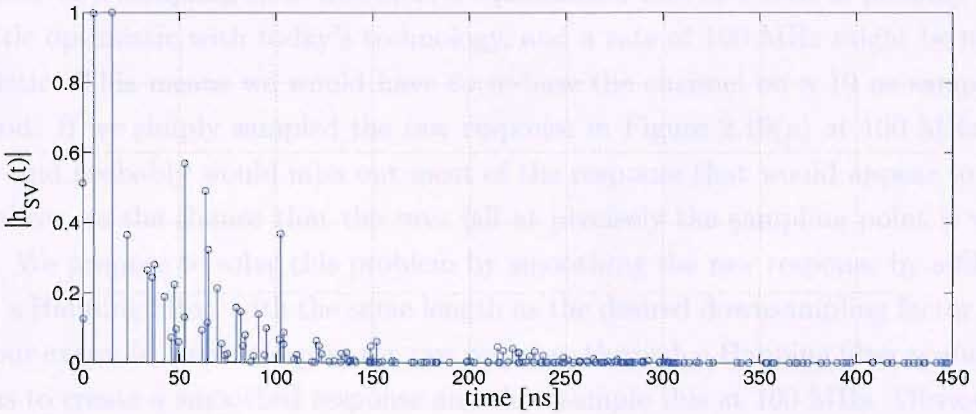

(a)

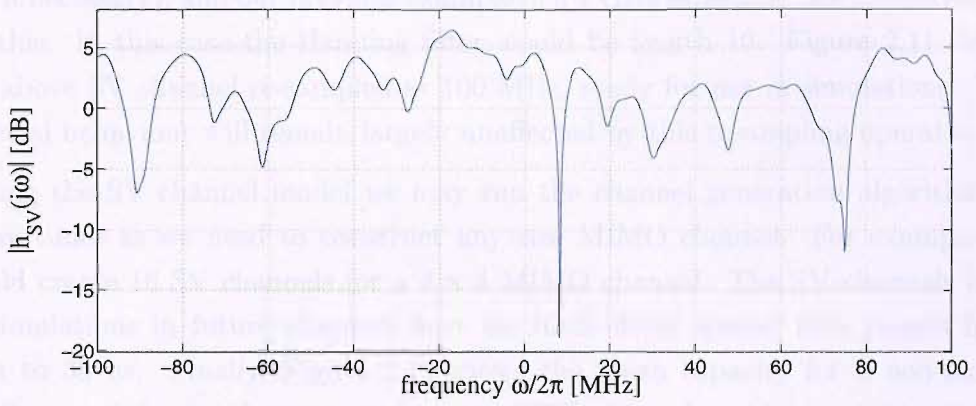

(b)

Fig. 2.10: Saleh-Valenzuela channel model realisation with $1/\Lambda = 300$ ns, $1/\lambda = 5$ ns, $\Gamma = 60$ ns and $\gamma = 20$ ns (a) impulse response (b) spectral behaviour.

were made using 1.5 GHz carrier pulses and the response was sampled at 200 MHz. They found that their model could be made to give a good fit to their measurements if they used the following parameters for their model: $1/\Lambda$ in the range 200-300 ns, $1/\lambda$ in the range 5-10 ns, $\Gamma = 60$ ns and $\gamma = 20$ ns. The channel impulse response and 200 MHz bandwidth portion of the spectral behaviour for an example of the SV model with $1/\Lambda = 300$ ns, $1/\lambda = 5$ ns, $\Gamma = 60$ ns and $\gamma = 20$ ns is shown in Figure 2.10.

If we are to use this channel in discrete time simulations we must decide on the receiver sampling rate, f_s, in real terms and sample the raw response at that rate. For example if we based the simulation on a 1 GHz sampling rate then we would sample every 1 ns and the channel response from the point of view of the equaliser would look very much that in Figure 2.10(a), with most of the ray responses falling

in their own sampling slot. However, a equalisation rate of 1 GHz is possibly still a little optimistic with today's technology, and a rate of 100 MHz might be more realistic. This means we would have to re-base the channel on a 10 ns sampling period. If we simply sampled the raw response in Figure 2.10(a) at 100 MHz we may and probably would miss out most of the response that would appear to the equaliser, as the chance that the rays fall at precisely the sampling point is very low. We propose to solve this problem by smoothing the raw response by a filter, e.g. a Hanning filter, with the same length as the desired downsampling factor. So for our example, we would pass the raw response through a Hanning filter spanning 10 ns to create a smoothed response and then sample this at 100 MHz. Obviously to do this we must start with a very high rate uniformly sampled realisation of the raw response that samples every ray (whilst moving the ray to the closest sampling slot if necessary), and our previous example of a 1 GHz sampling rate should suffice for this. In this case the Hanning filter would be length 10. Figure 2.11 shows the above SV channel re-sampled at 100 MHz, ready for use in simulations. The spectral behaviour will remain largely unaffected by this resampling operation.

Using the SV channel model we may run the channel generation algorithm as many times as we need to construct any size MIMO channel. For example we would create 16 SV channels for a 4×4 MIMO channel. The SV channels used in simulations in future chapters have an RMS delay spread that ranges from 5 ns to 35 ns. Finally, Figure 2.12 shows the mean capacity for a non-fading 2×2 non-minimum phase symbol-spaced SPIB channel and a non-fading Saleh-Valenzuela channel sampled at 100 MHz (SV100M) and Figure 2.13 shows the outage probability for the SV100M channel at a range of SNR values. These can be compared with the plots for flat fading channels shown in Figure 2.2 and 2.3.

2.4.1.4 Band-limiting

In Chapter 6 we will be considering fractionally-spaced equalisation of wideband MIMO channels, whereby the received signal are sampled at fractions of the symbol rate. Fractionally-spaced equalisation (FSE) will be briefly introduced in Section 4.1.4 but for now we state that we will require suitable channels. Simply generating higher bandwidth channels is unrealistic since by doing so we increase the transmission bandwidth and hence it will come as no surprise that a much improved BER can be expected. In realistic systems however, the channels will be band-limited to the symbol rate using some filter for reasons such as limiting extraneous emissions to conform to spectrum licenses, and limit noise power at the receiver. This band-limiting was seen in the spectrum of the fractionally-sampled SPIB channels in Section 2.4.1.2. For FSE simulations using the SPIB channels up

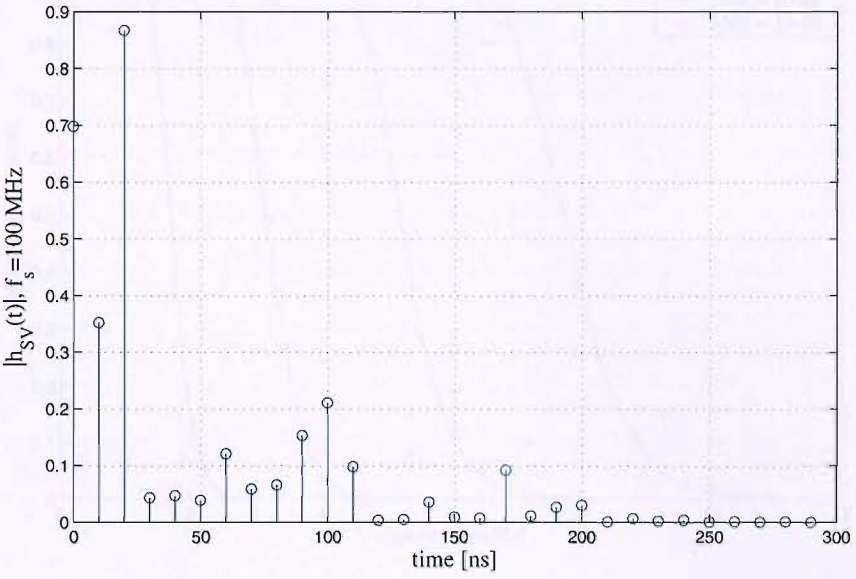

Fig. 2.11: Impulse response of Saleh-Valenzuela channel realisation sampled at 100 MHz.

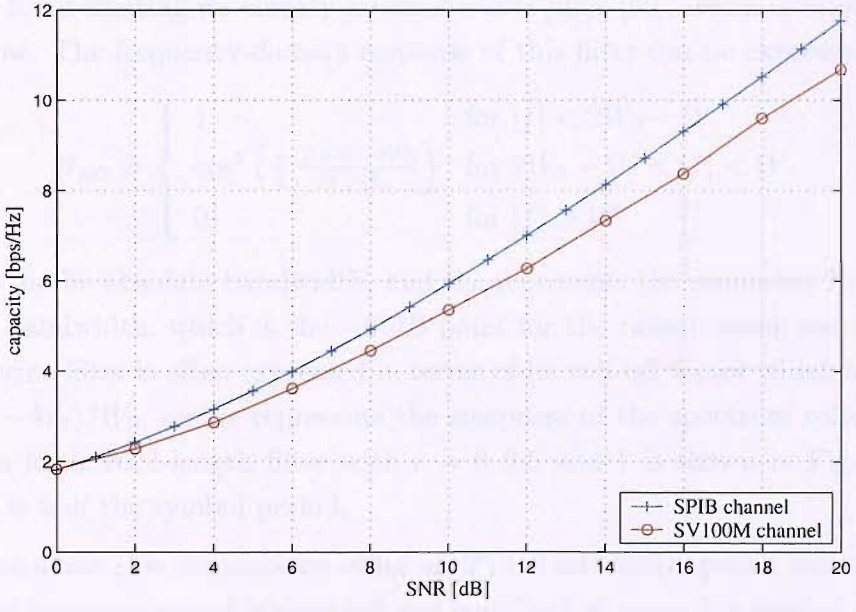

Fig. 2.12: Capacity of non-minimum phase 2×2 MIMO SPIB and SV100M channels.

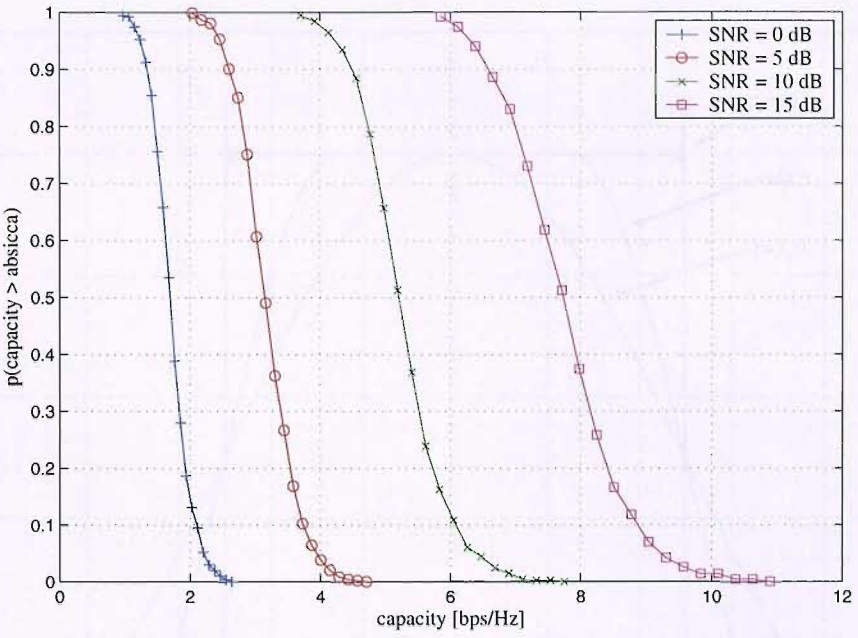

Fig. 2.13: Outage capacity of 2×2 MIMO SV100M channel.

to an oversampling factor of two we may simply use these measured responses (we will only be considering these so-called $T/2$ systems). The SV channels which are generated using the model in the previous section must be explicitly band-limited using a suitable filter.

For the band-limiting we employ a *raised cosine filter* [69], which is briefly introduced now. The frequency-domain response of this filter can be expressed as

$$H_{RC} = \begin{cases} 1 & \text{for } |f| < 2W_0 - W \\ \cos^2\left(\frac{\pi}{4}\frac{|f|+W-2W_0}{W-W_0}\right) & \text{for } 2W_0 - W < |f| < W \\ 0 & \text{for } |f| > W \end{cases} \tag{2.24}$$

where W is the absolute bandwidth, and W_0 represents the minimum Nyquist or nominal bandwidth, which is the -6 dB point for the raised cosine spectrum. A raised cosine filter is often expressed in terms of its *roll-off* factor which is defined $r = (W - W_0)/W_0$, and it represents the steepness of the spectrum roll-off. The spectrum for a 1024-length filter with $r = 0, 0.5$ and 1 is shown in Figure 2.14, where T is half the symbol period.

As an example, for simulations using an $T/2$ fractionally-spaced equaliser, i.e. where the incoming signal is sampled and equalised at twice the symbol rate, a 1 GHz SV channel can be generated in the usual way, sampled at 2 GHz and then band-limited to 1 GHz using a raised cosine filter with the desired roll-off factor. The magnitude response of such a band-limited channel is shown in Figure 2.15. Although the sharpest roll-off is achieved using $r = 0.1$, the stop-band attenuation

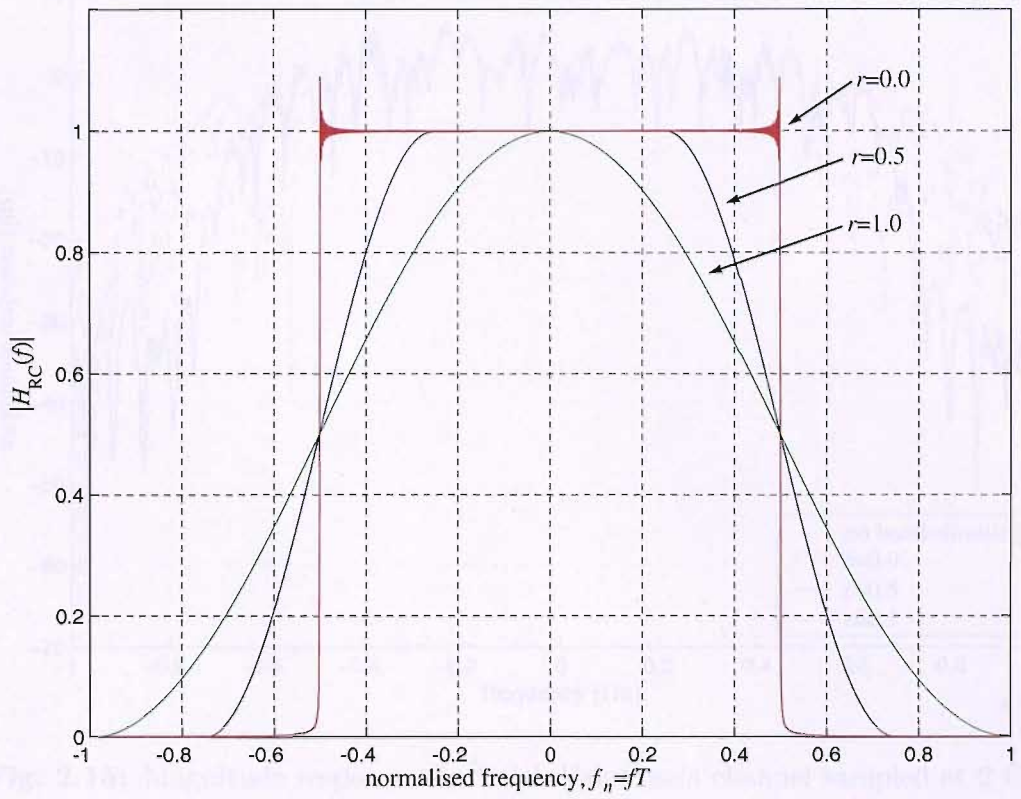

Fig. 2.14: Magnitude response of a 1024-length raised cosine filter for a roll-off factor $r = 0, 0.5, 1.0$.

is worse than the response for $r = 0.5$. The ringing with $r = 0$ is due to a finite filter length.

Finally, note that the method of creating a lower bandwidth channel from the 1 GHz-sampled SV channel in Section 2.4.1.3 is simply a basic form of band-limiting, but using a low-pass Hanning filter instead of a raised cosine response. Although the filtering is not perfect it is simple and serves its intended purpose, as basic low-pass filtering is sufficient to suppress aliasing to create a lower bandwidth channel based on the SV algorithm.

2.4.2 Temporal Dynamics

The previous section discussed the spectral behaviour of particular channels, but these channels were static. The impulse and spectral responses could either be considered to be long-term averages or a single sample realisation of the channel. Either way a channel may still vary in time due to movement of the MS and/or the

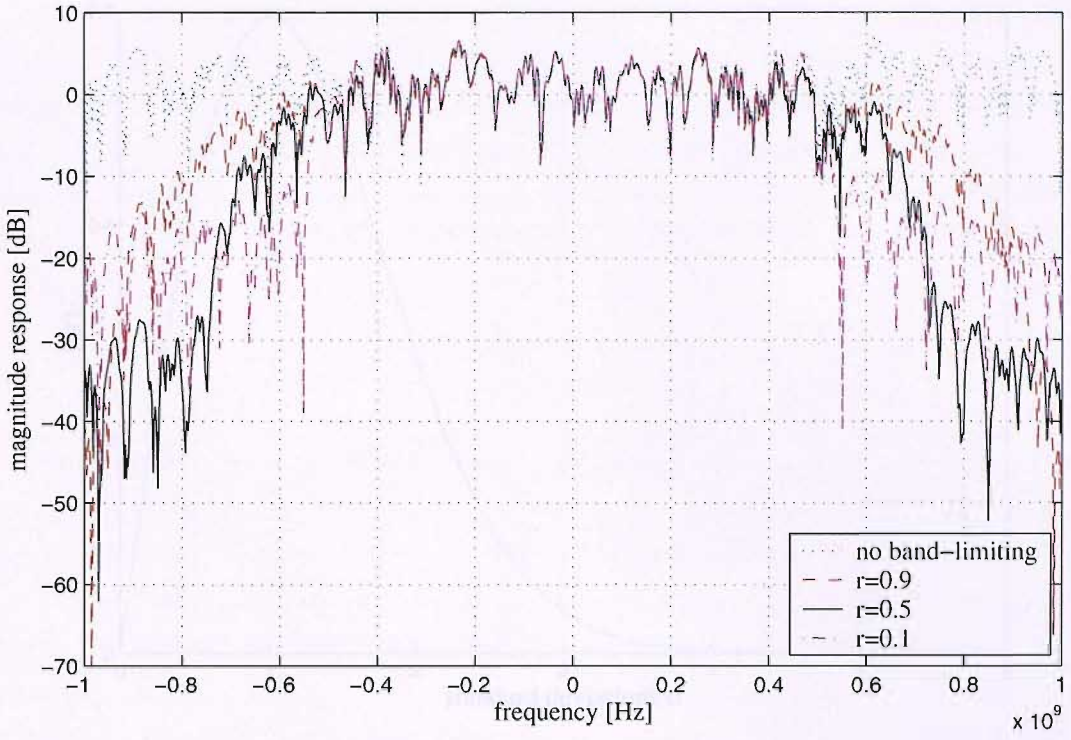

Fig. 2.15: Magnitude response of a Saleh-Valenzuela channel sampled at 2 GHz and band-limited using a raised cosine filter with $r = 0.1$, $r = 0.5$ and $r = 0.9$.

movement of objects within the vicinity of the MS. This section discusses these channel temporal dynamics.

2.4.2.1 Static Channel

When the MS is motionless, there are no moving objects in its vicinity and there are no other factors that may affect the channel, for example natural environmental conditions, we may assume that the channel is static. In this most basic case we consider it to be unchanging in every sense, both statistical and instantaneous. So, if we take the example of the flat channel in the previous section, the channel matrix is

$$\mathbf{H} = \begin{bmatrix} 1.0 & 0.6 \\ 0.2 & 0.9 \end{bmatrix} \tag{2.25}$$

at any instant and is time-invariant. We will use static channels most often in this thesis, as in later chapters when we come to consider adaptive channel identification and inversion, this is the most suitable channel to use when we are interested in the convergence behaviour of the adaptive algorithms for MIMO systems. If this channel were time-varying, this would affect the convergence results making

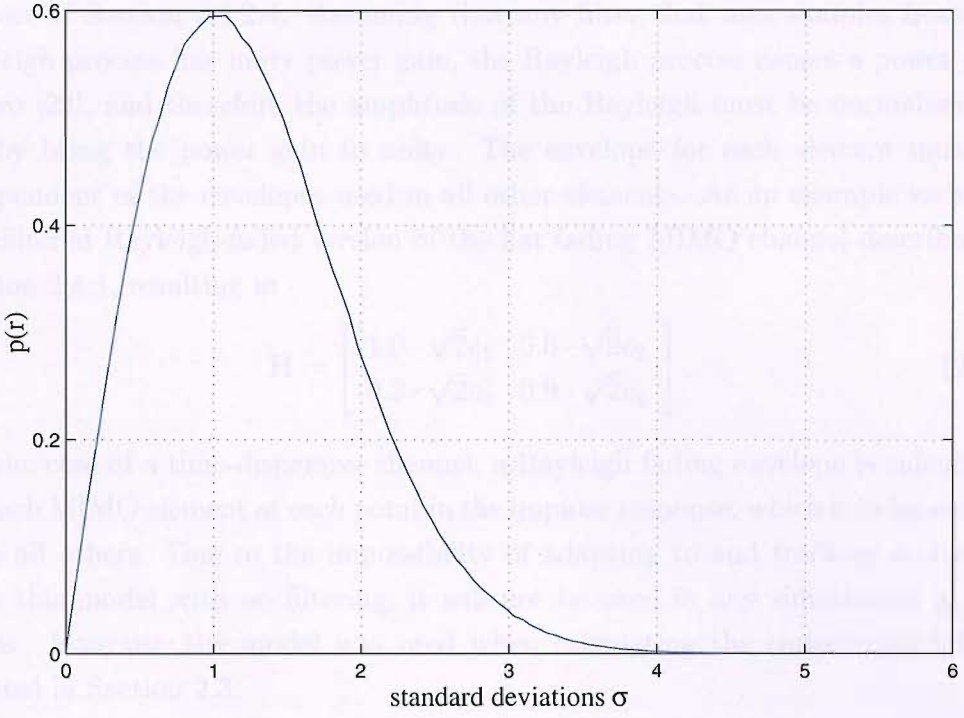

Fig. 2.16: The pdf of a Rayleigh process.

it more difficult to observe relative performance of the algorithms on different systems. However, if the channel were time-varying, the adaptive algorithms could be used to track this behaviour.

2.4.2.2 The Rayleigh Process

We now introduce the Rayleigh process, which we will need to use for both the quasi-static and Doppler-fading channels in the next two sections. The Rayleigh process is suitable for use in non line-of-sight channels and can be used to create a time-varying channel envelope where the phase is random and uniformly distributed in the range $[-\pi, \pi)$, and the gain is the magnitude of two orthogonal Gaussian random processes. The Rayleigh envelope can be expressed mathematically as

$$c = \mathcal{N}(0,1) + \mathrm{j} \cdot \mathcal{N}(0,1) \tag{2.26}$$

where $\mathcal{N}(\mu, \sigma^2)$ refers to a normally-distributed random process with mean μ and variance σ^2. Figure 2.16 shows the probability density function (pdf) of the Rayleigh process.

A Rayleigh-faded MIMO channel can be created by multiplying the relative average signal powers of each element in $\mathbf{H}$ by samples from a Rayleigh process passed through a relevant filter. One such filter is the Doppler filter and is the

subject of Section 2.4.2.4. Assuming that any filter that uses samples from the Rayleigh process has unity power gain, the Rayleigh process causes a power gain of two [23], and therefore the amplitude of the Rayleigh must be normalised by $\sqrt{2}$ by bring the power gain to unity. The envelope for each element must be independent of the envelopes used in all other elements. As an example we show a unfiltered Rayleigh-faded version of the flat fading MIMO channel described in Section 2.4.1, resulting in

$$\mathbf{H} = \begin{bmatrix} 1.0 \cdot \sqrt{2}c_1 & 0.6 \cdot \sqrt{2}c_2 \\ 0.2 \cdot \sqrt{2}c_3 & 0.9 \cdot \sqrt{2}c_4 \end{bmatrix}. \tag{2.27}$$

In the case of a time-dispersive channel, a Rayleigh fading envelope is calculated for each MIMO element at each point in the impulse response, which is independent from all others. Due to the impossibility of adapting to and tracking a channel from this model with no filtering, it will not be used in any simulations in this thesis. However, the model was used when calculating the capacity of MIMO channel in Section 2.3.

Although the majority of work on MIMO capacity has considered Rayleigh-fading channels, very recently there has been some work studying MIMO capacity for Ricean fading channels [73, 74], though in this work we shall continue to only consider Rayleigh-fading channels.

2.4.2.3 Quasi-Static Channel

A third way to model the time-varying behaviour of the channel is to use a quasi-static model, which is a combination of the static and Rayleigh fading channels. To use this model we must define a frame length consisting of a number of symbols. The channel is modelled as static within each frame, but exhibits Rayleigh fading between frames. So at the beginning of each frame, a new Rayleigh coefficient is calculated and this is then held for the duration of the frame.

This model is more useful than either the static or unfiltered Rayleigh-fading channel because, as with the static channel, we may adapt to it, as long as the frames are long enough, but it is more realistic than the static channel as the channel does vary in time. We must however re-adapt to the channel in each new frame.

2.4.2.4 Doppler Fading Channel

The Doppler Rayleigh-faded channel is the most realistic of the time-varying channel models we consider, where samples from a Rayleigh process are passed through

a Doppler filer. The time-varying nature of a real channel is essentially due to the movement of the MS, or equivalently the movement of objects within the vicinity of the MS. The Doppler model characterises the time-varying behaviour of the channel by directly relating it the movement of the MS, parameterised by its speed. An overview of the Doppler fading channel can be found in Appendix A, but a more thorough discourse can be found in [23].

2.4.3 Spatial Dynamics

The spatial dynamics of a MIMO channel refers to the correlation between the sub-channels from the multiple transmit antennas or to the multiple receive antennas. The spatial dynamics are closely related the temporal dynamics described in the previous section. It can be argued that this is because the time-varying nature of a moving channel is not a result of the movement itself, but of the change in location in space. For example, a stationary MS will have a static channel because it remains stationary at the same point in space. Different points in space have differing channels and the correlation of two channels at two different points in space is dependent on the distance between them. Lee [75] found that for the correlation between two identical signals arriving at two antennas to drop to below 0.7 a separation of 70 to 80 wavelength is required if the antennas are in line, and 15 to 20 wavelengths if they are broadside. For a carrier frequency of 1800 MHz this corresponds a spacing of 11.6 m to 13.3 m, and 2.5 m to 3.3 m respectively and these spacing would only be feasible at the BS. However, these distances tend to decrease in a rich-scattering environment which is the reason that it is often stated that MIMO systems require such an environment to work properly. In fact, if the antenna separations are large enough, 10 m for example, a rich-scattering environment is not required at all. Also, it has been experimentally shown that the antenna separation at the MS can be as low at half a wavelength, about 8 cm at 1800 MHz, and still the channel correlation is low enough to achieve most of the capacity promised by theory based on uncorrelated and independent sub-channels [45, 48]. It has been shown in Section 2.3.2 that the correlation of the sub-channel can have a large effect on the capacity of MIMO channels, hence the correlation caused by spatial proximity of antennas is clearly an important consideration.

2.5 Wideband MIMO Communication Problem

One of the aims in the use of MIMO systems is to increase achievable data rates to amounts previously unheard of. In this case, any real system employing MIMO channels is likely to also be transmitting symbols at a rate considerably greater than the RMS delay spread of the channel and consequently will be subject to both temporal and spatial dispersion as characterised by the channel models considered in the previous sections. At very high data rates the channel can be several tens or hundreds of coefficients long, when the channel is modelled using a uniformly spaced tapped delay line. In our review of the background work already performed in the field of MIMO systems, we saw that several methods have been researched to perform the detection of signals passed through the channels, such as ZF and MMSE equalisation, MLSE and OSIC methods such as D-BLAST and V-BLAST, as well as modified version of these. For very time-dispersive channels however, we must currently preclude the use the MLSE using methods such as Trellis or Viterbi equalisation due to the potentially tremendous computational cost of implementing such algorithms. Similarly, the BLAST algorithms and their derivates require multiple matrix inversions to decode each signal stream even for flat channels and these inversions must be performed repetitively for dynamic channels which will increase associated computational cost. For time-dispersive channels the problem is likely to worsen further. Since evidently the computational cost of implementing equalisation algorithms is likely to be limiting factor in their effectiveness, this thesis will examine cost reduction techniques and taking measures to reduce the cost at every available opportunity, while maintaining satisfactory MSE and BER performance. To this end, linear equalisation methods will be used to detect the transmitted data streams and low cost least mean squares (LMS) type adaptive algorithms. These will be covered next in Chapter 3. Later we use frequency-domain inversion and subband techniques in an attempt to lower the costs even further.

2.6 Summary

This chapter forms the basis for the rest of this thesis. It started by giving a brief history of the research conducted to date in MIMO systems, and an idea of what avenues remain unexplored. It formally described the MIMO channel, before explaining how it may be characterised by its behaviour in terms of spectral, temporal and spatial dynamics. It then covered the theoretical capacity of MIMO systems for both correlated and uncorrelated sub-channels, which demon-

Channel	Sampling Rate
Flat	Native
Two-tap	Native
SPIB	60 MHz at doubled symbol rate (T/2)
Minimum-phase SPIB	60 MHz at doubled symbol rate (T/2)
SV100M	100 MHz at symbol rate
SV1G	1 GHz at symbol rate

Tab. 2.1: Summary of Channels used in this thesis.

strated the great potential increase in capacity possible if the channels are properly exploited.

Table 2.1 shows a summary of all the channels that will be used for simulations in this thesis. The native sampling rate simply means that there is no natural sampling rate defined and any may be used.

We have made reference to the fact that if an equaliser is to be used in the receiver to detect the data streams, we need to obtain the frequency-selective MIMO channel inverse. This is no small feat and our background section has shown that there has not been a great deal of research done involved in this area for the application of multi-channel radio communications, especially for low complexity methods. The inverse can either be found by calculating it from the channel, or by using an adaptive system to find it directly. If we use the former method and bearing in mind that with wideband transmission systems we must assume that the channel will introduce ISI, we still need to find the channel. The best way to do this is again using an adaptive system. Hence, adaptive MIMO system identification and inversion is an important topic and one which we will cover in the next chapter. We will consider a particular class of adaptive systems – trained linear systems.

Chapter 3

Multi-Channel System Identification

Assuming a receiver is synchronised to the received signal stream, to perform coherent detection of signals sent through MIMO channels we will require a device known as an equaliser, whose task it is to remove the Cross-Channel Interference (CCI) and Inter-Symbol Interference (ISI) that can be introduced by a broadband MIMO channel. CCI is a spatial effect caused by the additive interference of a receiver picking up the transmissions from all transmitters, and ISI is a temporal effect caused by data being merged to some extent over time by the distortiveness of the channel. An essential part of creating an equaliser involves obtaining some information about the channel. We may create an equaliser directly using adaptive inversion or we may invert the channel analytically but even then we must identify the channel, and this can again be done using adaptive techniques. Work by Kyritsi *et al.* [76] and Rupp [77] show the effect that channel estimation errors can have on MIMO capacity and BER performance. Their results showed that, depending on the severity of the errors, the effect could be anywhere between negligible, causing little detriment to the theoretical capacity, and catastrophic, reducing the capacity to the SIMO case where the receiver benefits from receive diversity only. Evidently, accurate channel estimation, or alternatively channel inversion, is paramount. This section will cover adaptive filtering techniques that can be used in order to identify the MIMO channel for subsequent analytic inversion or to directly invert it.

The adaptive MIMO equaliser can be considered as a particular kind of linear filtering problem. After stating this filtering problem in Section 3.1 we will present optimum and adaptive filtering approaches in Section 3.2. In Section 3.3 we will develop and analyse the multi-channel Least Mean Squares adaptive filtering al-

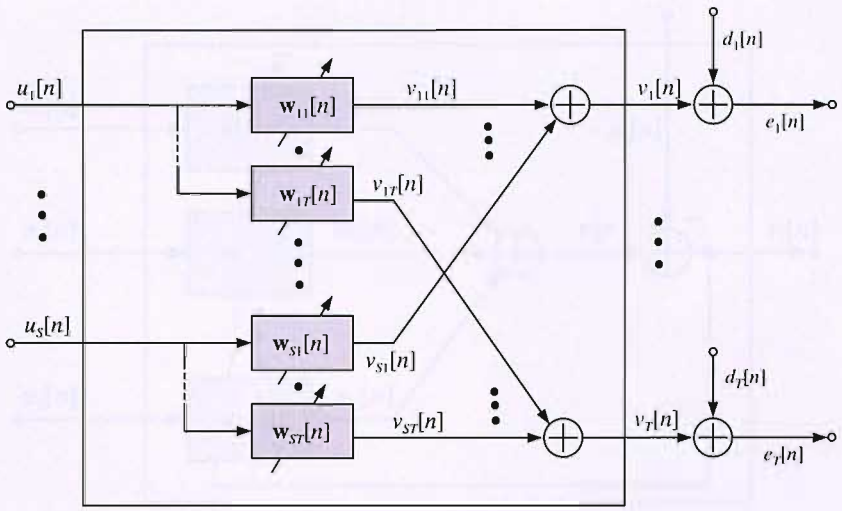

Fig. 3.1: A generic adaptive MIMO system.

gorithm, before considering its normalised version in Section 3.4. Next we briefly mention some other possible filtering algorithms in Section 3.5 that have been considering for the investigations in this thesis with reason for discounting them. Finally, we present some simulation results and discussions in Section 3.6, before summarising the chapter in Section 3.7. For a full discussion of this field the reader is referred to standard texts [78, 79].

3.1 MIMO Linear Filtering Problem

Figure 3.1 shows a generic adaptive MIMO system, where $\mathbf{w}_{st}[n]$ are the adaptive filters between input s and output t, $u_s[n]$ are the inputs and $v_t[n]$ are the outputs with $s = 1 \cdots S$ and $t = 1 \cdots T$, where S and T are the number of inputs and output, respectively. Previously, the number of MIMO inputs and outputs have been defined as M and P. If an adaptive filter is used for system identification, the adaptive filter will have M inputs and P outputs, while for equalisation, there are P inputs (the received signals) and M outputs. Therefore, we here use generic variables S and T to refer to the input and output dimensions. The outputs are compared to desired signals $d_t[n]$ thus forming error signals $e_t[n]$. We may break the problem down into T parallel independent systems shown in Figure 3.2. We

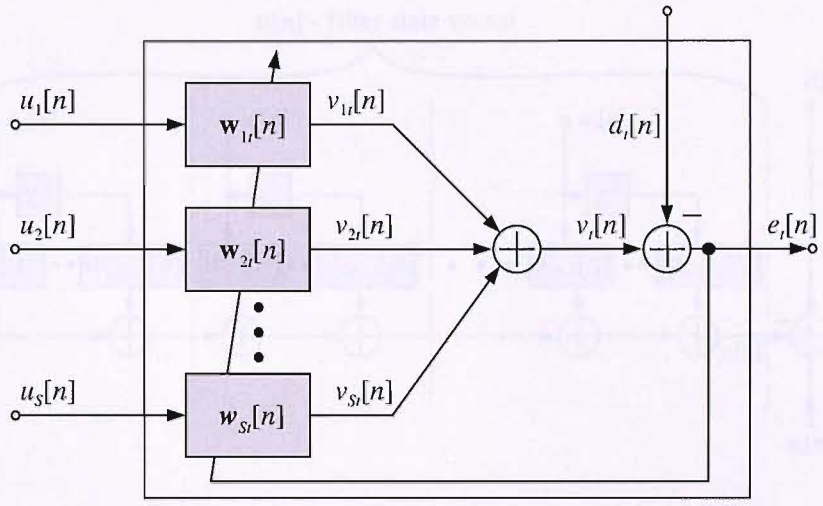

Fig. 3.2: A generic adaptive MISO system.

define vectors $\mathbf{w}_t[n]$ and $\mathbf{u}[n]$ as

$$\mathbf{w}_t[n] = \begin{bmatrix} \mathbf{w}_{1t}[n] \\ \mathbf{w}_{2t}[n] \\ \vdots \\ \mathbf{w}_{St}[n] \end{bmatrix} \quad \text{and} \quad \mathbf{u}[n] = \begin{bmatrix} \mathbf{u}_1[n] \\ \mathbf{u}_2[n] \\ \vdots \\ \mathbf{u}_S[n] \end{bmatrix}, \tag{3.1}$$

where $\mathbf{w}_{st}[n]$ hold the coefficients of a finite impulse response (FIR) filter $\mathbf{w}_{st}[n] = [\ w_{st,0}[n]\ \cdots\ w_{st,L_w-1}[n]\ ]^T$ of length L_w. Similarly $\mathbf{u}_s[n]$ are the filter state vectors comprising the signals currently at each filter tap, $\mathbf{u}_s[n] = [\ u_s[n]\ u_s[n-1]\ \cdots\ u_s[n-L_w+1]\ ]^T$ for $s = 1\ \cdots\ T$. For later notational convenience the tap-weight vectors are denoted using *complex conjugate* coefficients. Therefore the output of the MISO system is given by

$$v_t[n] = \mathbf{w}_t^H[n]\mathbf{u}[n], \tag{3.2}$$

where $\{\cdot\}^H$ denotes the Hermitian transpose and a notation familiar from SISO systems has been achieved, whereby the origin of the quantities $\mathbf{w}_t$ and $\mathbf{u}$ is highlighted in Figure 3.3. The estimation error of the filtering problem is

$$e_t[n] = d_t[n] - v_t[n] = d_t[n] - \mathbf{w}_t^H\mathbf{u}[n]. \tag{3.3}$$

In the following section we will aim at optimising $\mathbf{w}_t$ such that $e_t[n]$ is minimised in an appropriate sense.

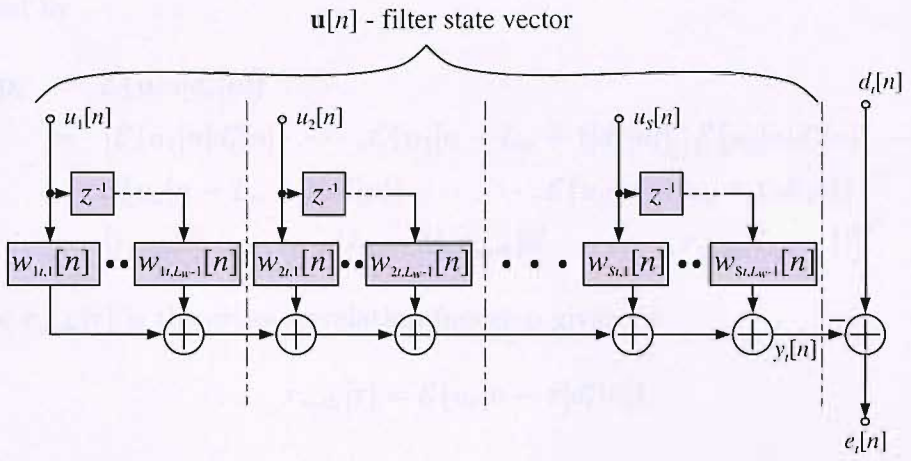

Fig. 3.3: Block diagram representation of a linear filtering problem.

3.2 Adaptive MIMO Filtering

3.2.1 Mean Squared Error

The mean squared error (MSE) is a common error criterion and is generally suitable if the input signals have a Gaussian distribution. The MSE cost function, ξ_{MSE}, is given by the statistical expectation, $\mathcal{E}\{\cdot\}$, of the squared error. We may develop a cost function for the MIMO problem described in the previous section. This results in T cost functions, $\xi_{\text{MSE},t}$, $t = 1, 2, \cdots, T$, one for each of the MISO systems

$$\begin{aligned}
\xi_{\text{MSE},t} &= \mathcal{E}\{e_t[n]e_t^*[n]\} && (3.4)\\
&= \mathcal{E}\left\{(d_t[n] - \mathbf{w}_t^H\mathbf{u}[n])(d_t^*[n] - \mathbf{u}^H[n]\mathbf{w}_t)\right\} && (3.5)\\
&= \mathcal{E}\{d[n]_t d_t^*[n]\} - \mathcal{E}\left\{\mathbf{w}_t^H\mathbf{u}[n]d_t^*[n]\right\} \\
&\quad -\mathcal{E}\left\{d_t[n]\mathbf{u}^H[n]\mathbf{w}_t\right\} + \mathcal{E}\left\{\mathbf{w}_t^H u[n]u^H[n]\mathbf{w}_t\right\} && (3.6)\\
&= \sigma_{d_t}^2 - \mathbf{w}_t^H\mathcal{E}\{\mathbf{u}[n]d_t^*[n]\} - \mathbf{w}_t^T\mathcal{E}\{d_t[n]\mathbf{u}^*[n]\} \\
&\quad +\mathbf{w}_t^H\mathcal{E}\left\{\mathbf{u}[n]\mathbf{u}^H[n]\right\}\mathbf{w}_t && (3.7)\\
&= \sigma_{d_t}^2 - \mathbf{w}_t^H\mathbf{p}_t - \mathbf{w}_t^T\mathbf{p}_t^* + \mathbf{w}_t^H\mathbf{R}\mathbf{w}_t, && (3.8)
\end{aligned}$$

where $\mathbf{p}_t$ is the cross-correlation vector between the filter state vector, $\mathbf{u}[n]$, and the conjugate of the desired response at time n, $d_t^*[n]$, and $\mathbf{R}$ is the auto-correlation matrix of the filter state vector, $\mathbf{u}[n]$. The cross-correlation vector is therefore

defined by

$$\begin{aligned}
\mathbf{p}_t &= \mathcal{E}\{\mathbf{u}[n]d_t^*[n]\} && (3.9)\\
&= \left[\mathcal{E}\{u_1[n]d_t^*[n]\}, \cdots, \mathcal{E}\{u_1[n-L_w+1]d_t^*[n]\}, \mathcal{E}\{u_2[n]d_t^*[n]\}, \cdots,\right.\\
&\quad \left.\mathcal{E}\{u_2[n-L_w+1]d_t^*[n]\}, \cdots, \cdots, \mathcal{E}\{u_S[n-L_w+1]d_t^*[n]\}\right]^T && (3.10)\\
&= \left[r_{u_1d_t}[0], \cdots, r_{u_1d_t}[L_w-1], r_{u_2d_t}[0], \cdots, \cdots, r_{u_Sd_t}[L_w-1]\right]^T && (3.11)
\end{aligned}$$

where $r_{u_sd_t}[\tau]$ is the cross-correlation function given by

$$r_{u_sd_t}[\tau] = \mathcal{E}\{u_s[n-\tau]d_t^*[n]\}. \tag{3.12}$$

It is assumed that the signals $u_s[n]$ and $d_t[n]$ are wide-sense stationary (WSS), and that $\mathbf{w}_t$ is statistically independent of both $\mathbf{u}[n]$ and $d_t[n]$. The elements of the auto-correlation matrix $\mathbf{R}$ are given by

$$\begin{aligned}
\mathbf{R} &= \mathcal{E}\{\mathbf{u}[n]\mathbf{u}^H[n]\} && (3.13)\\
&= \begin{bmatrix} \mathbf{R}_{11} & \mathbf{R}_{12} & \cdots & \mathbf{R}_{1S} \\ \mathbf{R}_{21} & \mathbf{R}_{22} & \cdots & \mathbf{R}_{2S} \\ \vdots & \vdots & \ddots & \vdots \\ \mathbf{R}_{S1} & \mathbf{R}_{S2} & \cdots & \mathbf{R}_{SS} \end{bmatrix}, && (3.14)
\end{aligned}$$

where

$$\begin{aligned}
\mathbf{R}_{s\bar{s}} &= \mathcal{E}\{\mathbf{u}_s[n]\mathbf{u}_{\bar{s}}^H[n]\}\\
&= \mathcal{E}\left\{\begin{bmatrix} u_s[n]u_{\bar{s}}^*[n] & u_s[n]u_{\bar{s}}^*[n-1] & \cdots & u_s[n]u_{\bar{s}}^*[n-L_w+1] \\ u_s[n-1]u_{\bar{s}}^*[n] & u_s[n-1]u_{\bar{s}}^*[n-1] & \cdots & u_s[n-1]u_{\bar{s}}^*[n-L_w+1] \\ \vdots & \vdots & \ddots & \vdots \\ u_s[n-L_w+1]u_{\bar{s}}^*[n] & u_s[n-L_w+1]u_{\bar{s}}^*[n-1] & \cdots & u_s[n-L_w+1]u_{\bar{s}}^*[n-L_w+1] \end{bmatrix}\right\}\\
&= \begin{bmatrix} r_{u_su_{\bar{s}}}[0] & r_{u_su_{\bar{s}}}[1] & \cdots & r_{u_su_{\bar{s}}}[L_w-1] \\ r_{u_su_{\bar{s}}}^*[1] & r_{u_su_{\bar{s}}}[0] & \cdots & r_{u_su_{\bar{s}}}[L_w-2] \\ \vdots & \vdots & \ddots & \vdots \\ r_{u_su_{\bar{s}}}^*[L_w-1] & r_{u_su_{\bar{s}}}^*[L_w-2] & \cdots & r_{u_su_{\bar{s}}}[0] \end{bmatrix}. && (3.15)
\end{aligned}$$

The elements of $\mathbf{R}$ are samples of the auto-correlation function, $r_{u_su_{\bar{s}}}[\tau]$, defined analogously to (3.12). The matrix $\mathbf{R}$ is block Töplitz, i.e. it consists of blocks $\mathbf{R}_{s\bar{s}}$ which have a band structure with identical elements on all diagonals and is Hermitian, i.e $\mathbf{R}^H = \mathbf{R}$, and as a result $\mathbf{R}$ is positive semi-definite with real-valued eigenvalues. Equation (3.8) shows that the cost functions, $\xi_{\mathrm{MSE,t}}$, are quadratic in the filter coefficients, $\mathbf{w}_t$, and due to the positive semi-definiteness of $\mathbf{R}$ have a minimum solution, which is unique when $\mathbf{R}$ is positive definite, i.e. of full rank.

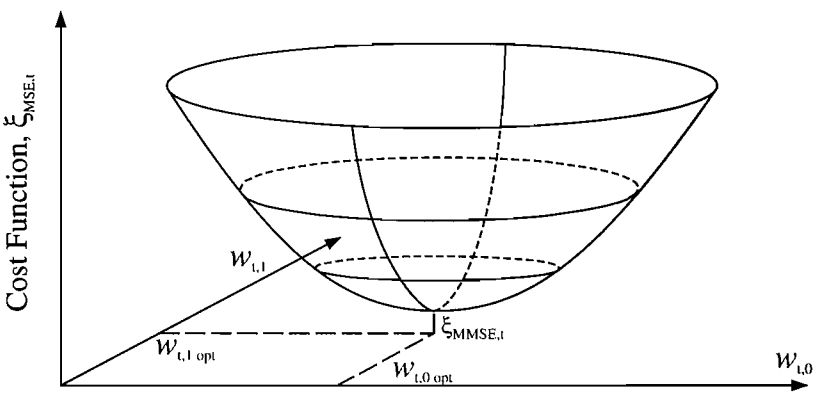

Fig. 3.4: Mean Squared Error (MSE) cost function, $\xi_{MSE,t}$, for a weight vector, $\mathbf{w}_t$, consisting of two elements.

The cost function forms an up-turned hyperparabola over the SL_w-dimensional space formed by all possible coefficient sets $\mathbf{w}_t$. This is shown in Figure 3.4 for the simplistic case where the weight vector, $\mathbf{w}_t$, consists of two elements only, $w_{t,0}$ and $w_{t,1}$.

3.2.2 Wiener-Hopf Solution

Assuming that $\mathbf{R}$ is positive definite, the cost function is minimised by a unique $\mathbf{w}_t$. The value of the vector $\mathbf{w}_t$ at this point forms the minimum MSE (MMSE) solution, $\mathbf{w}_{t,\text{opt}}$, to the MISO filtering problem described in Section 3.1.

A common method of finding the value of $\mathbf{w}_{t,\text{opt}}$ is to calculate the first derivative of the cost function, $\xi_{\text{MSE,t}}$, in (3.8). By setting the derivative to zero and solving for $\mathbf{w}_t$ we can find the optimum filter coefficient vector, $\mathbf{w}_{t,opt}$. Starting from (3.8) and exploiting the fact that [80]

$$\frac{\partial \mathbf{w}_t^T}{\partial \mathbf{w}_t} = \mathbf{I} \quad \text{and} \quad \frac{\partial \mathbf{w}_t^H}{\partial \mathbf{w}_t} = 0, \tag{3.16}$$

and

$$\begin{aligned} \frac{\partial}{\partial \mathbf{w}_t^*} \mathbf{w}_t^H \mathbf{R} \mathbf{w}_t &= \left(\frac{\partial}{\partial \mathbf{w}_t^*} \mathbf{w}_t^H \right) \mathbf{R} \mathbf{w}_t + \left(\frac{\partial}{\partial \mathbf{w}_t^*} \mathbf{w}_t^T \mathbf{R}^T \right) \mathbf{w}_t^* & (3.17) \\ &= \mathbf{R} \mathbf{w}_t & (3.18) \end{aligned}$$

we have

$$\begin{aligned} \nabla \xi_{\text{MSE},t}[n] = \frac{\partial \xi_{\text{MSE},t}}{\partial \mathbf{w}_t^*} &= \frac{\partial}{\partial \mathbf{w}_t^*} \left(\sigma_d^2 - \mathbf{w}_t^H \mathbf{p} - \mathbf{w}_t^T \mathbf{p}^* + \mathbf{w}_t^H \mathbf{R} \mathbf{w}_t \right) & (3.19) \\ &= -\mathbf{p} + \mathbf{R} \mathbf{w}_t, & (3.20) \end{aligned}$$

where ∇ is the gradient operator. By setting $\nabla\xi_{\mathrm{MSE},t}[n] = \mathbf{0}$ in (3.20) and re-arranging we obtain

$$\mathbf{w}_{t,\mathrm{opt}} = \mathbf{R}^{-1}\mathbf{p}_t, \tag{3.21}$$

which is known as the Wiener-Hopf solution. By substituting (3.21) into (3.8) and after some algebraic manipulation it can be shown that the value of the cost function at this point, the MMSE value, is given by

$$\min_{\mathbf{w}_t} \xi_{\mathrm{MSE},t}(\mathbf{w}_t) = \sigma_d^2 - \mathbf{p}_t^H \mathbf{R}^{-1}\mathbf{p}_t. \tag{3.22}$$

In practice, the Wiener-Hopf solution in (3.21) is difficult to obtain. Reliable estimation of $\mathbf{R}$ and $\mathbf{p}$ requires large time windows and becomes problematic in non-stationary situations. Apart from its large complexity of $\mathcal{O}(S^2L_w^2)$, the inversion of $\mathbf{R}$ can be impossible in the rank-deficient case and numerically unstable if $\mathbf{R}$ is ill-conditioned. To overcome problems with the Wiener-Hopf solution, we will review iterative methods for optimising $\mathbf{w}_t$ next.

3.2.3 Gradient Descent Adaptation Techniques

As derived in (3.8), the MSE is quadratic in the filter coefficients and therefore has a unique minimum. For convex functionals, such as the MSE, iterative gradient descent methods can be found which follow the negative gradient of the cost function. Starting from an arbitrary point this will eventually lead to the unique global minimum. This can be mathematically formulated as

$$\mathbf{w}_t[n+1] = \mathbf{w}_t[n] - \mu\nabla\xi_{\mathrm{MSE},t}[n] \tag{3.23}$$

where $\mathbf{w}_t[n]$ represents the weight vector at time n. The update takes a step in the direction of the negative gradient to give a new coefficient vector $\mathbf{w}_t[n+1]$ which is closer to the optimum solution in the l_2 (i.e. Euclidean norm) sense. The gradient of the MSE cost function, $\nabla\xi_{\mathrm{MSE},t}[n]$, has been derived in (3.20), and μ represents the step-size, which controls the innovation in (3.23). Hence the step-size determines the speed with which the iteration converges to the optimum solution. However, as will be shown in Section 3.3.2.2, too large a step-size may cause the update algorithm to become unstable.

Substituting (3.20) into (3.23) yields the so-called steepest descent algorithm [78, 79]. Using this algorithm, the auto-correlation matrix, $\mathbf{R}$, no longer needs to be inverted, but as well as the cross-correlation vector, $\mathbf{p}_t$, still needs to be reliably estimated. This can involve very long data windows and increase the need for memory while calculating $\mathbf{R}$ and $\mathbf{p}_t$. In the following, we will pursue a further simplification, where instead of calculating $\mathbf{R}$ and $\mathbf{p}_t$ exactly, estimates will be used.

1.	$v[n] = \mathbf{w}_t^H[n]\mathbf{u}[n]$
2.	$e_t[n] = d_t[n] - v_t[n]$
3.	$\mathbf{w}_t[n+1] = \mathbf{w}_t[n] + \mu\mathbf{u}[n]e_t^*[n]$

Tab. 3.1: The Multi-channel Least Mean Squares algorithm

3.3 Multi-Channel Least Mean Squares Algorithm

3.3.1 Algorithm Description

In order to further simplify iterative gradient methods this section gives an overview of the Multi-channel Least Mean Squares (M-LMS) algorithm, an exponent of the so-called stochastic gradient algorithms, thus called because the adaptation is subject to a statistical process. Due to the formulation in (3.2), the algorithm is identical to the better known single-channel LMS algorithm. The LMS algorithm is one of the simplest adaptation techniques while still performing satisfactorily. For a complete discussion of the LMS algorithm the reader is referred to e.g. [78,81,82].

The M-LMS algorithm is derived from the steepest descent algorithm. Instead of calculating $\mathbf{R}$ and $\mathbf{p}_t$ exactly using infinitely long data windows, single sample estimates $\hat{\mathbf{R}}$ and $\hat{\mathbf{p}}_t$ are used such that

$$\hat{\mathbf{p}}_t = \mathbf{u}[n]d_t^*[n] \tag{3.24}$$

$$\hat{\mathbf{R}} = \mathbf{u}[n]\mathbf{u}^H[n] \tag{3.25}$$

where the notation $\hat{(\cdot)}$ is used to indicate estimates of the respective variables. This method is equivalent to minimising the instantaneous squared error, rather than the MSE. Inserting the estimates into (3.20) yields

$$\hat{\nabla}\xi_{\mathrm{MSE},t}[n] = -\hat{\mathbf{p}}_\mathbf{t} + \hat{\mathbf{R}}\mathbf{w}_t[n] = -\mathbf{u}[n](d_t^*[n] - \mathbf{u}^H[n]\mathbf{w}_t[n]) = -\mathbf{u}[n]e_t^*[n]. \tag{3.26}$$

Substituting this gradient estimate into (3.23) gives the basis for the LMS algorithm,

$$\mathbf{w}_t[n+1] = \mathbf{w}_t[n] + \mu\mathbf{u}[n]e_t^*[n]. \tag{3.27}$$

To summarise, the complete M-LMS algorithm is shown in Table 3.1 and is executed in every sampling period. Unlike the method of steepest descent the M-LMS algorithm however performs a noisy update due to the error in the one-sample estimates of the parameters, which converges *on average* to the Wiener-Hopf solution.

3.3.2 Properties of the M-LMS algorithm

This section describes various properties of the M-LMS algorithm.

3.3.2.1 Computational Complexity

The computational complexity of the M-LMS algorithm can be expressed in terms of multiply-accumulate computations (MAC). Assuming we have complex-valued signals, the first step in Table 3.1 involves $4SL_w$ MACs, the second is just two MACs, and the final step involves $4SL_w + 4$ MACs, making the total complexity $C_{\text{M-LMS}} = 8SL_w + 6$ MACs. However, unlike the analytic optimisation in Section 3.2.2, this process must be performed many times until the algorithm converges to a suitably small MSE. Therefore, if we denote the number of iterations required to reach satisfactory convergence as N, then the final complexity is $N(8SL_w + 6)$. Even so, the algorithm is still order $\mathcal{O}(L_w)$, which is a great improvement of the $\mathcal{O}(L_w^2)$ of the Wiener-Hopf analytic optimisation. The advantage is even greater for large MIMO systems than SISO systems as the stacked multi-channel filter is S times longer than the equivalent SISO filter.

3.3.2.2 Stability Analysis

Due to the presence of feedback in the adaptation of the M-LMS algorithm there is the inherent possibility of instability. Convergence for the M-LMS can be derived in the mean, i.e. $\mathbf{w}_t[n] \rightarrow \mathbf{w}_{t,\text{opt}}$ for $n \rightarrow \infty$, or in the mean-squared, i.e. $\xi_{\text{MSE},t}[n] \rightarrow \xi_{\text{MMSE}}$ for $n \rightarrow \infty$. In the following we review convergence in the mean by inspecting the natural modes of the system [78] and we start by inserting (3.26) into (3.23) to obtain

$$\mathbf{w}_t[n+1] = \mathbf{w}_t[n] - \mu\left(-\hat{\mathbf{p}}_\mathbf{t} + \hat{\mathbf{R}}\mathbf{w}[n]\right). \tag{3.28}$$

By taking expectations of (3.28) and applying (3.21) we get

$$\begin{aligned}
\mathcal{E}\{\mathbf{w}_t[n+1]\} &= \mathcal{E}\{\mathbf{w}_t[n]\} + \mu\left(\mathcal{E}\{\hat{\mathbf{p}}_\mathbf{t}\} - \mathcal{E}\left\{\hat{\mathbf{R}}\mathbf{w}_t[n]\right\}\right) && (3.29)\\
&= \mathcal{E}\{\mathbf{w}_t[n]\} + \mu\left(\mathbf{p}_t - \mathbf{R}\mathcal{E}\{\mathbf{w}_t[n]\}\right) && (3.30)\\
&= \mathcal{E}\{\mathbf{w}_t[n]\} + \mu\left(\mathbf{R}\mathbf{w}_{t,\text{opt}} - \mathbf{R}\mathcal{E}\{\mathbf{w}_t[n]\}\right) && (3.31)\\
&= \mathcal{E}\{\mathbf{w}_t[n]\} + \mu\mathbf{R}\left(\mathbf{w}_{t,\text{opt}} - \mathcal{E}\{\mathbf{w}_t[n]\}\right). && (3.32)
\end{aligned}$$

Note that by taking expectations we have reverted to the noiseless gradient descent method where we assume that our estimates of $\mathbf{R}$ and $\mathbf{p}_t$ are perfect. We continue by defining a *weight-error vector* $\mathbf{c}_t[n]$ at time n as

$$\mathbf{c}_t[n] = \mathcal{E}\{\mathbf{w}_t[n]\} - \mathbf{w}_{t,\text{opt}} \tag{3.33}$$

where $\mathbf{w}_{t,\text{opt}}$ is the optimum weight vector, which translates the optimum solution for $\mathbf{w}_t[n]$ onto the origin. Subtracting $\mathbf{w}_{t,\text{opt}}$ from both sides of (3.32) and applying (3.33) we can write

$$\mathbf{c}_t[n+1] = (\mathbf{I}_{SL_w} - \mu\mathbf{R})\mathbf{c}_t[n]. \tag{3.34}$$

Using an eigenvalue-decomposition, we may express $\mathbf{R} = \mathbf{Q}\mathbf{\Lambda}\mathbf{Q}^{-1}$ where the matrix $\mathbf{Q}$ contains the eigenvectors of $\mathbf{R}$ and the matrix $\mathbf{\Lambda}$ is a diagonal matrix with elements equal to the eigenvalues of $\mathbf{R}$. Since $\mathbf{R}$ is Hermitian, $\mathbf{Q}$ is *unitary* with $\mathbf{Q}^{-1} = \mathbf{Q}^H$, i.e.

$$\mathbf{R} = \mathbf{Q}\mathbf{\Lambda}\mathbf{Q}^H, \tag{3.35}$$

and the eigenvalues, denoted by $\lambda_1, \lambda_2, \cdots, \lambda_{SL_w}$ are all positive semi-definite and real. Substituting (3.35) into (3.34) we get

$$\mathbf{c}_t[n+1] = (\mathbf{I}_{SL_w} - \mu\mathbf{Q}\mathbf{\Lambda}\mathbf{Q}^H)\mathbf{c}_t[n]. \tag{3.36}$$

Premultiplying both sides of (3.36) by $\mathbf{Q}^H$ and exploiting $\mathbf{Q}^{-1} = \mathbf{Q}^H$, we get

$$\mathbf{Q}^H\mathbf{c}_t[n+1] = (\mathbf{I}_{SL_w} - \mu\mathbf{\Lambda})\mathbf{Q}^H\mathbf{c}_t[n]. \tag{3.37}$$

Now we define a new set of rotated co-ordinates using

$$\begin{aligned} \boldsymbol{\upsilon}_t[n] &= \mathbf{Q}^H\mathbf{c}_t[n] && (3.38)\\ &= \mathbf{Q}^H[\mathbf{w}_t[n] - \mathbf{w}_{t,\text{opt}}], && (3.39) \end{aligned}$$

and re-write (3.36) in the transformed form as

$$\boldsymbol{\upsilon}_t[n+1] = (\mathbf{I}_{SL_w} - \mu\mathbf{\Lambda})\boldsymbol{\upsilon}_t[n]. \tag{3.40}$$

Thus, the filter coefficients have been decoupled into L_w *eigen* or *natural modes.* Assuming that the initial value of $\boldsymbol{\upsilon}_t[n]$, $\boldsymbol{\upsilon}_t[0]$, equals

$$\boldsymbol{\upsilon}_t[0] = \mathbf{Q}^H[\mathbf{w}_t[0] - \mathbf{w}_{t,\text{opt}}], \tag{3.41}$$

and that $\mathbf{w}_t[0] = \mathbf{0}$, (3.41) reduces to

$$\boldsymbol{\upsilon}_t[0] = -\mathbf{Q}^H\mathbf{w}_{t,\text{opt}}. \tag{3.42}$$

For the k^{th} natural mode of the LMS algorithm we have from (3.40)

$$\upsilon_{t,k}[n+1] = (1 - \mu\lambda_k)\upsilon_{t,k}[n] \qquad k = 0, 1, \cdots, S(L_w - 1), \tag{3.43}$$

where λ_k is the k^{th} eigenvalue of $\mathbf{R}$. Further (3.43) is a *first order homogeneous difference equation*, and can be written in terms of the initial value $v_{t,k}[0]$ as

$$v_{t,k}[n] = (1 - \mu\lambda_k)^n v_{t,k}[0] \qquad k = 0, 1, \cdots, S(L_w - 1), \tag{3.44}$$

where $v_{t,k}[0]$ is given by (3.42). Equation (3.44) shows the decoupled evolution of the M-LMS algorithm and creates a *geometric series* with a geometric ratio equal to $1 - \mu\lambda_k$. If the magnitude of this ratio is less than unity for all k, then the algorithm will be stable and converge to the optimum weights. Thus, the stability condition for the M-LMS algorithm requires that

$$-1 < 1 - \mu\lambda_k < 1 \qquad \forall k. \tag{3.45}$$

As n approaches infinity all natural modes of the algorithm will decay, irrespective of initial conditions. Considering the worst case of the largest geometric ratio, the convergence condition can be denoted as

$$0 < \mu < \frac{2}{\lambda_{max}}, \tag{3.46}$$

where λ_{max} is the largest eigenvalue of the auto-correlation matrix, $\mathbf{R}$. This forms the necessary and sufficient condition for stability of the deterministic method of steepest descent [78]. The upper convergence limit on μ can be safely approximated by

$$\lambda_{max} \leq \sum_{i=0}^{SL_w-1} \lambda_i = \mathrm{tr}\{\mathbf{R}\} = L_w \sum_{s=1}^{S} \sigma_{uu,s}^2, \tag{3.47}$$

where the positive semi-definiteness of $\mathbf{R}$ ensures the approximations by the trace of $\mathbf{R}$, $\mathrm{tr}\{\mathbf{R}\}$. According to (3.15), $\mathrm{tr}\{\mathbf{R}\}$ can be expressed by the power or variance $\sigma_{uu}^2 = r_{u_s u_s}[0]$ of the input signal $u[n]$ and the stacked filter length, SL_w, yielding

$$0 < \mu < \frac{2}{L_w \sum_{s=1}^{S} \sigma_{uu,s}^2} \tag{3.48}$$

as practically calculable convergence limits for μ [12].

3.3.2.3 Convergence Speed

An important property of adaptive algorithms is that of convergence speed. In the mean, the M-LMS algorithm exhibits an exponential convergence, which can be seen from the decoupled evolution of the algorithm in (3.44). It can be shown that the time constant of the exponential decay of the k^{th} eigen-mode, τ_k, can be given by

$$\tau_k = \frac{1}{\ln(1 - \mu\lambda_k)}. \tag{3.49}$$

A common simplification of this is

$$\tau_k \approx \frac{1}{\mu\lambda_k} \qquad \forall|\mu\lambda_k| \ll 1. \tag{3.50}$$

A more detailed analysis of the convergence speed is shown in [12] but two results are pointed out here:

- the overall convergence is governed by the slowest converging natural mode corresponding to the smallest eigenvalue, λ_{min}, of $\mathbf{R}$;
- the maximum speed of convergence has to be set according to (3.46) to accommodate for the largest eigenvalue, λ_{max}, of $\mathbf{R}$.

The *eigenvalue spread* or *condition number* of a matrix is defined as the ratio between the largest and smallest eigenvalue. Hence, if the condition number of $\mathbf{R}$ is large it follows that the convergence of the adaptive algorithm will be slow. The condition number can be shown to be less than or equal to the ratio between the minimum and maximum value of the power spectral density (PSD) of the input signals [12, 78]. If the S inputs to the algorithm are mutually independent and white Gaussian, then the condition number of $\mathbf{R}$ will be one and this scenario would achieve the fastest possible convergence. We will see in Chapter 4 that if we are performing system identification on an unknown MIMO channel then the eigenvalue spread may be close to one. However, if the task involves adaptive inversion of a frequency-selective channel, then the latter will impose correlation onto $\mathbf{u}[n]$, and slow the convergence for the M-LMS results.

3.3.2.4 Bias

The stability analysis in Section 3.3.2.2 showed that the adaptive filter vectors, $\mathbf{w}_t[n]$ approach the optimal values as $n \to \infty$ if the step-size coefficient remains within its convergence bounds. Hence if the underlying system to which the algorithm is converging remains stationary, the adaptation is free of bias in the *mean*. However if the underlying system is dynamic so that is spectral characteristics change over time the adaptation will lag behind the optimum filter vector which will produce a bias [12, 78, 83]. The bias depends on the step-size μ, there is an optimum step-size which will minimise the bias [83]. Too small a step-size means that the adaptive system is unable to follow the dynamic system at the rate it is fading, whereas if the step-size is too large the observation noise will be amplified by a greater amount than is necessary, degrading the performance. In a noiseless environment however there is no noise and we may use as great a step-size as is required to give good tracking.

1.	$v[n] = \mathbf{w}_t^H[n]\mathbf{u}[n]$
2.	$e_t[n] = d_t[n] - v_t[n]$
3.	$\mathbf{w}_t[n+1] = \mathbf{w}_t[n] + \tilde{\mu}\frac{\mathbf{u}[n]e_t^*[n]}{\mathbf{u}^H[n]\mathbf{u}[n]}$

Tab. 3.2: The Normalised Multi-Channel Least Mean Squares algorithm.

3.4 Multi-channel Normalised LMS Algorithm

This section gives a description of the Multi-channel Normalised LMS (M-NLMS) algorithm, and discusses its convergence characteristics with respect to the standard M-LMS algorithm and also the single-channel LMS algorithm.

3.4.1 Algorithm Description

In the standard M-LMS algorithm the step-size factor, μ, is fixed and has to be adjusted to cover the worst case with respect to λ_{max}. This has the drawback that if in a non-stationary environment the variance of the input signal is low, the convergence speed of the algorithm may be insufficient. The input signal power or variances, $\sigma_{uu,s}^2$, and λ_{max} are related as shown in (3.47). For this reason, a step-size normalisation with respect to the input signal power appears to be beneficial. In this case the step-size factor in effect varies so that it is small at times of high signal power, and vice versa.

If the variance of each input signal $u_s[n]$ is estimated over a rectangular window of length L_w and then these variances are summed to give the total power of the signals in the adaptive MISO filter, that is

$$\sigma_{uu}^2 \approx \frac{1}{SL_w}\sum_{s=1}^{S}\sum_{\tau=0}^{L_w-1}|u_s[n-\tau]|^2 = \frac{1}{SL_w}\mathbf{u}^H[n]\mathbf{u}[n], \tag{3.51}$$

and the step-size parameter, μ, can be substituted by

$$\mu = \frac{\tilde{\mu}}{\mathbf{u}^H[n]\mathbf{u}[n]}. \tag{3.52}$$

This results in the new update equation used in the M-NLMS algorithm, which can be summarised in Table 3.2. The substitution of μ by the normalised step-size, $\tilde{\mu}$, changes the stability condition to

$$0 < \tilde{\mu} < 2. \tag{3.53}$$

The cost of this algorithm is slightly higher than that of the M-LMS algorithm on account of the extra input signal power calculation. Exploiting computational

tricks the cost for the M-NLMS yields

$$C_{\text{M-NLMS}} = 8SL_w + 8S + 10 \tag{3.54}$$

MACs per sampling period.

3.4.2 Convergence Characteristics

The selection of $\tilde{\mu}$ sets a relative convergence speed independent of the variances of the input signals $u_s[n]$. This means that, whereas with the M-LMS the algorithm convergence is dependent on the total power of all the input signals, now it is normalised so that the convergence remains uniform during adaptation irrespective of fluctuations in the input signal power. This has the advantage that if one of the multiple inputs is prone to periods of high power relative to the others, we do not have to choose a small step-size at the expense of the convergence rate for the filters corresponding to the other inputs.

A comparison between the convergence of the M-NLMS for S inputs and the single-channel N-LMS algorithm is interesting. For the MISO case the filter state vectors are S times longer than the single-channel system, with only an L_w length filter. According to (3.50) the convergence speed is approximately inversely proportional to the step-size, μ. For the M-NLMS algorithm the step-size varies inversely with the total input signal power, so the approximate time-constant for the M-NLMS algorithm is

$$\tau_{k,\text{NMLMS}} = \frac{\mathbf{u}^H[n]\mathbf{u}[n]}{\mu\lambda_k} = \frac{S\mathbf{u}_s^H[n]\mathbf{u}_s[n]}{\mu\lambda_k} \quad \text{for any s} \in 1:\text{S}, \tag{3.55}$$

assuming that the power of all input signals are equal. Hence the convergence for the M-NLMS is S times slower than for the single-channel N-LMS algorithm.

3.5 Other Adaptive Algorithms

This section will give a very brief overview of some other adaptive filtering algorithms that may be of interest. We consider their use for the simulations in this thesis and give discussion why we discount them.

3.5.1 Recursive Least Squares

Whereas the LMS algorithm minimises the expectation of the squared error by use of gradient descent, an alternative is to optimise the the adaptive filter with respect

to the sum of squared errors, which arises in the so-called Least Squares (LS) methods. Like the LMS algorithm, this method will tend towards the Wiener-Hopf solution in a static environment. An exponent of the LS methods is the Recursive Least Squares (RLS) algorithm, where a recursive estimate of the quantities used in the algorithm is used. The cost function used for the LS methods is given by

$$\xi_{\mathrm{LS},n} = \sum_{\nu=0}^{n} \beta^{\nu} e[n-\nu]e^{*}[n-\nu], \tag{3.56}$$

where β is termed the *forgetting factor* and $0 < \beta \leq 1$. From this we see that the cost function depends upon the entire error signal up to the current time. The forgetting factor is used to de-emphasise the squared error of previous samples and plays a vital role if the target system is dynamic in time.

Analysis of the RLS algorithm shows that, like the LMS algorithm, the bias tends towards zero in the mean but unlike the LMS algorithm it also tends to zero in the mean squared, meaning that the final MSE tends to the MMSE both in statistical terms and in real terms. This is true if we assume a WSS signal and an infinite memory, i.e. $\beta = 1$. Generally, the RLS algorithm results in greatly superior performance it terms of both convergence speed and bias. However the RLS algorithm has two major drawbacks which make is less desirable than the N-LMS algorithm for the work contained in the thesis.

When the target system in non-stationary, a forgetting factor $\beta < 1$ must be chosen, and how small it must be depends on how dynamic the system is. The system must forget older statistics which change as the system changes so that it can continue to converge to the MMSE solution. Unfortunately, this can have a serious impact on the tracking behaviour of the algorithms, so much so that LMS-type algorithm can in certain situations achieve better performance [12, 84–87]. One of the intended applications of any equaliser architecture we develop in this thesis is for use within a MS which may be subject to movement. As such, we must assume that in general the MIMO channel will be dynamic and we require that the equaliser will be able to track changes in the channel over time.

The second and major drawback of the use of the RLS algorithm for use with MIMO channels is related to its computational complexity. The computational cost of the RLS algorithm is given by

$$C_{\mathrm{RLS}} = 3L_w + 3L_w^2, \tag{3.57}$$

MACs per iteration per SISO filter (i.e. not the stacked MISO filter), which is $\mathcal{O}(L_w^2)$ compared to $\mathcal{O}(L_w)$ of the LMS algorithm. Although it is true that the RLS algorithm would required fewer iterations until convergence this would only

be an advantage for a stationary system where continuous tracking is not required, and even in this case it is possible that the greater complexity order of the RLS algorithm would negate any advantage arising from the fewer required iterations for systems with a large L_w. This is especially likely for MIMO systems, where we would use the same stacked input vectors described in Section 3.1 as we used for the M-LMS algorithm to create the Multi-Channel RLS (M-RLS) algorithm. In this case, the complexity is increased by a factor of S^2 making the M-RLS even less attractive than the M-LMS algorithm.

For these two reasons and due to advantages of normalising the LMS algorithm described in Section 3.4 the M-NLMS algorithm is preferred over the RLS algorithm.

3.5.2 Frequency-Domain Adaptation

We have described the LMS class of adaptive filtering which is performed in the time-domain. An interesting alternative is to transform the problem into the frequency-domain via use of the FFT [78]. In this case, we call the technique *frequency-domain adaptive filtering* (FDAF) and the origins of this may be traced back to 1973 [88]. The attraction of FDAF lies in its potential to reduce the complexity of adaptive algorithms such as the LMS for long filters [89]. The technique combines two methods that were previously widely used in the field of signal processing, namely block processing and the FFT. Block processing involves, as its name suggests, the partitioning of the input data into blocks and performing the adaptive update once on each block to reduce the complexity of the algorithm [90, 91]. This will generally slow the convergence of the algorithm and this is the trade-off that must be paid, so that the lower complexity can be realised and it also opens up the possibility of the use of parallel processing, which could again increase the computational speed. The second technique is the use of the FFT, the use of which is made possible by the block processing. The FFT enables us to use computationally efficient techniques to process filters with a long impulse response. This approach leads us to the frequency-domain block LMS (FD-BLMS) algorithm that includes the standard LMS algorithm as a special case [92]. The FD-BLMS involves padding or forcing parts of the signals inside the algorithm to zero, which introduces a constraint to the error gradient and is required to ensure correct convergence to the MMSE solution.

The use of the FD-BLMS however brings with it some problems not present with the standard time-domain implementation. Foremost of these involves the *circular convolution* or *wrap-around* effect inherent in the use of the FFT, and

special precautions must be taken to combat this, such as the overlap-add or overlap-save methods [92]. Also, frequency-domain techniques are not suitable for every situation, for example for short filters of length below 64 taps the FD-BLMS will actually result in a more computationally costly solution [89], in addition to the worsened convergence.

The FD-BLMS can be implemented in two forms, *constrained* and *unconstrained*. The standard FD-BLMS as described above is the constrained version, with the constraint being on the error gradient, and as a result the FD-BLMS algorithm involves five FFTs per iteration. Two of these are involved in the constraint and it is possible to remove these to create the even less computationally costly unconstrained FD-BLMS algorithm that only uses three FFTs per algorithm iteration [93]. Of course by doing this performance is affected and the algorithm no longer converges to the MMSE solution as the number of block iterations approaches infinity [92]. A second point is that misadjustment of the algorithm is greater than that of the constrained FD-BLMS; in fact the unconstrained version can require twice as many iterations as the constrained algorithm to produce the same misadjustment [94].

More recently, there has been a renewed interested in frequency-domain processing techniques, mainly spurred on by the search for computational cost reduction of ever increasing more complex systems being developed and MIMO is an example of this. Complexity savings have been shown by using spatial-frequency adaptive equalization for diversity systems [95]. Recently, single-carrier frequency-domain equalisation for broadband wireless systems have been shown to compare favourably to the currently more popular OFDM [96]. Finally, a new method has been shown that applies an unconstrained FD-BLMS, where the constraint is different from the gradient constraint discussed previously, to multi-channel acoustic echo cancellation with favourable results in terms of misadjustment but also computational cost [97].

A fuller overview of FDAF can be found in Haykin [78] and Shynk [92] and the cited references in this section for specific details. Very recently there has been renewed great interest in frequency-domain adaptive equalisation for MIMO channels [67, 98, 99]. In this thesis, however, we will not deal much with FDAF, preferring instead subband processing techniques, discussed in Chapter 5, which have not yet attracted as much attention as frequency-domain techniques and seem to have given promising results in the past [12].

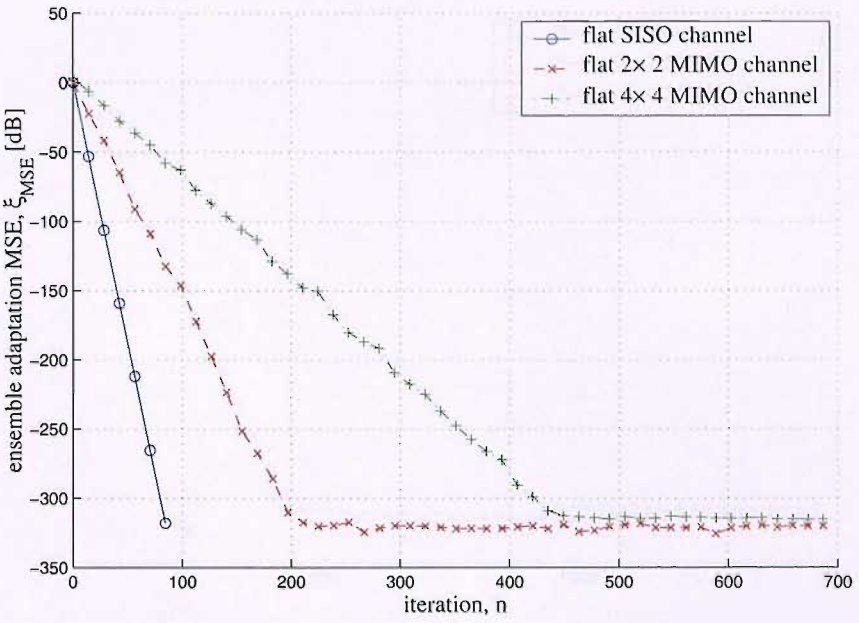

Fig. 3.5: System identification to flat SISO and MIMO channels using M-NLMS algorithm with $\tilde{\mu} = 0.18$.

3.6 Simulations and Discussion

This section presents various simulation results obtained by applying the adaptive tools to the channels described in Chapter 2.

3.6.1 System Identification

We start by applying the M-NLMS to SISO, 2×2 MIMO and 4×4 MIMO channels and the sub-channels comprising these all have flat frequency spectrums. The channels are static in both the mean and mean-squared as here we are just interested in observing the performance of the adaptive algorithm in identifying the unknown channels, starting from all-zero adaptive filter coefficients. Figure 3.5 shows the MSE over the duration of the adaptation, which is performed over many ensemble sets to obtain average results. In these simulations we have used $L_w = 1$, as this is the length of the sub-channels forming the systems, and $\tilde{\mu} = 0.18$. We see that as predicted by our discussion in Section 3.4.2 the convergence of the 4×4 MIMO system takes a little over twice as long as that to the 2×2 MIMO system, and the same is true for the 2×2 MIMO system over the SISO system. The final MSE values are around -320 dB and this is due to the machine accuracy of the simulation tool.

Figure 3.6 shows the convergence characteristic for the two-tap channels with

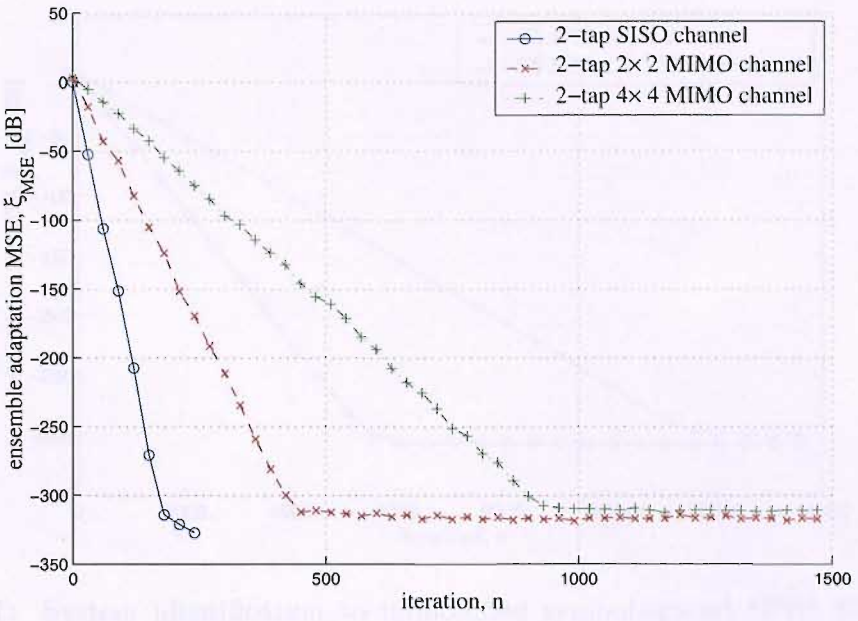

Fig. 3.6: System identification to two-tap SISO and MIMO channels using M-NLMS algorithm with $\tilde{\mu} = 0.18$.

$L_w = 2$. All the other parameters of the simulation remain the same as for the flat channel simulations. We see a similar pattern of behaviour as before with the convergence speed between the systems being related by a factor of 2 as the dimensions of the system double. The doubling in length of component sub-channels causes a doubling in the computational complexity, due to the $\mathcal{O}(L_w)$ M-NLMS algorithm, and a similar increase in real time to execute the simulations. Comparing these simulations with those of the flat channel we see an approximate doubling of convergence time between each of the corresponding simulations, due to the doubled filter length.

Next, the simulation results for adaptation to the symbol spaced (SS) SPIB channels are shown in Figure 3.7. Again we use the SISO and 2×2 MIMO channels, but not the 4×4 channel as there is insufficient data in the SPIB database [70] to form such a channel. We use the channels in an unmodified form as explained in Chapter 2, with the exception that we firstly downsample them to symbol-spacing and truncate them to length 50, which captures the significant part of the response. Unlike the flat and two-tap channels the SS SPIB channels have an associated sampling rate so we can relate the adaptation to real time. The channels are sampled at 30 MHz, therefore each iteration represents an 33 ns interval. The algorithm may be performed in real time at this rate, or if possible or required due to hardware limitations, for example, the data may be buffered or the algorithm iterated at a lower rate. The convergence time between these

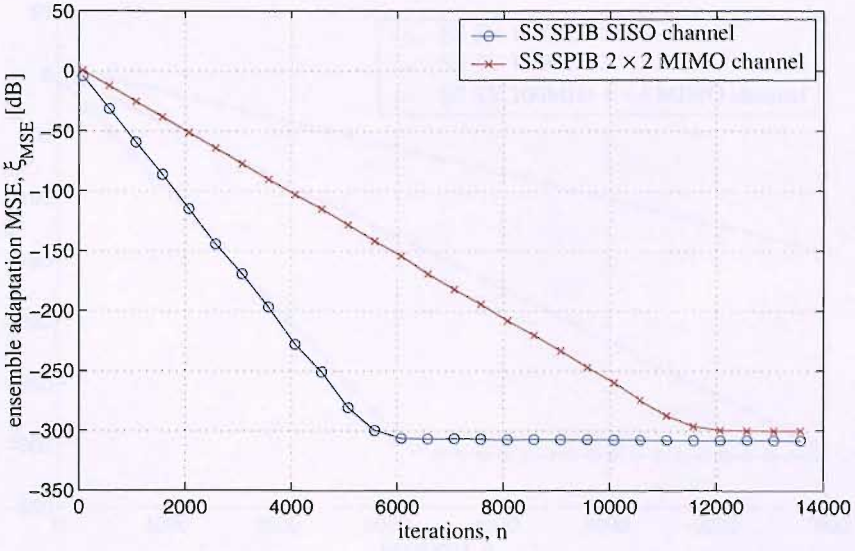

Fig. 3.7: System identification to unmodified symbol-spaced SPIB SISO and MIMO channels using M-NLMS algorithm with $\tilde{\mu} = 0.18$.

simulations and those of the flat sub-channels shows an increase of a little over 50, as expected. An increase in the final MSE now also becomes apparent- now around -300 dB. The reason for this is that the errors cause by the machine accuracy of the simulation tool combine additively for each adaptive tap. Hence we would expect an increase in the final MSE over the -320 dB of the flat channels equal to the number of adaptive taps, which in the SISO case in these SPIB simulations is 17 dB, and this is indeed roughly what we see in Figure 3.7.

Finally, for the system identification simulations, we look at the adaptation for the Saleh-Valenzuela channels, described in Chapter 2, with parameters $1/\Lambda = 300$ ns, $1/\lambda = 5$ ns, $\Gamma = 60$ ns and $\gamma = 20$ ns. The required number of channels were generated for each simulation, i.e. one for SISO, four for 2×2 MIMO and 16 for 4×4 MIMO. The channel impulse responses were truncated at 300 ns and given that for our channel realisations the RMS delay spread ranged from 5 ns to 35 ns this is reasonable as the truncated coefficients were of negligible magnitude. The impulse responses were temporally quantised, band-limited and sampled at 100 MHz. Again the M-NLMS algorithm with $\tilde{\mu} = 0.18$ was used. We see in Figure 3.8 that these length 30 adaptive filters converge at around 5/3 of the rate of the length 50 filters in the SPIB simulations. Again we see that as the simulations cover the SISO, 2×2 MIMO and 4×4 MIMO cases the convergence rate halved each time as the stacked multi-channel adaptive filters double in length. The final MSE is lower than for the SPIB simulations, due to reasons discussed earlier, as the filter lengths are now shorter.

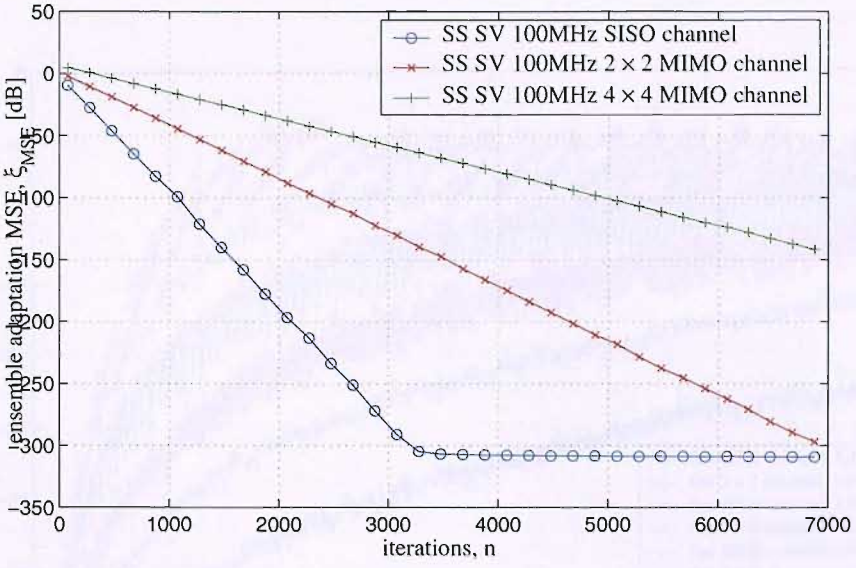

Fig. 3.8: System identification to 100 MHz bandwidth SV SISO and MIMO channels using M-NLMS algorithm with $\tilde{\mu} = 0.18$.

3.6.2 System Tracking

Up until this point we have shown the performance of the M-NLMS algorithm as it identifies the various unknown SISO and MIMO channels with an all-zero initial adaptive coefficient vector. Another interesting area relates to the tracking behaviour of the algorithm for non-stationary channels. When an MS travels at some speed the channel will be dynamic, as explained in Chapter 2, and we may model this behaviour using a Rayleigh Doppler-faded envelope, the characteristics of which are determined by the MS speed and carrier frequency. For these tracking simulations we assume that the adaptive system is privy to the channel coefficients at the start of the simulation, by previous identification for example, therefore the adaptive coefficients are initialised to the channel coefficients.

Firstly we look at the tracking behaviour for a SISO and 2×2 MIMO channel with flat sub-channels, shown in Figure 3.9. The simulation uses the M-NLMS algorithm with $\tilde{\mu} = 0.18$. Since we must relate the system to the real world to create the Rayleigh Doppler-faded faded channel, we must also associate a particular receiver sampling frequency, and for this we have chosen 10 kHz. To make the simulation more interesting, rather than an MS moving at constant velocity, we have it accelerating which causes an increasingly dynamic channel as the simulation progresses. Figure 3.9(b) shows that the MS accelerates from rest to 30 m/s, which is about 120 km/h, and we are using a carrier frequency $f_c = 1.8$ GHz. Looking at the time base we see a phenomenal acceleration far greater than the system will ever encounter, but this is simply to ensure the simulation takes

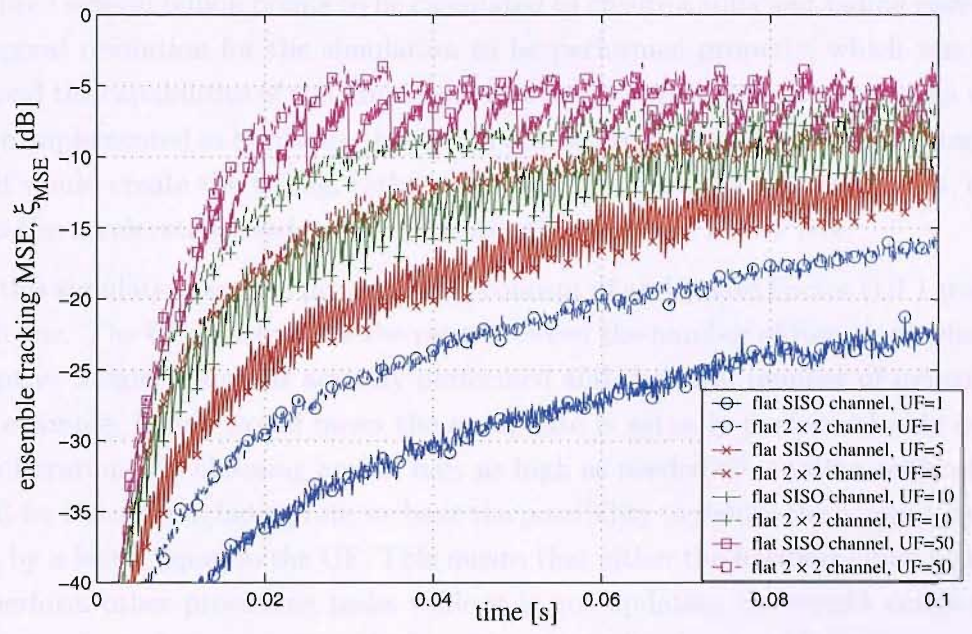

(a)

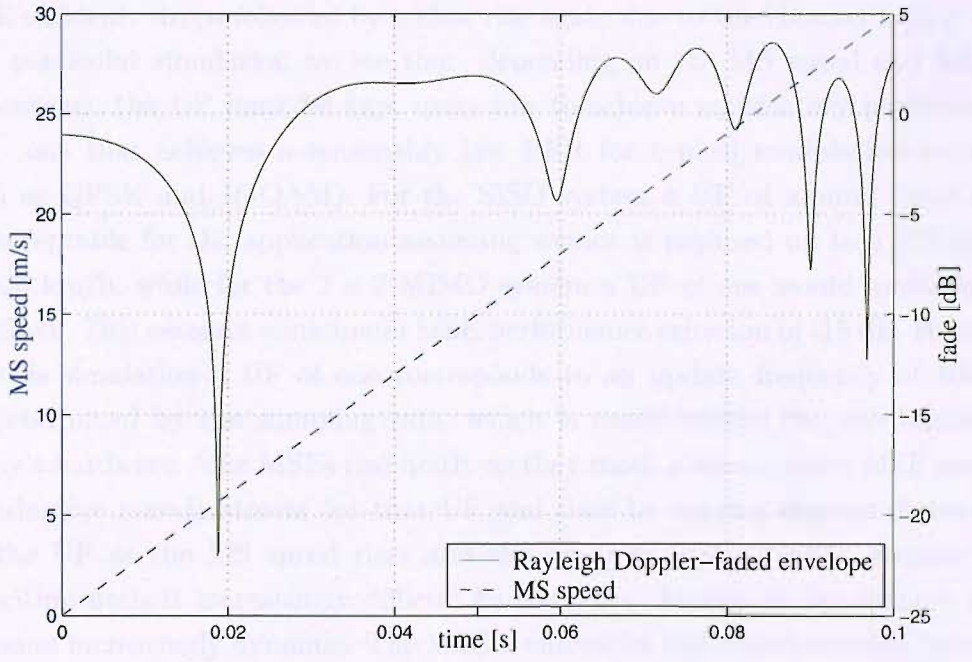

(b)

Fig. 3.9: System tracking behaviour for a Rayleigh Doppler-faded flat SISO and 2×2 MIMO channel for accelerating MS with $f_c = 1.8$ GHz (a) MSE for varying Update Factors (UF) (b) typical fading envelope as MS speed increases.

a reasonable amount of time; choosing a more realistic acceleration would have required several billion points to be calculated to ensure a sufficient fading envelope temporal resolution for the simulation to be performed properly, which was well beyond the capabilities of the simulation tool used. Fortunately, if the system were to be implemented in hardware this would not be problem as obviously the channel itself would create the fading, rather than the simulation tool. Nevertheless, even with the acceleration used, the results are still valid and instructive.

In this simulation we also introduce the concept of an Update Factor (UF) greater than one. The UF is defined as the ratio between the number of iterations where a adaptive weight update is actually performed and the total number of iterations. For example, UF=5 would mean the an update is actually performed only every fifth iteration. By choosing an UF only as high as needed to obtain a satisfactory MSE for the current fading rate we have the possibility to reduce the computational cost by a factor equal to the UF. This means that either the hardware may be used to perform other processing tasks while it is not updating the weight coefficient, for example analytic inversion which will be covered in Section 4.2, or lower power hardware may be used. Figure 3.9(a) shows results for UF=1,5,10 and 50. With the higher UFs we can actually see the adaptive updates being performed as the MSE suddenly drops followed by a slow rise again due to the channel fading. For this particular simulation we see that, depending on the MS speed and MIMO dimensions, the UF must be kept quite low to achieve satisfactory performance (i.e. one that achieves a reasonably low BER for typical modulation schemes such as QPSK and 16-QAM). For the SISO system a UF of around three may be acceptable for the application assuming service is required up to a MS speed of 120 km/h, while for the 2×2 MIMO system a UF of one would probably be required. This assumes a minimum MSE performance criterion of -15 dB. However for this simulation a UF of one corresponds to an update frequency of 10kHz, as determined by the sampling rate, which is easily within the capabilities of today's hardware. The MSEs rise firstly as they reach a steady-state MSE caused by adaptive misadjustment for that UF and then by varying degrees depending on the UF as the MS speed rises and the adaptive lag increases, because the algorithm finds it increasingly difficult to track the changes in the channel as it becomes increasingly dynamic. The MSE is caused by the misadjustment between the adaptive filter and the true channel co-coefficients between updates and also the adaptive filter lagging the channel which creates a bias as briefly mentioned in Section 3.3.2.4. For higher UFs it appears that the adaptation error due to a lower update rate becomes increasingly dominant over the bias caused by increasing lag due to the accelerating MS. Hence for higher UFs, after reaching the steady-state MSE for that UF, the MSE gradient decreases relative to lower UFs even as the

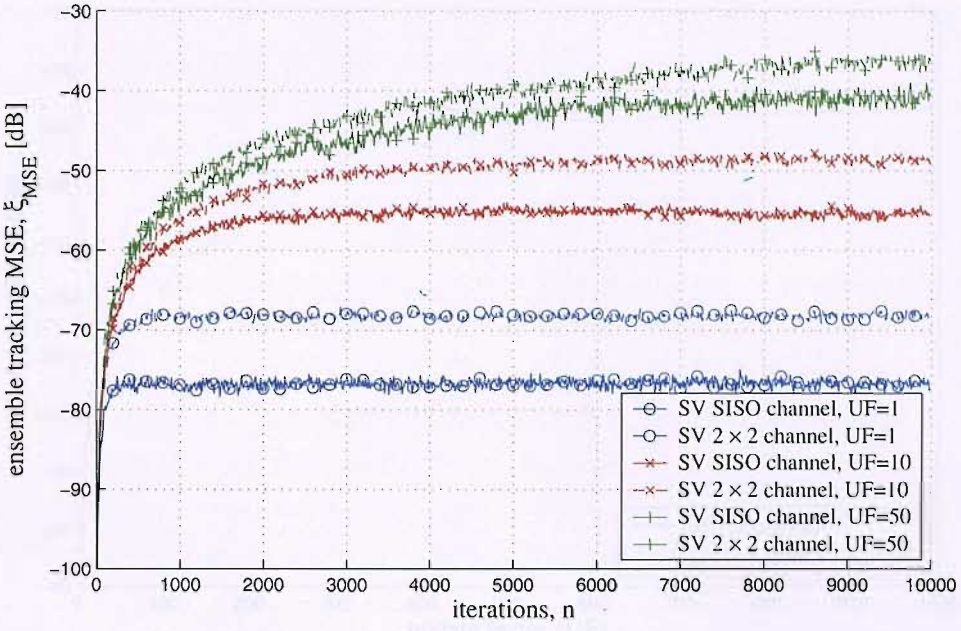

Fig. 3.10: System tracking for 100 MHz SV SISO and MIMO channels using M-NLMS algorithm with $\tilde{\mu} = 0.18$ and MS moving at 120 km/h.

MS speed increases, meaning that higher UFs are less sensitive to the fading effect of the channel but only because the misadjustment MSE dominates.

Our next tracking simulations show the performance of the M-NLMS following a dynamic Saleh-Valenzuela (SV) channel. As before, the parameters of the SV channel are $1/\Lambda = 300$ ns, $1/\lambda = 5$ ns, $\Gamma = 60$ ns and $\gamma = 20$ ns, the M-NLMS algorithm is used with $\tilde{\mu} = 0.18$, and the UF ranges from 1 to 50. The SV channels have been sampled at 100 MHz using the method outlined in Section 2.4.1.3, and hence the impulse responses are 30 taps long, assuming truncation after 300 ns as before. This is purely for processing reasons due to computational limitations of the simulation tool. Unlike for the flat channel tracking simulations previously the MS moves at a constant speed of 120 km/h and we plot the tracking MSE against the UF, shown in Figure 3.10, where again we have assumed that the adaptive system initialises with perfect channel knowledge at that moment in time. The Doppler bandwidth is 200 Hz or equivalently the coherence time is 2.1 ms [23]. Since the coherence time is many orders of magnitude greater than the receiver sampling period, 10 ns, we expect that the fading effect is negligible for low UFs. For example, UF=1 means that the adaptive algorithm updates at a period of 10 ns and therefore from the perspective of the algorithm the channel is near static. Figure 3.10 shows the MSEs for UF=1,10 and 50 we indeed see that the lower UFs achieve the lowest steady-state MSE. These steady-state MSEs are much lower than the flat channel MSEs in Figure 3.9 by virtue of the now much greater

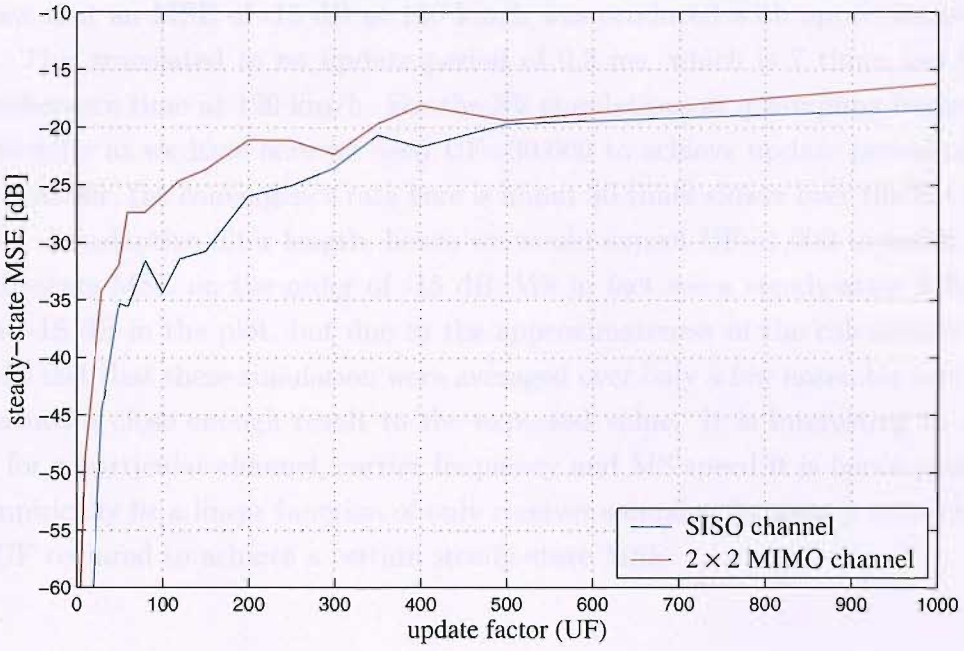

Fig. 3.11: Steady-state system tracking MSE for SV SISO and MIMO channels using M-NLMS algorithm with $\tilde{\mu} = 0.18$, MS moving at 120 km/h and varying update factors.

iteration rate in real time. Even though the MS is moving at a constant speed we still see the MSE curve converge to the steady-state value. The steady-state MSE is due to lag and the cases with a higher UF take longer to reach this MSE on account of their lower update rate. One point we should address is that the parameters we are using for the SV channel pertain to an indoor environment and hence it is unlikely that a MS would moving at 120 km/h. Nevertheless, the results are valid and instructive. It is feasible that in an harsh outdoor environment, such a dense urban, the channel would have a similar characteristics, only that the delay spread would be greater and the corresponding coherence bandwidth less. In this case a similar impulse response would be obtained by sampling at a lower rate. Hence these simulations form a worst-case scenario.

Finally, with the same SV channel and an MS moving at 120 km/h it is interesting to see how the steady-state MSE varies with the UF, and a plot of this is shown in Figure 3.11 for UF ranging from 1 to 1000. These simulations were very computationally intensive and for this reason it was feasible to run the simulation for only a few ensemble sets, hence the curves are not smooth. However they are of adequate quality to gain insight in the general behaviour and there are some interesting points to note. We see that the steady-state MSE degrades the most in the lower UF values. For the flat SISO tracking simulation in Figure 3.9(a)

we saw that an MSE of -15 dB at 120 km/h was produced with approximate UF of 3. This translated to an update period of 0.3 ms, which is 7 times less than the coherence time at 120 km/h. For the SV simulations at a sampling frequency of 100 MHz as we have here we need UF=30,000 to achieve update period of 0.3 ms. However, the convergence rate here is about 30 times slower over the flat case due to the adaptive filter length, hence we would expect UF=1,000 to result in a steady-state MSE on the order of -15 dB. We in fact see a steady-state MSE of about -18 dB in the plot, but due to the approximateness of the calculation and the the fact that these simulation were averaged over only a few ensemble sets this is deemed a close enough result to the expected value. It is interesting to note that for a particular channel, carrier frequency and MS speed it is hence possible to empirically fit a linear function of only receiver sampling frequency to calculate the UF required to achieve a certain steady-state MSE.

3.7 Summary

This chapter has covered the fundamentals of multi-channel adaptive filtering and given us the necessary grounding to continue with future chapters where the adaptive algorithms will used to identify unknown MIMO channels ready for analytic inversion or to adaptively invert the MIMO channel directly to create an equaliser. The chapter started by outlining the problem and devising a suitable multi-channel system model before then using this model to derive the optimum filter that translates a given input signal to a desired output signal, or Wiener-Hopf solution via use of the MSE cost function. We then explained the computational problems involved with the analytic calculation of the Weiner-Hopf which motivated us to develop lower complexity adaptive methods which converge to the optimum solution over time. We developed a gradient descent technique which led to the LMS family of adaptive algorithms. The properties of the LMS algorithm were discussed in terms of the computational complexity, where we showed its significant advantage over the analytic method, the algorithm stability, convergence speed and bias. We then derived a normalised version of this whereby the algorithm automatically adjusted itself for the input signal power as so not to become unstable and theorised that the convergence speed of the M-LMS relative the single-channel LMS algorithm would be slower by a factor equal to the number of transmitters. After briefly discussing other candidate adaptive algorithms and explaining the decision to favour the LMS type algorithm over these in this thesis we moved onto the application of the M-NLMS algorithm in various simulations. Two broad sets of simulation results were shown- static system identification and dynamic system

tracking. We saw that the convergence rate scaled inversely with the dimensions of the MIMO system and with the length of the adaptive filters. Finally, we saw that especially for high bandwidth systems we may choose an Update Factor greater than one and hence limit the computational power required for the adaptive tasks by either choosing a lower power processor or employ the freed power to perform other tasks such as analytic inversion. The analytic inversion of MIMO systems forms a important area for study and we have seen in Chapter 2 that studies in the literature covering the analytic inversion of frequency-selective MIMO channels are few and is still an open area for research which is explored in the next chapter.

Chapter 4

System Equalisation

This chapter explains the concepts and methods behind the equalisation of frequency-selective MIMO channels based on the basic domain-independent MIMO transfer function

$$\mathbf{y} = \mathbf{H}\mathbf{x} + \boldsymbol{\nu}, \tag{4.1}$$

where $\mathbf{y}$, $\mathbf{x}$ and $\boldsymbol{\nu}$ are vectors of multiple received, transmitted and noise signals respectively, and $\mathbf{H}$ is the MIMO channel matrix. Out of the adaptive methods, there are broadly two ways of creating a MIMO equaliser: (i) adaptively identify the MIMO channel as covered in Chapter 3 and then analytically invert it, or (ii) adaptively identify the inverse of the MIMO channel and hence converge to the equaliser directly. Each of these two methods are developed and their respective advantages and disadvantages are explained. We firstly cover the mathematical criteria behind the MIMO channel inverse and how it relates to the equaliser in Section 4.1. Techniques are covered to invert rectangular MIMO channels, i.e. $M \neq P$ as are ways to invert ill-conditioned MIMO channels. We also explain the possibility of using pre-distortion at the transmitter instead of equalisation at the receiver and justify our decision to favour the equalisation method. In Section 4.2, three analytic techniques are developed which perform the inversion in the z, time and frequency domain and the inversion criteria behind these techniques are covered. Also covered is the required FIR equaliser length, and the effects of channel estimation errors and noise during adaptive identification. We move onto the fully adaptive inversion technique, developing it and explaining the problems associated with it in Section 4.3. In Section 4.4, adaptive equaliser tracking for fading channels is covered and other adaptive equalisation techniques are mentioned in Section 4.5. Finally in Section 4.6, we present simulation results showing MSE and BER performances attainable in various scenarios, and end the chapter with a summary motivating the development of subband processing techniques, which are the topic of Chapter 5.

4.1 Inversion Methods and Criteria

The central problem of frequency-selective MIMO systems is that data streams transmitted from the multiple transmitters are mixed both in space and time and then combine additively at the multiple receivers. The frequency-selective, and hence time-dispersive, nature of the channel causes inter-symbol interference (ISI), while the MIMO property results in co-channel interference (CCI). The aim of this section is to discuss inversion methods for MIMO channels that can minimise both ISI and CCI in an appropriate sense.

The aim is to find a matrix, $\mathbf{G}$, that when applied to the vector of received signals, $\mathbf{y}$, we obtain an estimate $\hat{\mathbf{x}}$, for the transmitted data stream, $\mathbf{x}$. Hence, we have

$$\hat{\mathbf{x}} = \mathbf{G}_{M\times P}\mathbf{y} \tag{4.2}$$

$$= \mathbf{G}_{M\times P}\mathbf{H}_{P\times M}\mathbf{x}, \tag{4.3}$$

where $\mathbf{G}$ is an "unmixing" matrix whose purpose it is to undo the effects of the channel and the subscripts denote the dimension of the matrix. Note that at this point the criteria remain independent of representation domain. The structure of how the input and output signals and the time-dispersive nature of the channel are dependent on the representation domain, i.e. z, time or frequency and hence undefined at this point. It is useful to think of the elements of the vectors and matrices as blocks, the internal structure of which are as yet undefined. Notice that we are currently considering only a noiseless environment, and that we apply $\mathbf{G}$ to the input vector after the MIMO channel, and so it must be applied at the receiver. In this case, the unmixing matrix, $\mathbf{G}$ is termed a MIMO *equaliser*. Another possibility is to apply an unmixing matrix at the transmitter, in which case the matrix mixes the signals together before they are transmitted in such a way that the channel unmixes them so that $\hat{\mathbf{x}}$ arrives correctly at the receiver antennas. In this case we would call the unmixing matrix, $\mathbf{G}$, a MIMO *pre-distorter*. This will be discussed in Section 4.1.3 as well as our reasons for using equalisation. We will continue with the creation of an equaliser as an objective. To recover the input signals, $\mathbf{x}$, perfectly we require

$$\hat{\mathbf{x}}[n] = \mathbf{x}[n - \Delta], \tag{4.4}$$

where Δ is a delay required to place the significant portion of the response of $\mathbf{G}$ in the causal domain which is required if the channel determinant is non-minimum phase. The method of how to achieve this depends on the unmixing criterion. There are a number of these, however two of the best know are the zero-forcing

(ZF) and minimum mean squared error (MMSE) criteria. The ZF solution aims to perform a mathematically perfect inversion of the MIMO channel taking no account of noise or any other sources of error. Equivalently, it aims to make the Channel-Equaliser Response (CER) a delayed identity matrix. However if the signals are highly attenuated by the channel the ZF equaliser will have a high gain which can cause excessive errors and other problems in the presence of noise and other error-causing phenomena. The MMSE solution is an alternative which as its name suggests aims to minimise the error between the vector input to the MIMO channel and the vector output of the MIMO equaliser, which we will call the Channel-Equaliser Error (CEE), in any environment or in the presence of any noise sources. We have already seen the MMSE solution in Chapter 3, however in that case the adaptation error rather than the CEE was the minimisation objective.

We now consider the ZF solution of a MIMO channel, and to obtain this we must invert it. Assuming a rectangular channel where $M \neq P$, the inverse in the conventional sense, i.e. $\mathbf{H}^{-1}$, is undefined. However, in principle given a rectangular matrix it is possible to find another rectangular matrix of transposed dimensions such that the two result in an identity matrix when multiplied together. This forms the basis for the *pseudo-inverse* [100, 101]

$$\mathbf{G}_{M\times P} = (\mathbf{H}^{\dagger})_{M\times P}, \tag{4.5}$$

where $(\cdot)^{\dagger}$ represents the pseudo-inverse, and we assume that $\text{rank}(\mathbf{H}) = \min(M, P)$ to ensure its existence. There actually may be many solutions so that $\mathbf{H}^{\dagger}\mathbf{H} = \mathbf{I}$, but the pseudo-inverse is defined as the solution that has the minimum vector length. This is also known as the least squares solution to the inconsistent system $\mathbf{y} = \mathbf{H}\mathbf{x}$ [100].

There are two cases to consider, the first of which is the over-determined case, where the matrix has at least as many rows as columns, or $P \geq M$. The pseudo-inverse of a matrix $\mathbf{H}$ is then defined

$$\mathbf{H}^{\dagger}_{M\times P} = (\mathbf{H}^{H}_{M\times P}\mathbf{H}_{P\times M})^{-1}\mathbf{H}^{H}_{M\times P}, \tag{4.6}$$

which is termed the *left-inverse* of the matrix $\mathbf{H}$. Further, if the elements are functions of z, they must also be time-reversed [8, 102]. The second case is the under-determined problem where the matrix has at least as many columns as rows, or $P < M$. Now the pseudo-inverse is given by

$$\mathbf{H}^{\dagger}_{M\times P} = \mathbf{H}^{H}_{M\times P}(\mathbf{H}_{P\times M}\mathbf{H}^{H}_{M\times P})^{-1}, \tag{4.7}$$

and is termed the *right-inverse*. As will be shown in Section 4.1.3, when dealing with the application of signal processing, the choice of which pseudo-inverse to use

can be mapped directly to whether the system uses equalisation at the receiver or pre-distortion at the transmitter. The dimensions of the MIMO channel matrix and whether equalisation or pre-distortion is required are determined by the relationship between M and P. Finally, note that if $M = P$ both (4.6) and (4.7) reduce to the standard matrix inverse which is solvable assuming $\mathbf{H}$ is full rank.

4.1.1 Capacity of Equalised Channels

This section derives an expression for the capacity of a channel-equaliser system. We see from Figure 4.1 the effect that an equaliser has on a channel in isolation. Hence starting from (2.7) and accounting for the effect of the equaliser, the new capacity equation may be written as

$$C = \log_2 \frac{\det\left[\mathbf{R}_z + \mathbf{G}\mathbf{H}\mathbf{R}_x\mathbf{H}^H\mathbf{G}^H\right]}{M\det\mathbf{R}_z} \tag{4.8}$$

where $\mathbf{R}_z$ and $\mathbf{R}_x$ are the co-variance matrices of the post-equalised (coloured) noise and the inputs at the transmitters. Since

$$\mathbf{R}_z = \mathbf{G}\mathbf{R}_\nu\mathbf{G}^H, \tag{4.9}$$

then

$$C = \log_2 \frac{\det\left[\mathbf{G}(\mathbf{R}_\nu + \mathbf{H}\mathbf{R}_x\mathbf{H}^H)\mathbf{G}^H\right]}{M\det\left[\mathbf{G}\mathbf{R}_\nu\mathbf{G}^H\right]} \tag{4.10}$$

$$= \log_2 \det\left[\mathbf{I} + \frac{\rho}{M}\frac{\mathbf{G}\mathbf{H}\mathbf{H}^H\mathbf{G}^H}{\mathbf{G}\mathbf{G}^H}\right], \tag{4.11}$$

assuming that the input and noise powers are equal and the signals uncorrelated, and where $\mathbf{R}_\nu$ is the co-variance matrix of the noise at the receivers. Hence we see that in addition to the effect the equaliser has on the transmitted signal it also colours the noise. This equation will be used to evaluate the post-equaliser capacity in Chapter 7 where the equaliser is created using the various techniques covered in this thesis. This matrix applies to flat channels but it is clear how the capacity of frequency-selective equalised channel may be evaluated by applying the same principle as was used to evaluate the capacity of isolated frequency-selective channel in (2.11). In practice the capacity can be best evaluated via use of an FFT of suitable length.

4.1.2 Regularised Inversion and the MMSE Solution

The problem with the zero-forcing solution is that is places no constraint on the gain introduced by the equaliser so this solution is unsuitable for a noisy environment, a channel with deep spectral nulls in the determinant of the MIMO channel,

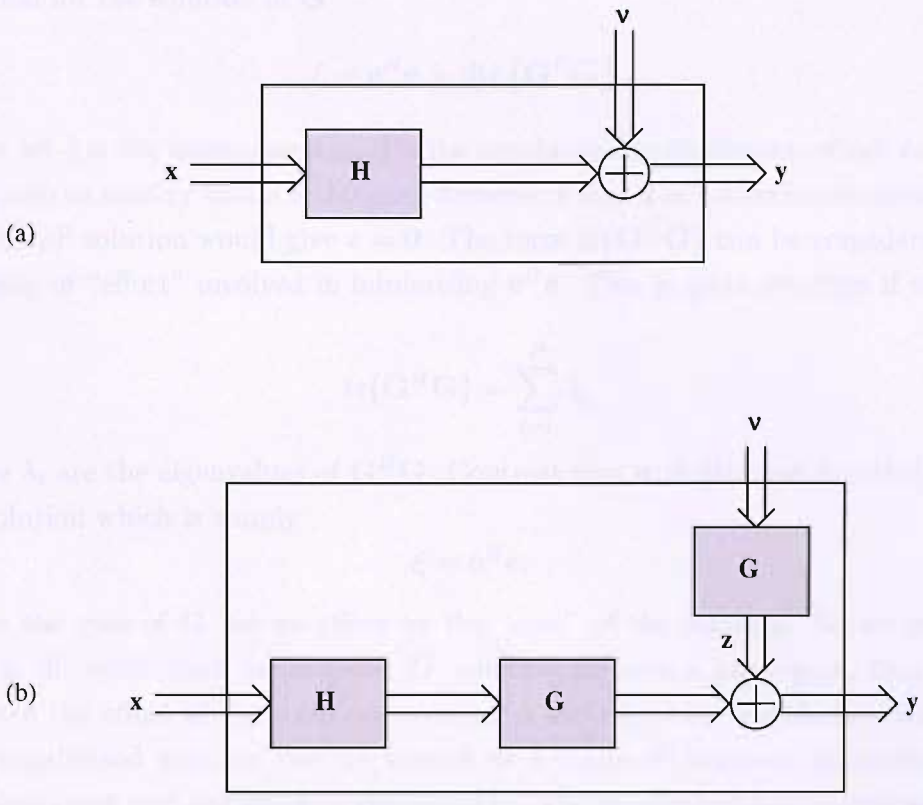

Fig. 4.1: Diagram showing (a) an isolated channel where the capacity is evaluated at the receivers, and (b) and channel-equaliser where the capacity is evaluated at the output of the equaliser.

where the zero-forcing solution may not exist, or when using inversion methods that themselves introduce errors due to their nature for example frequency-domain inversion discussed in Section 4.2.3. To demonstrate this consider a noisy version of (2.2), namely

$$\mathbf{y} = \mathbf{H} \cdot \mathbf{x} + \boldsymbol{\nu}, \tag{4.12}$$

where $\boldsymbol{\nu}$ is a vector of additive white Gaussian noise (AWGN) signals. If we now apply the equaliser of (4.5) we obtain

$$\hat{\mathbf{x}} = \mathbf{I}_{M\times M}\mathbf{x} + \mathbf{H}^{\dagger}_{M\times P}\boldsymbol{\nu}. \tag{4.13}$$

It is obvious from this equation that if $\mathbf{H}$ is ill-conditioned or near-singular then $\mathbf{H}^{\dagger}$ will greatly amplify the noise, effectively drowning out the desired signal, $\mathbf{x}$, and making $\hat{\mathbf{x}}$ a poor if not meaningless estimate of $\mathbf{x}$.

One way to alleviate this problem is to use the regularisation technique developed by Tihonov (also spelt Tikhonov) [103–106]. This technique introduces a cost

function for the solution of $\mathbf{G}$

$$\xi = \mathbf{e}^H\mathbf{e} + \beta \mathrm{tr}\left\{\mathbf{G}^H\mathbf{G}\right\}, \tag{4.14}$$

where $\mathrm{tr}\{\cdot\}$ is the trace operator, β is the regularisation coefficient, which can vary from zero to infinity, and $\mathbf{e}$ is the error between $\hat{\mathbf{x}}$ and $\mathbf{x}$ in a noiseless environment, i.e. the ZF solution would give $\mathbf{e} = \mathbf{0}$. The term $\mathrm{tr}\{\mathbf{G}^H\mathbf{G}\}$ can be considered as a measure of "effort" involved in minimising $\mathbf{e}^H\mathbf{e}$. This is quite intuitive if we note that

$$\mathrm{tr}\{\mathbf{G}^H\mathbf{G}\} = \sum_{i=1}^{P} \lambda_i, \tag{4.15}$$

where λ_i are the eigenvalues of $\mathbf{G}^H\mathbf{G}$. Contrast this with the cost function of the ZF solution which is simply

$$\xi = \mathbf{e}^H\mathbf{e}, \tag{4.16}$$

where the gain of $\mathbf{G}$ has no effect on the "cost" of the solution. So we see that if $\mathbf{H}$ is ill-conditioned causing the ZF solution to have a large gain, this would increase the effort of the solution, creating a less attractive regularised solution. The regularised solution can be viewed as a trade-off between minimising the noiseless error and the effort of the solution. The regularised left-inverse solution to the cost function (4.14) is given by

$$\mathbf{G} = (\tilde{\mathbf{H}}\mathbf{H} + \beta\mathbf{I})^{-1}\tilde{\mathbf{H}}. \tag{4.17}$$

The factor β guarantees that $\tilde{\mathbf{H}}\mathbf{H} + \beta\mathbf{I}$ is always non-singular for $\beta > 0$ and the greater β is, the better conditioned $\tilde{\mathbf{H}}\mathbf{H}+\beta\mathbf{I}$ becomes. So we see that by increasing β we can make the solution more well-behaved at the expense of moving away from the ZF true noiseless solution. By choosing β correctly we can ensure that the solution will be optimum for any noise power. The selection of β is not a precise art and any value that makes the ratio between the largest eigenvalue of $\tilde{\mathbf{H}}\mathbf{H}$ and β fall in the range between 1000 and 5000 generally gives a satisfactory solution [106].

There is one interesting case that merits further discussion. In Chapter 3 we developed the MMSE or so-called *Wiener-Hopf* solution, which is the optimum solution even for a noisy problem. It is possible to show that when the problem is represented in the time-domain, explained in Section 4.2.2, the MMSE solution is equivalent to the regularised solution for when $\beta = \sigma_\nu^2/\sigma_x^2$, where σ_ν^2 is the noise power and σ_x^2 the input signal power. This is developed and explained in Section 4.2.2 and the proof is contained in Appendix C.

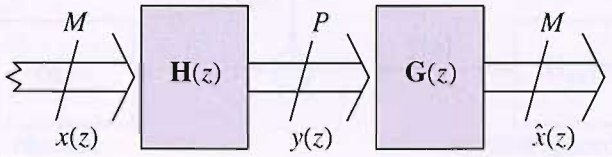

(a) Equalisation

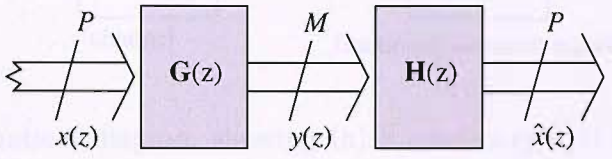

(b) Pre-distortion

Fig. 4.2: An equalisation and pre-distortion set-up.

4.1.3 Equalisation versus Predistortion

In Section 4.1 we showed that a rectangular matrix can have two pseudo-inverses, a left pseudo-inverse and a right pseudo-inverse. Although for the rest of this thesis we shall continue to only consider equalisation at the receiver, an alternative possibility of pre-distortion (sometimes called pre-equalisation) at the transmitter merits a brief look. It is an interesting area for application with mobile devices which are often physically small and hence may not have the space for many antennas. This can cause problems on the downlink if classic equalisation is used and some promising results have been shown using pre-distortion as an alternative [107].

Figure 4.2 shows the set-ups for equalisation and pre-distortion. With equalisation, shown in Figure 4.2(a), we use the left-inverse of the channel matrix and hence we require $M \geq P$. Conversely pre-distortion, shown in Figure 4.2(b), prescribes use of the right-inverse with $M \leq P$. In the special case where $M = P$ we may use either equalisation or pre-distortion. However, in radio communication equalisation is usually preferable, as pre-distortion has an associated problem that the response of the pre-distorter must either be calculated from the channel, which in general is unknown at the transmitter and must be identified, or adapted to directly. In either case, some feedback may be required from the receiver to the transmitter, which may require an extra overhead, although if the system uses time-division duplex (TDD) the uplink and downlink channel responses will be the same and hence known to both sides. Often pre-distortion and equalisation are

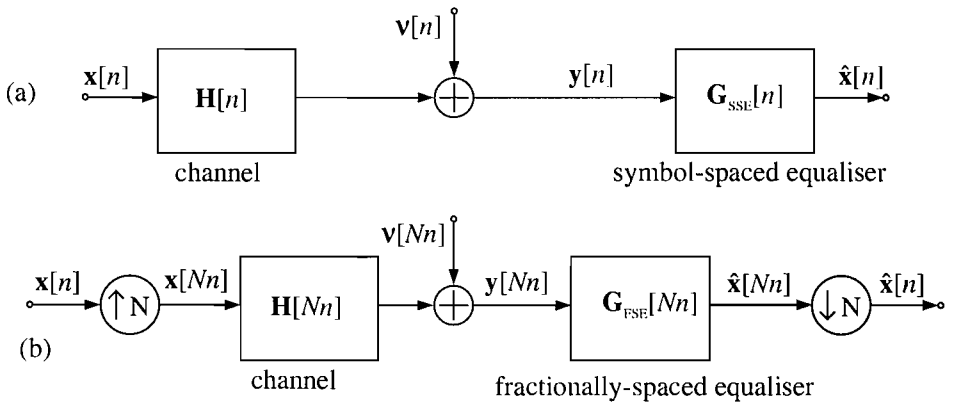

Fig. 4.3: Schematical diagram showing (a) a symbol-spaced equaliser, and (b) and fractionally-spaced equaliser

combined. Some applications use power control which can be considered a simple kind of pre-distortion. More sophisticated schemes exist where the inversion task is split between an equaliser and pre-distorter using a singular value decomposition of the channel [108], and some recent work has covered low-complexity pre-distorter design [109]. Such work however is outside the scope of this thesis.

4.1.4 Fractionally-Spaced Equalisation

We have made the implicit assumption up until this point that the equaliser samples and processes the input stream at the symbol rate, resulting in a so-called T-spaced or symbol-spaced equalisation (SSE). Most early receivers used symbol-spaced equalisation in order to simplify implementation and minimise computational cost. However, as performance requirements increased and digital processing systems became faster and cheaper, fractionally-spaced equalisers (FSE) started to be developed and are now almost ubiquitous in high-speed modems. Fractionally-spaced or T/N-equalisers sample the input data stream at a rate N times the symbol rate employing expanders and decimators, explained in Chapter 5, and hence the equaliser processing spacing is a fraction of the symbol spacing [110]. As such, the performance of the FSE is improved over that of the SSE, as shown in early papers [111, 112]. Other advantages include higher resolution equalisation [113, 114], equalisation of channels containing spectral zeros [115] and shorter equalisers if the sampled channel contains fractional delays [110].

The fractionally-spaced system is shown in Figure 4.3(a) next to the symbol-spaced system in Figure 4.3(b). The new samples that are placed between the samples that are defined by the original signal are a function of the expander;

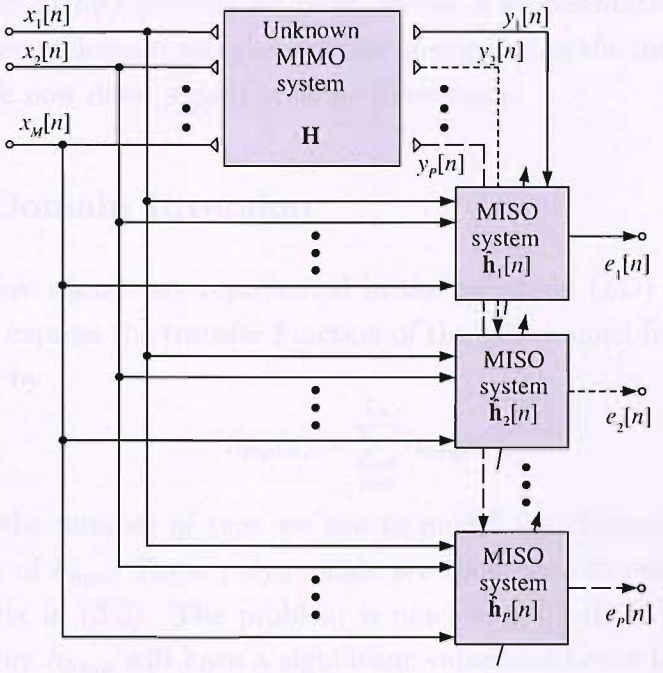

Fig. 4.4: System identification set-up used to obtain the response for an unknown MIMO system.

for example it may simply hold the previous signal sample or insert zeros for N samples. The FSE may be modelled using a polyphase representation [102, 115] so that the system is expressed as a multi-channel system. This is a very useful representation for us as we may simply use the multi-channel inversion techniques that will be developed in this chapter to easily find the FSE. This is an interesting topic, and is the subject of Chapter 6.

4.2 Analytic System Inversion

This section is devoted to developing and explaining the methods of calculating the system inverse and hence equaliser analytically. We assume that the MIMO channel has been previously identified using adaptive techniques discussed in Chapter 3, and the system that performs this is shown in more detail in Figure 4.4. The adaptive MISO blocks are those shown in Figure 3.2 in Chapter 3. It is possible that there may be some channel estimation error introduced at this point due to non-perfect estimation or the adaptation being terminated before full convergence due to time or processor power restrictions, for example. This is itself an interesting topic and discussed further in Section 4.2.5. Once the channel has been identified it can be inverted according to (4.6).

To invert the MIMO channel we must choose a representation domain, i.e. z, time or frequency-domain and the method of calculating the inverse is different in each case. We now discuss each of these three cases.

4.2.1 z-Domain Inversion

Time-dispersive signals are represented in the z-domain (ZD) using polynomials in z. We can express the transfer function of the sub-channel from transmitter M to receiver P by

$$h_{mp}(z) = \sum_{l=0}^{L_h} h_{l,mp} z^{-i} \tag{4.18}$$

where L_h is the number of taps we use to model the channel, and $h_{l,mp}$ is the l^{th} coefficient of h_{mp}. These polynomials are then used to construct the MIMO channel matrix in (2.3). The problem is much simplified for narrowband channels where only $h_{0,mp}$ will have a significant value and hence the MIMO channel matrix consists of scalar elements. In this case we may use a standard algebraic or numerical method to invert the matrix such as Gaussian elimination. With frequency-selective broadband channels however, the elements of the matrix will be polynomials in z and calculating the inverse is quite a difficult task.

The method we use here is to extend the standard inversion method to the polynomial element case. We use the pseudo-inverse in (4.6) and express the variables as functions of z, i.e.

$$\mathbf{H}^{\dagger}(z) = \left(\tilde{\mathbf{H}}(z)\mathbf{H}(z)\right)^{-1} \tilde{\mathbf{H}}(z), \tag{4.19}$$

where $\tilde{\mathbf{H}}(z)$ is the parahermitian of $\mathbf{H}(z)$, $\tilde{\mathbf{H}}(z) = \mathbf{H}^{H}(z^{-1})$ [12, 102]. Hence we may proceed in the same way using Gaussian elimination on polynomials instead of scalars. Unfortunately, the calculation of the pseudo-inverse in (4.19) will often involve many computationally intensive operations on complicated IIR systems.

This method will give the ZF inverse which takes no account of the noise. Unfortunately the regularisation method described in Section 4.1.2 cannot be easily applied to this z-domain method, only to the time-domain and frequency-domain methods discussed in the next sections. It is possible to devise an MMSE inverse in the z-domain [116,117] but the derivation is highly mathematical in nature and we will favour the time-domain and frequency-domain method for reasons discussed in their relevant sections.

We simplify our discourse here by considering a 2×2 polynomial MIMO channel. As the system is square we may use the standard inversion method but the same

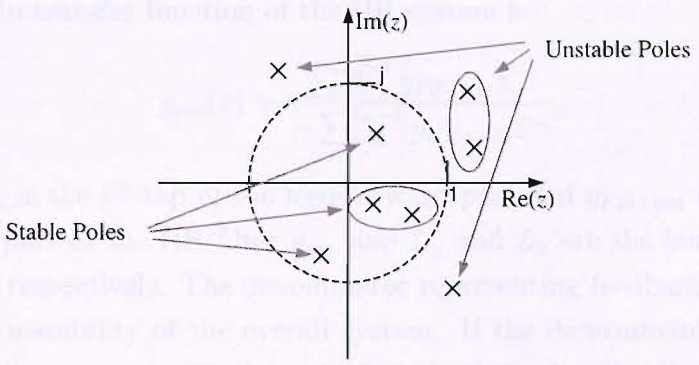

Fig. 4.5: z-plane plot of an overall unstable IIR system.

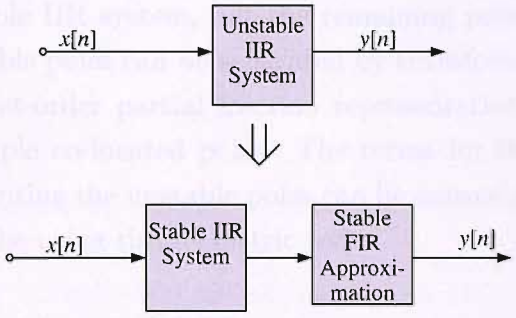

Fig. 4.6: Stabilisation of an unstable IIR system.

principles extend to non-square systems requiring the pseudo-inverse. The inverse is given by

$$\mathbf{H}^{-1}(z) = \frac{1}{\det(\mathbf{H}(z))} \begin{bmatrix} h_{22}(z) & -h_{21}(z) \\ -h_{12}(z) & h_{11}(z) \end{bmatrix}, \tag{4.20}$$

where $\det(\mathbf{H}(z))$ is given by $h_{11}(z)h_{22}(z) - h_{12}(z)h_{21}(z)$ and the polynomials are multiplied out as required.

The inverse of the channel in (4.20) generally has an infinite impulse response (IIR). If the determinant of the MIMO channel matrix is minimum-phase, then the inverse is stable. In this case all the poles of the MIMO inverse, which arise from the determinant in the denominator of the matrix inverse (4.20), lie strictly inside the unit circle in the z-plane. Problems arise when the determinant of the MIMO matrix is non-minimum phase, in which case the directly calculated inverse will be *unstable*, and some of the poles will lie outside the unit circle. A sketch of this is shown in Figure 4.5. We can attempt to stabilise the system by splitting it into two cascaded systems, one of which is an IIR system formed from the stable poles of the original system and the other a truncated FIR approximation of the unstable poles of the original system. This concept is outlined in Figure 4.6.

The z-domain transfer function of the IIR system is

$$g_{pm}(z) = \frac{\sum_{l=0}^{L_g-1} g_{FF,l,pm} z^{-l}}{-\sum_{i=0}^{L_b-1} g_{FB,i,pm} z^{-i}}, \tag{4.21}$$

where $g_{FF,l,pm}$ is the l^{th} tap of the feed-forward part and $g_{FB,i,pm}$ is the i^{th} tap of the feedback part of the IIR filter g_{pm} and L_g and L_b are the lengths of the FF and FB part, respectively. The denominator representing feedback is the cause of the potential instability of the overall system. If the determinant of the MIMO channel contains zeros outside the unit circle in the z-domain, the system is non-minimum phase and the inverse will be unstable. This was demonstrated in [118] with application to acoustics. The poles with a magnitude less than one may be used to form the stable IIR system, but the remaining poles must be stabilised. The stable and unstable poles can be separated by transforming the denominator polynomial into a first-order partial fraction representation, being sure to take precautions for multiple co-located poles. The terms for the now isolated first-order systems representing the unstable poles can be converted into an anti-causal stable system using the using the geometric series

$$\frac{1}{1+az} = \sum_{n=1}^{\infty} -a^n z^n \qquad \text{where } |a| < 1, \tag{4.22}$$

where a is the negative reciprocal of the pole. A significant portion of the series can be shifted into the causal domain by allowing a delay for the overall system. Hence by allowing a suitable delay, so that a^n has decayed to a suitably small value, the unstable IIR port can be approximated by a stable, causal FIR system.

There is an important difference between the z-domain inverse of SISO and MIMO systems, which relates to the locations of the zeros in the channels. With SISO systems, if there is a zero on the unit circle in the z-plane, the system inverse is marginally stable. However, with MIMO systems this may well not be the case, as even if one of the sub-channels comprising the MIMO channel has a zero on the unit circle the system may still be stable. Miyoshi and Kaneda [119] found that there must be no common zeros in all sub-channels. Another condition for invertibility is that the determinant must have no zeros on the unit circle in the z-plane. If this condition is not met then the inverse will be marginally stable with the impulse response of the inverse neither converging nor diverging but oscillating for infinite time. The inverse would have a pole directly on the unit circle causing infinite gain in the frequency response at the frequency corresponding to the pole. This infinite gain means that data at that frequency cannot be recovered using this method. Finally, there is a chance that the determinant of the MIMO matrix may be zero, in which case the matrix is singular and no inverse exists.

This method of finding the inverse is adequate for very small MIMO systems (i.e. 2×2), but once the system dimensions start to increase it becomes unfeasible. The direct calculation of the inverse becomes prohibitively complicated, as each element in the inverse MIMO system matrix would be a potentially considerably complicated IIR system. During the calculation of these IIR systems, inaccuracies during successive system stabilisations would accumulate and the resulting system is likely to be a rather poor or useless approximation of the inverse. Also if we are guaranteed that the determinant of the MIMO channel is minimum phase then we may cut out the stabilisation process and the complexity of this method with respect to L_h is $\mathcal{O}(L_h log_2 L_h)$. If this is not the case the stabilisation method will increase the complexity to a significant $\mathcal{O}(L_h^3)$. For these reasons we must turn to other methods for larger MIMO systems.

4.2.2 Time-Domain Inversion

A method for MIMO channel inversion which will always result in realisable stable FIR filter for the inverse was described by Miyoshi and Kaneda [119] and Kirkeby *et al.* [106]. Although it is more computationally costly than the z-domain method it has less accuracy problems associated when applied to arbitrarily large MIMO systems or where the inverse may be very difficult or impossible to calculate. The approach employs so-called *convolutional matrices* described in this section whereby both the time-dispersive and spatially-dispersive nature of the channel is modelled using scalar elements arranged in diagonals along the two dimensions of the matrix. As we only use scalars in a single matrix to describe the channel, as opposed to polynomials in the z-domain or, as we shall in the next section, multiple matrices for the bins in the frequency-domain method, we term this technique time-domain inversion. Again a delay will be required to move the significant portion of the solution into the causal domain.

We start by modifying the domain-independent MIMO transfer function in (4.1) so that we now have it in the convolutional domain, or as we are calling it, time domain

$$\mathbf{y}[n] = \mathbf{H}_c[n]\mathbf{x}[n] + \boldsymbol{\nu}[n] \tag{4.23}$$

where $\mathbf{x}[n]$, $\mathbf{y}[n]$ and $\boldsymbol{\nu}[n]$ are the multiple-channel input, output and noise vector, and the multiple channels are stacked in vectors analogously to $\mathbf{u}$ and $\mathbf{v}$ in Chapter 3. The dependency of the channel on n is as we have assumed the channel is dynamic in time, although we will now drop this for notational simplicity. The

convolutional channel matrix $\mathbf{H}_{\mathrm{c}}$ is defined

$$\mathbf{H}_{\mathrm{c}} = \begin{bmatrix} \mathbf{H}_{11,\mathrm{c}} & \cdots & \mathbf{H}_{M1,\mathrm{c}} \\ \vdots & & \vdots \\ \mathbf{H}_{1P,\mathrm{c}} & \cdots & \mathbf{H}_{MP,\mathrm{c}} \end{bmatrix} \tag{4.24}$$

with

$$\mathbf{H}_{mp,\mathrm{c}} = \begin{bmatrix} \mathbf{h}_{mp}^T & \cdots & \cdots & 0 & 0 \\ 0 & \mathbf{h}_{mp}^T & \cdots & \ddots & 0 \\ 0 & 0 & \ddots & \ddots & \vdots \\ 0 & 0 & \ddots & \mathbf{h}_{mp}^T & \cdots \end{bmatrix}, \tag{4.25}$$

where

$$\mathbf{h}_{mp} = [h_{mp}[0] \quad \cdots \quad h_{mp}[L_h - 1]]^T. \tag{4.26}$$

The dimensions of $\mathbf{x}$, $\mathbf{y}$, $\boldsymbol{\nu}$ and $\mathbf{H}_{\mathrm{c}}$ depend on the chosen equaliser length L_g per channel. To obtain a single output sample from an equaliser we require PL_g input samples to fill the L_g taps in the P equaliser filters. Hence $\mathbf{y}$ must be length PL_g. Given this fact, it is not difficult to deduce that $\mathbf{H}_{\mathrm{c}}$ must be of dimensions $PL_g \times M(L_g + L_h - 1)$, and from this we also see that $\mathbf{x}$ must be length $M(L_g + L_h - 1)$.

To calculate the equaliser we must invert $\mathbf{H}_{\mathrm{c}}$. To this end we may employ the Wiener-Hopf solution derived in Chapter 3, which is

$$\mathbf{g}_m = \mathbf{R}^{-1}\mathbf{p}_m, \tag{4.27}$$

where we calculate the optimum MMSE MISO equaliser system for each m to recover $x_m[n]$. The vector $\mathbf{g}_m$ is defined

$$\mathbf{g}_m = [\mathbf{g}_{m1}^T \quad \mathbf{g}_{m2}^T \quad \cdots \quad \mathbf{g}_{mP}^T]^T \tag{4.28}$$

where

$$\mathbf{g}_{mp} = [g_{mp}[0] \quad g_{mp}[1] \quad \cdots \quad g_{mp}[L_g - 1]]^T \tag{4.29}$$

and $g_{mp}[l]$ is the l^{th} filter coefficient for the MISO equaliser $\mathbf{g}_{mp}$. Figure 4.7 clarifies the situation where the dependencies on n reflect the potential dynamic channel and adaptive equaliser. Of course M of these MISO equalisers are required to create the full MIMO equaliser.

The matrix $\mathbf{R}$ is the multi-channel auto-correlation matrix defined in (3.13) in Chapter 3, but using $\mathbf{u} = \mathbf{y}$ as this is the input to the equaliser. Hence we have

$$\begin{aligned} \mathbf{R} &= \mathcal{E}\{\mathbf{y}\mathbf{y}^H\} && (4.30) \\ &= \mathcal{E}\{(\mathbf{H}_{\mathrm{c}}\mathbf{x} + \boldsymbol{\nu})((\mathbf{H}_{\mathrm{c}}\mathbf{x} + \boldsymbol{\nu})^H\} && (4.31) \\ &= \mathcal{E}\{\mathbf{H}_{\mathrm{c}}\mathbf{x}\mathbf{x}^H\mathbf{H}_{\mathrm{c}}^H + \boldsymbol{\nu}\boldsymbol{\nu}^H + \mathbf{H}_{\mathrm{c}}\mathbf{x}\boldsymbol{\nu}^H + \boldsymbol{\nu}\mathbf{x}^H\mathbf{H}_{\mathrm{c}}^H\} && (4.32) \\ &= \sigma_x^2\mathbf{H}_{\mathrm{c}}\mathbf{H}_{\mathrm{c}}^H + \sigma_\nu^2\mathbf{I}, && (4.33) \end{aligned}$$

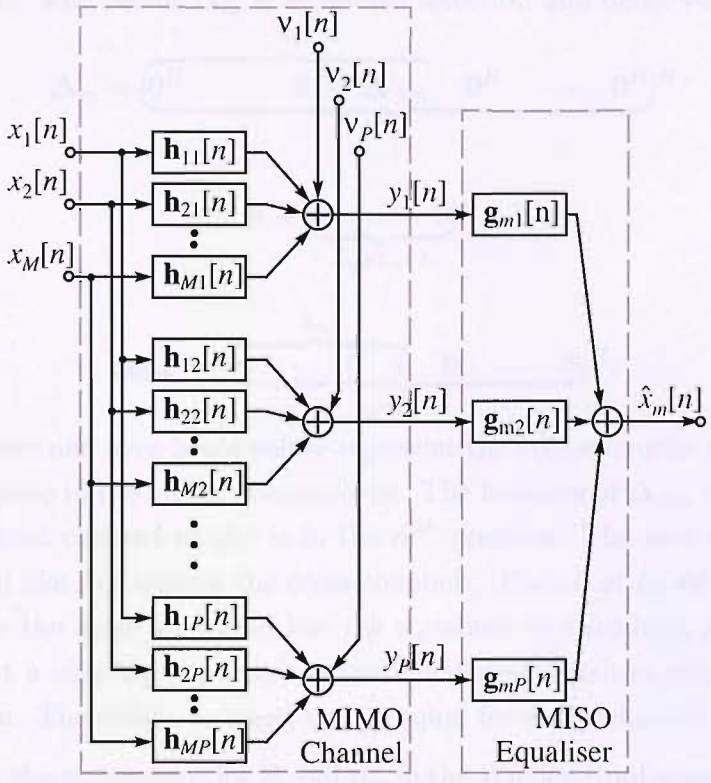

Fig. 4.7: A MIMO channel and MISO equaliser applied to input $x_m[n]$.

assuming that all the channel input variances σ_x^2 are equal, as are the noise powers σ_ν^2. We now see a problem that as equalisation is subject to the condition that $M < P$ then $\mathbf{H}_c\mathbf{H}_c^H$ will be rank-deficient and hence uninvertable as required by the Wiener-Hopf solution. However, we will later see the the pseudo-inverse can be used to invert $\mathbf{R}$ which will give the minimum norm solution for the inverse, and this will give the same solution as the pseudo-inverse of $\mathbf{H}_c$ regularised by the noise-to-signal ratio (NSR). Finally, notice that $\mathbf{R}$ is the same for all m input channels.

We continue now by developing the cross-correlation vector $\mathbf{p}_m$ for input channel m. We employ (3.9) but again substituting $\mathbf{u} = \mathbf{y}$ and also the desired signal $d_t = x_m$. Hence we specify which input channel the MISO equaliser should recover. Therefore we have

$$\begin{aligned}
\mathbf{p}_m &= \mathcal{E}\{\mathbf{y}x_m^*\} && (4.34)\\
&= \mathcal{E}\{(\mathbf{H}_c\mathbf{x} + \boldsymbol{\nu})x_m^*\} && (4.35)\\
&= \mathcal{E}\{\mathbf{H}_c\mathbf{x}x_m^*\} + \mathcal{E}\{\boldsymbol{\nu}x_m^*\} && (4.36)\\
&= \mathbf{H}_c\sigma_x^2\boldsymbol{\Delta}_m, && (4.37)
\end{aligned}$$

where we have again assumed that the input signal variance σ_x^2 is the same for all

channel inputs. The vector $\mathbf{\Delta}_m$ is a channel selection and delay vector defined

$$\mathbf{\Delta}_m = [\overbrace{\underbrace{\mathbf{0}^H \quad \cdots \quad \mathbf{0}^H \quad \mathbf{\Delta}_{\Delta m} \quad \mathbf{0}^H \quad \cdots \quad \mathbf{0}^H}_{M}}^{m}]^H \tag{4.38}$$

where

$$\mathbf{0} = [\underbrace{0 \quad \cdots \quad 0}_{L_g+L_h-1}]^H \tag{4.39}$$

and

$$\mathbf{\Delta}_{\Delta m} = [\overbrace{\underbrace{0 \quad \cdots \quad 0 \quad 1 \quad 0 \quad \cdots \quad 0}_{L_g+L_h-1}}^{\delta_m}]^H. \tag{4.40}$$

The under-brace and over-brace values represent the vector lengths and position of the relevant value in the vector, respectively. The location of $\mathbf{\Delta}_{\Delta m}$ in $\mathbf{\Delta}_m$ specifies the desired input channel m and is in the m^{th} position. The zero vectors specify that we would like to suppress the cross-channels. The offset δ_m of the impulse in $\mathbf{\Delta}_{\Delta m}$ specifies the delay we would like the equaliser to introduce, and is required to ensure that a significant portion of the calculated equaliser response is in the causal domain. The delays δ_m need not be equal for every channel.

Substituting the expressions for $\mathbf{R}$ and $\mathbf{p}_m$ in the Wiener-Hopf equation we obtain the MMSE solution

$$\mathbf{g}_m = (\mathbf{H}_c\mathbf{H}_c^H + \frac{\sigma_\nu^2}{\sigma_x^2}\mathbf{I})^\dagger \mathbf{H}\mathbf{\Delta}_m, \tag{4.41}$$

where we have used the pseudo-inverse to invert $\mathbf{R}$ as it will be rank-deficient in a noiseless environment and we have assumed that the the channel inputs are of power σ_x^2 and the noise power is σ_ν^2 at all the receivers. Notice that $\mathbf{g}_m$ is a row vector. It is relatively straight-forward, although algebraicly tedious, to generalise the derivation for when the input signal powers or receiver noise powers are unequal. In this case the optimum solution for the m^{th} input stream is given by

$$\mathbf{g}_m = (\mathbf{H}_c\mathbf{R}_x\mathbf{H}_c^H + \mathbf{R}_\nu)^\dagger \mathbf{H}_c\sigma_{x_m}^2\mathbf{\Delta}_m, \tag{4.42}$$

where

$$\mathbf{R}_x = \begin{bmatrix} \sigma_{x_1}^2 & 0 & \cdots & 0 \\ 0 & \sigma_{x_2}^2 & \ddots & 0 \\ \vdots & \ddots & \ddots & \vdots \\ 0 & \cdots & 0 & \sigma_{x_M}^2 \end{bmatrix} \tag{4.43}$$

is a matrix containing the input signals powers on the main diagonal, and

$$\mathbf{R}_\nu = \begin{bmatrix} \sigma_{\nu_1}^2 & 0 & \cdots & 0 \\ 0 & \sigma_{\nu_2}^2 & \ddots & \vdots \\ \vdots & \ddots & \ddots & 0 \\ 0 & \cdots & 0 & \sigma_{\nu_P}^2 \end{bmatrix} \tag{4.44}$$

is a matrix containing the noise powers on the main diagonal. Finally, to create an equaliser matrix $\mathbf{G}$ we may simply stack the optimum MISO equaliser vectors $\mathbf{g}_m \forall m \in 1:M$, i.e.

$$\mathbf{G} = [\mathbf{g}_1 \quad \mathbf{g}_2 \quad \cdots \quad \mathbf{g}_M]^H. \tag{4.45}$$

Hence we have the MMSE inverse as required.

It may be shown that the multi-channel Wiener-Hopf solution is equal to the pseudo-inverse of the MIMO channel regularised by the NSR, i.e.

$$\mathbf{g}_m^H = ((\mathbf{H}_c\mathbf{H}_c^H + \frac{\sigma_\nu^2}{\sigma_x^2}\mathbf{I})^\dagger \mathbf{H}_c\mathbf{\Delta}_m)^H \tag{4.46}$$

$$= \mathbf{\Delta}_m^H \left(\mathbf{H}_c^H\mathbf{H}_c + \frac{\sigma_\nu^2}{\sigma_x^2}\mathbf{I}\right)^{-1} \mathbf{H}_c^H. \tag{4.47}$$

where we have assumed that the input signal powers and noise powers are equal for simplicity. The full derivation uses the singular value decomposition (SVD) of the channel $\mathbf{H}_c$ and is quite tedious so is found in Appendix C. Notice that to calculate the pseudo-inverse of $\mathbf{H}_c$ we must now invert the term $\mathbf{H}_c^H\mathbf{H}_c + \frac{\sigma_\nu^2}{\sigma_x^2}\mathbf{I}$. This is now invertible even in a noiseless environment.

Superficially, this time-domain inversion seems ideal, but we have yet to perform the complexity analysis. Before we do this, we must first apply some opportunities to reduce the complexity of the inversion. Note that $\mathbf{R}$ is the same for all m and therefore the inversion need only be performed once. Secondly, the selection and delay vector $\mathbf{\Delta}_m$ extracts one column of the preceding $\mathbf{H}_c$ in (4.41) and this vector is multiplied by $\mathbf{R}^\dagger$. Hence, we may save ourselves the computational steps involved in multiplying $\mathbf{R}^\dagger$ with $\mathbf{H}_c$ since $\mathbf{\Delta}_m$ will discard all but one column of the result. If we define a vector $\mathbf{h}_{\mathbf{H},m}$ as the $(m(L_h + L_g - 1) + \delta_m)^{\text{th}}$ column of $\mathbf{H}_c$ then the optimum MISO equaliser vector for channel m is given by

$$\mathbf{g}_m = \mathbf{R}^\dagger \mathbf{h}_{\mathbf{H},m}, \tag{4.48}$$

and the complexity required to calculate this for all $m \in 1:M$ is given by

$$C(G) = 2MP^2L_g^2(L_g + L_h - 1) + M(2PL_g - 1) + C(T), \tag{4.49}$$

MACs, where $C(T) = \mathcal{O}(PL_g(\log(PL_g))^2)$ is the complexity of a fast inversion algorithm which we may use as $\mathbf{R}$ is Töeplitz, see e.g. [120,121]. Note that this is lower complexity than the standard Levinson-Durbin algorithm [101,104,122,123] for inverting Töeplitz matrices, which is order $\mathcal{O}(L_g^2)$, however this is still less than the $\mathcal{O}(L_g^3)$ that dominates the inversion and hence the extra effort required in implementing a $\mathcal{O}(PL_g(\log(PL_g))^2)$ fast inversion algorithm over the well-known Levinson-Durbin algorithm may not be worth the potentially insignificant computational saving in relative terms. As the inversion is $\mathcal{O}(L_g^3)$ even after these

complexity reduction techniques it is advantageous to keep L_g as small as possible, but if this still results in a process that is too computationally costly we must seek other inversion techniques such as the frequency-domain method described in the next section or shorten the channels that needs to be inverted, and hence L_g, through use of subband techniques, which are introduced in Chapter 5.

4.2.3 Frequency-Domain Inversion

Frequency-domain techniques are often thought of as low complexity methods when compared with their equivalents performed for example in the time domain. An associated problem with frequency-domain processing is that of circular convolution, also known as wrap-around effects [92], that occurs when the inverse is calculated at a finite number of discrete frequencies. Kirkeby [124] proposed a solution which involved the use of a regularisation term to suppress the error-induced effects of the circular convolution.

We start by stating the zero-forcing condition in the frequency-domain, which is

$$\mathbf{H}^{\dagger}(f)\mathbf{H}(f) = \mathbf{I} \qquad |f| < 1/2T_s, \tag{4.50}$$

where $\mathbf{H}(f)$ is the frequency response matrix of the MIMO channel, $\mathbf{H}^{\dagger}(f)$ is the MIMO equaliser response matrix and T_s is the sampling interval. The channel matrix $\mathbf{H}(f)$ contains in its elements the spectral characteristic of each sub-channel evaluated at a finite number of frequencies. A SISO algorithm which satisfies this criterion was developed by Lucky [125]. The SISO inverse can be found by obtaining the frequency domain representation of the channel, using a length L_g DFT or FFT, calculating the reciprocal of the coefficient in each frequency bin and converting back to a time domain representation, using an length L_g inverse DFT or FFT. The resulting coefficients form the impulse response of a FIR filter that is the inverse of the channel. For a MIMO system, instead of finding the reciprocal of each frequency bin, the pseudo-inverse must be used to find the inverse of a MIMO matrix for each frequency bin. The advantage over the z-domain and time-domain methods discussed in the previous sections is that in each frequency bin the MIMO system is represented by a matrix of scalar Fourier coefficients and that these matrices at each frequency are independent of the matrices at any other frequency, hence they can be inverted independently. The inversion of such matrices can be readily solved with a straight-forward Gaussian elimination for example. An inverse FFT applied to each frequency response in the inverse MIMO system yields the final zero-forcing inverse MIMO matrix in the time domain.

There are two problems associated with this solution. The method results in the zero-forcing inverse and therefore will not work well in the presence of noise

when the channel causes significant attenuation over any of the sub-channels. This noise may overwhelm the desired signal at the receiver, which may then not be able to detect the transmitted symbols correctly. The second problem arises from the error caused by the circular convolution effect, mentioned previously, which are implicit to frequency-domain methods. A well-known method of combating wrap-around effects is to use zero-padding of the intermediate signals and to use only a portion of the results. This approach leads to the so-called overlap-add and overlap-save methods [92]. However, if we attempt to deconvolve the channel coefficients out of the received signal by dividing their FFTs, or in the case of MIMO systems, applying the inverse matrix, this zero-padding method does not prevent the circular convolution effects from affecting the outcome [124]. The reason is that the frequency response of the optimal filters is inevitably that of a filter whose impulse response is of infinite duration, so while we can reduce the impact of the circular convolution by increasing the padding length to some value that will result in an acceptable error, in reality this may result in unacceptable computational complexity, and we would need an infinitely long zero-padding sequence to remove the wrap-around effect completely.

A regularisation term [104, 106, 124] goes some way to counteracting the effects of both the problems of equalisation in a noisy environment and combating the circular convolution effects. If we use the pseudo-inverse of each frequency bin, we may include a regularisation term β to limit the gain of the inverse matrix. We use the pseudo-inverse as a function of $e^{j2\pi fT_s}$, and apply a regularisation factor β

$$\mathbf{H}^{\dagger}[e^{j2\pi fT_s}] = \left(\mathbf{H}^{H}[e^{j2\pi fT_s}]\mathbf{H}[e^{j2\pi fT_s}] + \beta\mathbf{I}\right)^{-1}\mathbf{H}^{H}[e^{j2\pi fT_s}], \tag{4.51}$$

where we have used the square bracket notation as the variables are only defined at a finite number of discrete frequencies. Notice that the complex conjugation performed by the Hermitian operator reverses the phase frequency term, which is the reason why the parahermitian time index is reversed in the z-domain representation in Section 4.2.1. The regularisation term β can be used to control the "duration" of the inverse filters, and thereby provides a mechanism to avoid the undesirable wrap-around effect associated with filter methods based on sampling in the frequency-domain [124]. The regularisation essentially controls the longest time constant of the optimal filters [126], and a high β favours a low power solution with a short time constant at the expense of the zero-forcing performance error. If β is too small there may be sharp peaks in the frequency responses of the optimal filters. Conversely if β is too large the deconvolution will not be very accurate. Fortunately, the precise value of β is not usually critical and values anywhere in the region of the optimal β are likely to produce acceptable results. The effect of varying β in the frequency-domain inversion method will be seen in Section 4.6.1.

Notice the similarity between the regularisation term β in this method and in the time-domain method where it is equal to the NSR σ_ν^2/σ_x^2. Unfortunately the analysis of the optimum solution for the time-domain technique does not apply to the frequency-domain method, mainly because of the wrap-around effects. However, regularisation by the NSR at low SNRs does still provide benefit, as we will see in the simulations. In fact, at these low SNRs the performance of the frequency-domain method regularised by the NSR approaches that of the optimum MMSE performance of the time-domain technique. This is because at low SNRs the noise dominates over the wrap-around effects and hence and the best solution is given by regularising by the NSR. At higher SNRs however, the errors caused by the circular convolution will become apparent, and if we were to continue regularising by the NSR the performance would worsen again. We can counteract this effect by switching to a fixed regularisation factor at some critical SNR to deal with the wrap-around effects. Hence we can call the frequency-domain method regularised by an appropriate quantity a sub-optimal technique whose performance approaches optimality at low SNRs but worsens at higher values relative to the MMSE performance.

Like the time-domain technique, this method will always result in a stable FIR inverse and a delay must usually be applied to the method to make the solution realisable. The usual way to do this is to multiply the inverse MIMO matrix by a linear phase characteristic with a constant gradient or equivalently a constant group delay, i.e. $e^{j2\pi f\Delta}$ where Δ is the symbol delay. After all the inversions have been performed we transform the filters back into the time-domain using an IFFT applied to each element over all the scalar frequency-bin matrices in turn, which will result in an impulse response from which the filter-tap coefficients can be easily extracted.

This process will generate L_g scalar valued $M \times P$ matrices in the frequency-domain which must be inverted. Hence, the number of inversions required will scale linearly with L_g. The FFT and IFFT are $\mathcal{O}(L_g \log_2 L_g)$ processes and as these dominate over the $\mathcal{O}(L_g)$ number of inversions that must be performed, the computational complexity of this frequency-domain method is $\mathcal{O}(L_g \log_2 L_g)$, which is lower than time-domain and the stabilised z-domain method in all cases except the unlikely case where we choose $L_g \log_2 L_g > L_h^3$. The complexity of the inversions of the matrices will not dominate as it is a function of only M and P. Although the frequency-domain has a higher complexity than the unstabilised z-domain, where we assumed that we would choose $L_g > L_h$ we cannot in general rely on the determinant of the MIMO channel being minimum phase, as described in Section 4.2.1.

In conclusion, although the frequency-domain method has the considerably lower complexity, the time-domain will give the true MMSE solution. There is a trade-off here and a system designer must assess whether the time-domain MMSE solution is worth the extra computational overhead when the frequency-domain technique may provide an acceptable solution. We may either be satisfied with the performance of the frequency-domain method or investigate techniques to lower the complexity of the time-domain method, which at $\mathcal{O}(L_g^3)$ may be too great to be feasible.

4.2.4 FIR Equaliser Length

With both the time-domain and frequency-domain methods we must choose an FIR equaliser length L_g, but a question remains what is the best way to choose this parameter. If we ignore the effects of noise and use of a regularisation factor, the FIR solution to the channel equalisation problem will be an FIR model that most closely matches the IIR impulse response of the perfect ZF inverse as calculated using the z-domain technique. Hence we require a length-L_g filter that can model the IIR system for long enough until the impulse response of this system has died down to a suitably small value. The length of this response is determined primarily by the location of the poles of $(\mathbf{H}(z))^{-1}$, but also to a lesser extent but number of poles and zeros in $(\mathbf{H}(z))^{-1}$.

With no loss of generality, for simpler expression we may consider the problem for a full-rank 2×2 MIMO system. Referring to (4.20) it is clear that the inverse consists of a length L_h FIR part (in the matrix elements) and a length $2L_h$ IIR part (the reciprocal of the determinant). The channel inverse will consist of L_h non-zero zeros and $2L_h$ non-zero poles. In addition to this, the dominant factor in the selection of L_g is the rate of decay of the IIR part, which is determined by the proximity of the poles to the unit circle in the z-domain. We must consider the unstable poles separately, although we have practically already covered the unstable case when explaining the stabilisation technique in Section 4.2.1. As the unstable IIR part of the reciprocal of the determinant of $\mathbf{H}(z)$ is transformed into stable FIR approximation, then the length of the impulse response due to this is determined simply by the length of the FIR system. To evaluate the response of the stable IIR part we use a slightly modified version of the same geometric series in (4.22),

$$\frac{1}{1 - bz^{-1}} = \sum_{n=0}^{\infty} b^n z^{-n} \qquad |b| < 1, \tag{4.52}$$

where b is the location of a pole, and thus we may convert each stable pole into an infinite length "FIR" series. Then for the pole with the largest magnitude we

simply evaluate for what value of n we consider b^n to have decayed to a suitably small value and, since this will usually dominate of over all the other various constituent FIR impulse responses, we choose L_g accordingly.

While this is the mathematically best way to choose L_g it is an admittedly long-winded process and anyone actually charged with the task may find it considerably easier to use a pragmatic approach and try an initial guess for a value of L_g, observe the impulse response of the resulting equaliser and, if required, modify L_g appropriately. A more detailed analysis of MIMO equaliser lengths is given in [127].

4.2.5 Channel Estimation Errors

The effects of channel estimation errors on the performance of the equaliser which is calculated from the estimation has not received a great deal of attention in the literature. We use adaptive techniques to identify the channel but for the analytic inversion methods discussed in the previous sections we have always assumed that the channel is known perfectly for the purpose of inversion. The adaptive methods may be subject to misadjustment or lag due to a potential time-varying MIMO channel, as well as error caused if the adaptation has not been executed until convergence due to time limitations for example and the analytic inversion is based on this estimate.

Rupp [77] showed the effect of channel estimation errors on the SNR vs BER curves for narrowband MIMO systems with conditions numbers of 40 and 416, in the form of varying amounts of added noise and decoding using ML, MMSE, ZF-VBLAST and MMSE-VBLAST techniques. The error appeared to result in a constant offset in the BER vs SNR curves for the ML, MMSE and MMSE-VBLAST on the order of the added channel estimation noise relative to the observation noise. For the ZF-VBLAST simulation the BER performance actually improved with channel estimation noise. The reason for this was put down to that for when the channel estimation noise is of similar power to the observation noise it behaves like a regularisation term in the channel inversion and actually starts to behave like the MMSE-VBLAST system, as explained in Sections 4.1.2 and 4.2.2. While this work showed the effects through simulation little mathematical analysis was shown, and the work considered only narrowband flat channels. Very recently there has been a significant amount of work mathematically deriving expressions for the effect on channel capacity of channel estimation error and varying amount of channel state information at the receiver and/or transmitter [76, 128–132]. The work by Kyritsi *et al.* [76] showed that the effect on capacity is essentially de-

termined by the dimensions of the MIMO system, the observation noise and the channel estimation noise. This work however did not show the resulting effect on the inverse of a broadband MIMO channel when calculated from the noisy channel estimation.

We consider the problem in the time-domain using convolutional matrices as this is the most intuitive method. We start by modelling the channel estimation error as a noise term that is added to the MIMO channel matrix and assume that the error is constant for a particular tap in a sub-channel, h_{mp}. Hence the channel estimation error is given by the convolutional matrix constructed in a similar manner to (4.24) except where

$$\mathbf{M}_c, mp = \begin{bmatrix} \mathbf{m}_{mp}^T & \cdots & \cdots & 0 & 0 \\ 0 & \mathbf{m}_{mp}^T & \cdots & \ddots & 0 \\ 0 & 0 & \ddots & \ddots & \vdots \\ 0 & 0 & \ddots & \mathbf{m}_{mp}^T & \cdots \end{bmatrix} \tag{4.53}$$

where

$$\mathbf{m}_{mp} = [m_{mp}[0] \quad \cdots \quad m_{mp}[L_h - 1]]^T \tag{4.54}$$

and $m_{mp}[l_h]$ is the channel tap estimation error or misadjustment.

Following a similar analysis as in Section 4.2.2, but with no noise as we are only interested in the effect of the channel estimation error, we find the auto-correlation matrix and cross-correlation vector of the filter state vector by

$$\begin{aligned} \mathbf{R} &= \mathcal{E}\{(\mathbf{H}_c + \mathbf{M}_c)\mathbf{x}\mathbf{x}^H(\mathbf{H}_c + \mathbf{M}_c)^H\} && (4.55) \\ &= \sigma_x^2(\mathbf{H}_c\mathbf{H}_c^H + \mathcal{E}\{\mathbf{M}_c\mathbf{M}_c^H\}) && (4.56) \\ &= \sigma_x^2(\mathbf{H}_c\mathbf{H}_c^H + L_h\sigma_{M_c}^2\mathbf{I}) && (4.57) \end{aligned}$$

$$\begin{aligned} \mathbf{p}_m &= \mathcal{E}\{(\mathbf{H}_c + \mathbf{M}_c)\mathbf{x}x_m^*\} && (4.58) \\ &= \mathbf{H}_c\sigma_x^2\mathbf{\Delta}_m, && (4.59) \end{aligned}$$

and hence

$$\begin{aligned} \mathbf{g}_m &= \left(\sigma_x^2(\mathbf{H}_c\mathbf{H}_c^H + L_h\sigma_{M_c}^2\mathbf{I})\right)^\dagger \mathbf{H}_c\sigma_x^2\Delta_m && (4.60) \\ &= (\mathbf{H}_c\mathbf{H}_c^H + L_h\sigma_{M_c}^2\mathbf{I})^\dagger\mathbf{H}_c\Delta_m, && (4.61) \end{aligned}$$

where $\sigma_{M_c}^2$ is the variance of the channel estimation error. Note that this is the ZF inverse of $\mathbf{H}_c + \mathbf{M}_c$. It is interesting to note that when $L_h\sigma_{M_c}^2 = \sigma_\nu^2$ in a noisy environment the ZF inverse results in an MMSE equaliser. Rupp [77] found a similar result in [77] using flat channels for certain channel estimation error variances.

At first, it may seem therefore to be possible to utilise this fact by deliberately terminating the adaptive channel identification before full convergence to give a better inverse when calculated using the unregularised pseudo-inverse. However closer inspection of the problem reveals that this is only true *in the mean*. Notice that we have taken expectations in the analysis above and therefore it is only valid for a large ensemble set. In a real system, the adaptation would only be performed once, and the error at the termination of the adaptations for this one realisation will be effectively random. Hence, this performance may even be worse than if we had adapted to full convergence and manually inserted the correct regularisation factor in the inversion. Therefore a better approach is still to try to obtain the best channel estimate possible and manually apply a regularisation factor that results in the best BER performance for any SNR point, as in this case we have precise control over this factor and are not subject the adaptation performance.

Returning to the analysis, notice that the size of the effective regularisation term is directly proportional to the channel length L_h. Therefore the longer the channel the greater the effective regularisation factor over a large ensemble and hence the adaptation needs to be left to converge for longer to result in the same misadjustment effect. This is coupled with the fact that the M-NLMS converges slower for longer channel anyway. These factors indicate that it is beneficial to keep the length of the adaptive filter that identifies the channel as short as possible, possibly even at the expense of loosing some of the smaller tailing channel coefficients. Inevitably the parameters to use must be decided upon using a heuristic approach.

4.2.6 Noisy Adaptation

Whereas the previous section considered the behaviour of the inversion of a channel estimate from an adaptation that is terminated before full convergence, we now consider the case where the adaptation is performed in the presence of noise, which although similar is sufficiently different to warrant its own section. Real systems will usually have to identify the channel in the presence of noise determined by the channel SNR, so it is important to consider this problem.

We start with the LMS algorithm set up for system identification in a noisy channel. For simplicity, but with no loss of generality, we consider the single channel case. Hence we have

$$\hat{y}[n] = \hat{\mathbf{h}}[n]\mathbf{x}[n], \tag{4.62}$$

and

$$\begin{aligned} e[n] &= y[n] - \hat{y}[n] && (4.63)\\ &= \mathbf{h}^T\mathbf{x}[n] + \nu[n] - \hat{\mathbf{h}}^T[n]\mathbf{x}[n] && (4.64)\\ &= (\mathbf{h}^T - \hat{\mathbf{h}}^T[n])\mathbf{x}[n] + \nu[n], && (4.65) \end{aligned}$$

and

$$\begin{aligned} \hat{\mathbf{h}}[n+1] &= \hat{\mathbf{h}}[n] + \mu\mathbf{x}[n]e^*[n] && (4.66)\\ &= \hat{\mathbf{h}}[n] + \mu\mathbf{x}[n]\left((\mathbf{h}^H - \hat{\mathbf{h}}^H[n])\mathbf{x}^*[n] + \nu^*[n]\right) && (4.67)\\ &= \hat{\mathbf{h}}[n] + \mu\mathbf{x}[n](\mathbf{h}^H - \hat{\mathbf{h}}^H[n])\mathbf{x}^*[n] + \mu\mathbf{x}[n]\nu^*[n] && (4.68) \end{aligned}$$

where $\hat{y}$ is the output of the adaptive system, $\hat{\mathbf{h}}$ is the adaptive coefficient vector, $\mathbf{x}$ is the adaptive filter state vector, y is the output of the unknown channel, e is the adaptive error, ν is the channel noise and μ is the adaptive step-size. From these equations we may draw some conclusions:

1. The total coefficient update will deviate from the "correct" update, $\mu\mathbf{x}[n](\mathbf{h}^H - \hat{\mathbf{h}}^H[n])\mathbf{x}^*[n]$ by a random amount determined by the noise, $\mu\mathbf{x}[n]\nu^*[n]$.

2. While the power of the "correct" update is much greater than the noise power, i.e. $\mathcal{E}\left\{((\mathbf{h}^H - \hat{\mathbf{h}}^H[n])\mathbf{x}^*[n])^2\right\} \gg \sigma_\nu^2$, the effect of the noise is insignificant and will not affect the convergence.

3. Once the algorithm has converged to such a point where $\mathcal{E}\left\{((\mathbf{h}^H - \hat{\mathbf{h}}^H[n])\mathbf{x}^*[n])^2\right\}$ becomes comparable to the noise power, the noise power will dominate the error in (4.65) causing the MSE to reach a lower limit meaning no further meaningful adaptive innovation is possible.

Hence for adaptation where the output signals are corrupted by noise such that the average SNR is for example 20 dB, the MSE would not fall below -20 dB on average for a unity power signal. It is now immediately possible to use this noisy channel estimate in the calculation of the equaliser by analytic inversion, however clearly the error in the channel estimate will cause an undesirable increase in BER when some modulation scheme is used. A simple technique to solve this is to recognise that after the adaptation has reached the limit imposed by the noise the system is steady-state, as hence we may use a temporal average over the steady-state portion of the adaptation to remove some of the effect of the noise and gain a better channel estimate. In the previous section this was not possible as the system was still converging when the adaptation was terminated and hence not ergodic, but now we may continue to execute the algorithm even after it has

stopped converging for this purpose. The longer we take the average over, the better the channel estimate will be but in reality we calculate the mean over a finite number of samples so there will still be a small misadjustment afterwards. The simulations will show that taking the mean over about a thousand samples will ensure that the BER performance approaches that of the system with perfect channel knowledge. Finally, with systems that adapt very slowly we may wish to terminate the adaptation before the noise floor has been reached and use the current adaptive tap values. Even though the adaptation was still converging when it was terminated and thus the signal are not completely ergodic it is still often advantageous to average the taps over the last few samples to remove some of the noise. However, in this case we must keep the number of samples over which we average relatively small, although we will see from the simulations that even this will result in a significant improvement in channel estimation as most of the advantage arises from taking a average over a relatively small number of the most recent adaptive iterations.

4.3 Adaptive System Inversion

Whereas the previous section considered the method of analytically inverting a MIMO channel which was previously found using an adaptive identification technique, we now consider the alternative method of fully adaptive system inversion, where the equaliser is converged over time with no channel knowledge.

4.3.1 System Architecture

Fortunately, we have already developed all the adaptive tools we required in Chapter 3, and here we simply need to apply them correctly by creating a suitable system architecture to invert the channel. The required system is shown in Figure 4.8, where we have m MISO blocks, the structure of which is shown in Figure 4.9. The MIMO channel has M inputs and P outputs, the equaliser has P inputs and M outputs, and there are P noise sources applied at the receiver.

The system is a simple application of the adaptive techniques developed in Chapter 3. We will be using the M-NLMS algorithm to adaptively invert the system and hence this will result in the MMSE inverse which properly compensates for receiver noise. The analysis of this system follows the same procedure as the time-domain inverse in Section 4.2.2. In the absence of noise this will result in a zero-forcing solution. The computational cost of this method is that of the adaptation algorithm used, hence $\mathcal{O}(L_g)$ for the M-NLMS.

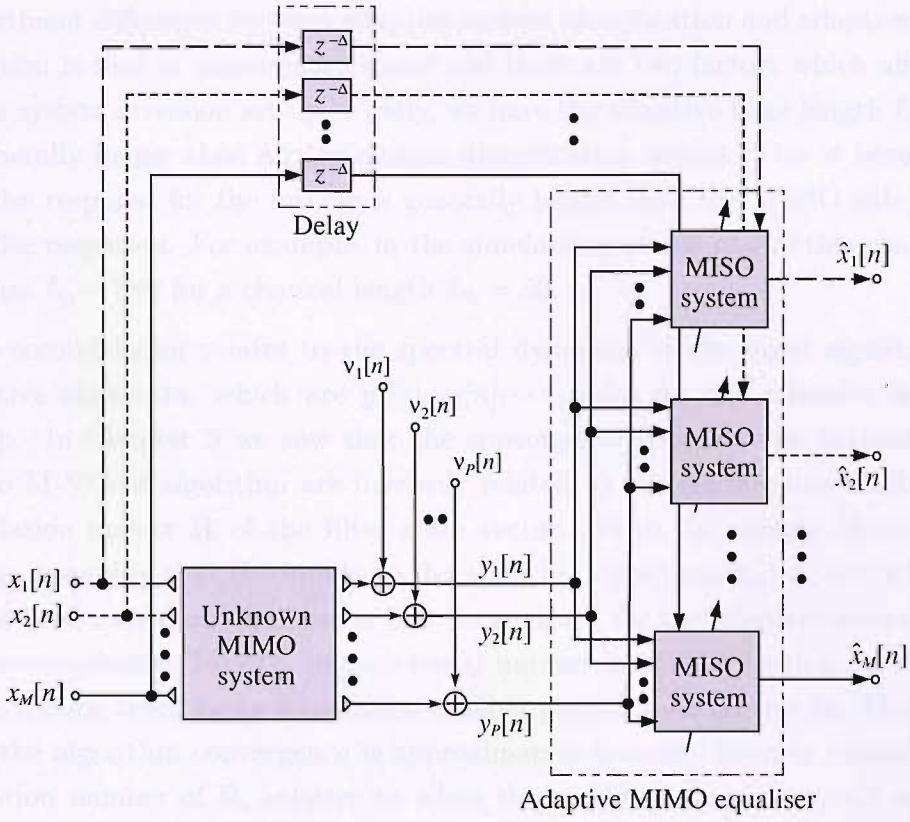

Fig. 4.8: Block diagram showing adaptive system set-up to obtain the response for the inverse of the unknown MIMO channel.

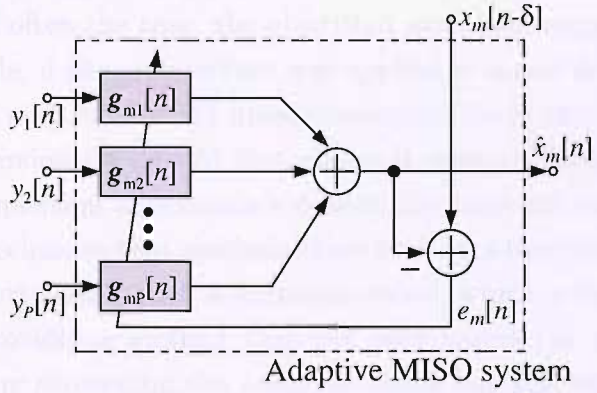

Fig. 4.9: An adaptive MISO system.

4.3.2 Convergence Characteristics

A pertinent difference between adaptive system identification and adaptive system inversion is that of convergence speed and there are two factors which affect this in the system inversion set-up. Firstly, we have the adaptive filter length L_g which is generally longer than for the system identification set-up. This is because the impulse response for the inverse is generally longer than the MIMO sub-channel impulse responses. For example, in the simulations at the end of this chapter we will use $L_g = 280$ for a channel length $L_h = 50$.

The second factor relates to the spectral dynamics of the input signals to the adaptive algorithm, which are $y_1[n], y_2[n], \cdots, y_P[n]$ for the adaptive inversion set-up. In Chapter 3 we saw that the convergence speed of the natural modes of the M-NLMS algorithm are inversely related to the eigen-values of the auto-correlation matrix $\mathbf{R}$ of the filter state vector. With the system identification set-up, assuming that the inputs to the adaptive algorithm, $x_m[n]$, are 'white', $\mathbf{R}$ would have a condition number of one. In contrast, for the adaptive inversion, the frequency-selective MIMO channel would impose spectral colouring on the algorithm inputs, resulting in a condition number greater than one for $\mathbf{R}$. This means that the algorithm convergence is approximately inversely linearly related to the condition number of $\mathbf{R}$, relative to when the condition number equals one. We would therefore expect that adaptive inversion set-up would converge slower than for adaptive identification and depending of the severity of the spectral dynamics of the MIMO sub-channels this can result in a significant slowing of convergence. In extreme cases for highly frequency-selective channels the number of algorithm iterations required to reach a suitably small adaptation MSE can mean that the adaptive inversion method is unfeasible, as not only would this required a greater computational overhead but, if the processing power available to the algorithm is restricted as if often the case, the algorithm would converge too slowly in real time. For example, if the architecture was applied to a real device such as a MS, the performance may be deemed unsatisfactory. This is the main draw-back of the adaptive inversion set-up. At first glance it seemed like an ideal solution as it is simple to implement and avoids a potentially awkward analytic inversion. If we could find a technique that combats these problems then this would be greatly advantageous. Fortunately such a technique exists, which is that of subband processing. This provides a method that not only lowers the computational cost of this solution by shortening the adaptive filters but also effectively "whitens" the algorithm inputs for the adaptive inversion set-up resulting in an increased convergence speed. Subband techniques are the topic of Chapter 5.

4.4 Adaptive Equaliser Tracking

An important potential application of the adaptive inversion set-up described in the previous section is tracking of the equaliser with a temporally dynamic channel. If we consider a channel that fades over time and which can be modelled using the methods described in Chapter 2, then the MMSE equaliser will also vary over time. Adaptive system inversion can be used to track the actual equaliser to the MMSE solution with some lag. A problem with this method is that it would require a training sequence known to the receiver to transmitted for the entire time while the channel is fading, which clearly leaves no available time to transmit actual data. If however we were to transmit data the equaliser could not track variations in the channel, and the MSE and hence BER would degrade and eventually no meaningful data could be transmitted.

A solution is to run the adaptive algorithm in a *decision-directed* mode [72]. Previously we have assumed the use of a training sequence known to both transmitter and receiver and the adaptive algorithm can converge from this. If however for a particular point in time, the equaliser is known to be MMSE, if for example it has been found using an analytic method and we assume the post-decision output of the equaliser is error-free, the adaptive algorithm may use this as the desired signal instead of the training sequence. Hence it may be considered as a partially-blind method, since the receiver does not need to know the transmitted signal in order to track. In this case the adaptation curve gained from when a training sequence is used for adaptation is the best performance bound of an adaptive filter running in decision-directed mode, i.e. if the equaliser output is error-free the performance of the decision-directed system is the same as that of the trained system. Later we will show these best-performance-bound results for the adaptive tracking of an equaliser to a fading MIMO channel.

4.5 Other Adaptive Equalisation Techniques

No chapter on adaptive equalisation would be complete without at least a mention of other adaptive equalisation techniques based on other adaptive algorithms, and also so-called blind adaptive techniques where no training sequence is required. We have concentrated exclusively on LMS-type algorithms in this thesis, however another algorithm of note is the recursive least squares (RLS) in its standard and various modified forms. One application of note was shown in [133, 134] the where a state-space approach [135] with Riccati recursions was used to perform adaptive equalisation of frequency-selective MIMO channels. The proposed method

resulted in an optimum least squares solution, which is the same as the MMSE solution in stationary channels. Another interesting method was shown in [122, 136] and although the application was for cross-talk cancellation in acoustics it should also be possible to use the method for adaptive equalisation of communication signals through a frequency-selective MIMO channel. The method is an interesting variation of the time-domain analytic inversion but where the inversion is performed using a recursive technique closely related to the RLS algorithm. As it is essentially an analytic inversion technique it requires channel knowledge which must be obtained using adaptive identification, but unlike the analytic methods already considered in this chapter which required full channel knowledge before the analytic inversion can be performed, the proposed algorithm finds the optimum inverse filters, in a least squares sense, in a time-recursive manner whereby if we arrange for the adaptive identification system to find the impulse response of the channel one tap at a time, then the algorithm iteratively converges to the optimum inverse filters over time as new channel knowledge is gained. This means that by the time the adaptive identification process is complete, the optimum inverse filters have already been found and a second post-identification analytic inversion stage is not required. The algorithm was shown to be computationally robust with a computational cost comparable to the $\mathcal{O}(L_g^2)$ of the Levinson-Durbin algorithm briefly mentioned in Section 4.2.2.

In the area of fully blind adaptive equalisation of frequency-selective MIMO channels, two interesting works have been selected. The first shows a performance analysis of a blind adaptive MIMO equaliser based on the Constant Modulus Algorithm (CMA) [137]. The authors proposed a new CMA algorithm which can recover all channel inputs simultaneously while removing all ISI and CCI and demonstrated its favourable behaviour through use of simulations. The second work of note develops a direct blind equalisation algorithm based on the periodic auto-regressive (AR) model matching of multi-channel FIR systems, which can use either the LMS or circular lattice adaptive algorithms for convergence, and results where shown using this algorithm [138]. For further background on blind adaptive equalisation algorithms the reader is referred to [138] and the references therein.

Here we have given a very brief overview of other MIMO adaptive equalisation methods, but we shall not mention any of these further, concentrating instead on the analytic and adaptive techniques developed previously in this chapter.

4.6 Simulations and Discussion

This section presents various simulation results obtained by applying the methods, algorithms and techniques discussed in this chapter.

4.6.1 Analytic System Inversion

We start by applying the analytic inversion techniques developed in Section 4.2, namely the z, time and frequency-domain methods. We show MSE versus SNR performance results for a range of static MIMO channels chosen from those outlined in Chapter 2 with AWGN added at the receiver. We consider the cases where the receiver has perfect channel knowledge, found by a previous identification for example.

Firstly we examine the results from the two-tap 2×2 MIMO channel which has a non-minimum phase determinant in the z-domain. The stabilisation technique will need to be used, and length-32 FIR filters are used to approximate the unstable part of the IIR determinant in the inverse, however remembering that this technique unlike the time and frequency-domain methods still has a stable IIR part. For the time and frequency-domain inverses length-32 filters are also used. The Channel-Equaliser Response (CER) MSE values in a noiseless environment and the CER MSE versus SNR behaviour for the three different inversion techniques are shown in Table 4.1 and Figure 4.10 respectively. We see that in a noiseless environment, the z-domain method results in the best performance, better than the MMSE time-domain method, due to its IIR part. Although it uses the unfavourable ZF inversion criterion this does not cause any ill effects in a noiseless environment. The frequency-domain method performs the worst due to the circular convolution effects inherent in this method, but still quite satisfactorily at significantly lower computational cost. In the MSE versus SNR plots we see that at low SNRs the time-domain and frequency-domain techniques perform similarly to each other and both are better than the z-domain technique on account of the different inversion criterion, i.e. the MMSE inverse will perform better than the ZF inverse in the presence of significant noise. At mid SNR levels all the performances are similar. It was explained in Section 4.2.3 that a regularisation factor should be used even in a noiseless environment on account of the circular convolution effects but here the optimum factor is found to be approximately zero, so this is the best performance possible with the frequency-domain technique. Calculating the complexity orders for relative comparison, the z-domain order evaluates to 8, the time-domain to 32,768, and the frequency-domain to 160. Hence, the frequency-domain method appears to have the best overall performance since at

Inversion	z-domain	time-domain	frequency-domain
Noiseless MSE [dB]	-52	-46	-32

Tab. 4.1: Noiseless CER MSE values for two-tap channels

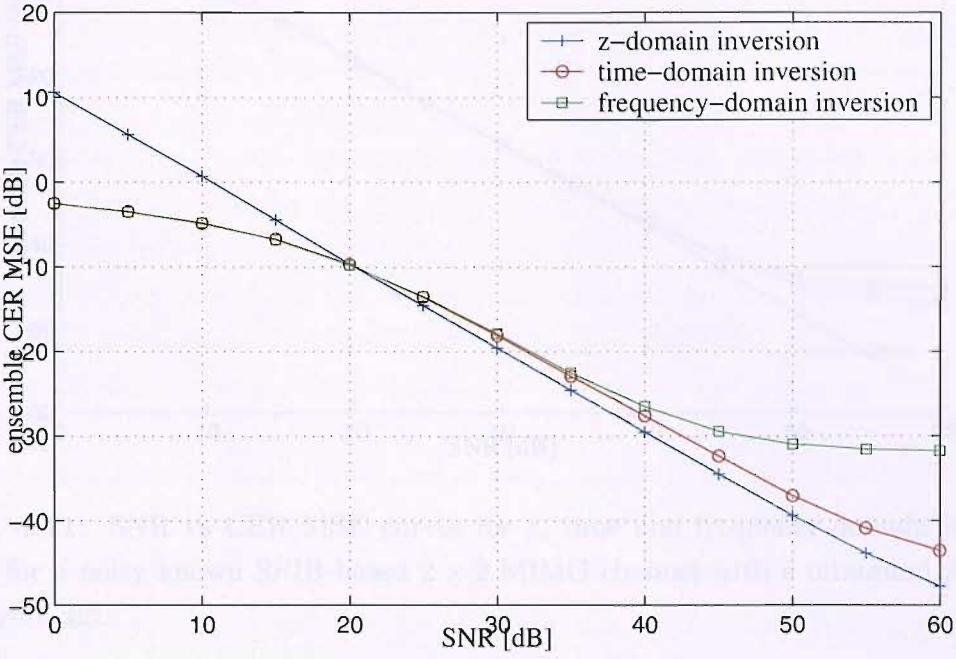

Fig. 4.10: SNR vs Channel-Equaliser Response (CER) MSE curves for z, time and frequency-domain inversion for a noisy known two-tap 2×2 MIMO channel.

the more realistic lower SNR values its performance is same as the optimum MMSE time-domain method, but at approximately 0.5% of the computational cost.

Table 4.2 and Figure 4.11 respectively show the noiseless CER MSE and CER MSE versus SNR performance results for the analytic inversion of the SPIB-based 2×2 MIMO channel with a minimum phase determinant. Length-280 filters are used for the time-domain and frequency-domain equalisers. The theoretical noiseless MSE is zero for z-domain inversion and in practice the calculation is limited by the numerical accuracy of the simulation tool. Again we see the worst performance is given by the frequency-domain method due to circular convolution effects, but the margin between this and the time-domain method it now not as great as it

Inversion	z-domain	time-domain	frequency-domain
Noiseless MSE [dB]	$-\infty$	-47	-46

Tab. 4.2: Noiseless CER MSE values for SPIB-based channels with a minimum phase determinant.

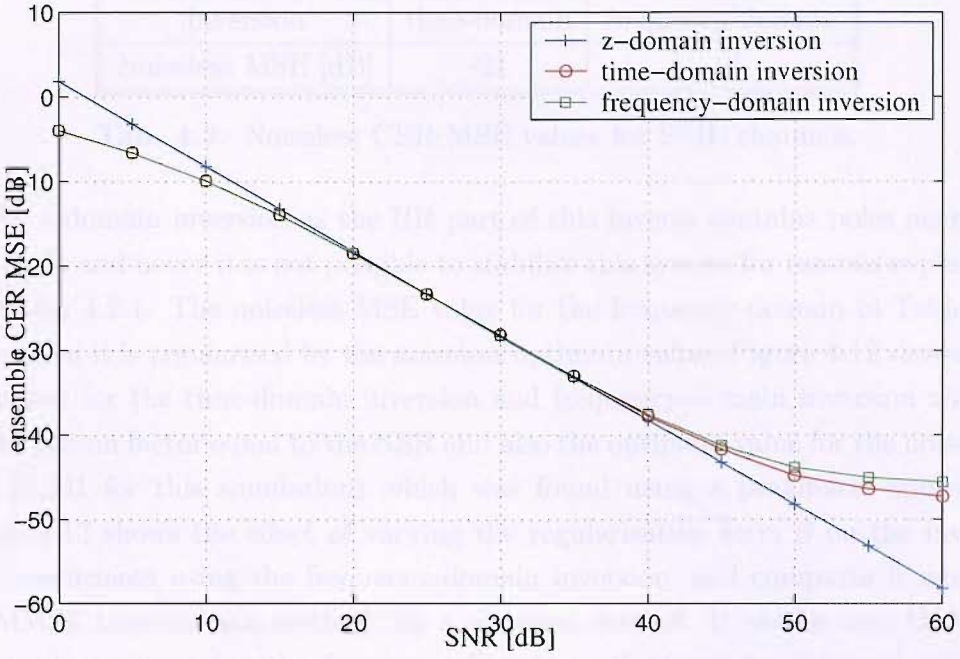

Fig. 4.11: SNR vs CER MSE curves for z, time and frequency-domain inversion for a noisy known SPIB-based 2×2 MIMO channel with a minimum phase determinant.

was for the two-tap channel. Also, for these channels the best performance was given for a regularisation factor of zero in the noiseless environment. In the MSE versus SNR plot, at low and mid SNR the relative performances are similar to the two-tap channel. At high SNR the z-domain method is still the best as with the two-tap channel but the time-domain and frequency-domain inverse performances are much closer to each other now. As the determinant is minimum phase, no stabilisation is required for the z-domain inversion and with a complexity order that evaluates to approximately 282 has a significantly lower computational complexity than the other two methods. The time-domain method has a complexity order of 2.2×10^7 and for the frequency-domain method it is approximately $2,276$. Hence, for this channel, the z-domain method seems to give the best overall performance compromise between the MSE and computational cost, given that the MSE is only about 3 dB worse that the MMSE performance at SNR=0.

Now we move on to the performance of the unmodified symbol-spaced (SS) SPIB channels. For the purposes of fast simulations these were truncated to length 50 responses so that the whole of the significant part of the responses were retained but the relative alignment between the channels was unaltered. Table 4.3 and Figure 4.12 show the noiseless CER MSE and CER MSE versus SNR behaviour, respectively, for length 280 inverse systems. Firstly notice that there is no result

Inversion	time-domain	frequency-domain
Noiseless MSE [dB]	-21	-16

Tab. 4.3: Noiseless CER MSE values for SPIB channels.

for the z-domain inversion as the IIR part of this inverse contains poles near the unit circle and hence it is not possible to stabilise this system for reasons explained in Section 4.2.1. The noiseless MSE value for the frequency-domain in Table 4.3 is for when it is regularised by the noiseless optimum value. Figure 4.12 shows the behaviour for the time-domain inversion and frequency-domain inversion with a regularisation factor equal to the NSR and also the optimum value for the noiseless case (0.001 for this simulation) which was found using a pragmatic approach. Figure 4.13 shows the effect of varying the regularisation term β on the inverse filter coefficients using the frequency-domain inversion, and compares it against the MMSE time-domain method, for a noiseless channel. It can be seen that the best performance using the frequency-domain method can be obtained using a non-zero β. Hence from this it is clear that when regularising by the NSR the performance will begin to worsen once the SNR rises above some value.

It is interesting to see that the performance of the frequency-domain method regularised by the NSR approaches that of the MMSE time-domain method at low SNR values, where the noise dominates the error performance over the circular-convolution effects inherent in this method. At higher SNRs the frequency-domain method achieves the best MSE using a fixed regularisation factor of 0.001, which is specific to this channel. Hence at the cross-over at around a SNR of 20 dB the regularisation factor could be switched to give the best possible performance. Although the time-domain method still outperforms at higher SNRs, at the more realistic lower SNR values the frequency-domain method performs just as well and at a considerably lower computational cost. Since inverse filters of the same length as for the previous SPIB-based minimum phase determinant channel are being used, similar computational savings are possible with the frequency-domain method.

Finally for this section, the performance for the 100 MHz bandwidth Saleh-Valenzuela (SV) channels is simulated. Parameters used for this channel are $1/\Lambda = 300$ ns, $1/\lambda = 5$ ns, $\Gamma = 60$ ns and $\gamma = 20$ ns, making it a suitable model for indoor environments. The channel is resampled at 100 MHz using the method explained in Chapter 2 and truncated to length 30, which retains the significant part of the response of the channel. The inverse filters used are length 280 as in the previous simulations. There is one fundamental difference between this simulation and the previous ones, which is that the SV channels are realised using

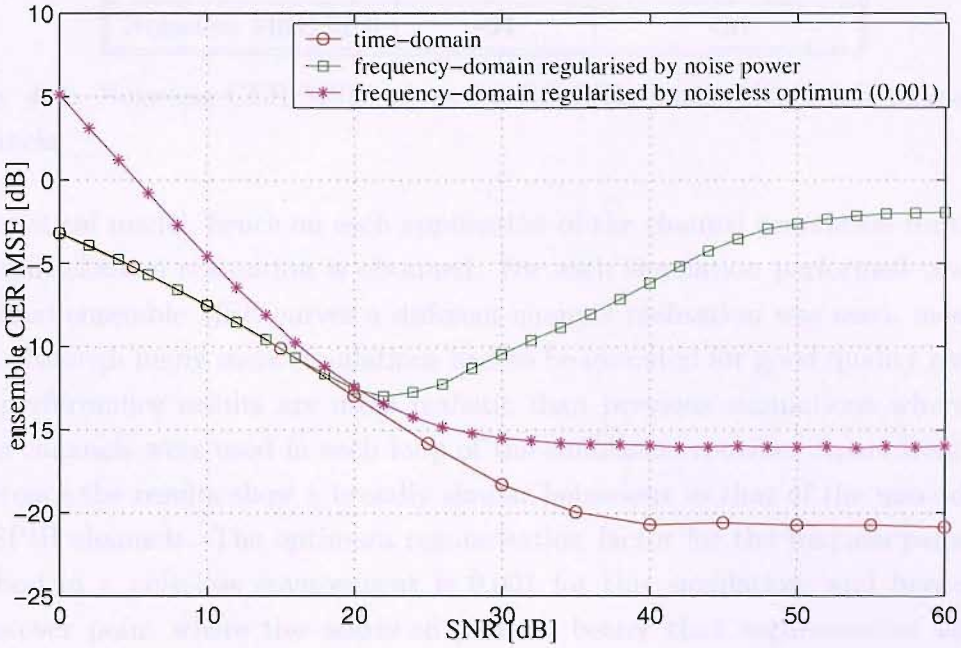

Fig. 4.12: SNR vs CER MSE curves for z, time and frequency-domain inversion for a noisy known SS SPIB 2×2 MIMO channel.

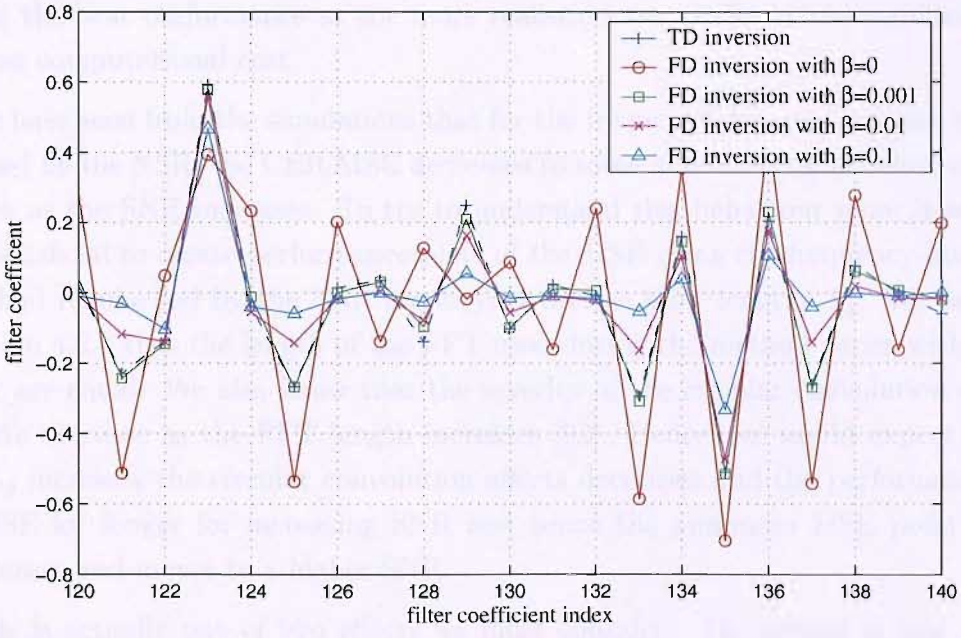

Fig. 4.13: Portion of inverse filter coefficients for a noiseless known SS SPIB 2×2 MIMO channel, calculated using the time-domain (MMSE) and the frequency-domain techniques with a range of regularisation factors.

Inversion	time-domain	frequency-domain
Noiseless MSE [dB]	-34	-26

Tab. 4.4: Noiseless CER MSE values for 100 MHz bandwidth Saleh-Valenzuela channels.

a statistical model; hence on each application of the channel generation routine a different channel realisation is obtained. For each simulation performed towards the final ensemble MSE curves a different channel realisation was used, meaning that although many more simulations had to be executed for good quality results, the performance results are more realistic than previous simulations where the same channels were used in each loop of the simulation routine. Apart from this difference the results show a broadly similar behaviour to that of the unmodified SS SPIB channels. The optimum regularisation factor for the frequency-domain method in a noiseless environment is 0.001 for this simulation, and hence the cross-over point where this starts to perform better than regularisation by the NSR is at an SNR of 30 dB. The better performance of inversions of this channel when compared to the unmodified SS SPIB channel is due to the shorter channel length, i.e. 30 for the SV channels and 50 for the SPIB channels. The complexity comparison is the same as previously as again length-280 inverse filters are used. Hence we again come to the same conclusion that the frequency-domain method gives the best performance at the more realistic lower SNRs at the significantly lowest computational cost.

We have seen from the simulations that for the frequency-domain inversion regularised by the NSR, the CER MSE decreases to some minimum value before rising again as the SNR increases. To try to understand this behaviour more it would be beneficial to create performance plots of the MSE using the frequency-domain method regularised by the NSR for varying inverse filter lengths L_g. We saw in Section 4.2.3 that the length of the FFT used during the method varies with L_g they are equal. We also know that the severity of the circular convolution error effects decrease as the FFT length increases [92]. Hence, we would expect that as L_g increases the circular convolution effects decreases and the performance is MMSE for longer for increasing SNR and hence the minimum MSE point also decreases and moves to a higher SNR.

This is actually one of two effects we must consider. The second is that with smaller L_g we can expect the MSE performance to worsen as the filters can only model a decreasing amount of the true inverse filter response, in addition to the worsened circular convolution effect. On approaching an L_g where all the significant part of the true inverse response is modelled by the inverse filter, increasing

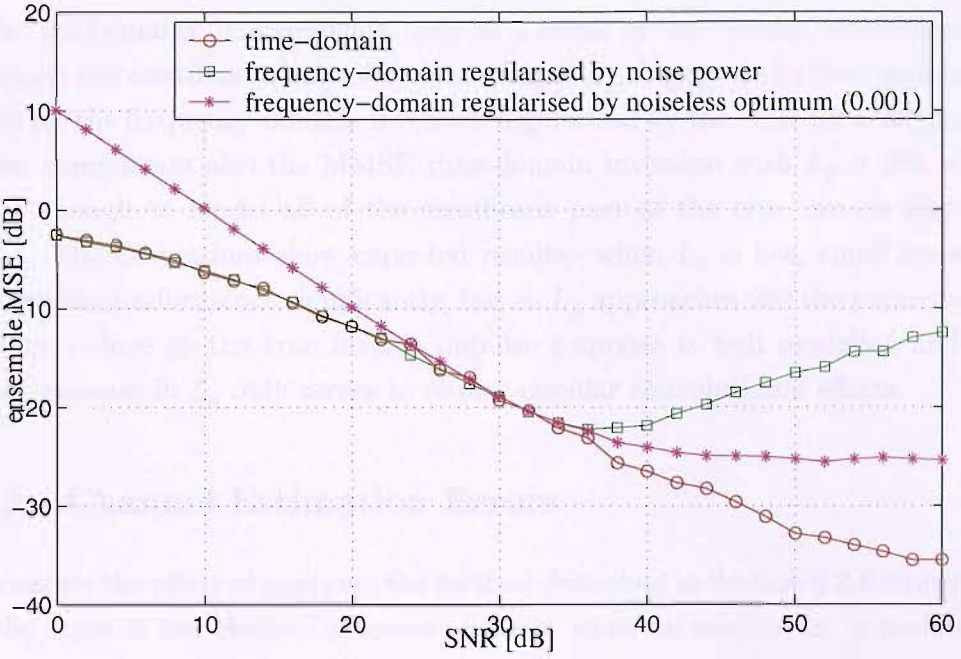

Fig. 4.14: SNR vs CER MSE curves for z, time and frequency-domain inversion for a noisy known 100 MHz bandwidth Saleh-Valenzuela 2×2 MIMO channel.

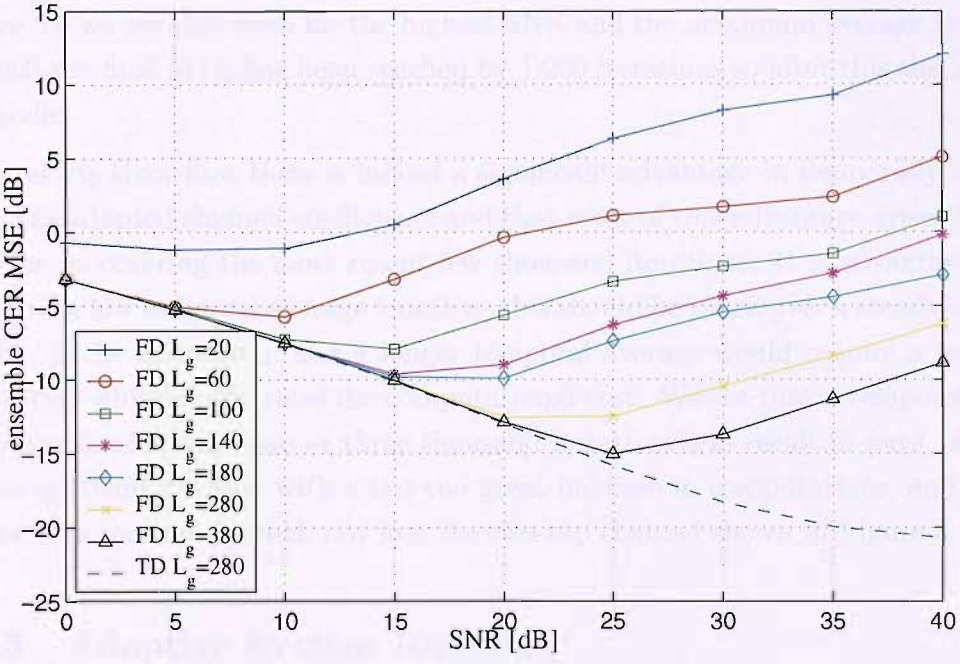

Fig. 4.15: SNR vs CER MSE curves for frequency-domain (FD) inversion for a noisy known SS SPIB 2×2 MIMO channel with variable equaliser length (L_g), and MMSE time-domain (TD) inverse with $L_g = 280$ for comparison.

L_g will improve the MSE due to the modelling error no further and we can expect smaller performance improvements only as a result of the circular convolution effect which will continue to reduce with increasing L_g. Figure 4.15 shows simulation results for the frequency-domain inversion regularised by the NSR for a varying L_g and for comparison also the MMSE time-domain inversion with $L_g = 280$ which is long enough to model all of the significant part of the true inverse filter response. The simulations show expected results– when L_g is low, small increases improves the performance significantly, but as L_g approaches 280 the performance increases reduce as the true inverse impulse response is well modelled and the further increase in L_g only serves to reduce circular convolutional effects.

4.6.2 Channel Estimation Errors

We consider the effect of applying the method described in Section 4.2.6 to average out the noise in the channel estimates present when an adaptation is performed in a noisy environment. Figure 4.16 shows the vectorial difference between the adapted channel estimate and the actual channel for the two-tap channel after the final MSE attained has been reached for a range of SNRs. The adaptation was executed for 10,000 iterations and results are shown for a temporal average of the channel coefficients for up to the final 9,000, of these iterations. Referring to Figure 3.6 we see that even for the highest SNR and the maximum average length of 9,000 the final MSE has been reached by 1,000 iterations so after this the MSE is ergodic.

The results show that there is indeed a significant advantage in temporally averaging the adapted channel coefficients and that most of this advantage arises from the average covering the most recent few thousand iterations. It is advantageous to choose a low temporal average length as this should be taken over a steady-state portion of the adaptation and a longer temporal average would require a longer adaptation which would raise the computational cost. We see that a temporal average length of around two or three thousand iterations will result in most of the advantage being realised with a not too great increase in computations, and this will be true for any channel, not just the two-tap channel shown in Figure 4.16.

4.6.3 Adaptive System Inversion

This section examines the convergence characteristics of a fully adaptive inversion of unknown static noiseless MIMO channels as explained in Section 4.3. The convergence behaviour of the M-NLMS algorithm is shown in Figure 4.17 for the

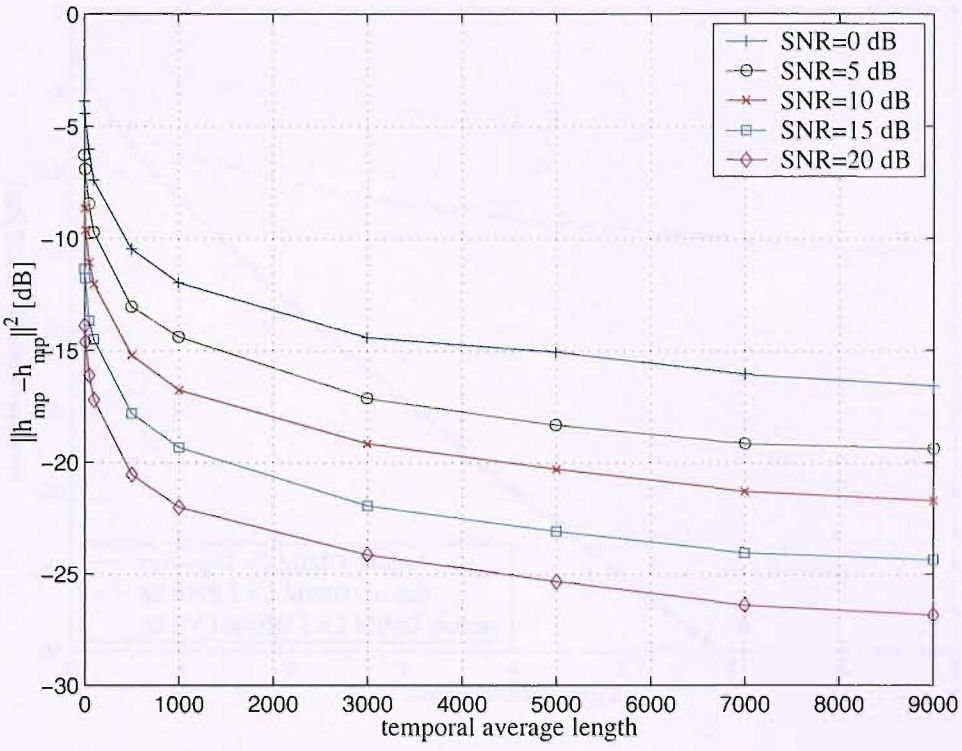

Fig. 4.16: Channel estimation error against temporal average length for a two-tap 2×2 MIMO channel, a 10,000 iteration adaptation and a range of SNRs.

two-tap, unmodified SS SPIB and 100 MHz bandwidth SS Saleh-Valenzuela (SV) 2×2 MIMO channels, which we discuss in turn. For all the simulations an adaptive step-size coefficient $\tilde{\mu} = 0.18$ was used and the algorithm was executed for 80,000 iterations. In all the simulations we see overall behaviour of fast initial convergence as the fastest eigen-modes converge before reaching a constant gradient which represents the convergence of the slowest eigen-mode. For the two-tap channel a length-32 adaptive system was used and we see that after 50,000 the MSE has reached -35 dB. The two-tap channels are frequency-selective and the spectral range of the four channels comprising the MIMO channel over the full band varies between 2 dB and -7 dB, so even though the multi-channel adaptive filters are 64 taps long (i.e. 2×32) the convergence is considerably slower than the identification for even the length-50 SPIB channel in Chapter 3 for example, which converges from white inputs. Both the SPIB and SV inversions use length-280 filters, hence they are both slower than the two-tap channel inversion but notice that the SV inversion converges slower than the SPIB inversion. This can be explained by referring to the magnitude response plots of the channels in Chapter 2. The SS SPIB magnitude responses vary very little over the 30 MHz channel bandwidth (i.e. -15 MHz to +15 MHz) and hence colours the signal very little, however the SV channels are far more frequency-selective, meaning that the signals at the output

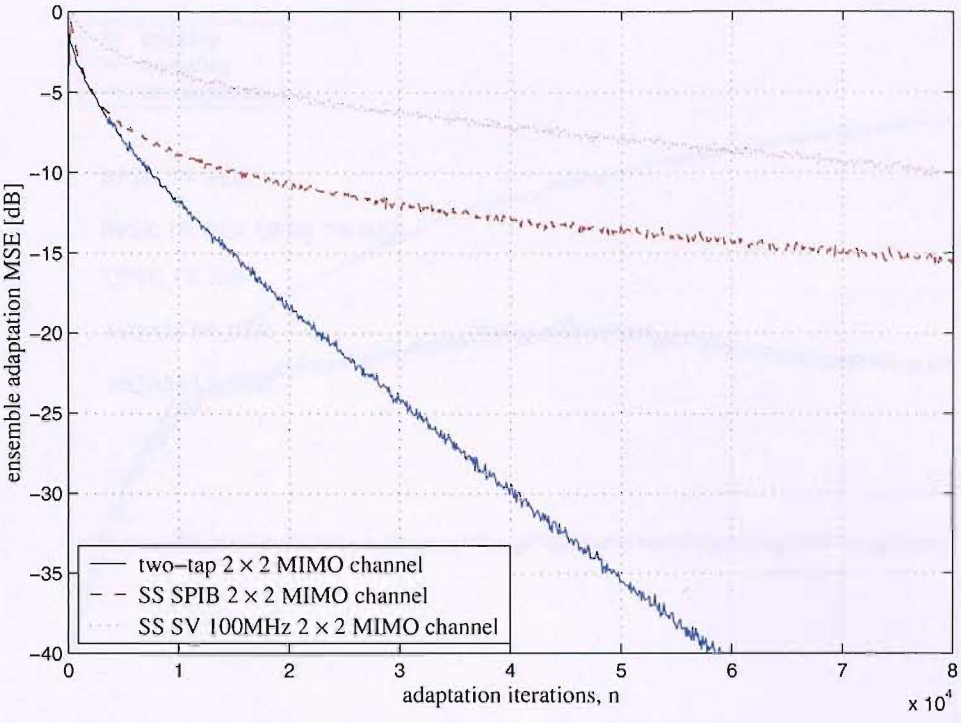

Fig. 4.17: Adaptation MSE curves for adaptive inversion for unknown static noiseless two-tap, SS SPIB and 100 MHz bandwidth Saleh-Valenzuela 2×2 MIMO channels.

of this channel will result in a comparatively slower convergence.

These results confirm the proposition in Section 4.3.2, which was that the convergence of the MIMO adaptive inversion especially for a frequency-selective channel will be too slow in comparison to the analytic method. In fact as the algorithm would be required to converge for several of tens of thousands of iterations for any of the channels the computational cost is likely to be considerably greater than the frequency-domain analytic method. Although the M-NLMS algorithm has $\mathcal{O}(L_g)$ cost per iteration against the $\mathcal{O}(L_g \log_2 L_g)$ of the frequency-domain method, it is obvious that the analytic method would result in the lowest computational cost due to the fact that the computation would only have to be performed once.

4.6.4 Adaptive Equaliser Tracking

In this section we examine the tracking capability of the M-NLMS algorithm, where the inverse of the channel is tracked. The SPIB and SV100M channels are used, with an MS moving at 120 km/h, which is assumed to be the highest speed at which the system will be expected to have to function. Both the SPIB and SV100M channel are considered to be harsh compared to the channels that

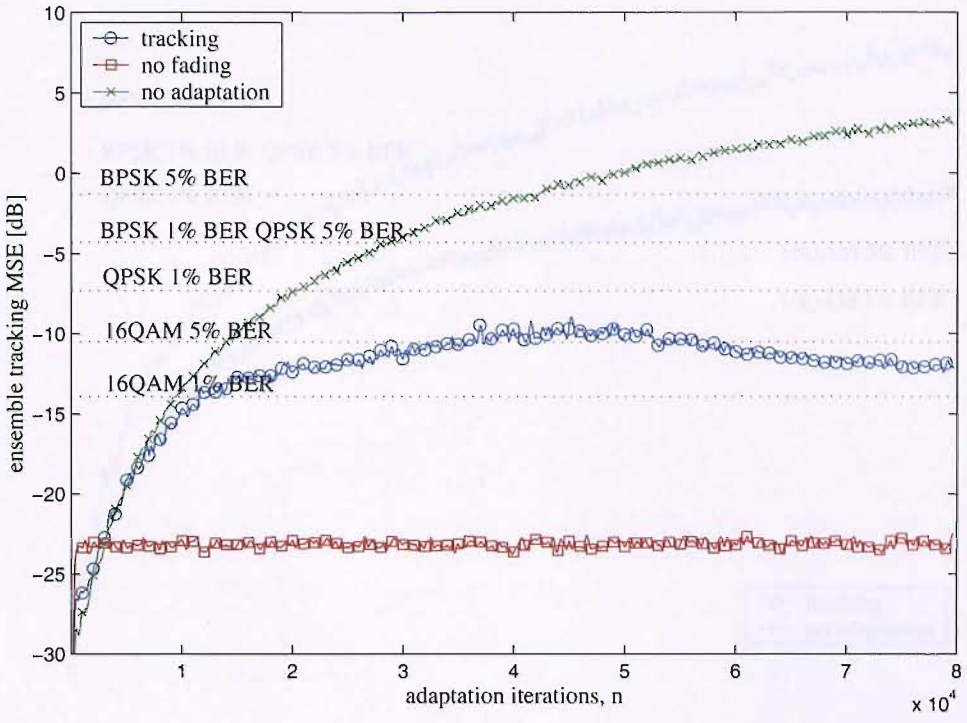

Fig. 4.18: Adaptive equaliser tracking MSE for Doppler-filtered Rayleigh-fading 2×2 MIMO SPIB channel using M-NLMS algorithm with $\tilde{\mu} = 0.18$, and MS moving at 120 km/h.

current day mobile systems experience. Hence the harshest set of conditions that the system is likely to encounter is chosen and this is investigated as a worst case scenario.

Figure 4.18 shows the tracking performance to the inverse of the SPIB channel. Also shown are plots for a channel which does not fade and the equaliser adaptive algorithm is iterated, and for when the channel fades but the adaptation is not performed. These represent the best and worst cases respectively and we would expect a system tracking when the channel is fading to perform somewhere between these two extremes. Further, the proximity of the tracking result to either extreme gives an idea of the performance of the algorithm. The systems are initialised with near-MMSE equaliser knowledge at the start, calculated using the frequency-domain inversion method. After this the channel begins to fade, hence the MMSE equaliser will vary and the system must track these changes. Also shown are theoretical error probability levels for BPSK, QPSK and 16-QAM modulation, where the error is assumed to be white. This is a reasonable assumption when the error characteristic is averaged over many channel realisations. Here the performance is approximately half way in between the extremes by the end of the simulation and is able to maintain an MSE that would result in a BER of

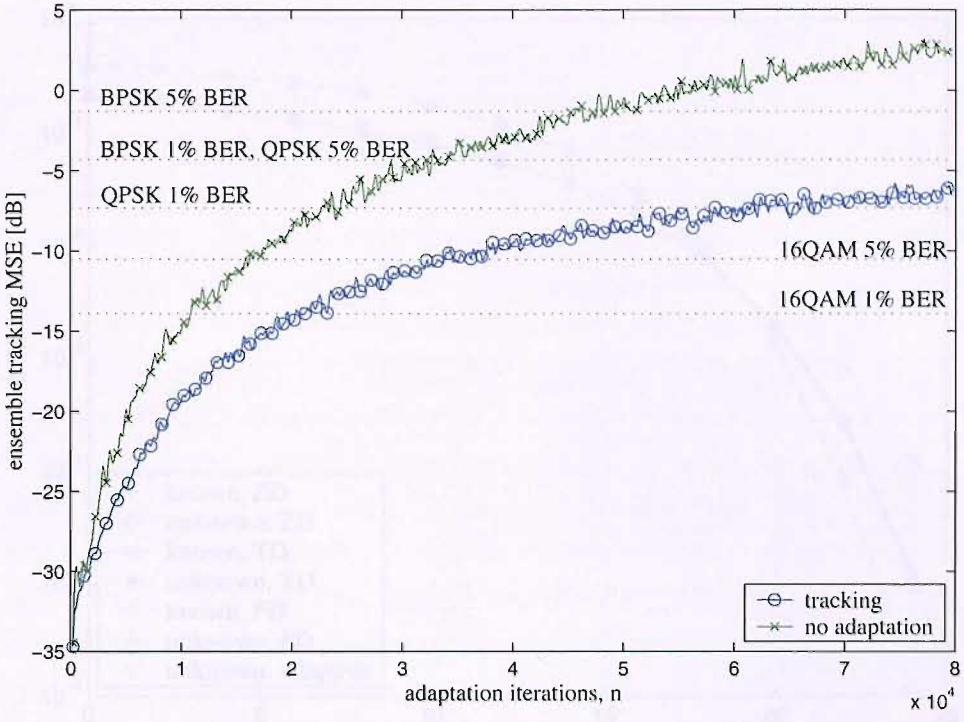

Fig. 4.19: Adaptive equaliser tracking MSE for Doppler-filtered Rayleigh-fading 2×2 MIMO SV channel sampled at 100 MHz using M-NLMS algorithm with $\tilde{\mu} = 0.18$, and MS moving at 120 km/h.

between 1% and 5% with 16-QAM modulation, or less that 1% with QPSK.

Figure 4.19 shows the tracking performance to the inverse of the SV100M channel and also the trajectories when there is no adaptation and no fading. The performance with no fading here is well below the -35 dB representing the lower range of the result axis, hence not shown. We see that the performance is reasonable but not great, with the MSE having crossed above the 1% BER level for QPSK by the end of the simulation. The tracking performance is very close to the worst case of using no adaptation relative to the best case. The trajectory when there is no adaptation shows that the fading would cause useless performance by the end of the simulation. However even by the end of the simulation the tracking MSE is still slowly rising and it is likely that the performance would worsen even further. Also, the performance shown in the figure shows the best case tracking, since a real system would function in decision-directed mode if it is to continually track, in which case the convergence would be worsened by decision errors.

Hence we are motivated to find an alternative technique which will perform adequately. A possible method is to track the channel itself as shown in Chapter 3 which gives better performance and then periodically analytically invert the system as and when required to re-calculate the current equaliser. This has the disad-

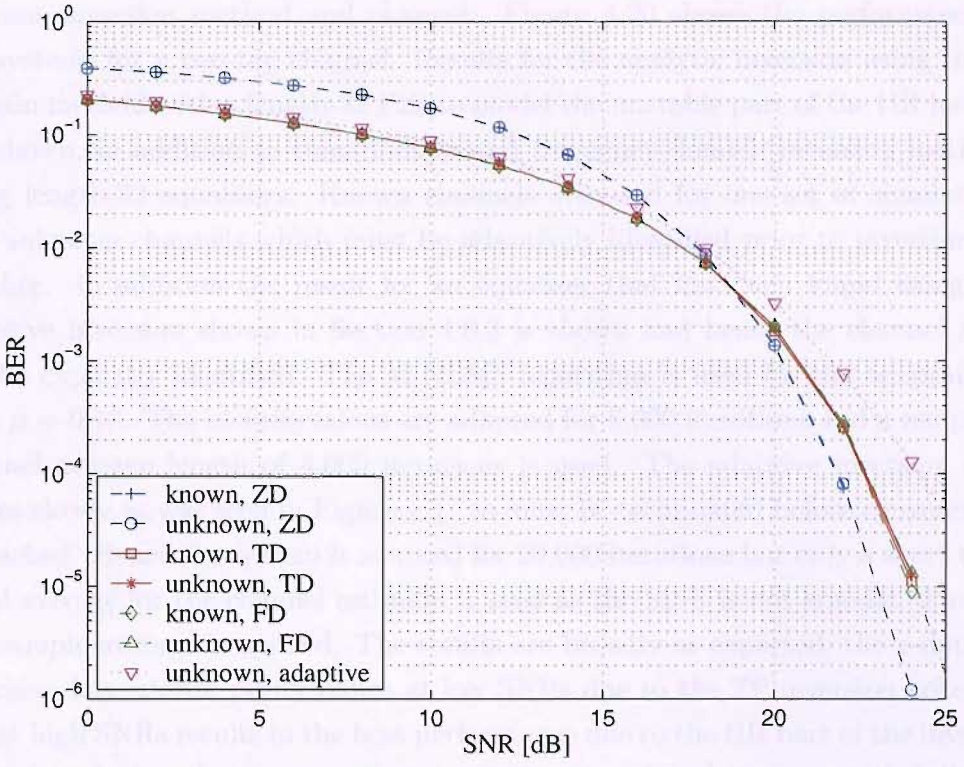

Fig. 4.20: SNR vs BER curves for z-domain, time-domain, frequency-domain and adaptive inversion for an unknown noisy static two-tap 2×2 MIMO channel using BPSK.

vantage that between the periodic updates the system performance will worsen, and then jump back to a lower MSE. This will result in a cyclical MSE and hence BER performance which is not ideal. Also, the rate at which the channel inversions must be performed is dependent on the MS speed and at high speed this method may result in a high computational cost. An alternative technique is to employ subband adaptive systems which have been shown to result in superior convergence speed at significantly reduced computational cost and hence we could expect the tracking behaviour to be better. Subband systems are the subject of the next chapter.

4.6.5 System BER Performance

We now show simulations for the BER versus SNR performance characteristics for various full systems created using the tools we have developed in this section for the two-tap, unmodified SS SPIB and 100 MHz bandwidth SS SV 2×2 MIMO channels, using BPSK modulation. For the inversion methods we consider, the inverse filter parameters are the same as those in Sections 4.6.1 and 4.6.3 for the

relevant inversion method and channel. Figure 4.20 shows the performance of the systems for a two-tap channel. Results for the analytic inversion using the z-domain method with a length-32 FIR to model the unstable part of the IIR inverse are shown, in addition to time-domain and frequency-domain inversion methods using length-32 equalisers. Known channels are used for one set of simulations and unknown channels which must be adaptively identified prior to inversion for another. In addition the result for an equaliser that has been found using the adaptive inversion shown in Section 4.6.3 is shown and hence the channel need not be explicitly identified. The M-NLMS algorithm is used for the adaptations with $\tilde{\mu} = 0.18$. The identifications are adapted for 6,000 iterations and a temporal channel average length of 4,000 iterations is used. The adaptive inversion converges slowly as was seen in Figure 4.17 so must be terminated before convergence is reached. Hence the system is adapted for 20,000 iterations but only a short temporal average for the channel estimate is used as the MSE is not ergodic. Thus, a 500 sample average is applied. The results are broadly as expected; the z-domain inversion has inferior performance at low SNRs due to the ZF inversion criterion but at high SNRs results in the best performance due to the IIR part of the inverse. Even though the adaptive inversion simulations are the most computationally intensive due to the long adaptation required, sub-optimal performance is obtained as the adaptation is terminated before convergence. Both the time-domain and frequency-domain methods result in the optimal FIR MMSE performance over all SNRs, as the optimum noiseless regularisation factor is approximately zero. This, coupled with the lowest computational cost of all the methods, makes the frequency-domain inversion the most attractive. The BER performance for the systems adaptively identifying the unknown channels perform as well as the systems with a known channel, showing the noisy adaptations have no ill effect when the channel coefficient temporal averaging technique is used.

Figure 4.21 shows the BER performance for the SS SPIB channels, and has some interesting differences from the two-tap channels. Firstly, we notice that there is no result for a z-domain inversion as this would be unsuccessful for this channel due to stability problems. There are results for time-domain and frequency-domain inversion of the known channel and for the unknown channel where prior identification is required. There is also a result for adaptive inversion where channel knowledge is not required. A step-size $\tilde{\mu} = 0.18$ is used for all adaptations and $L_g = 280$. The time-domain gives the optimum MMSE result and hence best performance. The frequency-domain method has results for a regularisation factor of the NSR and the fixed noiseless optimum value (0.001 for this simulation). For the regularisation factor equal to the NSR we see the BER performance improves until the SNR reaches approximately 22 dB, above which the performance worsens again as the

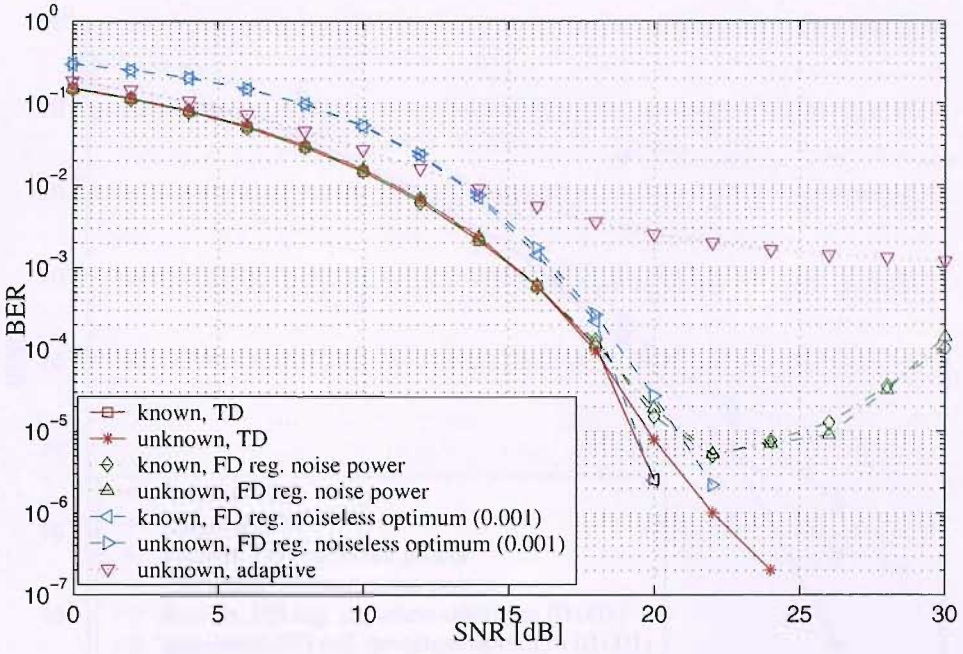

Fig. 4.21: SNR vs BER curves for time-domain, frequency-domain and adaptive inversion for an unknown noisy static SS SPIB 2×2 MIMO channel using BPSK.

regularisation factor moves below the noiseless optimum. Correspondingly, the point where the performance of the method regularised by the noiseless optimum crosses and becomes better than that of the NSR regularisation curve is slightly lower. For these higher SNRs it is beneficial to switch to a fixed regularisation factor. The adaptive identifications that are performed prior to analytic inversion are executed for 8,000 iterations, of which the tap coefficients of the last 4,000 iterations were averaged to give a better channel estimate. At lower SNRs this results in the same BER performance as for the known channels as the noise error dominates over the adaptation error, but at higher SNRs the the performances diverge slightly. Evidently, the adaptation time and channel estimate averaging length should be chosen according to the SNR range in which the system is likely to have to function. The adaptive inversion terminated at 20,000 iterations with a length-500 adaptive coefficient temporal average shows the worst performance, although if the adaptation was left until full convergence MMSE performance would result; however as the adaptation takes so long this is unfeasible. The adaptive inversion performance is worse here than for the two-tap channel as the MSE attained during the 20,000 iteration adaptation is worse. Finally, it is interesting to notice that the MMSE SPIB channel performance is better than that of the two-tap channel despite the fact that the ratio between L_g and L_h is much greater for the two-tap channel. This is due to the fact that the chosen L_g for the SPIB simulation is very long given that the channel is spectrally quite flat and the two-

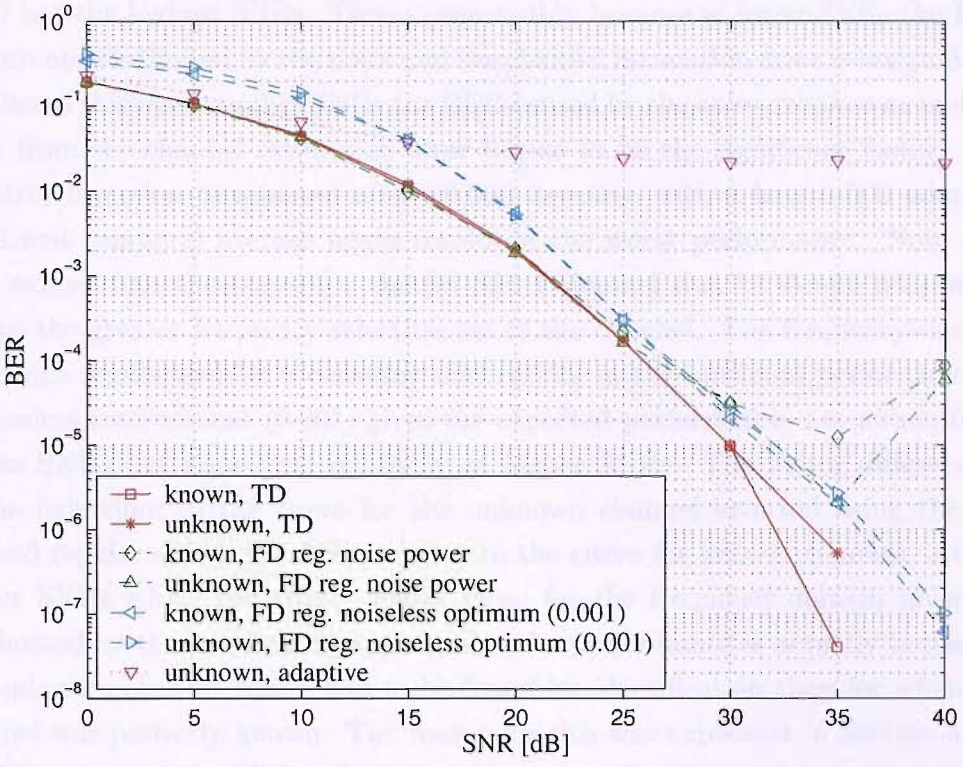

Fig. 4.22: SNR vs BER curves for time-domain, frequency-domain and adaptive inversion for an unknown noisy static 100 MHz bandwidth SV 2×2 MIMO channel using BPSK.

tap channel is more frequency-selective than the SPIB channel. Hence, despite first impressions based on the impulse response of the SPIB channel, it is evident that it really is rather benign.

Finally, for the BER performance curves, Figure 4.22 shows the BER versus SNR performance for a 2×2 MIMO 100 MHz bandwidth SS SV channel. As mentioned previously, unlike the earlier channels, the SV channel uses a statistical model and hence the channel realisation is different in every simulation run towards the ensemble mean. As a result, to obtain smooth curves requires a very large number of simulations but this was unfeasible due to computational limitations, hence the curves are not completely smooth – 1,000 different channel realisations are used in this simulation. Nevertheless they are of adequate quality to study the behaviour and there are some interesting points in the result. The system is adapted for 12,000 iterations with $\tilde{\mu} = 0.18$, and again uses length-280 equalisers and a length-4,000 adaptive coefficient temporal average for the identifications and analytic inversions. The overall shapes of the curves are similar to the SS SPIB simulations and for the same reasons. The TD inversion of the known channel results in MMSE performance, and the TD inversion of the adapted channel matches this

at all but the highest SNRs. This is presumably because at lower SNRs the BER performance is limited by the noise and the channel estimation error is insignificant relative to this but at higher SNRs the BER caused by the noise drops away and the BER from the channel estimation error begins to be the significant factor. The adaptive inversion terminated after 20,000 iteration with a length-500 adaptive coefficient temporal average again results in the worst performance. Note that it is worse than the curve for the SS SPIB channel due to slower adaptation due to the greater frequency-selectiveness of the channel. The frequency-domain inversions regularised by a constant that results in the optimum performance in a noiseless environment (0.001) gives the expected performance, i.e. sub-optimal at low SNRs but improving relatively at higher SNRs. The major difference is in the behaviour of the curve for the unknown channel inverted using the FD method regularised by the NSR relative to the curve for known channels. At the higher SNRs where the curve crosses those for the frequency-domain inversion regularised by the noiseless optimum value the performance is actually better for the unknown channel which had to be found by identification than for when the channel was perfectly known. The reason for this was explained in Section 4.2.5, and is because at the SNRs where the noise power has dropped to a value below the noiseless optimum regularisation factor the channel estimation error that arises from the adaptation goes some way to raising the effective regularisation factor towards the noiseless optimum value and hence the performance is better in the mean than if the channel was known perfectly. In fact, we see that between SNRs of 25 and 35 dB this estimation error generates an extra effective regularisation factor such that the performance is similar to that of manually regularising by the noiseless optimum value and using perfectly known channels. This result is valid however in the mean over many adaptations but when performing a single adaptation to single channel realisations the BER will not be deterministic and hence unreliable if this phenomenon is relied upon. Therefore it is still better to attempt to identify the channel as accurately as possible and manually insert the noiseless optimum value for the regularisation factor, which will result in the same performance.

4.7 Summary

This chapter has covered the essentials of inverting an unknown broadband MIMO channel to create an equaliser and has concentrated on minimising the computational cost of this process while maintaining a satisfactory BER performance. It started by explaining the overall inversion methods and criteria that would be

used, covered the useful regularisation method and discussed the alternative of using predistortion at the transmitter instead of equalisation at the receiver. The fractionally-spaced equalisation structure was briefly mentioned. The core of this chapter then explained three analytic inversion methods, namely z-domain, time-domain and frequency-domain and covered the potential performance and associated computational costs. A process involved in choosing the FIR equaliser length was explained but we stated it is often easier to use a pragmatic approach in the selection of this parameter. Also covered in some detail were the effects of channel estimation error on the performance, which arise when the channel is unknown and adaptive identification is used, and also the effects of the presence of noise during the adaptation. The chapter moved on to the alternative method of adaptive inversion to directly find the equaliser from an unknown channel and explained the advantages and disadvantages in terms of computational cost and potential BER performance. Finally, the existence of some other common adaptive equalisation methods was mentioned. The chapter finished with a sizeable section covering and discussing simulation results of systems created from the various techniques covered in this and previous chapters. Broadly, the conclusions we may draw are that the frequency-domain analytic inversion technique results in the best overall compromise in term of computational cost and BER performance and that it is advantageous to switch from regularisation by the NSR to a fixed value at some critical SNR which depends on the equaliser length and the channel. Further, it is beneficial to perform some temporal averaging on adapted filter coefficients when performed in the presence of noise. Finally, we saw that tracking performance is clearly inadequate for a worst-case but realistic future scenario of a 100 MHz bandwidth SV channel model and a MS moving at 120 km/h. A technique that has shown great potential in the past to solve this problem is that of subband processing. Not only can this result in faster adaptive convergence and thus solve the tracking problem, but it can also significantly reduce the computational cost of many signal processing algorithms, which is a primary motivator in this thesis. Hence subband systems are introduced in the next chapter and they are applied to the broadband adaptive MIMO equalisation problem.

Chapter 5

Subband MIMO Equalisation

The splitting of a signal into a number of narrowband frequencies has long been recognised as a powerful technique to reduce the computational cost of signal processing algorithms, as well as in some cases improving the performance of such algorithms against their fullband counterparts [72, 92, 139–141]. The narrowband frequency bands are termed subbands and their band-limited nature often allows us to reduce the sampling or processing rate of signal processing algorithms by up to a rate equal to the number of subbands. As a result, we may also reduce the length of filters operating in the subbands by a factor of up to the decimation rate, explained later in this chapter. Also, in theory, the method offers the possibility of parallelising the signal processing tasks due to the independent nature of the subbands and hence provides a way of efficiently implement algorithms. Although subband processing has is roots in acoustics, the technique may just as well be applied to adaptive and analytic equalisation or system inversion for radio communications.

A problem with the adaptive inversion discussed in the previous chapter was that of potentially slow convergence of LMS-type algorithms for frequency-selective broadband channels. Subband processing can potentially increase the convergence speed of such algorithms without having to resort to computationally costly fast convergent adaptive algorithms such as RLS [12, 12, 142, 143]. Such advantages have been shown for both adaptive identification and inversion in static and dynamic environments [144]. However there has been only very limited work in the area of multi-channel processing in subbands, especially with the application of equalisation for communication systems. Yamada *et al.* [145] showed an advantage in using subbands for multi-channel problems but this work was only limited to a 1×2 system and two subbands. More recently Weiss *et al.* [8] showed the benefit of performing adaptive equalisation of MIMO systems but again was of limited

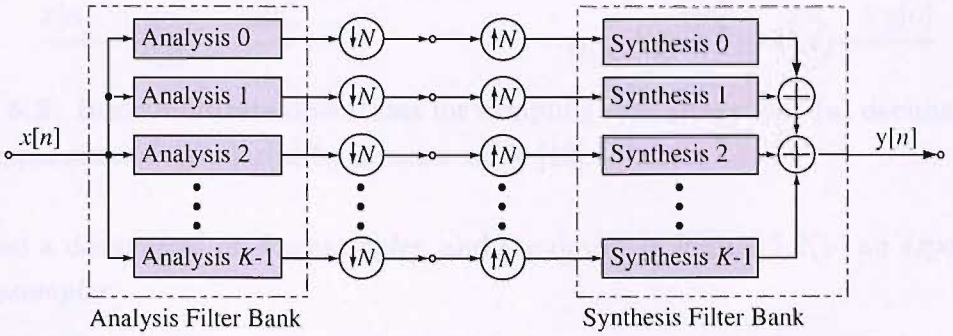

Fig. 5.1: A simple subband system.

scope. Further both of these works were in the area of acoustics.

We start in Section 5.1 by reviewing some essential aspects of multirate signal processing. In Section 5.2 we briefly cover the performance characteristics of subband systems, such as how they can result in an increase in convergence of some adaptive algorithms, as well as the effect on final MSE and modelling accuracy. We then move on to describing how we may use these subband building blocks to create MIMO adaptive and analytic inversion systems which enjoy the benefits afforded using the technique in Section 5.3. Finally in Section 5.4 we provide a comparative study between subband MIMO systems and their fullband counterparts shown in the previous chapters, before summarising in Section 5.5.

5.1 Subband Concepts

The most basic subband system was shown in Figure 1.2 and is reproduced for convenience in Figure 5.1. The aim of this section is to analyse and understand this system. We start by introducing basic multirate operations.

5.1.1 Multi-Rate Systems

A multirate system comprises components running at different sampling frequencies. The filter banks in Figure 5.1 are a typical example of a multirate system, where each of the K subband signals between the analysis and synthesis filter banks is sampled slower by a factor of N compared to the input or output fullband signal. There are two basic operations to change the sampling rate, decimation and expansion, which are shown in Figure 5.2. The device in Figure 5.2(a) is

Fig. 5.2: Basic multirate operations for sampling rate alteration: (a) decimation; (b) expansion of signal $x[n]$ by a factor of N [12].

termed a *decimator*[1] or *downsampler*, and the device in Figure 5.2(b) an *expander* or *upsampler*.

Decimation. When a signal is fed through a decimator in Figure 5.2(a) only every N^{th} sample is retained in the output signal, that is

$$y[n] = x[Nn], \tag{5.1}$$

where $N \in \mathbb{Z}^*$, i.e. a non-negative integer. As an example, Figure 5.3(b) shows the result of decimating the signal in Figure 5.3(a) by a factor of 2.

Although fractional values of N are possible and lead to non-uniform sampling [146], this is not considered here. In the frequency domain, (5.1) can by expressed by [102]

$$Y(z) = \frac{1}{N} \sum_{n=0}^{N-1} X(z^{1/N} e^{-j2\pi n/N}). \tag{5.2}$$

Thus, the spectrum $Y(e^{j\omega})$ is assembled by superimposing $X(e^{j\omega})$ stretched by a factor of N with $N-1$ versions shifted by multiples of 2π. This superposition leads to a spectral overlap (or *aliasing*) if $x[n]$ is not suitably band-limited. As an example for a decimation by $N = 2$, the spectrum in Figure 5.3(e) emerges from the input shown in Figure 5.3(d).

Expansion. The expander in Figure 5.2(b) inserts $N-1$ zeros between every original sample, that is

$$y[n] = \begin{cases} x\left[\frac{n}{N}\right] & n = \lambda N \\ 0 & n \neq \lambda N \end{cases}, \tag{5.3}$$

where λ is an integer. An example is depicted in Figure 5.3(c), which results when Figure 5.3(a) is expanded by $N = 2$. In the frequency domain, expansion can be expressed by

$$Y(z) = X(z^N), \tag{5.4}$$

which for the spectrum $Y(e^{j\omega})$ means a re-scaling of the frequency axis with respect to $X(e^{j\omega})$ by a factor of N. An illustration for the expansion of Figure 5.3(d) by

[1] Technically, decimation refers to downsampling by a factor of 10, however the terms decimation and downsampling are often used interchangeably, and we shall continue to do so in this thesis.

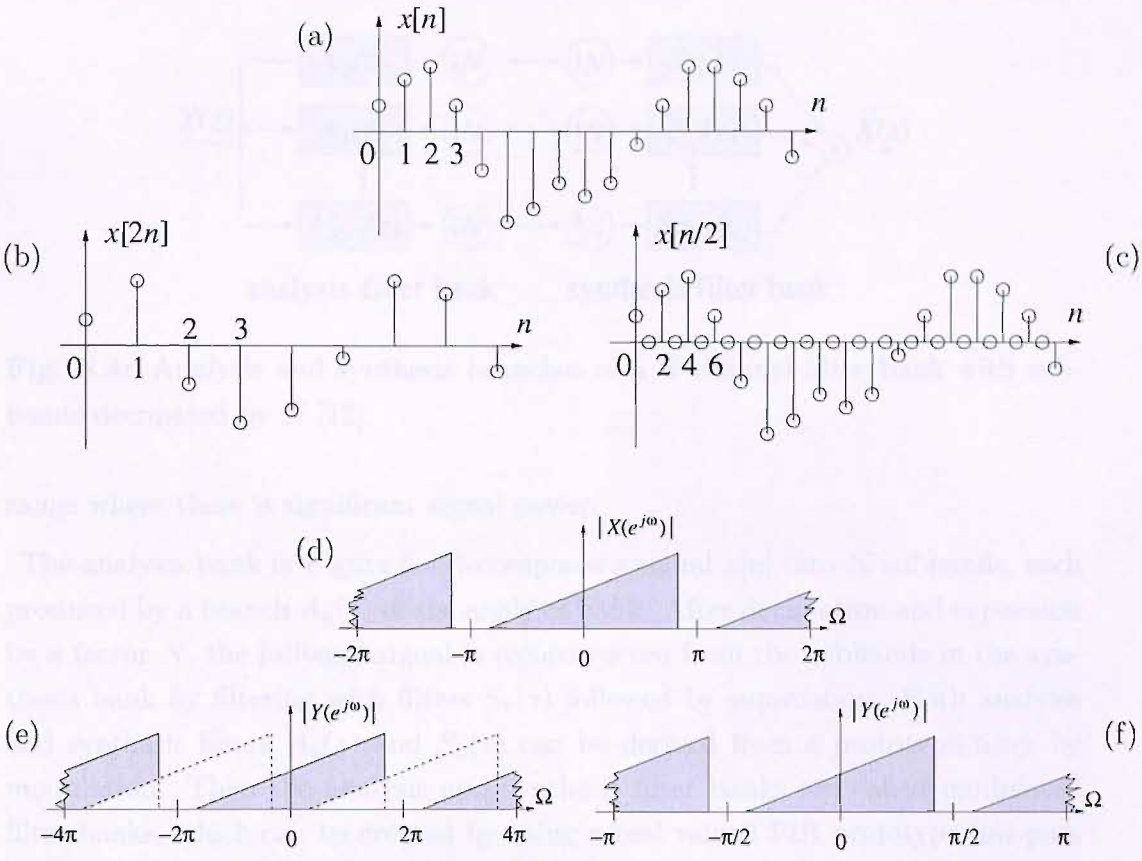

Fig. 5.3: Example for decimation and expansion by 2: (a) original time domain signal; (b) decimated signal; (c) expanded signal; (d) frequency domain of a complex signal; (e) frequency domain of decimated signal; (f) frequency domain of expanded signal [12].

$N = 2$ is given in Figure 5.3(f). Good tutorials on multirate processing and a detailed text can be found in [102, 147–149].

5.1.2 Modulated Filter Banks

Now that the decimation and expansion processes have been covered, we will look at the actual analysis and synthesis filter banks more closely. Figure 5.4 shows the same system as Figure 5.1, but it illustrates the analysis and synthesis filter banks in more detail. Broadly speaking the purpose of each filter in the analysis filter bank is to extract a frequency band of interest, while removing the remaining frequency bands. For example the first filter will pass only the lowermost frequencies. Due to the limited bandwidth of the subband signals, according to Shannon's sampling theorem [150, 151] each of the K bands can be downsampled by a factor $N \leq K$, and the subband signals are said to be *critically decimated* when the equality holds. The bandwidth is defined as the width of a frequency

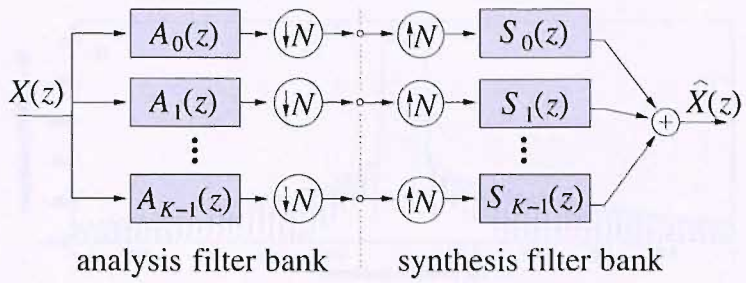

Fig. 5.4: Analysis and synthesis branches of a K-channel filter bank with subbands decimated by N [12].

range where there is significant signal power.

The analysis bank in Figure 5.4 decomposes a signal $x[n]$ into K subbands, each produced by a branch $A_k(z)$ of the analysis bank. After decimation and expansion by a factor N, the fullband signal is reconstructed from the subbands in the synthesis bank by filtering with filters $S_k(z)$ followed by summation. Both analysis and synthesis filters $A_k(z)$ and $S_k(z)$ can be derived from a prototype filter by modulation. Then the analysis and synthesis filter banks are called modulated filter banks, which can be created by using a real valued FIR prototype low-pass filter $p[n]$ of length L_p and modulating it with a generalised discrete Fourier transform (GDFT). Modulated filter banks created in this way are termed generalised discrete Fourier transform (GDFT) filter banks. The GDFT which modulates the prototype filter to the correct frequency can be expressed mathematically as

$$h_k[n] = t_{k,n} \cdot p[n], \qquad t_{k,n} = e^{j\frac{2\pi}{K}(k+k_0)(n+n_0)}, \tag{5.5}$$

where k and n are positive integers. The term *generalised* DFT arises from the offsets k_0 and n_0 applied to the frequency and time indices, which are responsible for important properties of the modulated filter bank such as the band position of the analysis filters and linear phase of the modulated filters. The GDFT is a memory-efficient way of performing the analysis and synthesis filtering as we must only store one set of prototype filter coefficients. For a detailed understanding of the parameters, the reader should refer to the more detailed texts on this subject cited earlier in this chapter. Further we may use the GDFT to create a paraunitary analysis filter bank, i.e. $\tilde{\mathbf{A}}(z)\mathbf{A}(z) = z^{-\Delta}\mathbf{I}$, where $\tilde{\mathbf{A}}(z)$ is the parahermitian of the polyphase matrix of the analysis filter bank $\mathbf{A}(z)$, which has the useful property that the polyphase synthesis filter bank $\mathbf{S}(z)$ is simply given by $\tilde{\mathbf{A}}(z)$ [12, 72]. Figure 5.5(a) and Figure 5.5(b) respectively show a prototype filter and the result of the modulation operation resulting in a set of filters suitable for use in a filter bank.

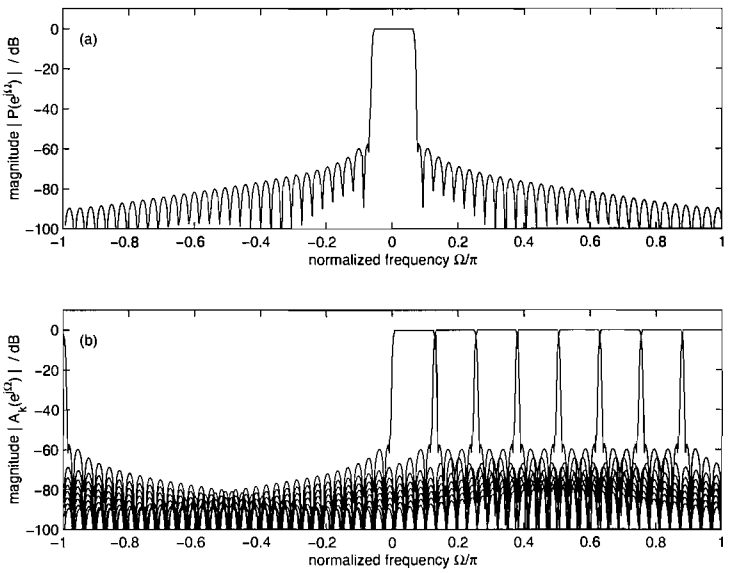

Fig. 5.5: (a) Real valued prototype lowpass filter $P(e^{j\omega})$ with bandwidth $B = 2\pi/16$; (b) modulated GDFT filter bank derived from the prototype lowpass filter $P(e^{j\omega})$ with $K/2 = 8$ filters covering the frequency range $\omega = [0; \pi]$ [12].

5.1.3 Polyphase Representation

In this section we will introduce the polyphase representation of the basic subband system in Figure 5.1 as an alternative form which is convenient to analyse. We introduce this equivalent form as it (i) leads to further insights into the subband approach, (ii) enables a computationally efficient implementation of filter banks, and (iii) will be used when developing the fractionally-spaced subband MIMO equaliser in Chapter 6. The term "polyphase" refers to the decimation of the fullband signals and that there are N possibilities of which sample set to keep. Each set is as good as any other and they differ only in phase but not magnitude in the frequency-domain. The polyphase approach in fact uses all N phases.

We follow the approach in [12] and [102] to analyse a SISO realisation of the system for simplicity. Extension to a fractionally-spaced MIMO implementation will be performed in Chapter 6. We start by expressing analysis and synthesis transfer functions, $A_k(z)$ and $S_k(z)$ respectively, for the k^{th} subband in terms of their polyphase components $A_{k|n}(z), k = 0(1)N-1$ and $S_{n|k}(z), k = 0(1)N-1$ as

$$A_k(z) = \sum_{n=0}^{N-1} z^{-n} A_{k|n}(z^N) \quad \text{type 1 polyphase} \tag{5.6}$$

$$S_k(z) = \sum_{n=0}^{N-1} z^{-(N-1-n)} S_{n|k}(z^N) \quad \text{type 2 polyphase} \tag{5.7}$$

where

$$A_{k|n}(z) = \sum_{\kappa=-\infty}^{\infty} a_k(N\kappa + n)z^{-\kappa} \tag{5.8}$$

$$S_{n|k}(z) = \sum_{\kappa=-\infty}^{\infty} s_k(N\kappa + N - 1 - n)z^{-\kappa}. \tag{5.9}$$

In vector-matrix form the analysis and synthesis filter banks can be expressed

$$\underline{\mathbf{a}}(z) = \underline{\mathbf{A}}(z^N) \cdot [1 \; z^{-1} \; \cdots \; z^{-(N-1)}]^T \tag{5.10}$$

$$\underline{\mathbf{s}}^T(z) = [z^{-(N-1)} \; z^{-1} \; \cdots \; 1] \cdot \underline{\mathbf{S}}(z^N) \tag{5.11}$$

respectively, where

$$\underline{\mathbf{A}}(z) = \begin{bmatrix} A_{0|0}(z) & A_{0|1}(z) & \cdots & A_{0|N-1}(z) \\ A_{1|0}(z) & A_{1|1}(z) & \cdots & A_{1|N-1}(z) \\ \vdots & \vdots & \ddots & \vdots \\ A_{K-1|0}(z) & A_{K-1|1}(z) & \cdots & A_{K-1|N-1}(z) \end{bmatrix} \tag{5.12}$$

$$\underline{\mathbf{S}}(z) = \begin{bmatrix} S_{0|0}(z) & A_{0|1}(z) & \cdots & A_{0|K-1}(z) \\ S_{1|0}(z) & A_{1|1}(z) & \cdots & A_{1|K-1}(z) \\ \vdots & \vdots & \ddots & \vdots \\ S_{N-1|0}(z) & A_{N-1|1}(z) & \cdots & A_{N-1|K-1}(z) \end{bmatrix} \tag{5.13}$$

The matrices $\underline{\mathbf{A}}(z)$ and $\underline{\mathbf{S}}(z)$ are known as the polyphase matrices of the analysis and synthesis filter banks, respectively. Notice the native sampling rate corresponding to z is of the decimated signals inside the filter banks. Similarly, we can put the input signal into polyphase form such that

$$\underline{\mathbf{x}} = [X_0(z) \; X_1(z) \; \cdots \; X_{N-1}(z)]^T, \tag{5.14}$$

where $X_i(z) \bullet\!\!-\!\!\circ\, x_i[n] = x[Nn + N - 1 - i]$, $i = 0(1)N - 1$. Hence the output of the analysis filter bank is

$$\underline{\mathbf{y}}(z) = \underline{\mathbf{A}}(z)\underline{\mathbf{x}}(z) \tag{5.15}$$

where $\underline{\mathbf{y}}(z)$ is a vector containing the K subband signals. Further we may reconstruct the polyphase input signal by

$$\hat{\underline{\mathbf{x}}}(z) = \underline{\mathbf{S}}(z)\underline{\mathbf{y}}(z) = \underline{\mathbf{S}}(z)\underline{\mathbf{A}}(z)\underline{\mathbf{x}}(z) \tag{5.16}$$

where $\hat{\underline{\mathbf{x}}}(z)$ is an estimate of $\underline{\mathbf{x}}(\mathrm{z})$.

The system we have developed is shown in Figure 5.6(a). Two problems with this result from the fact that the decimation and expansion is performed inside the filter banks. The filters banks run at the full rate, increasing computational

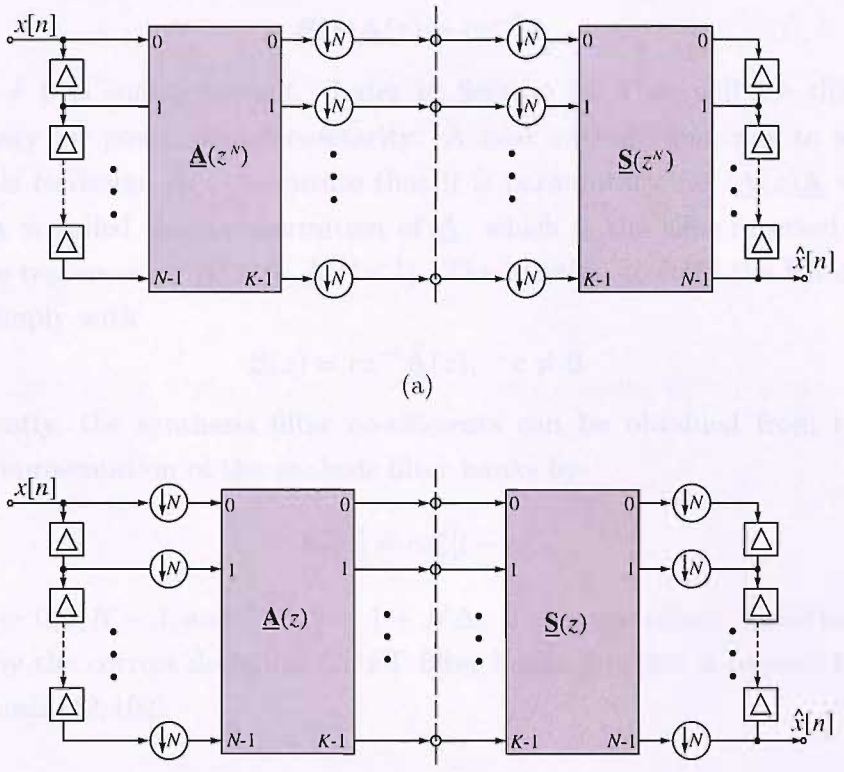

Fig. 5.6: (a) Polyphase representation of a K subband system decimated by factor N; (b) re-arrangment using Noble identities.

requirements, and when further processing tasks are inserted in the decimated stage the overall system is difficult to analyse, since the decimators and expanders are non-linear devices. To tackle both these problems we employ the Noble identities [102]

$$A(z)(\downarrow N) = (\downarrow N)A(z^N) \tag{5.17}$$

$$(\uparrow N)S(z) = S(z^N)(\uparrow N) \tag{5.18}$$

where $(\downarrow N)$ and $(\uparrow N)$ denotes decimation and expansion by factor N respectively. Applying these to Figure 5.6(a) we obtain Figure 5.6(b). Now the analysis and synthesis operations are performed at the same rate as any other potential signal processing tasks that may be performed in subbands, which is at the decimated rate hence the filtering can be performed using fewer computations.

Perfect Reconstruction. The perfect reconstruction (PR) property is important as it minimises the error between $\underline{\hat{\mathbf{x}}}(z)$ and $\underline{\mathbf{x}}(z)$. The necessary and sufficient

condition for PR is

$$\underline{\mathbf{S}}(z)\underline{\mathbf{A}}(z) = cz^{-\Delta}\mathbf{I} \tag{5.19}$$

where $c \neq 0$ is some constant. Later in Section 5.2.4 we will see that $c = 1$ is necessary for power complementarity. A neat and efficient way to solve this problem is to design $\underline{\mathbf{A}}(z)$ to ensure that it is paraunitary, i.e. $\tilde{\underline{\mathbf{A}}}(z)\underline{\mathbf{A}} = \mathbf{I}$. The matrix $\tilde{\underline{\mathbf{A}}}$ is called the parahermitian of $\underline{\mathbf{A}}$, which is the time-reversed complex conjugate transpose or $\tilde{\underline{\mathbf{A}}}(z) = \underline{\mathbf{A}}^H(z^{-1})$. The solution to fulfil the PR condition follows simply with

$$\underline{\mathbf{S}}(z) = cz^{-l}\tilde{\underline{\mathbf{A}}}(z), \quad c \neq 0. \tag{5.20}$$

Subsequently, the synthesis filter co-efficients can be obtained from the time-domain representation of the analysis filter banks by

$$S_k[n] = ca_k^*[l - n], \tag{5.21}$$

where $k = 0(1)K - 1$ and $l = N - 1 + N\Delta$. The paraunitary condition can be fulfilled by the correct design of GDFT filter banks but this is beyond the scope of this thesis [12, 102].

5.1.4 Critically Decimated versus Oversampled Subbands

Given the number of subbands K, we are now still left with a choice for the decimation factor N. Critically decimated subbands, i.e. where $N = K$, with respect to adaptive filtering were first analysed by Gilloire [141] and Gilloire and Vetterli [140, 142]. The problem with critically decimated subband systems is that there may be aliasing in the subbands due to the finite attenuation in the transition bands of the analysis and synthesis filters which can be seen as overlap of adjacent bands in Figure 5.5. Aliasing has been identified as a problem when performing comparison or correlation-type operations in the subbands, such as subband adaptive filtering, and generally the alias level will limit the achievable MMSE [12, 152]. A solution to the aliasing problem suggested by Gilloire and Vetterli [140–142] leads to a modified subband structure with cross-terms between adjacent bands. Another solution, called gap-filters, is to leave guard bands between adjacent analysis filters, which removes the aliasing problem but introduces a loss of frequency components within the guard bands [153–156]. The first solution leads to bulky implementations, while the second approach is clearly undesirable.

The simplest and preferred solution to this problem is to have the analysis filters overlapping but oversample each subband such that no aliasing results. This avoids the need for any special subband structure such as the use of cross-terms

in Gilloire's solution or gap-filters. In this case $N < K$, i.e. the subband signals are decimated by a factor which is less than the number of subbands, the system is termed an oversampled subband system. An advantage of this approach is that now independent processing in the subbands is possible, enabling the possibility of parallel processing of subbands for numerically intensive signal processing tasks.

5.2 Performance of Subband Systems

In this section we briefly examine the performance characteristics of subband processing.

5.2.1 Computational Complexity

One of the main incentives for using the subband approach for solving signal processing problems is that it can be used to reduce the computational complexity when compared to the equivalent fullband problem. Admittedly there is the overhead of having to use an analysis and synthesis filter to interface with the fullband domain, and also having filtering occurring in several subband branches, however the advantages offered by subband system often outweigh these overheads. The main advantages of the subband approach is that the processing rate within the subbands is lower by a factor of N and also each subband filter may be shorter by up to a factor of N compared to the fullband counterpart. Clearly, the first fact reduces the computation cost of any process performed in subband by a factor of N, and the second fact makes the task of converging each filter much quicker as shown in Chapter 3, in addition to reducing the computational cost by a further factor of up to N. A commonly used relationship [140] for adaptive filtering is that if a task requires a fullband filter of length L_f then subband filters of length

$$L_s = \frac{L_f + 2L_p}{N}, \tag{5.22}$$

may be used, where L_p is the length of the prototype filter, although we will see in the simulations that $L_s = L_f/N$ can also work well and has the advantage of quicker convergence due to the shorter subband filters; a similar result was found in [72]. Another advantage offered by this method is the parallelisation of the signal processing tasks into several subbands, as the computation of each branch is independent of any other and can therefore be computed by a dedicated processor for each subband, if the task warrants it [140]. Also, by following the approach in [157–160] for real-valued signals only $K/2$ complex subbands need

be calculated since the remaining subbands are complex conjugate and therefore redundant.

One last point to mention is that the subband method has a computational overhead arising from the analysis and synthesis filtering operations, which is not present with fullband processing. The overhead for a single filter bank is [161]

$$C_{\text{filter bank}} = \frac{1}{N}(2L_p + 4K\log_2 K + 8K), \tag{5.23}$$

where L_p is the length of the prototype filter. Hence the savings offered by the method must be great enough to outweigh these overheads.

5.2.2 Convergence Speed

For LMS-type algorithms the convergence speed is governed by the *eigenvalue spread*, also known as the *condition number*, of the auto-correlation matrix, $\mathbf{R}$, of the input as defined in Chapter 3 [12, 78, 143]. The eigenvalue spread is upper bounded by the ratio between the minimum and maximum value of its power spectral density (PSD) [12, 143]. Because the subband approach separates the input signal into spectral intervals, the spectral dynamics will be less than in the fullband case, resulting in a lower eigenvalue spread within each subband. This effect is often referred to as "pre-whitening". Therefore, compared to the fullband case, the subband version of the algorithm is expected to converge faster for spectrally coloured input signals. The performance increase depends on how coloured the input signal is or, in other words, the dynamic range of its PSD. The performance was analysed and simulated for several LMS adaptation schemes in [162] and showed that for the application of acoustic echo cancellers the subband adaptive system resulted in improved convergence.

This improvement in convergence speed becomes particularly important in the case of adaptive system inversion. The input to the adaptive system is filtered by the frequency-selective MIMO channel and may therefore exhibit considerable spectral dynamics, which can create severe difficulties for the convergence of a fullband adaptive system as shown in Figure 4.17. The spectral separation inherent to the subband approach results in a greatly improved convergence [8]. Conversely, in a system identification set-up, as the input to the adaptation algorithm is the original input signal and assuming that this signal is spectrally white and random, we do not expect the subband algorithm to perform better that its fullband counterpart. In fact, a worse performance is expected due to the distortive effects of the analysis and synthesis filter banks, discussed further in Section 5.2.4. Another reason is that in oversampled subband adaptation the total number of adaptive

tap coefficients over all subbands is greater than the number of adaptive tap coefficients for the fullband case, so the subband adaptation will take longer. One final point is that the subband analysis filters introduce spectral gaps, or guard bands, at the band edges in order to avoid aliasing, and hence colour the signal. Therefore there is a trade-off for the number of subbands between pre-whitening and this "self-colouring" effect.

5.2.3 Final MSE

A main disadvantage of the subband approach is that it imposes limitations on the final MSE. In general the subband approach will result in a higher final MSE than the fullband approach, since aliased signal components in the subbands appear as observation noise to the adaptive algorithm. Another reason is the distortive effects of the analysis and synthesis filter banks, discussed further in Section 5.2.4. Weiss *et al.* [12, 143] developed a relative measure of the error performance called the *signal-to-alias ratio* (SAR) in the subbands and this can be related to the stop-band attenuation of the prototype filter used in the analysis and synthesis filter banks.

A filter bank essentially consists of a number of band-pass filters centred on different frequencies. If we consider a filter bank derived from a prototype filter the best attainable adaptive MSE will be limited by the energy escaping from adjacent bands, which will appear as noise. Since the escaping energy is determined by stop-band attenuation of the prototype filter bank the SAR can be shown to be [12]

$$SAR = \frac{\int_0^{\pi/N} |P(e^{j\Omega})|^2 d\Omega}{\int_{\pi/N}^{\pi} |P(e^{j\Omega})|^2 d\Omega}, \tag{5.24}$$

where $|P(e^{j\Omega})|$ is the magnitude response of the prototype filter and the denominator measures the stop-band energy. The MMSE limitations for subband adaptive systems were examined in [163]. Further insight into sources of subband error is given in [159, 164].

5.2.4 Modelling Accuracy

Besides the final MSE it is also possible to assess the accuracy of the subband adaptive system with respect to the optimal solution. This can be done by finding the vector distance between the converged subband weights and the optimum solution in the l_2 sense. This of course implies knowledge of the optimum subband solution, which is usually not known. An alternative is to compare the distance

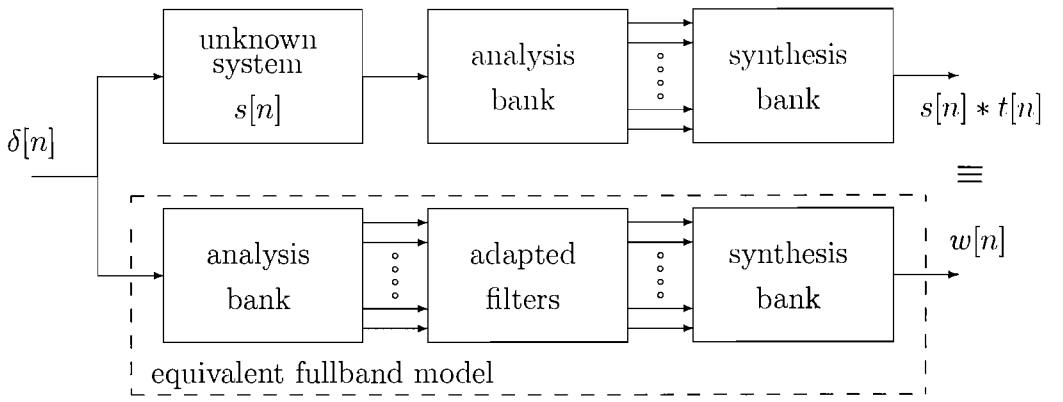

Fig. 5.7: Separation of system identification structure for reconstruction of fullband equivalent model [12].

between the subband final weight and the fullband final weights, where we take advantage of the fact that the fullband adaptation performs better in the final MSE sense. To be able to compare the two we need to obtain the *fullband equivalent model* of the final subband coefficients.

Figure 5.7 shows a way to find the equivalent fullband model using the response of the subband system. As the analysis and synthesis banks in the lower branch cause a slightly distorted delay, $t[n]$, the same distortion must be introduced in the upper branch, so that any difference between the output signals of the two branches is caused by the misadjustment of the subband adaptive filters only. This distortion is produced by the analysis and synthesis filter banks in the upper branch. Hence, after the adaptive filters have converged, the impulse response of the upper and lower branches should be close.

From this, a limitation to the modelling accuracy can be shown, which results in a second limitation to the final attainable MSE, the first being the limitation by aliasing. This is know as limitation by power complementarity, which becomes an issue when aliasing is sufficiently suppressed. The PR condition then reduces to the requirement that [12]

$$\sum_{k=0}^{K-1} S_k^*(z^{-1})A_k(z) = \underline{\tilde{\mathbf{s}}}(z)\underline{\mathbf{a}}(z) \triangleq z^{-l}. \tag{5.25}$$

If the analysis-synthesis cascade deviates from a perfect unity gain delay, then it introduces distortion, which can be modelled by means of the distortion function, $t[n]$. However, in reality, if the analysis and synthesis filter banks are well designed the distortion rarely causes any problems.

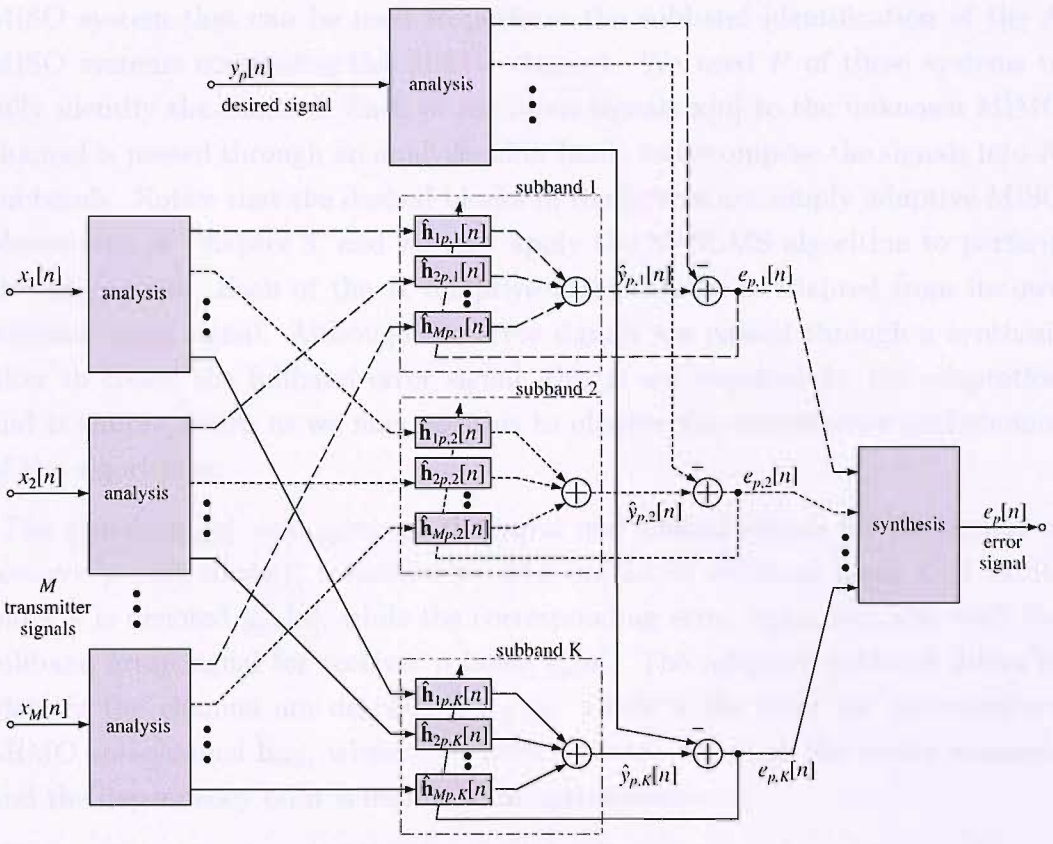

Fig. 5.8: A MISO subband adaptive system arranged for identification.

5.3 Subband MIMO Inversion

We may now tackle the task of combining the subband processing techniques explained in this chapter with the analytic and adaptive MIMO inversion methods in Chapter 4 to create a subband adaptive MIMO equaliser. As in Chapter 4 there are two approaches to doing this- an adaptive system identification followed by a system inversion or a fully adaptive system inversion. Subband processing offers us interesting new combinations, such as subband identification, followed by a subband analytic inversion, and then using the subband inverse for the equaliser or finding from this the fullband equivalent system and using this instead. This section will cover each possible combination and show how they can be implemented.

5.3.1 Subband Adaptive System Identification

We consider the method of identifying the unknown system in subbands for a future analytic inversion, which is the topic of Section 5.3.2. Figure 5.8 shows a

MISO system that can be used to perform the subband identification of the P MISO systems comprising the MIMO channel. We need P of these systems to fully identify the channel. Each of the input signals $\mathbf{x}[n]$ to the unknown MIMO channel is passed through an analysis filter bank, to decompose the signals into K subbands. Notice that the dashed blocks in the figures are simply adaptive MISO blocks seen in Chapter 3, and we may apply the M-NLMS algorithm to perform the adaptation. Each of the K adaptive MISO blocks is adapted from its own subband error signal. Although the error signals are passed through a synthesis filter to create the fullband error signal, this is not required for the adaptation and is simply shown as we may use this to observe the convergence performance of the algorithms.

The signals $x_m[n]$, and $y_p[n]$ are the input and desired signals for the output of receiver p (not shown), respectively. The output of subband block k of MISO block p is denoted $\hat{y}_{p,k}[n]$, while the corresponding error signal is $e_{p,k}[n]$ with the fullband error signal for receiver p being $e_p[n]$. The adaptive subband filters to identify the channel are denoted $\hat{\mathbf{h}}_{mp,k}[n]$, which is the filter for the unknown MIMO sub-channel $\mathbf{h}_{mp}$, where the coefficients are stored in the vector elements and the dependency on n is due to its adaptive nature.

The computational cost of this approach is of interest, as computation reduction is one of the main drivers behind the subband approach. The cost of a single GDFT analysis or synthesis filter bank operation in a fast implementation is given by [161]

$$C_{\text{filter bank}} = \frac{1}{N}(2L_p + 4K\log_2 K + 8K), \tag{5.26}$$

MAC operations per fullband sampling period, where N, K and L_p are the decimation factor, number of subbands and prototype filter length, respectively. Thus, the complexity of the MISO adaptive identification system in Figure 5.8 (excluding the unnecessary fullband error synthesis) using the M-NLMS algorithm can be found to be

$$C_{\text{MISO Identification}} = \frac{K}{N}(8ML_{h,s}+8M+10)+\frac{M+1}{N}(2L_p+4K\log_2 K+8K), \tag{5.27}$$

where M is the number of transmitters, $L_{h,s}$ is the length of the subband adaptive filter that converges to the unknown MIMO sub-channels and can be chosen according to (5.22), and (3.54) has been used for the cost of the M-NLMS algorithm. The adaptation must be performed in each subband, but within each subband the update rate relative to the fullband adaptation is reduced by the decimation rate, hence the K/N factor in the first term. For the cost of the full MIMO system P of these blocks are needed, but notice that the analysis for the input signals $x_m[n]$ only needs to be performed once as all P MISO blocks used the same signals.

Hence the complexity of the MIMO adaptive identification system is given by

$$C_{\text{MIMO Identification}} = \frac{PK}{N}(8ML_{h,s} + 8M + 10) + \frac{M+P}{N}(2L_p + 4K\log_2 K + 8K) \tag{5.28}$$

MACs per fullband sampling period. As K and N are usually of similar magnitude but $L_{h,s}$ is up to N times smaller than $L_{h,f}$ we would expect the complexity of this method to be up to N times less than for the fullband method. In reality the reduction may be less than N as a longer subband filter length than $L_{h,s} = L_{h,f}/N$ may be required, according to Section 5.2.1. This computational cost saving arises for algorithms that are of order $\mathcal{O}(L_h)$, however for more complex algorithms, such as RLS which is order $\mathcal{O}(L_h^2)$, subband processing can reduce the complexity of the algorithm over fullband methods by an even more significant amount. In fact, we can generalise this behaviour and say that subband processing offers computational savings of up to the complexity order of the algorithm considered.

If the signals are guaranteed to be real-valued there are two opportunities for complexity-reduction. Firstly, the number of operations required in multiplying two real numbers is a quarter that of complex-value numbers, and for addition the ratio of half. The second, less obvious method arises from the fact that the filters in the second half of the subbands, i.e. subband K/2+1 to K, are simply the complex conjugates of the filters in the lower subbands, and therefore redundant.

5.3.2 Subband Analytic System Inversion

Once the MIMO channel has been identified in subbands it must be analytically inverted to obtain the equaliser. In Chapter 4 we have covered three inversion methods, namely in the z, time and frequency domains. We found that the z-domain method generally had problems or was unusable for all but the most benign channels, and hence here we shall only consider the time and frequency-domain methods.

5.3.2.1 Subband Time-Domain Inversion

Assuming that subbands can be processed independently from each other, a time-domain MISO inversion can be invoked for each of the K subbands, following the method laid out in Chapter 4. This is advantageous since the shortening of the filter response lengths in the decimated subband domain helps to contain the dimensions of the convolutional matrices and hence the computational complexity required for the inversion. However, the guard bands in the subband domain will contribute to an ill-conditioning of the problem and at least some degree of

regularisation will be required. Fortunately, this regularisation is implicit to the time-domain inversion and is manually added to the frequency-domain inversion.

We now consider the computational cost of this method in detail and compare it to the same fullband inversion technique. The complexity of the time-domain inversion method is $\mathcal{O}(L_g^3)$, where L_g is the length of the FIR filter chosen to model the inverse impulse response. Recalling (5.22) for the length of the subband filter $L_{g,s}$ then the cost orders of the subband and fullband inversions are related by a factor

$$\frac{\mathcal{O}(C_{\text{fullband inversion}})}{\mathcal{O}(C_{\text{subband inversion}})} = \frac{N^3}{K}\left(\frac{L_{g,f}}{L_{g,f}+2L_p}\right)^3, \tag{5.29}$$

where the factor K is included as K such inversions are required for the subband case. From this it would appear that it would be beneficial to make N and K very high, subject to $N < K$. However, increasing the number subbands necessitates an increase in L_p to maintain the same alias and distortion levels which means that $L_{g,s}$ may need to be greater too, to model the prototype filter response adequately. Ideally, we would choose as great a value for K so that the necessary value for L_p is small comparable to $L_{g,f}$, otherwise we may reach the peculiar case where the subband filters may actually need to be longer than the fullband filter to model the response of the prototype filter accurately enough.

Example. Considering the inversion simulations in Chapter 4 which used $L_{g,f} = 280$ for the SPIB channels, performing in subbands using GDFT analysis filters with $L_p = 448$, $K = 16$ subbands and $N = 14$ decimation factor results in approximately 43% of the number of MACs over the fullband case.

This can be lowered further as we will see in the simulations that

$$L_{g,s} = \frac{L_{g,f}}{N} \tag{5.30}$$

can result in satisfactory results for long inverse filters, i.e. where $L_{g,f}$ is not insignificant relative to $2L_p$. This new relationship will result in a ratio between the cost orders

$$\frac{\mathcal{O}(C_{\text{fullband inversion}})}{\mathcal{O}(C_{\text{subband inversion}})} = \frac{N^3}{K}. \tag{5.31}$$

Example. For the same scenario this could result in a much more impressive approximate 0.6% of the MACs over the fullband case. Of course, we may use a pragmatic approach in choosing $L_{g,s}$ anywhere between these two extremes to give the performance required with a corresponding computational saving.

Figure 5.9 shows the ratio of fullband to subband computational cost order against $L_{g,f}$, for three different rules for $L_{g,s}$ and different subband parameters.

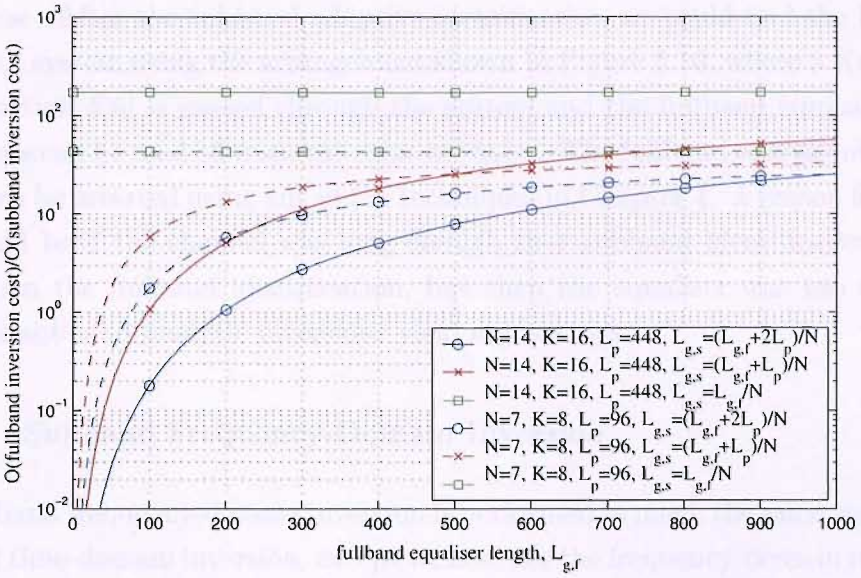

Fig. 5.9: Ratio of fullband to subband time-domain analytic inversion computational cost orders.

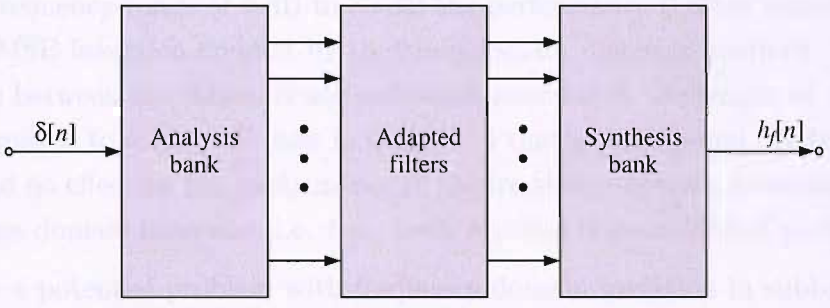

Fig. 5.10: A system for finding the fullband equivalent filter coefficients from a subband system.

The subband inversion becomes less costly once the ratio has reached over unity. With $K = 16$, $N = 14$ and $L_p = 448$, for low values of $L_{g,f}$ we are more likely to need $L_{g,s} = (L_{g,f} + 2L_p)/N$ to satisfactorily model the prototype filter response, and hence the subband method becomes favourable for value of $L_{g,f}$ above about 200. For much higher values of $L_{g,f}$, $L_{g,s} = L_{g,f}/N$ may suffice in which case the upper limit of N^3/K is reached for cost saving. Where $K = 8$, $N = 7$ and $L_p = 96$ is used, not only are the values for $L_{g,f}$ for which $L_{g,s} = L_{g,f}/N$ should result in satisfactory performance lower, but even where $L_{g,s} = (L_{g,f} + 2L_p)/N$ is required for very low $L_{g,f}$ the subband method becomes less costly above around $L_{g,f} = 75$. Clearly it is desirable to ensure that L_p is not large compared to $L_{g,f}$, which in turns places limits on K and N to maintain certain alias and distortion levels.

We should, for completeness, mention an alternative possibility of calculating

the inverse. After the subband adaptive identification we could find the fullband equivalent system using the arrangement shown in Figure 5.10, where a Kronecker delta function $\delta[n]$ is passed through the system and the fullband equivalent tap coefficients can be read off from the response $h_f[n]$. The fullband equivalent system could then be inverted using any of the techniques in Chapter 4. A reason for doing this would be if the channel was long enough that subband identification is less costly than the fullband identification, but then the equaliser was too short to make the subband analytic inversions yield any savings.

5.3.2.2 Subband Frequency-Domain Inversion

The subband frequency-domain inversion is performed in much the same way as the subband time-domain inversion, except we now use the frequency-domain inversion technique described in Chapter 4. We saw that this method has an associated problem of circular convolution effects, however in the simulations in Chapter 4 we saw that this only causes a degradation at very high SNR values. In the more realistic frequency range of 0 dB to 30 dB the performance is often similar to that of the MMSE inversion created by the time-domain inversion method. The only difference between the fullband and subband inversion is the length of the filters we are required to invert. We saw in Chapter 4 that at low to mid SNRs the filter length had no effect on the performance of the frequency-domain inversion relative to the time-domain inversion, i.e. they both resulted in near-MMSE performance.

There is a potential problem with frequency-domain inversion in subbands that is actually caused by the shorter filters that partially motivate the subband technique. Where shorter subband identified channels are used, shorter equaliser filters can often be used too. We know from Chapter 4 that the length of the FFT used in the inversion is the same as the chosen length of the equaliser filters, hence we use shorter FFTs for inversion of subband filters. However, the severity of the circular convolution effect is also governed by the length of the FFT, i.e. the shorter the FFT the more severe the undesirable effect of circular convolution. A further problem is that the narrowband assumption of frequency bins becomes less true as the number of bins is reduced. If the error-causing effects of these problems become unacceptable the only solution is to choose a longer equaliser $L_{g,s}$. We will see later in this section however that if we raise $L_{g,s}$ we may reach the point were the fullband frequency-domain inverse is less computational costly than the subband method.

The main advantage offered by the subband frequency-domain method is that of potential complexity reduction over the time-domain method, although the difference will not be as marked as for the fullband case due to the shorter filters and

the $\mathcal{O}(L_g \log_2 L_g)$ order of this method and in some cases may cause a complexity increase. Again we consider the cases of $L_{g,s}$ being defined by the two extremes in (5.22) and (5.30). The ratio between subband and fullband inversion complexity order using the first relationship can be shown to be

$$\frac{\mathcal{O}(C_{\text{fullband inversion}})}{\mathcal{O}(C_{\text{subband inversion}})} = \frac{N}{K} \cdot \frac{L_{g,f}}{L_{g,f} + 2L_p} \cdot \frac{\log_2 L_{g,f}}{\log_2(L_{g,f} + 2L_p) - \log_2 N}. \tag{5.32}$$

From this we see we should make the oversampling ratio $K/N > 1$ as small as possible, given that L_p is not under our control for a given K. In contrast, using (5.30) gives a ratio between complexity orders of

$$\frac{\mathcal{O}(C_{\text{fullband inversion}})}{K\mathcal{O}(C_{\text{subband inversion}})} = \frac{N}{K} \cdot \frac{\log_2 L_{g,f}}{\log_2 L_{g,f} - \log_2 N}. \tag{5.33}$$

Example. For the simulations in Chapter 4 using $L_{g,f} = 280$, and with $L_p = 448$, $N = 14$ and $K = 16$ this method results in a computational increase of about 377% of the fullband case. This is due to the fact that the complexity order of the frequency-domain method does not outweigh overhead caused by L_p and the fact that $N < K$. Using (5.30) results in computational savings of 60% of the fullband case.

Evidently the benefit of subband processing for frequency-domain inversion, if any, is nowhere near as great as for the time-domain inversion due to the complexity order of the frequency-domain method. While the computational savings would increase if we chose a higher value for K and hence could increase N also, this must be weighed against the worsening in MSE performance that would arise in the identification of Section 5.3.1, due to distortion and aliasing effects, which in turn would worsen the performance of the equaliser derived from it.

For cases where we need to use a value for $L_{g,s}$ such that the subband frequency-domain inversion would result in a more computationally costly process than the fullband method, i.e. where $L_{g,f}$ is relatively short with respect to L_p, we may invert the fullband equivalent model of the channel generated from the subband identification in Section 5.3.1. This was considered but discounted for time-domain inversion since the subband processing always results in computational savings. Considering the above example, $L_{g,s} \approx 29$ will mean the subband frequency-domain inversion is about as costly in terms of MACs as the fullband method. If MSE performance is unsatisfactory however then instead of raising $L_{g,s}$ to improve prototype filter response modelling, a computationally cheaper method would be to revert back to the fullband with $L_{g,f} = 280$ by determining the fullband equivalent system using the system in Figure 5.10, and analytically invert this in the frequency-domain. The conversion to fullband is a computationally insignificant

task. Not only would the MSE performance improve since we are no longer required to model the prototype filter response, but also the equaliser is now unaffected by the slight distortion introduced by the analysis and synthesis filter banks that would have been present if performing the inversion in subbands. Even in this scenario however it is still better to perform the prior adaptation in subbands as this will still result in the lower cost than the fullband identification due to the lower adaptive update rate.

The main disadvantage of converting back into the fullband involves subsequent tracking of the equaliser for dynamic channels. We will see in Section 5.3.4 that subband adaptive equaliser tracking can potentially outperform the fullband version, but to use this we must start off with the inverse in subbands. If the channel is static or very slowly time-varying this will not matter as we may perform a periodic re-identification and fullband analytic inversion as and when required. With dynamic channels we must determine whether it is better overall to perform a potentially more costly subband frequency-domain analytic inversion so that we may benefit from the advantages of subband adaptive tracking or whether we should convert to the fullband after subband identification and perform the adaptive tracking in the fullband. We will see in Section 5.4 that generally the adaptive processes dominate the cost over the analytic inversion and hence the fully subband method will still usually be the computationally least costly, i.e. where the adaptive identification, analytic inversion and subsequent tracking are all performed in subbands.

Figure 5.11 shows the ratio of fullband to subband computational cost order against $L_{g,f}$ for frequency domain inversion. We see that as $L_{g,f}$ increases and the effects of L_p and N become less significant in (5.32) and (5.33) all the ratios tend to K/N, which causes the subband methods to be slightly more costly than the fullband. Also note that for $L_{g,s} = L_{g,f}/N$ the greatest savings are given for the lowest values of $L_{g,f}$, since the $\log_2 N$ term in (5.33) has the greatest effect at these values. Clearly, frequency-domain inversion in subbands does not produce any worthwhile computational savings and, more often than not, results in a cost increase.

In conclusion, even though subband frequency-domain inversion does not result in great computationally savings we still benefit from the savings that arise from the prior identification required in this method. It also allows later implementation of subband adaptive tracking for dynamic channels which may also have better tracking performance. The computational savings in the adaptive tasks can outweigh potential computational increases in subband frequency-domain inversion. As far as frequency-domain analytic inversion in subbands is concerned on its own

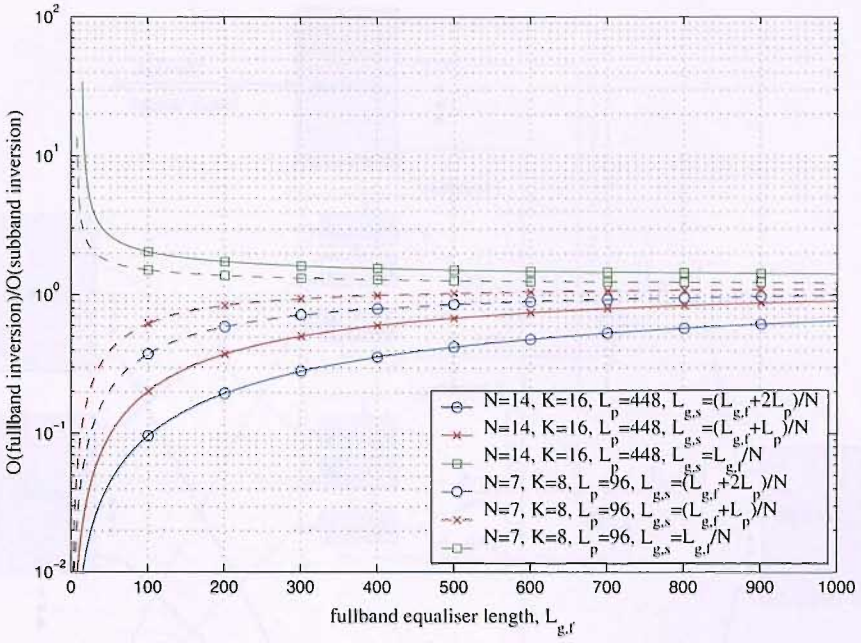

Fig. 5.11: Ratio of fullband to subband frequency-domain analytic inversion computational cost orders.

merits, if we are not concerned with these related benefits, if the channel is static for example, the computational savings, if any, do not warrant the effort involved in using the subband implementation especially as the lower values for $L_{g,s}$ which are necessary to achieve computational savings often result in an unsatisfactory BER performance due to excessive circular convolutional effects and inadequate modelling of the prototype filter response. We would be better off inverting the fullband equivalent of the subband identified channel. The effort may be warranted however if we require the superior BER performance of the time-domain inversion method where the computational savings are much more impressive.

5.3.3 Subband Adaptive System Inversion

Considering a fading communications channel, adaptive tracking of the equaliser is required. As an initialisation we utilise the inversion result of Section 5.3.2 based on an identification of the channel, which converges faster and at a lower complexity than the direct adaptive inversion. The benefit of performing the tracking in subbands is expected to be in the pre-whitening of the received signals whose PSD is governed by the spectral dynamics of the frequency-selective MIMO channel.

Modifying the subband MISO adaptive system in Figure 5.8, the equalisation

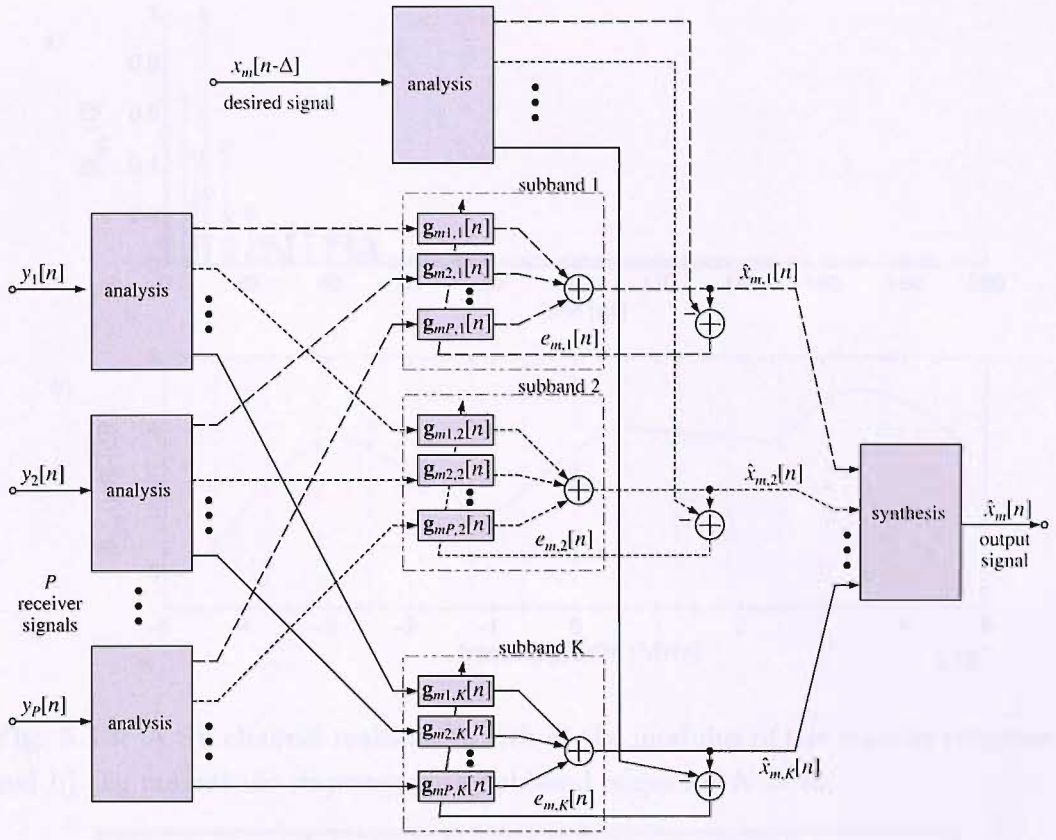

Fig. 5.12: A MISO subband adaptive system arranged for inversion.

architecture shown in Figure 5.12 arises. Using P received signals as inputs, M such MISO blocks have to be solved for the M transmitted data streams, $x_m[n]$. Note that the adaptive filters are now converging to the subband inverses $\mathbf{g}_{mp,k}[n]$ relating the p^{th} receiver to the m^{th} transmitter in subband k, whereas for the identification the system converged to estimate of the channel itself.

We now look at an example for the performance advantages offered by performing adaptive inversion in subbands. Figure 5.13(a) shows a CIR realisation of a Saleh-Valenzuela (SV) channel described in Chapter 2, with parameters $1/\Lambda = 300$ ns, $1/\lambda = 5$ ns, $\Gamma = 60$ ns, $\gamma = 20$ ns with two ray clusters and 40 rays per cluster. In Figure 5.13(b) the magnitude response of this channel exhibits spectral dynamics of approximately 5 dB. For an uncorrelated signal $x_m[n]$ transmitting over this channel Figure 5.13(b) also represents the PSD of the received signal, which will degrade the convergence of the LMS-type adaptive filters as outlined in Chapter 3. Figure 5.13(b) also displays the location of the band edges for a subband system with $K = 16$, demonstrating the whitening effect on the received signals by reducing the spectral dynamics within each subband.

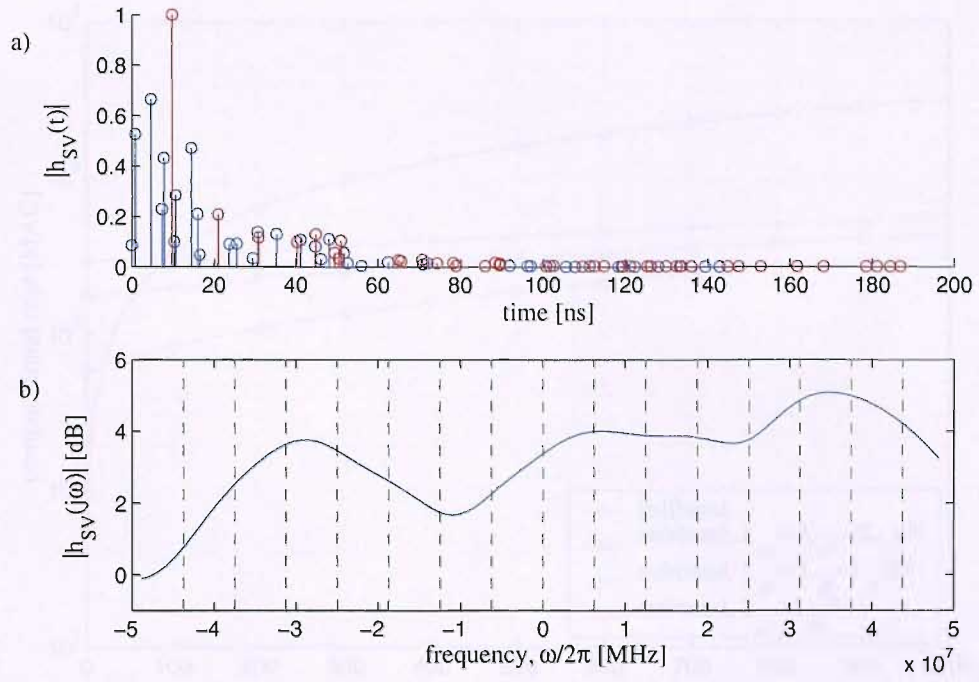

Fig. 5.13: A SV channel realisation with a) the modulus of the impulse response, and b) the magnitude response with subband edges for $K = 16$.

subband k	1	2	3	4	5	6	7	8
dynamic [dB]	0.8	1.8	1.1	0.3	0.85	0.9	0.65	1.1
subband k	9	10	11	12	13	14	15	16
dynamic [dB]	0.6	0.1	0.05	0.15	1.05	0.25	0.8	0.95

Tab. 5.1: Approximate spectral range within each subband.

This is highlighted in Table 5.1, listing the approximate spectral dynamics[2] within each subband of Figure 5.13(b), which are considerably lower than the 5 dB across the entire 100 MHz band.

Next, we look at the complexity of the subband MIMO adaptive inversion. The complexities of the fullband and subband systems are related by

$$C_{\text{subband}} = \frac{K}{N^2} C_{\text{fullband}} + \frac{2M+P}{N}(2L_p + 4K\log_2 K + 8K), \tag{5.34}$$

for the M-NLMS and assuming $L_{g,s} = L_{g,f}/N$, where the second term is due to the analysis and synthesis operations. Figure 5.14 shows the computational cost per fullband sampling period for a range of fullband adaptive equaliser lengths, with three different equivalent subband equaliser lengths. Here we see the overheads caused by the analysis filtering operation and by the prototype filter length. For

[2]For simplicity, the influence of the guard bands is neglected here.

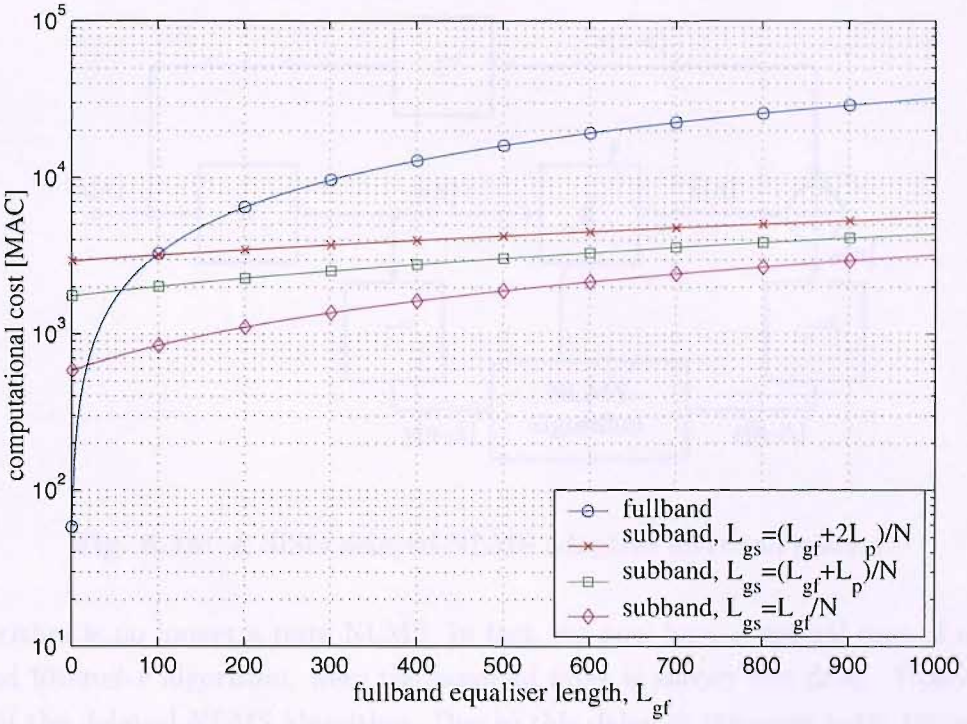

Fig. 5.14: Computational cost per fullband sampling period of adaptive inversions for fullband and subband with three different equaliser lengths, for a 2×2 MIMO equaliser with $N = 14$, $K = 16$ and $L_p = 448$.

low values of $L_{g,f}$ we are more likely to have to use $L_{g,s} = (L_{g,f} + 2L_p)/N$ for the subband equaliser to model the prototype filter response adequately, however for greater values of $L_{g,f}$, $L_{g,s} = L_{g,f}/N$ may suffice. This makes the point that subband systems are generally more suitable for systems where a long equaliser length relative to L_p is required.

5.3.4 Subband Adaptive Equaliser Tracking

As with the fullband systems, an application of subband adaptive inversion is to perform equaliser tracking of a fading channel. Unfortunately there is a complication with the subband system that means the error-free decision-directed performance is not the same of that using a training sequence. Adaptation is performed in subbands, and referring to Figure 5.12 we note if the desired signals are to be generated from the subband equaliser output, they must first be passed through a synthesis bank, the decision or slicing operation must be performed and then the signal must be projected back into the subband domain using an analysis bank. Together these two filter banks caused an extra delay of L_p/N in the error path of the adaptive algorithm on the order of the filter bank length and hence the

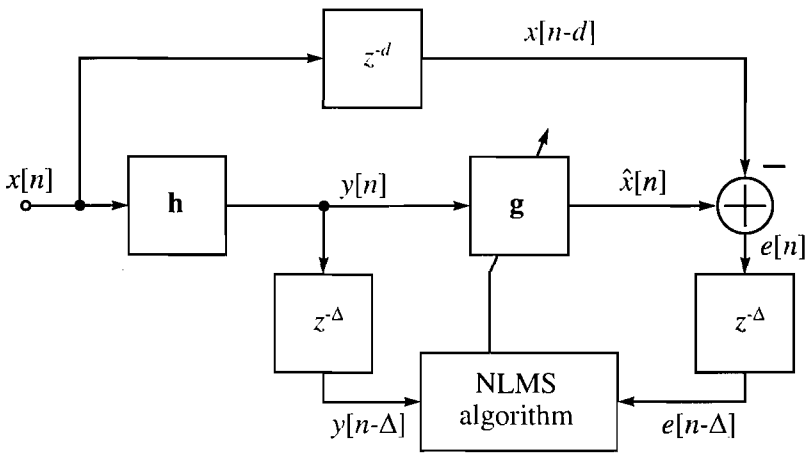

Fig. 5.15: A SISO delayed-NLMS adaptive inversion system.

algorithm is no longer a pure NLMS. In fact, we now have a special case of a so-called filtered-x algorithm, were the nominal filter is simply the delay. Hence we call it the delayed-NLMS algorithm. Due to this delay in the error path, the same delay must be applied to the input to the algorithm, i.e. the received signal, but *not* to the branches that lead to the synthesis filter bank. Figure 5.15 shows the set-up of a delayed NLMS algorithm, whereby for simplicity the delay introduced by the analysis and synthesis filter banks has been modelled as a perfect delay Δ and the delay introduced by the channel and equaliser is d. Note that Δ and d are generally unrelated. The figure also only shows a SISO system, again for simplicity. Both the input and desired signals are delayed to the standard NLMS algorithm.

The same method was used in [72] to combat a similar problem, but the convergence of the delayed-NLMS algorithm is known to often be inferior to that of the standard NLMS algorithm [79, 165]. Hence in the simulation results for subband equaliser tracking results are shown for both the standard NLMS algorithm using a sequence known to the receiver and for a system using the delayed-NLMS algorithm. In the former case no actual data can be sent. These results will represent the error-free performance bound for the subband adaptive tracking system running in decision-directed mode.

5.4 Simulations and Discussion

This section presents results obtained from various systems employing subband techniques, and puts them into context based on the discussions in this chapter.

Channel Length	SB $L_{h,s} = 4$	SB $L_{h,s} = 12$	SB $L_{h,s} = 68$	FB $L_{h,f} = 50$
Cost (MACs)	571	864	2,912	1,652
% of fullband	35%	52%	176%	100%

Tab. 5.2: Computational cost per fullband sampling period for the SS SPIB adaptive inversions in Figure 5.16.

In all simulation 16 subbands are used since is seems to give a good compromise between adaptive algorithm performance improvement, computational cost reduction and sources of error, i.e. error floor.

5.4.1 Subband Adaptive System Identification

We start with the performance of noiseless subband adaptive channel identification, which would be followed by an analytic inversion to create the channel equaliser.

For the simulations, the SS SPIB 2 × 2 MIMO channel as shown in Chapter 2 is employed. Subband parameters $K = 16$, $N = 14$ and a $L_p = 448$ GDFT filter bank are used for the analysis and synthesis. Results are shown in Figure 5.16 for three different values for $L_{h,s}$ for the subband adaptive identification, compared to a fullband adaptation with $L_{h,f} = 50$ as performed in Section 3.6.1. The simulation for $L_{h,s} = 4$ approximately corresponds to $L_{h,s} = L_{h,f}/N$ and hence the initial adaptation rate is approximately the same as for the fullband adaptation. However, the subband filters are too short to model the prototype filter response, resulting in a very high final MSE of about -11 dB. For $L_{h,s} = 12$ a lower final MSE of about -27.5 dB is reached at the cost of slower convergence. Finally, a curve for $L_{h,s} = 68$ is shown which approximately corresponds to $L_{h,s} = (L_{h,f} + 2L_p)/N$, yielding a final MSE of approximately -39 dB. As in a noisy environment the final MSE will be limited by the channel noise and of the three subband simulations $L_{h,s} = 12$ provides a good compromise between convergence speed and final MSE.

Table 5.2 shows the computational cost per fullband sampling period associated with the curves in Figure 5.16. The subband adaptation with $L_{h,s} = 12$ shows a 48% computational saving over the fullband adaptation. An interesting aspect is to consider the total cost required to reach a specific MSE value. For example to reach an MSE of -20 dB the subband adaptation for $L_{h,s} = 12$ needs to be executed about 3.8 times longer than the fullband adaptation. The latter consumes a total of about 1.5×10^6 MACs while the $L_{h,s} = 12$ subband adaptation requires 3×10^6 MACs.

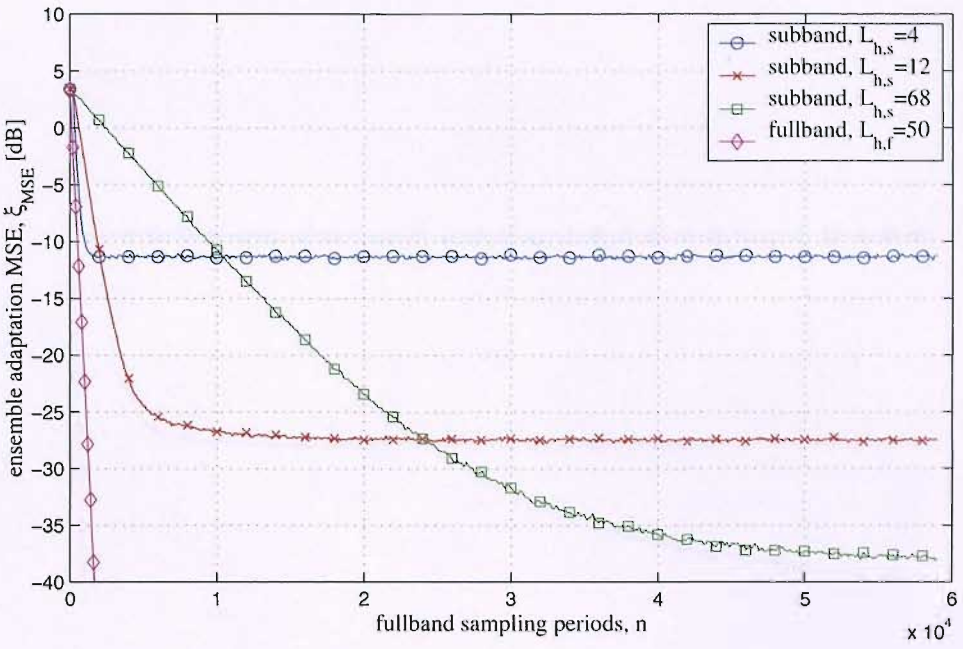

Fig. 5.16: Subband adaptive system identification of a SS SPIB 2×2 MIMO channel for a range of subband adaptive channel lengths, and the corresponding fullband adaptation for comparison.

Channel Length	SB $L_{h,s} = 3$	SB $L_{h,s} = 12$	SB $L_{h,s} = 66$	FB $L_{h,f} = 30$
Cost (MACs)	535	864	2,839	1,012
% of fullband	52%	85%	280%	100%

Tab. 5.3: Computational cost per fullband sampling period for the 100 MHz bandwidth SV adaptive identifications in Figure 5.17.

Figure 5.17 shows the adaptations for the length-30 100-MHz bandwidth SV channels, with the same parameters as before, and we see a similar behaviour. Compared to SPIB simulation, the curve corresponding to $L_{h,s} = L_{h,f}/N$ now has a greater final MSE of about -9 dB as the filters are shorter and hence smaller compared to L_p which is fixed for all these simulations.

The computational costs for the 100 MHz bandwidth SV adaptations are shown in Table 5.3. To reach an MSE of -20 dB, the subband adaptation with $L_{h,s} = 12$ takes 6.3 times longer than the fullband adaptations. The subband adaptation again consumes a total of 3×10^6 MACs, while the fullband system only requires 5.6×10^5 MACs to reach the required MSE value.

Finally, we look at the adaptation of a much longer channel where the subband technique is likely to result in computational savings, namely a SV channel sampled at 1 GHz introduced in Chapter 2. This channel is 300 coefficients long, and the

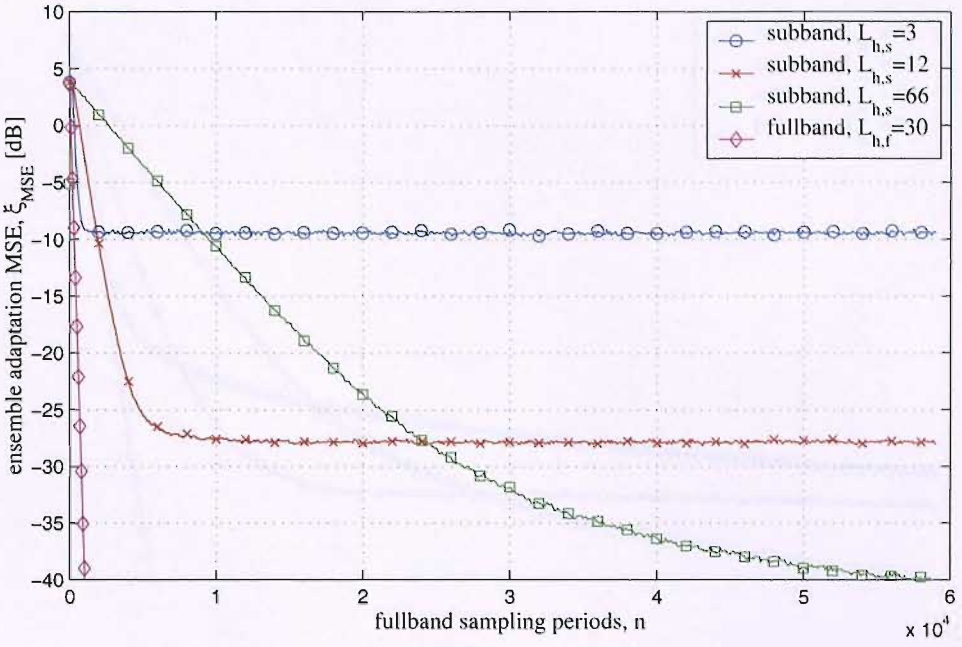

Fig. 5.17: Subband adaptive system identification of a 100 MHz bandwidth SV 2 × 2 MIMO channel for a range of subband adaptive channel length, and the corresponding fullband adaptation for comparison.

Channel Length	SB $L_{h,s} = 22$	SB $L_{h,s} = 44$	SB $L_{h,s} = 86$	FB $L_{h,f} = 300$
Cost (MACs)	1,230	2,034	3,570	9,652
% of fullband	13%	21%	37%	100%

Tab. 5.4: Computational cost per fullband sampling period for the 1 GHz bandwidth SV adaptive identifications in Figure 5.18.

adaptation curves are shown in Figure 5.18. The subband curve with $L_{h,s} = L_{h,f}/N = 22$ now has a much improved final MSE compared to the SS SPIB and 100 MHz SV channels, as the filter is longer. Additionally shown is the curve for $L_{h,s} = 44$ which reaches -30 dB MSE much quicker, and for $L_{h,s} = (L_{h,f} + 2L_p)/N \approx 86$, which has the slowest convergence but attains the lowest final MSE.

Table 5.4 shows the computational cost per fullband sampling period for the adaptations, where the subband adaptations have the lowest cost. If we consider the curve with $L_{h,s} = 44$, -20 dB is reached after 2.8×10^7 MACs but the fullband adaptation consumes 6.1×10^7 MACs. Thus, for this longest channel in terms of the number of taps, the subband adaptation does result in a computational saving.

In conclusion significant computational savings will only arise for long channels where the fixed analysis filter overhead becomes relatively less significant and

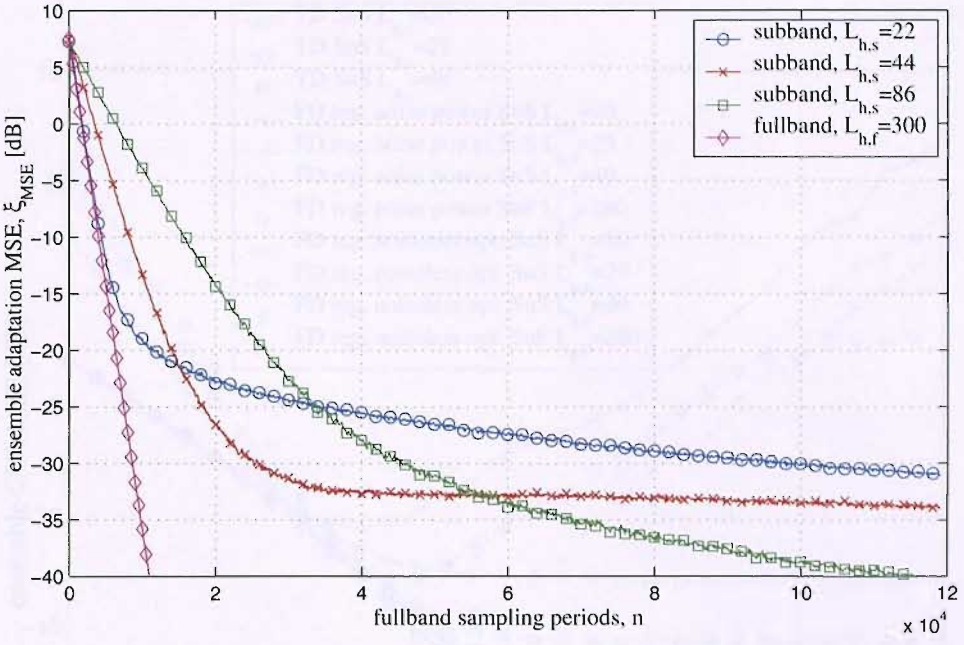

Fig. 5.18: Subband adaptive system identification of a 1 GHz bandwidth SV 2×2 MIMO channel for a range of subband adaptive channel length, and the corresponding fullband adaptation for comparison.

$L_{h,s}$ is sufficiently large compared to L_p. We can generalise by saying that the longer the channel, the greater the computational savings offered by the subband technique. This is fortunate as the longer channels are those that consume the most computational power during adaptation.

One final point relates to the tracking of a dynamic channel itself. If we wish to perform a periodic analytic inversion of the channel when required, we may desire continuous tracking of the channel for this purpose, rather than re-identifying it prior to each inversion. In this case the number of iterations required to reach a specific MSE becomes irrelevant since the adaptation must be performed continually anyway, and we may directly compare the cost per fullband sampling period for the subband and fullband adaptations. For example, the SS SPIB channel identification with $L_{h,s} = 12$ requires only 864 MACs per fullband sampling period whereas the fullband method consumes 1,652 MACs, and therefore the former is clearly the most favourable solution.

5.4.2 Subband Analytic System Inversion

In this section the simulation results for the Channel-Equaliser Response (CER) MSE are shown for equalisers created by identifying an unknown channel in sub-

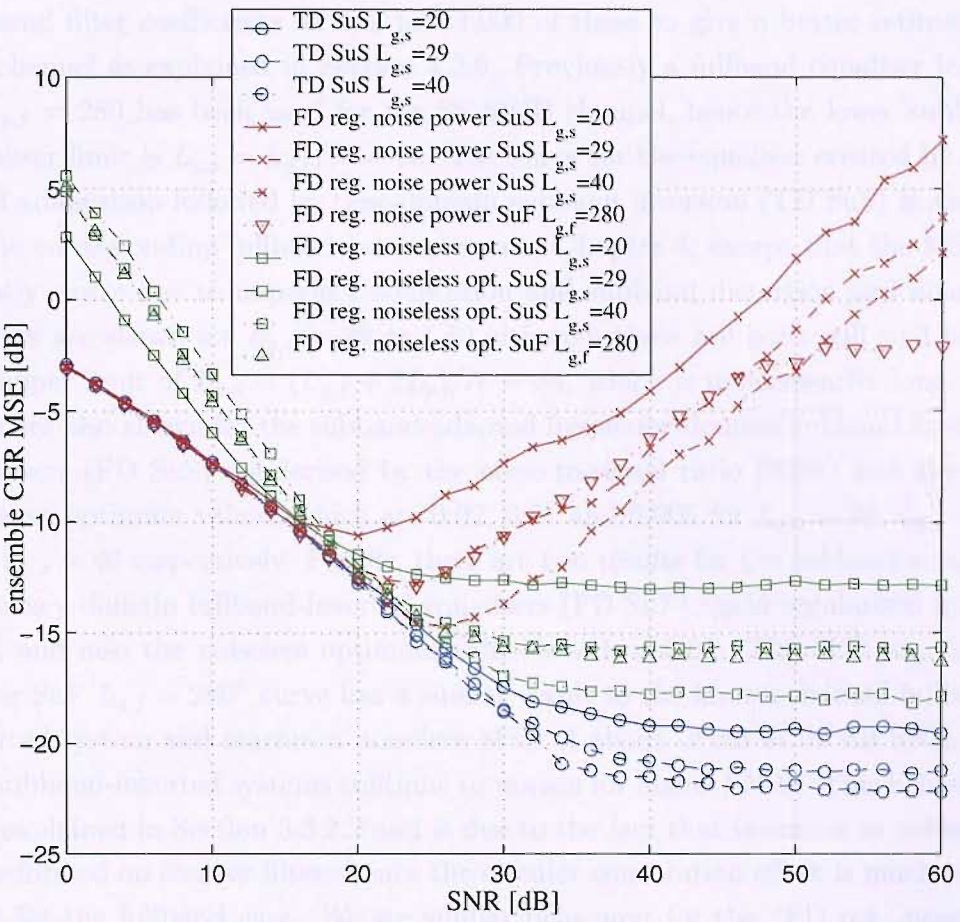

Fig. 5.19: SNR versus Channel-Equaliser Response (CER) MSE for a noisy unknown SS SPIB 2 × 2 MIMO channel.

bands prior to analytically inverting it. The inversion is performed either based on the fullband equivalent system which, as shown in Section 5.3.2.2, may be computationally less costly when calculated in the DFT domain, or on the subband adapted system. The results in this section show broadly similar behaviour to the fullband CER MSE in Section 4.6.1, although a notable difference in the implementation is that the channel was known for the fullband results but here the channel must be identified in subbands, hence it is effectively unknown.

We start by looking at the results for the unmodified SS SPIB channel, shown in Figure 5.19. The reasons behind the overall behaviour of this result have already been explained in Section 4.6.1, so here we shall concentrate on differences in terms of the subband MSE relative to the fullband and computational cost. For each inversion method, results are shown for a number of different subband equaliser lengths, although for the subband adaptations $L_{h,s} = 12$ is always used, based on satisfactory result displayed in Figure 5.16. In all simulations the system adapted to the channel for 14,000 fullband sampling periods and temporally averages the

subband filter coefficients for the last 4.000 of these to give a better estimate of the channel as explained in Section 4.2.6. Previously a fullband equaliser length of $L_{g,f} = 280$ has been used for the SS SPIB channel, hence the lower subband equaliser limit is $L_{g,s} = L_{g,f}/N = 20$. The curve for the equaliser created by subband adaptation followed by time-domain subband inversion (TD SuS) is similar to the corresponding fullband curve shown in Chapter 4, except that the MSE is slightly worse due to imperfect adaptation and subband distortion and aliasing. Results are shown for $L_{g,s} = 29$ and 40 although these are both still well below the upper limit of $L_{g,s} = (L_{g,f} + 2L_p)/N = 84$, which is unnecessarily long. Results are also shown for the subband-adapted frequency-domain subband-inverted equalisers (FD SuS) regularised by the noise-to-signal ratio (NSR) and also the noiseless optimum values, which are 0.02, 0.01 and 0.005 for $L_{g,s} = 20$, $L_{g,s} = 29$ and $L_{g,s} = 40$ respectively. Finally, there are two results for the subband-adapted frequency-domain fullband-inverted equalisers (FD SuF) again regularised by the NSR and also the noiseless optimum value, which is 0.01. The "FD reg. noise power SuF $L_{g,f} = 280$" curve has a similar result to the known-channel fullband-inverted system and reaches a noiseless MSE of about -2 dB at 50 dB SNR, but the subband-inverted systems continue to worsen for higher SNRs. This behaviour was explained in Section 5.3.2.2 and is due to the fact that inversion in subbands is performed on shorter filters hence the circular convolution effect is much worse than for the fullband case. We see similar behaviour for the "FD reg. noiseless opt. SuS $L_{g,s} = 20$" curve. We would have expected this to give similar performance to the "FD reg. noiseless opt. SuF $L_{g,f} = 280$" curve, which does give the similar performance to the known-channel fullband-inverted system, but as the circular convolutional effects are now worse and the filters are of inadequate length to model the prototype filter response well, the performance is also significantly worse.

Table 5.5 shows the evaluated complexity orders for the inversions involved in the SS SPIB simulations, but does not include the cost of the prior adaptations. We see that, as expected, performing the time-domain inversions in subbands provides considerable computational savings over the fullband. Also shown are the frequency-domain inversion costs. The reason for the choice to simulate the equaliser with $L_{g,s} = 29$ is because this represents a cross-over point where subband FD inversion is about as costly as the fullband. Evidently, the best compromise between MSE performance and cost is to calculate the equaliser using the frequency-domain method, switching to a fixed regularisation factor at between 15 dB and 25 dB SNR depending on which equaliser length is deemed to give adequate performance. Bit error rate performance will help decide this and BER curves will be shown in Section 5.4.5.

Equaliser Length	TD SuS $L_{g,s} = 20$	TD SuS $L_{g,s} = 29$	TD SuS $L_{g,s} = 40$	TD SuF $L_{g,f} = 280$
Total Cost	1.28×10^5	3.9×10^5	1.02×10^6	2.2×10^7
Equaliser Length	FD SuS $L_{g,s} = 20$	FD SuS $L_{g,s} = 29$	FD SuS $L_{g,s} = 40$	FD SuF $L_{g,f} = 280$
Total Cost	1.38×10^3	2.25×10^3	3.41×10^3	2.28×10^3

Tab. 5.5: Evaluation of computational complexity order of analytic inversion in subbands and fullband for a range of equaliser lengths for the SS SPIB and 100 MHz-sampled SV channel.

Comparing the inversion costs to the adaptation costs in the previous section highlights the fact that the channel adaptation will dominate the overall cost involved in calculating the equaliser, assuming frequency-domain inversion is used. As we saw that the SS SPIB channel is too short (i.e. 50 coefficients long) for the subband adaptation to provide any computational savings over the fullband we must conclude that the fullband identification and inversion will give the best performance in terms of MSE and cost.

Figure 5.20 shows the CER MSE results for a SV channel sampled at 100 MHz. The behaviour is similar to Figure 5.19 with the exception that the MSEs are generally better than for the SS SPIB channel because this channel is shorter, i.e. length 30, and inverses of the same length are used. For the same reason the frequency-domain inversion regularised by the NSR does not reach as bad an MSE as the SNR increases. The complexities are also those shown in Table 5.5 because the inverse lengths are the same. Even though the channel identification is faster and less computationally intensive than before it still dominates the overall cost and hence the fullband method is better than the subband. Further as the channel is even shorter the difference between the fullband and subband methods is even greater than before.

Since it is evident that the subband method gives no benefit for the initial identification and inversion of short channels, we now look at a much longer channel, i.e. the length 300 SV channel sampled at 1 GHz. Figure 5.21 shows the CER MSE behaviour but only for a single subband equaliser length in each case. The channels are identified in subbands using length 44 adaptive filters, which is double the minimum of $L_{h,s} = L_{h,f}/N \approx 22$, and the equalisers are length 70. The behaviour follows similar patterns as in the previous two simulations but here we are particularly interested in the computational costs. Table 5.6 shows the evaluated complexities for the subband inversions for $L_{g,s} = 70$, and also for the equivalent fullband inversions where $L_{g,f} = NL_{g,s} = 980$. These fullband inversions were not

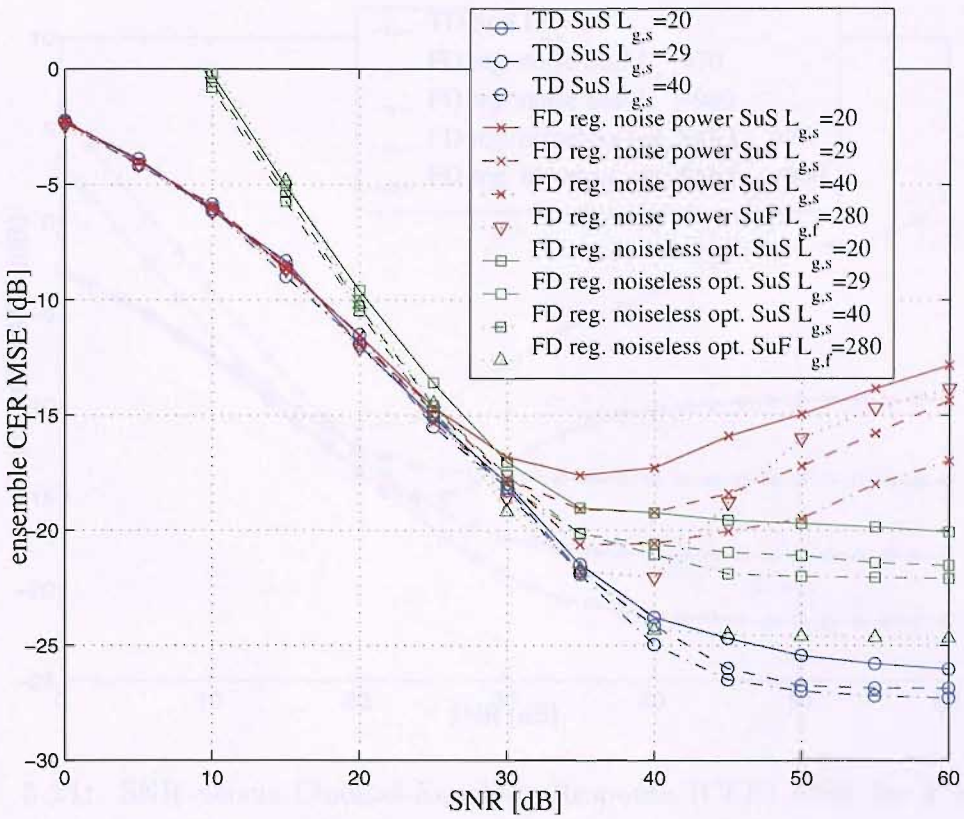

Fig. 5.20: SNR versus Channel-Equaliser Response (CER) MSE for a noisy unknown 100 MHz SV 2 × 2 MIMO channel.

simulated in Chapter 4 as the computational cost involved in the time-domain inversion was too large. The table shows that for time-domain inversion the subband method reduces the computational cost to about 0.58% of the fullband inversion, which is clearly a great advantage. The subband frequency-domain inversion now also has a lower cost than the fullband inversion which was not the case for the channels where a shorter inverse sufficed— it reduces the cost by about 30%.

Equaliser Length	TD SuS $L_{g,s} = 70$	TD SuF $L_{g,s} = 980$	FD SuS $L_{g,s} = 70$	FD SuF $L_{g,f} = 980$
Total Cost	5.49×10^6	9.41×10^8	6.86×10^3	9.74×10^3

Tab. 5.6: Evaluation of computational complexity order of analytic inversion in subbands and fullband for an range of equaliser lengths for the 1 GHz-sampled SV channel.

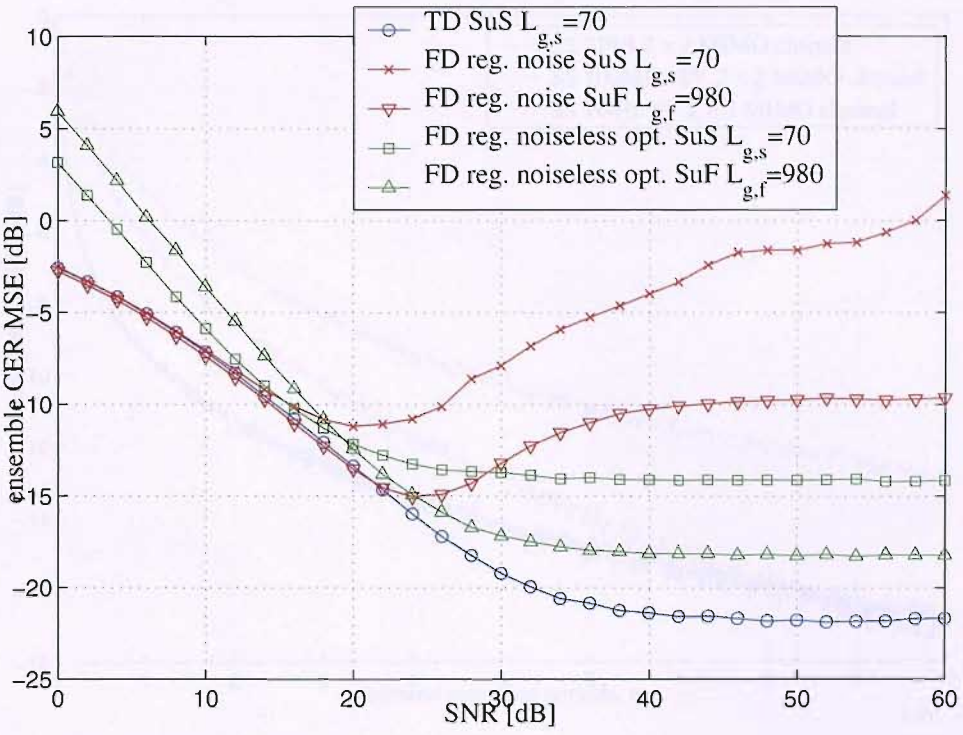

Fig. 5.21: SNR versus Channel-Equaliser Response (CER) MSE for a noisy unknown 1 GHz SV 2×2 MIMO channel.

5.4.3 Subband Adaptive System Inversion

In this section we look at the performance results of subband adaptive inversion. Figure 5.22 shows the adaptation curves for the subband inversion of the 2×2 symbol-spaced (SS) SPIB, 100 MHz-sampled SV and 1 GHz-sampled SV channels. The M-NLMS algorithm with $\tilde{\mu} = 0.18$ is used in all cases. For the SS SPIB and 100 MHz-sampled SV inversions, $L_{g,s} = L_{g,f}/N = 20$ is used, and for the 1 GHz inversion $L_{g,s} = 70$ is used. We expect faster convergence with the subband inversion of frequency-selective channels than with the fullband inversion due to the spectral whitening effect as discussed in Sections 5.2.2 and 5.3.3. Comparing these results with the corresponding ones in Section 4.6.3 we see that the fullband inversion of the 2×2 SS SPIB channels reaches a MSE of about -15.5 dB after 80,000 fullband sampling periods and the subband inversion shows almost the same performance, reaching -16 dB. However as the SS SPIB channel is nearly flat we do not expect any great improvement. The 100 MHz SV channel is very frequency-selective and we see that whereas the fullband inversion reaches only about -10 dB after 80,000 fullband sampling periods the subband inversion performs much better, reaching about -16 dB. The SS SPIB initially converges at the faster rate as it is relatively flat, but the 100 MHz SV channel inversion attains a lower final

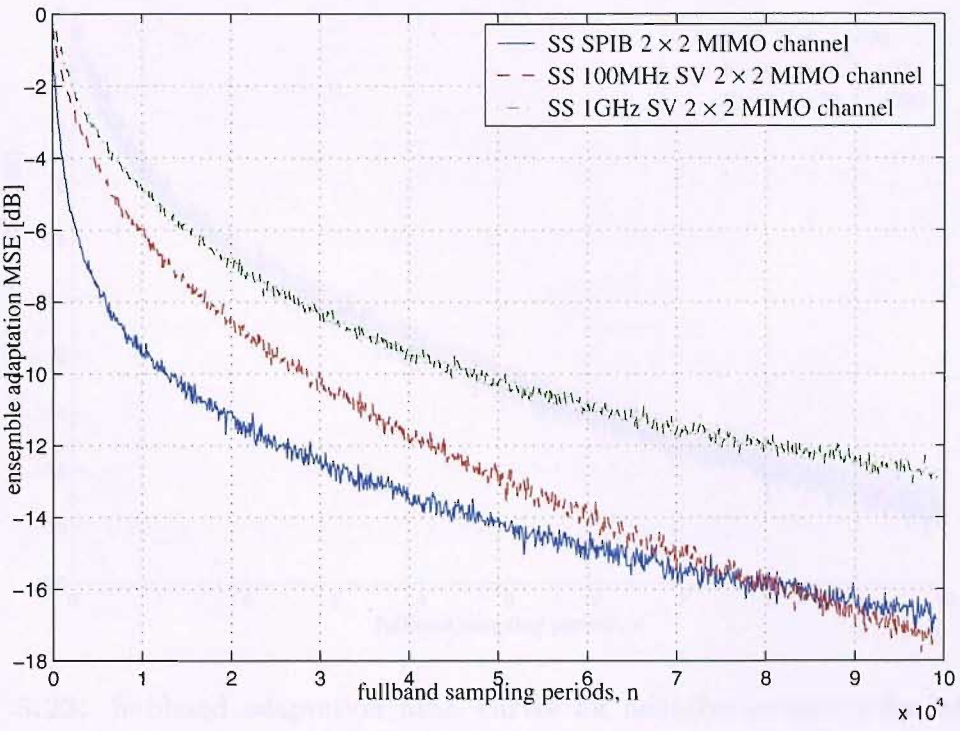

Fig. 5.22: Subband adaptation MSE curves for adaptive inversion for unknown static noiseless SS SPIB, 100 MHz and 1 GHz bandwidth Saleh-Valenzuela 2×2 MIMO channels.

MSE as it is shorter than the SS SPIB channel for the same $L_{g,s}$. Finally, we show an adaptation curve for the inversion of the SV channel sampled at 1 GHz, and this converges at the slowest rate. A corresponding curve is not shown in the fullband inversion in Chapter 4 because not only would the convergence have been very slow but also the computational cost of this adaptation would have been unfeasibly great due to the required length of the fullband equaliser.

Though up until this point in this chapter we have only considered a system consisting of 16 subbands, we briefly now examine using varying numbers of subbands during an adaptive inversion. Figure 5.23 shows the performance for $K = 8, 16$ and 32 subbands inverting a symbol-spaced 100 MHz sampled SV 2×2 MIMO channel. We see that the adaptation profile is almost identical in each case, meaning that for this particular spectral profile, 8 subbands achieve almost all the adaptation improvement possible. Using more subbands will achieve better adaptation only for channels that exhibit greater spectral dynamics; however it is in out best interest to keep this number as low as possible since increasing it unnecessarily limits the final attainable adaptation MSE. The final MSE with 16 subbands however is not prohibitive and we can expect it to perform better with a channel such as the 1 GHz sampled SV channel, hence we continue to use 16 subbands for the

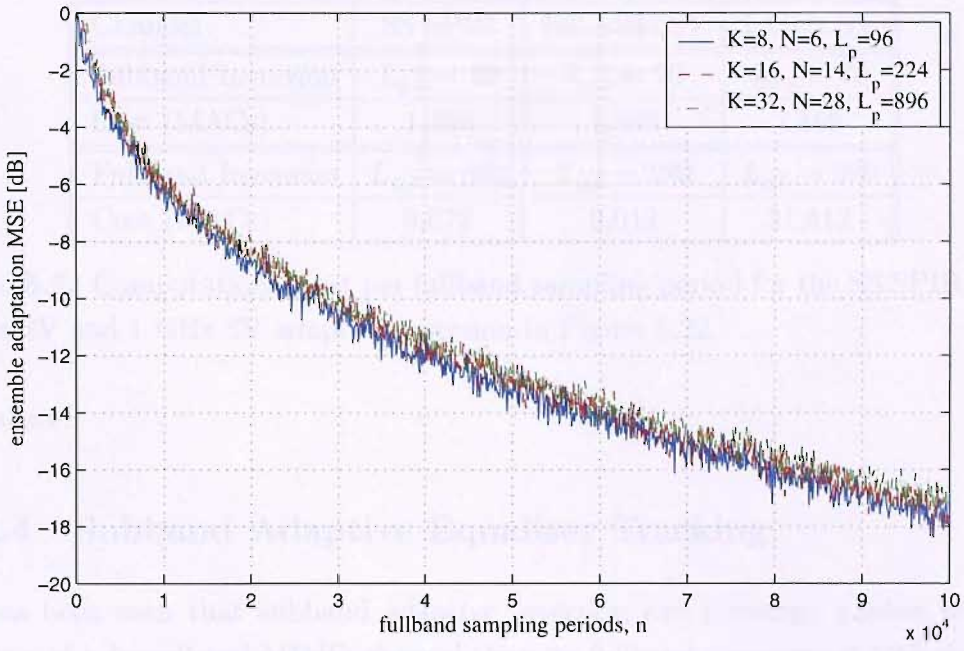

Fig. 5.23: Subband adaptation MSE curves for adaptive inversion for known static noiseless SS 100 MHz Saleh-Valenzuela 2×2 MIMO channels with number of subbands $K = 8, 16$ and 32.

remainder of the chapter.

Since a broadband channel equaliser is generally much longer than the channel itself, we expect the computational cost advantages offered by the subband technique to be greater than for the subband channel identification in Section 5.4.1. Table 5.7 shows the computational cost per fullband sampling period of the inversion, with the fullband costs shown for comparison. Both the SS SPIB and 100 MHz-sampled SV channel equalisers are length-20 in subbands, and we see that only about 15% of the MACs are required compared to the fullband inversion. The advantage for the longer 1 GHz-sampled SV channel is even greater as the fixed overheads of the analysis and synthesis filtering operations become less significant from the cost perspective and the subband approach results in only 10% of the MACs of the fullband method.

In conclusion, not only does the subband approach result in faster convergence to the inverse of frequency-selective channels but the arising computational cost of the method is considerably lower. Although the benefits of the subband method are not convincing for the adaptive identification and analytic inversion in previous sections, the advantages offered here can far outweigh this if a dynamic channel is to be tracked where the adaptation must run continuously. To use the subband method for tracking we must invert the channel in subbands to initialise the

Channel	SS SPIB	100 MHz SV	1 GHz SV
Subband Inversion	$L_{g,s} = 20$	$L_{g,s} = 20$	$L_{g,s} = 70$
Cost (MACs)	1,339	1,339	3,168
Fullband Inversion	$L_{g,f} = 280$	$L_{g,f} = 280$	$L_{g,f} = 980$
Cost (MACs)	9,012	9,012	31,412

Tab. 5.7: Computational cost per fullband sampling period for the SS SPIB, 100 MHz SV and 1 GHz SV adaptive inversion in Figure 5.22.

equaliser.

5.4.4 Subband Adaptive Equaliser Tracking

It has been seen that subband adaptive inversion can converge quicker to the inverse of a broadband MIMO channel than its fullband counterpart. We saw in Section 4.6.4 that the fullband algorithm tracking performance for an MS moving at 120 km/h in a 100 MHz-sampled SV MIMO channel bordered on acceptable for low order constellation patterns but even then the MMSE inverse would have probably needed to be recalculated at some point beyond the simulated time. Figure 5.24 and 5.25 show the equivalent subband tracking simulations with BER error probability levels superimposed. For the SPIB channel the subband approach results in no benefit due to the small spectral range of the channel. When tracking the inverse of the SV100M channel the subband algorithm performs slightly better with the tracking MSE reaching just below the QPSK 1% BER error threshold by the end of the simulation. Performing decision-directed tracking however will require the use of the delayed subband algorithm. Using this with the M-NLMS algorithm with $\tilde{\mu} = 0.18$ it appears the algorithm becomes unstable, with the MSE growing without bound. It would appear that for dynamic channels the delay in the feedback can cause stability problems. Reducing $\tilde{\mu}$ to 0.1 corrects the stability issue but the performance is now slightly worse than for the fullband system. Since the tracking curves are closer to the curves with no adaptation, clearly this channel inverse is more difficult to track than the SPIB channel for any algorithm. Finally, the subband method however enables the tracking to be executed at a significantly lower computational cost shown, which is shown in Table 5.7.

A seemingly greater challenge is to track the SV channel equaliser sampled at 1 GHz for an MS moving at 120 km/h. In this case the required equaliser is longer— length-70 subband equaliser filters are used, equivalent to a 980-tap fullband filter with $N = 14$. Further, this channel exhibits spectral dynamics such that within each subband the eigenvalue spread of the auto-correlation matrix is likely to

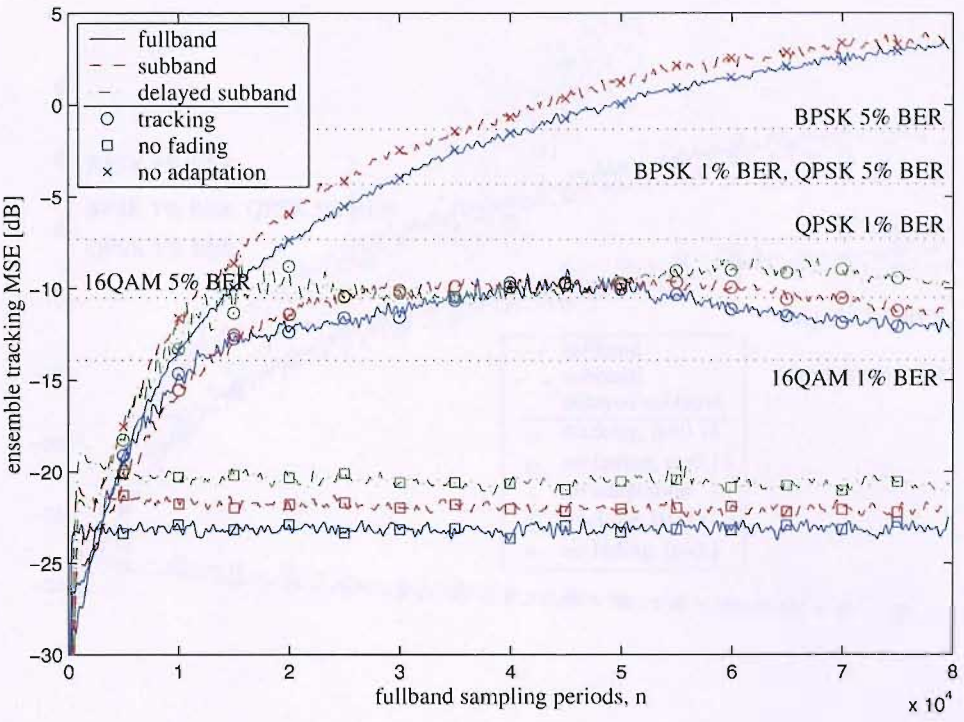

Fig. 5.24: Subband, delayed subband and fullband adaptive equaliser tracking MSE for Rayleigh Doppler-faded 2×2 MIMO SPIB channel using M-NLMS algorithm with $\mu = 0.18$, and MS moving at 120 km/h.

be close to that of the fullband case. Hence we would not expect the subband method to produce a great improvement in tracking ability over the fullband. Note there are no simulations for the fullband system due to the computational requirements of such a simulation. Comparing the tracking results in Figure 5.26 to the "no adaptation" and "no fading" curves we see that they are closer to the worst-case, meaning that the system has difficulty tracking the inverse. For the equaliser initialisation in this simulation the frequency-domain inversion method is used due to the excessive computational cost that would be required to perform a better time-domain inversion. As before, the delayed subband adaptation with $\tilde{\mu} = 0.18$ becomes unstable but setting $\tilde{\mu} = 0.1$ corrects this. Curiously, this results in a better tracking ability than the delayless subband structure with $\tilde{\mu} = 0.18$– clearly the step size coefficient is an important parameter for dynamic tracking. A further important point about this simulation relates to the fact that the Doppler frequency relative to the symbol rate is smaller and so the channel fades relatively slower. Hence the degradation in the delayless subband tracking MSE gradient is much lower than for the SPIB and SV100M channels, reaching about -17 dB MSE by the end of the simulation. The simulation can not be executed until the MSE curves approach a steady-state since the associated computational intensity

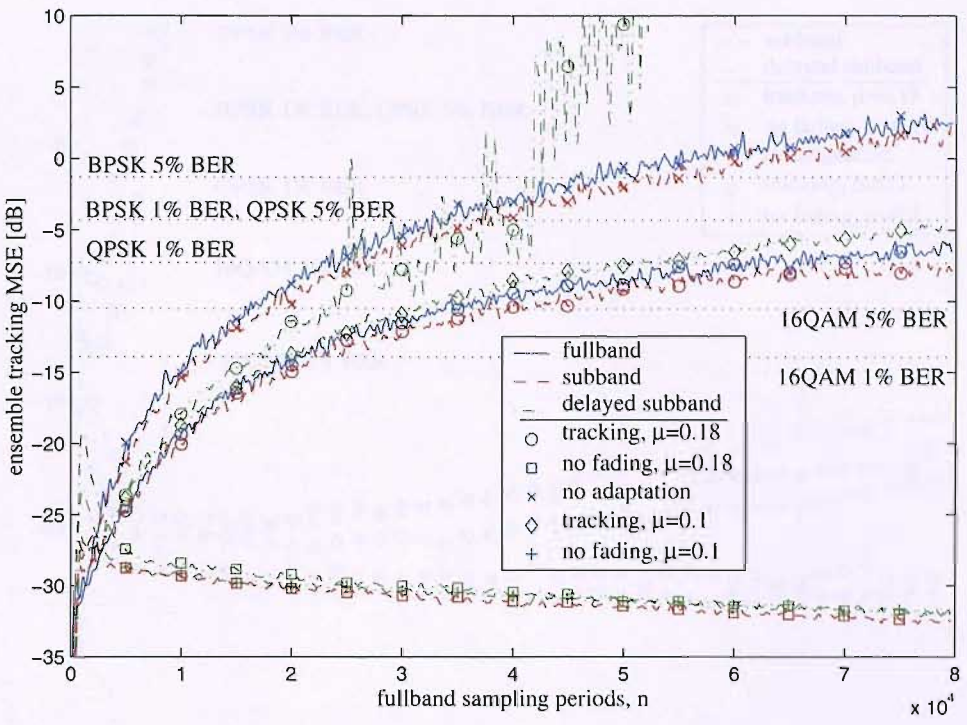

Fig. 5.25: Subband, delayed subband and fullband adaptive equaliser tracking MSE for Rayleigh Doppler-faded 2 × 2 MIMO SV channel sampled at 100 MHz using M-NLMS algorithm with $\mu = 0.18$, and MS moving at 120 km/h.

makes this unfeasible, but some interesting conclusions may still be drawn. The slow fading rate provides greater scope to re-identify the channel via the use of a training sequence and perform an analytic inversion once the MSE has degraded too far. In conclusion, even though the 1 GHz-sampled SV channel is much harsher than the SPIB and 100 MHz-sampled SV channel, it appears that maintaining an acceptable MSE for a greater number of fullband sampling periods is possible.

5.4.5 Subband System BER Performance

In this final section we show simulations for the BER performance of the various subband systems developed in this chapter using a BPSK modulation pattern and compare these to each other as well as the equivalent fullband performance noted in Section 4.6.5. The parameters of the simulated systems are the same as those used for the CER MSE simulations in Sections 5.4.1, 5.4.2 and 5.4.3. We do not consider the two-tap channel because it is too short for the subband method to provide any advantage, as explained in Section 5.4.1. The BER performance of the systems communicating over the SS SPIB channel is shown in Figure 5.27. Even though we saw in Section 5.4.2 that the larger values of $L_{g,s}$ resulted in a

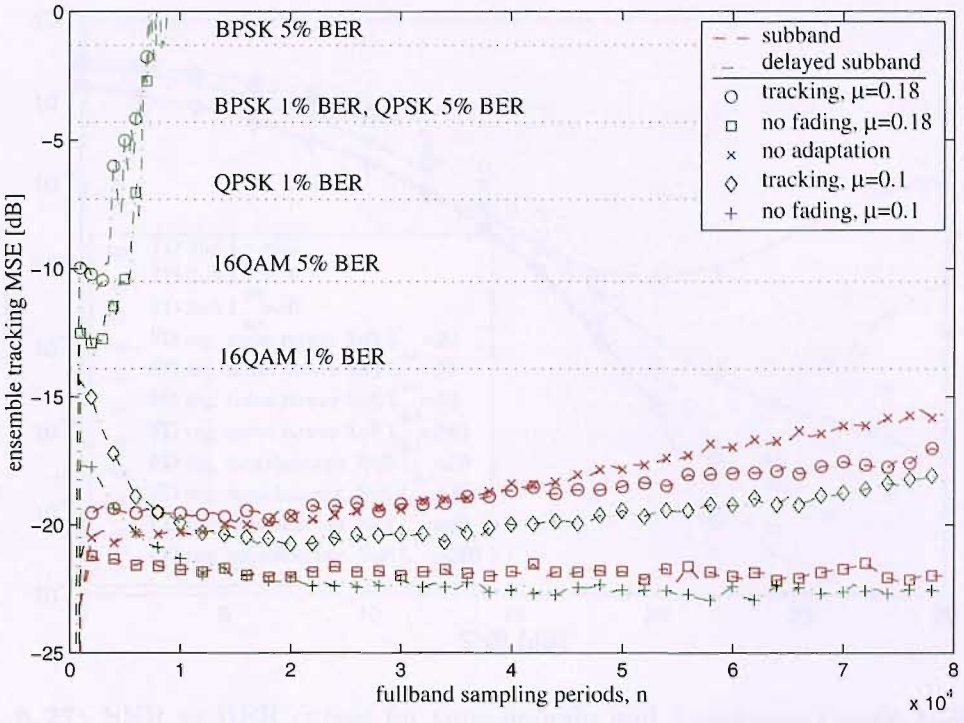

Fig. 5.26: Subband, delayed subband and fullband adaptive equaliser tracking MSE for Rayleigh Doppler-faded 2×2 MIMO SV channel sampled at 1 GHz using M-NLMS algorithm with $\mu = 0.18$, and MS moving at 120 km/h.

lower MSE, this does not translate to any significant improvement in the BER performance for the time-domain inversion (TD). Hence it appears sufficient to use $L_{g,s} = L_{g,f}/N = 20$. With the frequency-domain (FD) method there are differences between the results for the different equaliser lengths and a value of $L_{g,s}$ below 29 will result in computational savings over the fullband frequency-domain inversion. If the $L_{g,s} = 20$ curve is regularised by the NSR at SNR values below about 16 dB and then switched to a fixed regularisation factor (in this case 0.02), the performance is quite reasonable, although not as good as the fullband inversion BER performance shown in Section 4.6.5. Using $L_{g,s} = 29$, where the computational cost is the same as for the fullband inversion and again switching to a fixed regularisation factor (now 0.01) above an SNR of 21 dB, slightly worsens the performance compared to a fullband inversion. A subband equaliser length $L_{g,s} = 40$ is required before the subband (SuS) performance becomes comparable to the fullband (SuF), but the cost has now risen by about 50%. Beyond an SNR of about 17.5 dB the fullband frequency-domain inversion regularised by NSR (FD reg. noise power SuF $L_{g,f} = 280$) method becomes the most favourable as it outperforms the subband inversion with $L_{g,s} = 29$ (FD reg. noise power $L_{g,s} = 29$) but has a similar computation cost. There is no performance curve for an adaptive

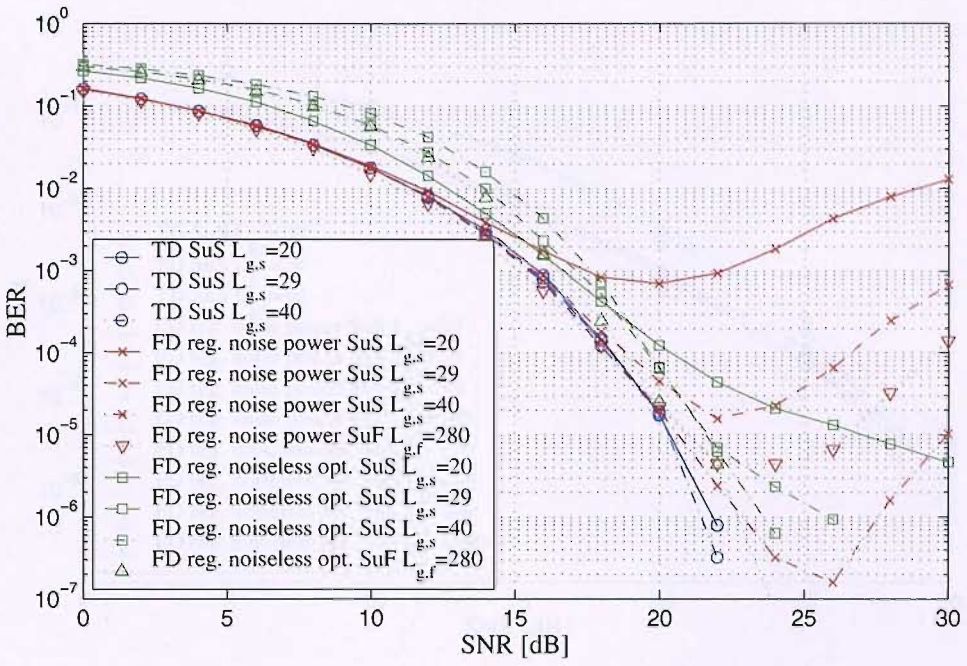

Fig. 5.27: SNR vs BER curves for time-domain and frequency-domain analytic inversion of the subband identified noisy static SS SPIB 2×2 MIMO channel using BPSK.

inversion as the performance is highly dependant on the number of iterations that the adaptation is performed for, and we have already seen that the computational cost in converging to the inverse so that it reaches an MSE comparable to the analytic methods is much greater than these methods. The adaptive inversion is more suitable for tracking an equaliser to a dynamic channel.

The BER performance results for the SS SV channels sampled at 100 MHz are shown in Figure 5.28. The results do not differ much, with little variation within different values for $L_{g,s}$. The only significant difference for each of the inversion methods with varying values of $L_{g,s}$ occurs at above 30 dB. Below this both the time-domain inversion and frequency-domain inversion regularised by the NSR result in near optimal MSE performance. The point where the circular convolution effect will degrade the performance of the frequency-domain method occurs above 30 dB, as we saw in Figure 5.20. As before, the frequency-domain inversion regularised by a fixed value, providing the best possible performance for the frequency-domain method in a noiseless environment, results in a worse performance at low SNR values, as the system is "under-regularised". Overall we see that for this channel the frequency-domain inversion is less susceptible than the SS SPIB channel to circular convolution problems, as this channel is shorter for the same equaliser length. Note that for the fullband frequency-domain inver-

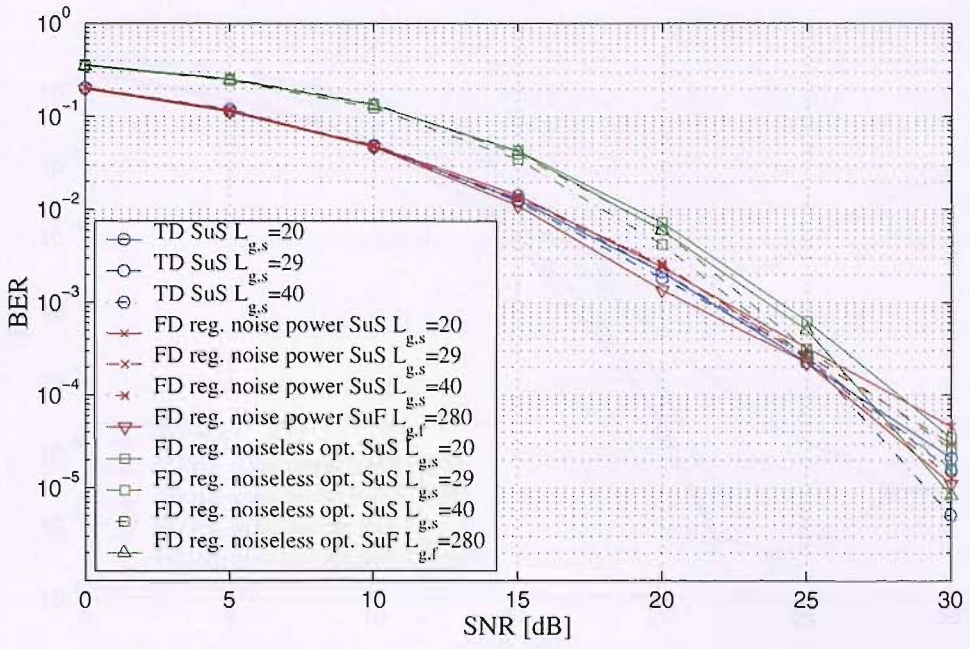

Fig. 5.28: SNR vs BER curves for time-domain and frequency-domain analytic inversion of the subband identified noisy static 100 MHz SV 2×2 MIMO channel using BPSK.

sion regularised by the NSR, i.e. the curve labelled "FD reg. noise power SuF, $L_{g,f} = 280$", the MSE performance in the mid-SNR values is the best— even better than the TD SuS $L_{g,s} = 40$ curve, which has given the best performance in the past. Actually, the TD SuS $L_{g,s} = 40$ curve does give the best performance out of the subband inversions. The reason for the worse performance of the subband inversion is partly due to circular convolution effects and partly due to the distortion introduced by the subband filter banks, mentioned in Section 5.2.4. The effects of circular convolution are worse for a shorter FFT and since the FFT length is determined by the equaliser length, the effect will be smaller for the 280 length fullband equaliser than for any of the subband equalisers.

Finally, we see the BER performance results for the SV channel sampled at 1 GHz in Figure 5.29. As for the corresponding MSE performance curves in Figure 5.21, $L_{g,s} = 70$ is used to model the subband-adapted channel with $L_{h,s} = 44$. Since these parameters result in satisfactory performance no other values for $L_{g,s}$ are simulated as this would only serve to raise the computational cost for little improvement in BER. For the fullband inversions of subband-adapted channels (SuF), $L_{g,f} = NL_{g,s} = 980$ is used to show the best possible fullband inversion BER performance while still keeping the comparison fair. At mid-SNR values, the improvement in BER for the fullband frequency-domain inversion regularised by the NSR over the time-domain subband inversion is now more pronounced. This

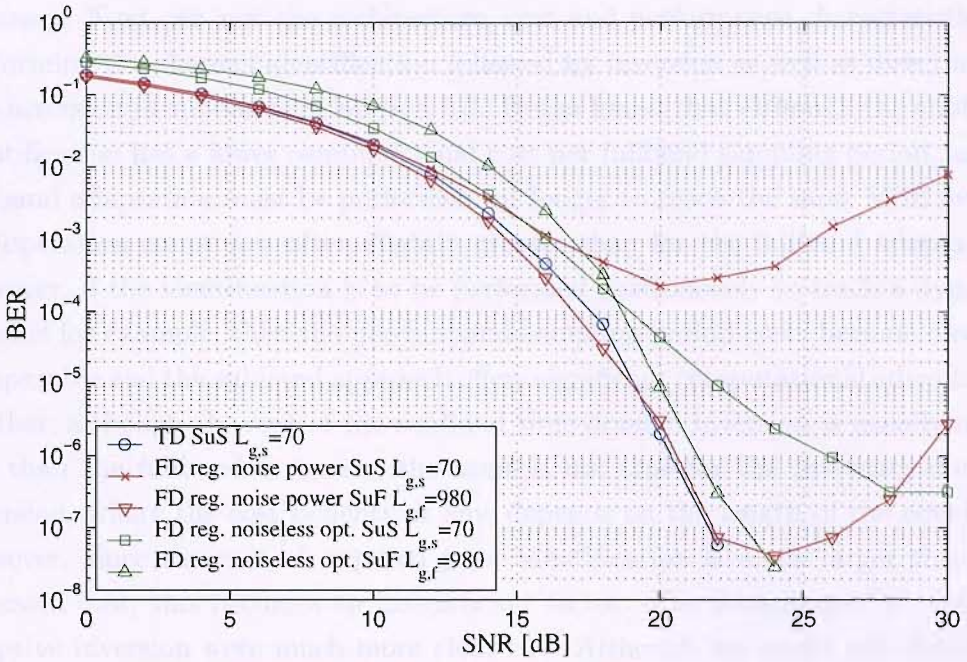

Fig. 5.29: SNR vs BER curves for time-domain and frequency-domain analytic inversion of the subband identified noisy static 1 GHz SV 2 × 2 MIMO channel using BPSK.

is since the length-980 FFTs used for the fullband inversion are much longer than the length-70 for the subband inversion, and this causes the circular convolution effect to be relatively less severe.

5.5 Summary

Because of the problems of inadequate MSE and BER performance of fullband equalisers in Chapter 4, as well as a high associated computational cost, we were motivated to examine the application of subband systems to solve this problem. Subband systems are known to potentially reduce the cost of signal processing algorithms and in some case be able to improve MSE and BER performance. This chapter has covered the execution of the various signal processing tasks involved in the calculation and tracking of an adaptive broadband MIMO channel equaliser in subbands. It started by introducing some of the concepts behind the techniques including multi-rate operations, modulated filters banks and the trade-offs between critical and oversampled subband decimation in Section 5.1. Section 5.2 briefly covered some performance measures and enhancement offered by the approach such as faster adaptive convergence and lower computational costs, as well as some of the limitations of a greater final MSE and potential worsened modelling

accuracy. Next, we saw the architecture, cost and performance characteristics of performing the channel identification followed by inversion as well as direct adaptive inversion in subbands in Section 5.3. It was found that although the subband identification has a lower computational cost per fullband sampling period, as the subband adaptation must be performed for longer to reach the same MSE overall the operation count was often slightly greater than for the fullband adaptation. However, if the identification is to be performed continuously to track a dynamic channel for example, then the per-fullband-sampling-period costs become directly comparable and the subband approach offers significant computational advantages. Further, although the cost of the subband time-domain inversion is usually much less than the fullband inversion, the same is not true for the frequency-domain inversion, where the cost benefits, if any, depends on the length of the equaliser. However, since the cost of required prior identification is much larger than the inversion cost, this becomes an insignificant factor. The advantages for subband adaptive inversion were much more clear-cut. Although we would not choose to use this method to invert the channel from an unknown initial equaliser as the total computational cost and time required to reach an acceptable MSE is far too great and the analytic methods result in superior performance, this method showed good results for the tracking of the equaliser for a dynamic channel. Not only can the subband system converge to a frequency-selective system quicker than the fullband and hence maintain a lower steady-state adaptation MSE for a dynamic channel, this may be performed at a fraction of the cost, which approached the decimation factor, N.

The chapter concluded by showing the results of simulations in Section 5.4. It showed that the subband adaptive identification converges more slowly than the fullband and can only reach a much greater, but still generally acceptable final MSE. We then saw the subband analytic inversion CER MSE performance, assuming a previously subband-identified channel and these showed similar overall behaviour to the fullband inversion in Chapter 4 such as the worsening MSE for the frequency-domain method regularised by the NSR above a certain SNR. There were some differences and these were explained. Next we saw the performance of the equaliser tracking a dynamic channel, which is where the real power of the subband technique becomes evident, as not only is it able to maintain a slightly better MSE but it could do so at a fraction of the computational cost of the fullband tracking. To be able to take advantage of this superior performance however, a prior channel identification and analytic inversion in subbands is required to initialise the equaliser. Finally, various BPSK BER performance results for an equaliser created from the analytic inversion of the subband-adapted system were presented. They showed that over the more realistic SNR ranges there was no

significant degradation in BER compared to the fullband systems, although the fullband frequency-domain inversion showed a slightly better BER performance compared to corresponding subband inversion.

In conclusion, the subband technique seems most suitable for

- highly frequency-selective and time-dispersive channels, with an impulse response which is comparable to or long relative to the subband prototype filter length, and
- time-varying fading channels where tracking is required.

Chapter 6

Fractionally-Spaced Equalisation

It is now well-known that sampling at a frequency greater than the symbol rate can result in significant improvement in equaliser performance both in terms of MSE and even the computational complexity involved in calculating or adapting to the inverse of a channel. This oversampling of the received signals is known as fractionally-spaced equalisation. This chapter introduces and develops the technique of fractionally-spaced MIMO equalisation in some detail and applies the method to the subband MIMO equalisation developed in previous chapters. Advantages offered by fractionally-spaced equalisation include higher resolution [114], shortening of equalisers [110] and the capability of equalising channels that contain spectral zeros [115].

Before we start to develop the concept further, it is helpful to remind ourselves of what a fractionally-spaced MIMO equaliser (FSE) looks like. We touched upon this briefly in Chapter 4 and the comparison between a symbol-spaced equaliser (SSE) and an FSE is shown in Figure 6.1. Simply put, the FSE acts on a version of the received signals that is sampled R as frequently relative to an SSE.

6.1 Phase Behaviour

We start the analysis by a brief explanation of the source of the potential performance improvements offered by the FSE. It is well-known that the optimum receiver is a cascade of a filter matched to the channel and an SSE [166]. An SSE alone cannot perform matched filtering since its sampling rate is the same as the symbol rate. The FSE however can perform the task of both matched filtering and equalisation by virtue of its increased sampling rate. Consider a channel whose spectral response around the lower band edge $-f_s/2$, where f_s is the sampling frequency, differs distinctly from the response around the upper band edge

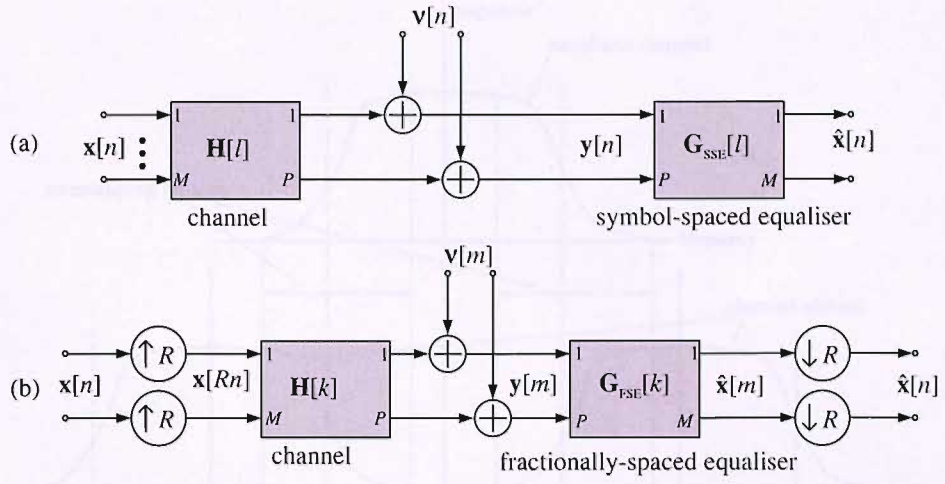

Fig. 6.1: Schematical diagram showing (a) a symbol-spaced equaliser, and (b) fractionally-spaced equaliser.

$f_s/2$. Since a SSE is subject to aliased versions of the spectrum with respect to $\pm r/T$, $r \in \mathbb{Z}$ the aliased frequency-response is likely to have a rapid transition in these areas. For a standard SSE to equalise over this area presents a difficult problem requiring a great many taps. However, since the FSE manipulates the frequency-response at the band-edges before symbol-spaced sampling, and hence the aliasing, the performance can markedly improve.

A consequent advantage offered by the FSE is that, in contrast to the SSE, it is less sensitive to the sampling phase. To explain this we first consider the SSE where aliasing causes spectral overlap at the band edges. If we assume that the phases of the baseband spectrum near the top and bottom band edges differ by π then the alias signal will interfere destructively with the baseband signal causing a weakened signal in this region, as shown in Figure 6.2, which an SSE would have difficulty manipulating. Conversely, we now assume that we vary the receiver sampling timing so that an offset, which results in a constant gradient in the phase response, is added to the baseband signal. If for example this results in no phase offset just above $f = -1/2T_s$ but an extra π phase offset just above $f = 1/2T_s$ then the alias will interfere constructively with the baseband signal causing enhancement of the aliased signal in direct contrast to the previous case. Evidently an SSE will be able to equalise this frequency now much better than when there was a null present. Hence the SSE MSE performance is highly dependent on the receiver timing offset. In the extreme, if the timing is such that the interference causes a null, the SSE equaliser cannot equalise the spectrum to unity gain, whereas adding a timing offset can improve the performance hugely.

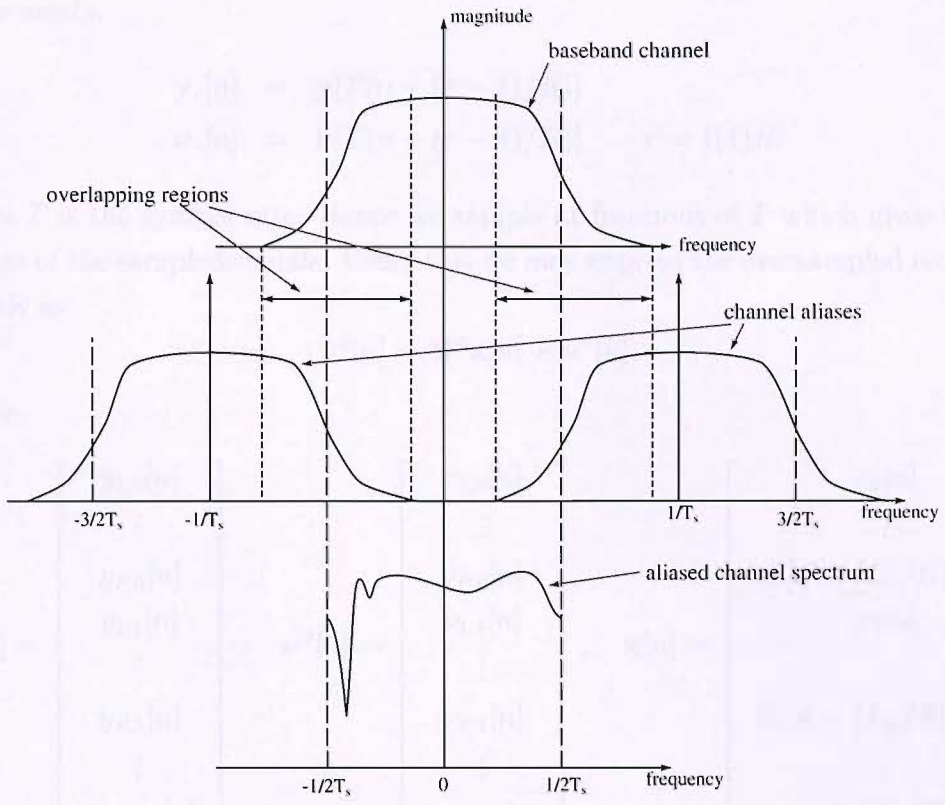

Fig. 6.2: Effect of destructive interference of alias signals in a symbol-spaced sampled signal.

The FSE equaliser avoids this problem since it samples at a frequency greater than the SSE, hence there is no aliasing at the FSE input. Not only does this mean that the FSE is able to function on a signal that will not suffer from nulls due to alias interference, but also the FSE performance is less sensitive to the phase of the receiver timing. As a result, the MSE performance is typically much better than that of an SSE even when the total number of equaliser taps remains the same [110].

6.2 Polyphase Representation

We develop a polyphase representation for MIMO FSE which is convenient for analysis. In its standard form FSE with its resampling operations is awkward to analyse, but the polyphase description expresses the system using a single sampling rate through-out. We start by splitting the signals in Figure 6.1(b) into polyphase

components,

$$\mathbf{y}_r[n] = \mathbf{y}[T(n+(r-1)/R)] \tag{6.1}$$

$$\boldsymbol{\nu}_r[n] = \boldsymbol{\nu}[T(n+(r-1)/R)] \qquad r = 1(1)R, \tag{6.2}$$

where T is the symbol rate. Hence we sample at fractions of T which gives the R *phases* of the sampled signals. Using this we may express the oversampled received signals as

$$\mathbf{y}^{\phi}[n] = \mathbf{H}^{\phi}\mathbf{x}[n] + \boldsymbol{\nu}^{\phi}[n], \tag{6.3}$$

where

$$\mathbf{y}^{\phi}[n] = \begin{bmatrix} y_{1,0}[n] \\ \vdots \\ y_{P,0}[n] \\ y_{1,1}[n] \\ \vdots \\ y_{P,1}[n] \\ \vdots \\ y_{P,R-1}[n] \end{bmatrix}, \quad \boldsymbol{\nu}^{\phi}[n] = \begin{bmatrix} \nu_{1,0}[n] \\ \vdots \\ \nu_{P,0}[n] \\ \nu_{1,1}[n] \\ \vdots \\ \nu_{P,1}[n] \\ \vdots \\ \nu_{P,R-1}[n] \end{bmatrix}, \quad \mathbf{x}[n] = \begin{bmatrix} x_0[n] \\ \vdots \\ x_0[n-\lceil L_h/R \rceil + 1] \\ x_1[n] \\ \vdots \\ x_1[n-\lceil L_h/R \rceil + 1] \\ \vdots \\ x_M[n-\lceil L_h/R \rceil + 1] \end{bmatrix}, \tag{6.4}$$

and

$$\mathbf{H}^{\phi} = \begin{bmatrix} \mathbf{H}^{\phi}_{11} & \cdots & \mathbf{H}^{\phi}_{M1} \\ \vdots & \cdots & \vdots \\ \mathbf{H}^{\phi}_{1P} & \cdots & \mathbf{H}^{\phi}_{MP} \end{bmatrix}. \tag{6.5}$$

The matrix $\mathbf{H}^{\phi}$ is the polyphase MIMO channel. Further

$$\mathbf{H}^{\phi}_{mp} = \begin{bmatrix} h_{mp,0}[0] & \cdots & h_{mp,0}[\lceil L_h/R \rceil - 1] \\ \vdots & \cdots & \vdots \\ h_{mp,R-1}[0] & \cdots & h_{mp,R-1}[\lceil L_h/R \rceil - 1] \end{bmatrix}, \tag{6.6}$$

where $h_{mp,r}$ is phase r of sub-channel mp.

As an example, the polyphase representation of a $T/2$ spaced 2×2 MIMO channel-equaliser system, i.e. $R = 2$, is shown in Figure 6.3. We see from this that the problem is effectively no different to equalising a 2×4 MIMO channel. This is the system we would use for analysis, i.e. when analytically inverting the channel, we require the channel expressed in polyphase form, which can be found by adaptation. Of course in a real implementation, the channel would not be decomposed into its phases, but function at the upsampled rate. Hence we use the multi-rate description of the channel but the polyphase description of the equaliser, shown in Figure 6.4.

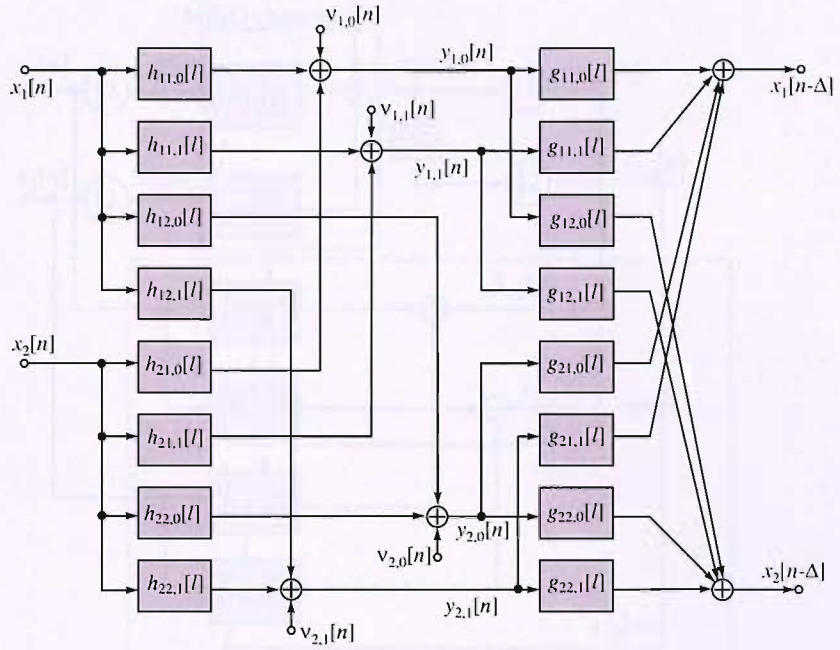

Fig. 6.3: Polyphase representation of channel and equaliser for $T/2$ 2×2 MIMO system.

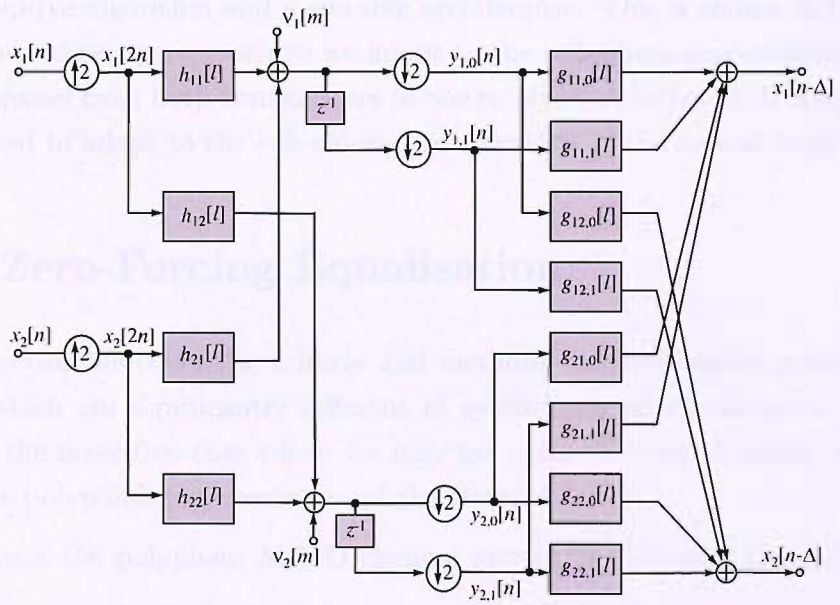

Fig. 6.4: Polyphase representation of equaliser for $T/2$ 2×2 MIMO channel, used for implementation.

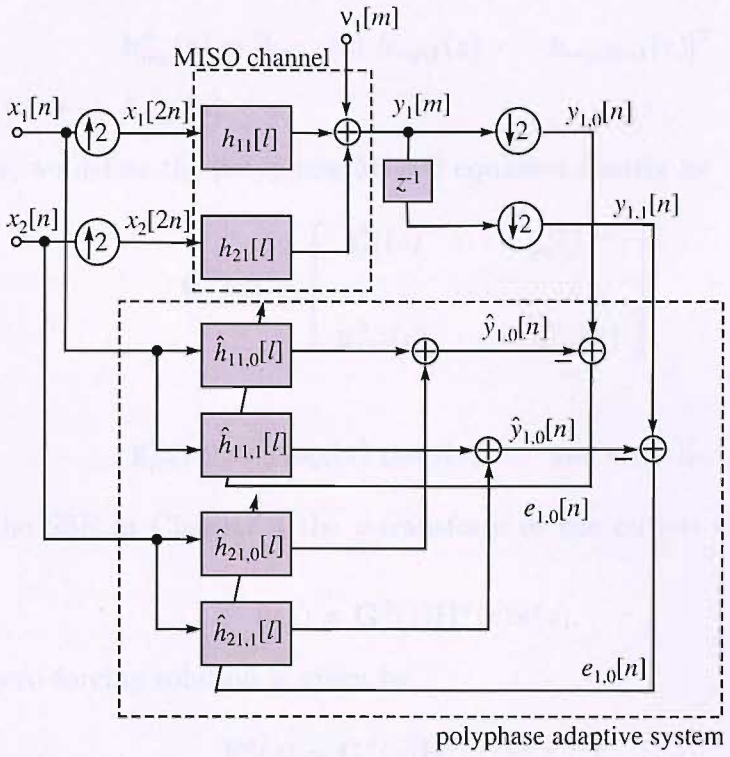

Fig. 6.5: Adaptive system to identify MIMO sub-channels to one receiver.

If we are to invert the channel analytically we must identify it first, by means of an adaptive algorithm and a suitable architecture. This is shown in Figure 6.5 for a two-channel system, where we adapt to the polyphase representation of the MISO channel from both transmitters to one receiver. Another such system would be required to adapt to the sub-channel terminating at the second receiver.

6.3 Zero-Forcing Equalisation

In this section we cover the criteria and methods for fractionally-spaced equalisation, which are significantly different to symbol-spaced equalisation. We first consider the noise-free case where we may use a zero-forcing equaliser to exactly invert the polyphase representation of the channel.

We convert the polyphase MIMO channel matrix in (6.5) into the z-domain so we have

$$\mathbf{H}^{\phi}(z) = \begin{bmatrix} \mathbf{h}_{11}^{\phi}(z) & \cdots & \mathbf{h}_{M1}^{\phi}(z) \\ \vdots & \cdots & \vdots \\ \mathbf{h}_{1P}^{\phi}(z) & \cdots & \mathbf{h}_{MP}^{\phi}(z) \end{bmatrix} \tag{6.7}$$

where

$$\mathbf{h}_{mp}^{\phi}(z) = [h_{mp,0}(z)\ h_{mp,1}(z)\ \cdots\ h_{mp,R-1}(z)]^T \tag{6.8}$$

and $h_{mp,r}(z) \bullet\!\!-\!\!\circ\ h_{mp,r}[n]$.

Similarly, we define the polyphase MIMO equaliser matrix as

$$\mathbf{G}^{\phi}(z) = \begin{bmatrix} \mathbf{g}_{11}^{\phi}(z) & \cdots & \mathbf{g}_{P1}^{\phi}(z) \\ \vdots & \cdots & \vdots \\ \mathbf{g}_{1M}^{\phi}(z) & \cdots & \mathbf{g}_{PM}^{\phi}(z) \end{bmatrix} \tag{6.9}$$

where

$$\mathbf{g}_{pm}^{\phi}(z) = [g_{pm,0}(z)\ g_{pm,1}(z)\ \cdots\ g_{pm,R-1}(z)]. \tag{6.10}$$

As for the SSE in Chapter 4 the z-transform of the output of the equaliser is given by

$$\hat{\mathbf{x}}(z) = \mathbf{G}^{\phi}(z)\mathbf{H}^{\phi}(z)\mathbf{x}(z), \tag{6.11}$$

and the zero-forcing solution is given by

$$\mathbf{F}^{\phi}(z) = \mathbf{G}^{\phi}(z)\mathbf{H}^{\phi}(z) = z^{-\Delta}\mathbf{I}. \tag{6.12}$$

Since we have shown the problem to be equivalent to a multi-channel system, we have already developed all of the required inversion techniques in Chapter 4. The solution to this problem can be found using the time-domain or frequency-domain methods described in Section 4.2.

6.3.1 FIR Equalisability

A major difference between FSE and SSE is that the zero-forcing equaliser can be implemented using an FIR system without any approximations or filter truncation and without needing additional antennas, assuming that a condition (described later) is met. The analysis in this section assumes FIR MIMO sub-channels. It can be shown that if $\mathbf{H}^{\mathrm{H}}$ is full-rank then the minimum polyphase equaliser length required to perform ZF FIR equalisation is [167]

$$L_g = \frac{L_h/R - 1}{R - 1}. \tag{6.13}$$

So for a $T/2$ 2×2 MIMO equaliser ZF equalisation may be performed using eight length-$(L_h - 1)$ filters, set up as in Figure 6.4.

In the more general case if any of the matrices $\mathbf{H}_{mp}^{\phi}$ is rank-deficient because some of the fractional phases are linearly dependant, the minimum length for the corresponding equaliser is given by [115]

$$L_{g_{pm}} = \frac{L_h/R - 1}{\text{rank}\{\mathbf{H}_{mp}^{\phi}\} - 1}. \tag{6.14}$$

The outcome of this is that for the system to be equalisable at all, the row rank of $\mathbf{H}^{\phi}$ must be at least as great as its column rank. Further, if they are equal and $\mathbf{H}^{\phi}$ is hence square, the equaliser will be IIR but if the row rank is at least twice the column rank then all the equalisers will be FIR, with lengths determined by (6.14). Anywhere between these two limits causes some of the equalisers making up the full MIMO equaliser to be FIR and the remainder to be IIR. It is also clear that if the SS MIMO system is rank-deficient because some of the sub-channels are linearly dependent, then some of the degrees of freedom provided by the fractional-spacing can be used to invert those sub-channels at the expense of other benefits provided by FSE. This interesting possibility of using the linearly independent rows if $\mathbf{H}^{\phi}$ to provide degrees of freedom where required is the topic of Section 6.5. Another condition for the system to be ZF equalisable using FIR filters is that there must be no zeros common to all MIMO sub-channels and phases from one channel input to one channel output, i.e. each column of (6.7) must have no common zeros. This is the same condition as for the SISO FSE [115, 168, 169] except since $\mathbf{H}^{\phi}$ is made up of more sub-channels for the MIMO case it is more likely that this condition will be fulfilled. There is also an increased possibility that inversion is possible (either FIR or IIR), where there is no spectral zero common to any column of $\mathbf{H}^{\phi}(z)$ in (6.7), i.e. from one input to all outputs, and based on all polyphase components. This condition is quite intuitive since if there is a common zero in any column of (6.7) then that zeros can be factored out into a SISO system where ZF equalisation can be only performed using an IIR filter.

Proof of the existence of an FIR equaliser solution to the problem can be shown by writing (6.12) in polyphase form

$$\mathbf{B}_{ij}(z) = \sum_{p=1}^{P} \sum_{r=0}^{R-1} g_{pj,r}(z) h_{ip,r}(z) = \begin{cases} z^{-\Delta} & j = i \\ 0 & j \neq i \end{cases} \quad \forall i, j = 1(1)M. \tag{6.15}$$

This is solvable as long as $M \geq PR$, although for each sub-channel to be fractionally-sampled by R we require $P \geq M$. The interesting case of $M/R \leq P < M$ where we may use the extra degrees of freedom provided by fractional-sampling to invert rank-deficient MIMO systems rather than for other possible benefits of FSE is the topic of Section 6.5, but for now we will assume the fractional-sampling

is used to perform FSE and that $P \geq M$. The matrix $\mathbf{B}_{ij}(z) = z^{-\Delta}$ is known as Bézout's identity for $\Delta = 0$ [170]. The identity states the existence of FIR equalisers for FIR channels as long as they are relatively prime, or in our context there are no common zeros. Generally speaking, for the multi-channel case, assuming there are no common zeros in each column in (6.7), for the channel to be invertible using FIR filters there needs to be more than one degree of freedom for each constraint in $\mathbf{G}^{\phi}(z)\mathbf{H}^{\phi}(z)$.

So for the example of the $T/2$ equaliser for the 2×2 MIMO channel there are two constraints so we need four degrees of freedom. Two are provided by the sub-channels in the paths from a MIMO input to both MIMO outputs and a further two are provided by the $T/2$ fractional-spacing, hence the system is equalisable using FIR filters. Simply put, this just means that all filters comprising the MIMO equaliser need to be fractionally-sampled.

6.3.2 Frequency-Domain Equalisability

We now express the multi-rate system shown in Figure 6.1(b) in the z-domain and then transform it into the frequency-domain to further explain the conditions of equalisability and gain further insight.

The fractional MIMO channel co-efficients can be related to the polyphase representation by

$$h^{\mathrm{F}}_{mp}(z) = \sum_{r=0}^{R} h_{mp,r}(z^R) z^{-r}. \tag{6.16}$$

Using this we build a fractional MIMO channel matrix

$$\mathbf{H}^{\mathrm{F}}(z) = \begin{bmatrix} h^{\mathrm{F}}_{11}(z) & \cdots & h^{\mathrm{F}}_{M1}(z) \\ \vdots & \cdots & \vdots \\ h^{\mathrm{F}}_{1P}(z) & \cdots & h^{\mathrm{F}}_{MP}(z) \end{bmatrix} \tag{6.17}$$

with $h^{\mathrm{F}}_{mp}(z) \bullet\!\!-\!\!\circ\, h_{mp}[k]$. A multi-rate equaliser matrix $\mathbf{G}^{\mathrm{F}}(z)$ may be built similarly.

If we define the channel-equaliser response

$$\mathbf{B}^{\mathrm{F}}(z) = \mathbf{G}^{\mathrm{F}}(z)\mathbf{H}^{\mathrm{F}}(z) \tag{6.18}$$

then the output of the equaliser is

$$\hat{\mathbf{x}}(z) = \left(\frac{1}{R} \sum_{r=0}^{R-1} \mathbf{B}^{\mathrm{F}}(e^{-jr2\pi/R} z^{1/R}) \right) \mathbf{x}(z), \tag{6.19}$$

where we use the multi-rate operations described in Chapter 5. Decomposing this into single signals we have

$$\hat{x}_m(f) = \sum_{j=1}^{M} \left(\left(\frac{1}{R} \sum_{r=0}^{R-1} b_{mj}(e^{-jr2\pi/R} e^{j2\pi fT/R}) \right) x_j(e^{j2\pi fT}) \right), \tag{6.20}$$

where we have used $z = e^{j2\pi fT}$, and

$$\mathbf{B}^{\mathrm{F}}(z) = \begin{bmatrix} b_{11}(z) & \cdots & b_{1M}(z) \\ \vdots & \cdots & \vdots \\ b_{M1}(z) & \cdots & b_{MM}(z) \end{bmatrix}. \tag{6.21}$$

After some manipulation and using $\mathbf{B}^{\mathrm{F}}(f) = \mathbf{B}^{\mathrm{F}}(z)|_{z=e^{j2\pi fT/R}}$, we obtain the frequency response

$$\hat{x}_m(f) = \sum_{j=1}^{M} \left(\left(\frac{1}{R} \sum_{r=0}^{R-1} b_{mj}\left(f - \frac{r}{T}\right) \right) x_j(e^{j2\pi fT}) \right). \tag{6.22}$$

Hence for ZF equalisation we require

$$\frac{1}{R} \sum_{r=0}^{R-1} b_{mj}\left(f - \frac{r}{T}\right) = \begin{cases} e^{j2\pi f\Delta T} & m = j \\ 0 & m \neq j \end{cases} \quad -\frac{1}{2T} < f < \frac{1}{2T};\ m, j = 1(1)M. \tag{6.23}$$

where Δ is the delay in symbol periods. Finally, decomposing b into its component channel and equaliser parts we obtain

$$\sum_{p=1}^{P} \left(\frac{1}{R} \sum_{r=0}^{R-1} g_{pi}\left(f - \frac{r}{T}\right) h_{jp}\left(f - \frac{r}{T}\right) \right) = \begin{cases} e^{j2\pi f\Delta T} & i = j \\ 0 & i \neq j \end{cases} \quad i, j = 1(1)M. \tag{6.24}$$

In matrix form this is

$$\frac{1}{R} \sum_{r=0}^{R-1} \mathbf{G}^{\mathrm{F}}\left(f - \frac{r}{T}\right) \mathbf{H}^{\mathrm{F}}\left(f - \frac{r}{T}\right) \triangleq e^{j2\pi f\Delta T}\mathbf{I}. \tag{6.25}$$

From this we may infer the conditions that must be fulfilled so that the fractionally spaced MIMO channel is equalisable. Firstly, note that although $h_{mp}(f)$ and $g_{mp}(f)$ are periodic with period R/T, the functions in (6.24), i.e. $h_{mp}(f - \frac{r}{T})$ and $g_{pm}(f - \frac{r}{T})$ are periodic with period $1/T$. For the SISO case it has been shown that the condition for equalisability is that there needs to be some aliasing between these adjacent polyphase characteristics, i.e. the bandwidth of the channel $f_b > 1/(2T)$ [115]. A MIMO channel however is equalisable using only FIR filters when $\mathbf{H}^{\mathrm{F}}(f - r/T)\ \forall f \in (-R/2T, R/2T)$ is full-rank.

A physical interpretation of this is quite difficult for a general fractionally-spaced MIMO channel, so for simplicity we consider the example of $M = 2$ and $P = 2$.

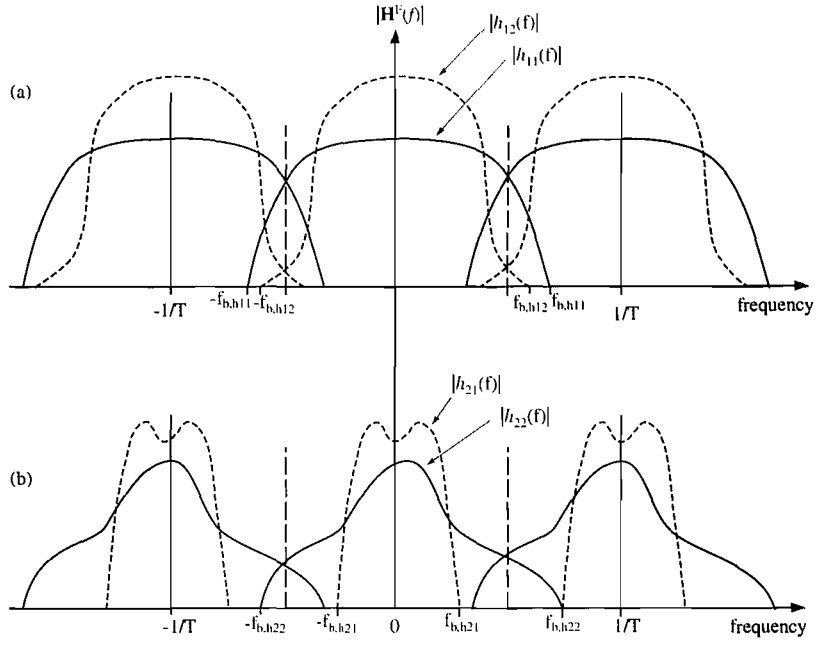

Fig. 6.6: Frequency response of an oversampled 2 × 2 MIMO channel- (a) sub-channels h_{11} and h_{12}, and (b) sub-channels h_{21} and h_{22}.

Figure 6.6 shows the case for when channels h_{11}, h_{21} and h_{22} exceed the minimum required bandwidth of $\frac{1}{2T}$, but channel h_{21} does not. This channel is still equalisable however, since even at the frequencies where h_{21} can pass no power, the MIMO matrices are still triangular and hence invertible. If however either the bandwidth of either h_{22} or h_{11} was also less than $\frac{1}{2T}$ the channel would become singular at the frequencies which exceeds the bandwidth and hence become uninvertible. More generally, we can say the condition for invertibility using FIR filters is this: P (i.e. all) of the sub-channels in one of the columns of $\mathbf{H}^{\mathrm{F}}(z)$ must have a bandwidth $f_b \in \frac{1}{2T}, \frac{R}{2T})$; $P-1$ of the sub-channels in a different column must have a bandwidth $f_b \in (\frac{1}{2T}, \frac{R}{2T})$, and so on until all the columns of $\mathbf{H}^{\mathrm{F}}(z)$ are accounted for. In this way the MIMO channel matrix at each frequency is at least triangular and hence invertible. Incidentally, it is the fact that the bandwidth may exceed $\frac{1}{2T}$ and still be equalisable using FSE and FIR filters that means that the method can alone perform both the tasks of matched filtering and SSE and generally better than either alone. This is therefore the necessary condition for equalisability using FIR filters in the frequency-domain; note however it is not sufficient. The necessary and sufficient condition was seen in the previous section, i.e. no zeros common to all paths between a MIMO channel input and all its outputs.

6.3.3 Noise-Enhancement

In this section we study the problem of noise enhancement in ZF equalisers. Consider the polyphase representation of the fractionally-sampled MIMO channel in (6.9). It is clear that when $P \geq M$ and $R > 1$ this matrix will always have more rows than columns. As such it is an over-determined system (assuming the rank is greater than M) and as was explained in Chapter 4 has an infinite number of solutions to perform zero-forcing equalisation (ZFE), as long as the equaliser length is longer than the minimum required [115]. This is in contrast to the SSE where there is generally a unique solution. For the FSE the infinite number of solutions will enhance any noise at the equaliser input by varying amounts. The solution that will enhance the noise by the smallest amount is the minimum norm solution, which as explained in Chapter 4 can be calculated using the pseudo-inverse. Hence this solution will minimise the MSE at the equaliser output in the presence of noise. Further, by increasing the FSE length further, we increase the number of degrees of freedom of the solution and hence the pseudo-inverse further optimises the solution to give an FSE with even better performance (lower MSE). We call this solution the Minimum Mean Squared Zero Forcing Error (()MMSZFE), i.e. the solution that results in the MMSE from all the ZFE solutions. This is different from the true MMSE solution which is not constrained by the ZF criterion.

Putting this argument mathematically, consider white noise at the P equaliser inputs, which for simplicity all have the same power, such that

$$\mathcal{E}\left\{\boldsymbol{\nu}^{\phi}[n]\left(\boldsymbol{\nu}^{\phi}[n]\right)^{H}\right\} = \sigma_{\nu}^{2}\mathbf{I} \tag{6.26}$$

The variance at output m of the MIMO FSE is

$$\sigma_{m,\mathrm{ZFE}}^{2} = \sum_{p=1}^{P}\left(\sigma_{\nu,p}^{2}\sum_{r=0}^{R-1}\sum_{n=1}^{L_h/R-1}|g_{pm,r}[n]|^{2}\right) = \sigma_{\nu}^{2}\sum_{p=1}^{P}\sum_{r=0}^{R-1}\int_{-\frac{1}{2}}^{\frac{1}{2}}|g_{pm,r}(f)|df. \tag{6.27}$$

where we have used Parseval's Identity and assuming $\sigma_{\nu,p} = \sigma_{\nu}$ for $p = 1(1)P$. Hence it can be shown [115] that the optimisation criterion to minimise $\sigma_{m,\mathrm{ZFE}}^{2}$ is

$$\begin{cases} \arg\min\limits_{g_{pm,r}(f)} \sum\limits_{r=0}^{R-1}|g_{pm,r}(f)|^{2} & m = 1(1)M, p = 1(1)P \\ \text{subject to } \mathbf{G}^{\phi}(f)\mathbf{H}^{\phi}(f) = e^{j2\pi f\Delta T}\mathbf{I} \end{cases}, \tag{6.28}$$

where the delay Δ ensures causality. The well-known solution to this, as mentioned earlier, is the pseudo-inverse of $\mathbf{H}^{\phi}(f)$, i.e.

$$\mathbf{G}_{\mathrm{MMSZFE}}^{\phi}(f) = \left(\left(\mathbf{H}^{\phi}(f)\right)^{H}\mathbf{H}^{\phi}(f)\right)^{-1}\left(\mathbf{H}^{\phi}(f)\right)^{H}. \tag{6.29}$$

Since this solution has been developed in the frequency-domain, it represents the infinite length solution, i.e. using infinite length equalisers. Finite length equalisers can also be found using this solution using finite length FFTs during computation, however they will give an approximation to the MMSZFE solution, due to the effect of circular convolution discussed in Chapter 4. We have already seen a way to combat this, namely using regularisation.

Now we have found the MMSZFE, an interesting question is if and how much better than the MMSZFE would the true MMSE solution be, i.e. not constrained to be ZF. Both the MMSE solution and the method of regularisation can be used together to result in better equaliser performance (i.e. lower MSE).

6.4 MMSE Equalisation

Minimum mean squared error (MMSE) equalisation has already been covered in previous chapters, so in this section we shall restrict ourselves to only cover the differences between FSE MMSE and SSE MMSE equalisation.

FSE MMSE equalisers differ since we now have more degrees of freedom to minimise the cost function, which are given by the fractional-sampling. The cost function of FSE MMSE for the m^{th} input is

$$\begin{aligned}\sigma^2_{m,\text{MMSE}} = \min_{g_{pm,r}(f)} \sum_{p=1}^{P} \int_{-\frac{1}{2}}^{\frac{1}{2}} \Bigg\{ \sigma_x^2 \left| \sum_{r=0}^{R-1} g_{pm,r}(f) h_{mp,r}(f) - k_{mp} \right|^2 \\ + \sigma_\nu^2 \left(\sum_{r=0}^{R-1} |g_{pm,r}(f)|^2 \right) \Bigg\} df \end{aligned} \tag{6.30}$$

where

$$k_{mp} = \begin{cases} e^{j2\pi f \Delta T} & m = p \\ 0 & m \neq p \end{cases} \tag{6.31}$$

assuming that the signal power σ_x^2 is the same at all transmitters, as is the noise power σ_ν^2 at the receivers. The infinite-length solution to this is the pseudo-inverse regularised by the noise power

$$\mathbf{G}^{\phi}_{\text{MMSE}}(f) = \left((\mathbf{H}^{\phi}(f))^H \mathbf{H}^{\phi}(f) + \sigma_\nu^2 \mathbf{I} \right)^{-1} (\mathbf{H}^{\phi}(f))^H \tag{6.32}$$

assuming the signal power is normalised $\sigma_x^2 = 1$. In the presence of noise the MMSE has superior performance to the MMSZFE since is clear that

$$\sigma^2_{\text{MMSE}} \leq \sigma^2_{\text{MMSZFE}} \tag{6.33}$$

due to the presence of the regularisation term $\sigma_\nu^2\mathbf{I}$ arising from the noise in the solution.

The solutions expressed as functions of frequency of the MIMO fractionally-sampled polyphase channel result in an infinite length solution. However, since the FSE is capable of creating FIR equalisers we will want to calculate a finite length solution. Such finite length deconvolution is subject to circular convolution problems and discussed in Chapter 4. The technique we used to combat this was regularisation. Fortunately often at realistic SNRs the error effect of the receiver noise will be greater than the error caused by the circular convolution. However when this is not the case we may use a fixed regularisation co-efficient in (6.32) to limit the error caused. Using (6.32) to calculate a finite length solution no longer results in the MMSE, rather an approximation to it. However as we found in Chapter 4 the performance is still quite acceptable especially when also considering the greatly reduced computational cost involved in performing the inversion when compared to the alternative time-domain method that does give the MMSE solution. Hence the equaliser can be calculated using

$$\mathbf{G}^{\phi}_{\mathrm{MMSE}}(f) = \left((\mathbf{H}^{\phi}(f))^H\mathbf{H}^{\phi}(f) + \max(\sigma_\nu^2, \beta)\mathbf{I}\right)^{-1}(\mathbf{H}^{\phi}(f))^H \tag{6.34}$$

where β is a fixed regularisation factor which minimises $\sigma^2_{m,\mathrm{MMSE}}$ in (6.30) in a noiseless environment when using finite length FFTs.

6.5 Rank-Deficient MIMO Equalisation

In Section 6.3.1 we briefly introduced the possibility of using the extra degrees of freedom (DOF) provided by sampling at fractional intervals to invert MIMO systems that would otherwise be rank-deficient and hence uninvertible. If after doing this there were no DOF left, the responses of the filters comprising the MIMO equaliser would be IIR, as with SSE (assuming the condition for equalisability is fulfilled). This arises from an extension of the discussion of DOF in [115] to the MIMO case. If however there were one or more DOF left, other benefits associated with FSE could still be realised using these, resulting in FIR filters with appropriately modified lengths if necessary.

Consider the polyphase representation of a T/2 2×2 MIMO system shown in Figure 6.3. For this system, the polyphase channel matrix (defined in (6.5)) has dimensions 2×4 and assuming it has full column-rank it is an over-determined system. We only require row-rank of two, but we have four. Hence if for some reason the sub-channels to the second receiver are blocked or linearly related to the sub-channels to the first receiver, the polyphase channel matrix will only have

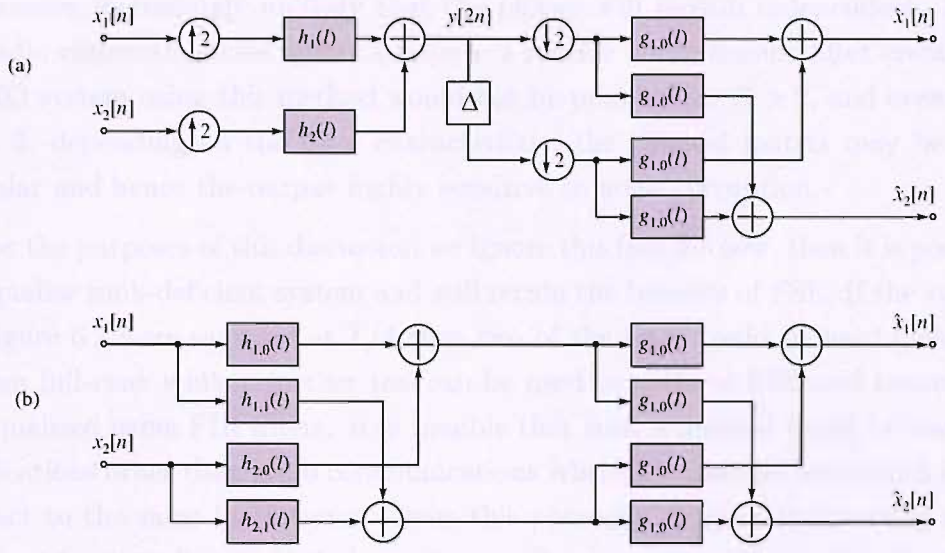

Fig. 6.7: A $T/2$ 2×1 system (a) in a form for implementation, and (b) in analysis form.

row-rank two. However by sacrificing the other benefits of FSE (e.g. FIR equaliser responses) we may still invert and hence equalise this channel (using IIR filters though, or an FIR approximation to them). This is potentially a powerful technique since we may now equalise rank-deficient systems, something that was not possible with symbol-spaced sampling. Speculatively, it may be possible, as an alternative application, to gain the benefit of some (though certainly not all) of the capacity increase associated with MIMO systems, with using fewer receivers than transmitters (in an equalisation set-up), by exploiting imperfect band-limiting channel filtering.

Figure 6.7(a) shows the example of a system with two transmitters and one receiver. In a T-spaced equaliser this would be uninvertible and hence unequalisable. However since it is fractionally-sampled at $T/2$ we express it in polyphase form in Figure 6.7(b) and from this it is clear that this is just the same as a SSE 2×2 system (for the moment ignoring band-limiting transmit and receive filters) and hence equalisable using IIR filters. If this system was sampled at $T/3$ we could invert a 3×1 system and so on. The size of the system we may invert is limited mainly by the characteristic of the transmit and receive filters and also to some extent the radio channel. The system remains equalisable as long as the phases of the channel are linearly independent, and as we decrease the period between sampling when fractionally-spaced this becomes less likely. When the transmit and receive filters are accounted for the bandwidth of the channel is typically about 10% to 40% greater than the signal bandwidth [110]. Hence when $R > 2$

it becomes increasingly unlikely that the phases will remain independent. Since all radio communications systems require a receive and transmit filter creating a MIMO system using this method would not be possible for $R > 2$, and even with $R = 2$, depending on the filter characteristic, the channel matrix may be near singular and hence the output highly sensitive to noise corruption.

If for the purposes of this discussion we ignore this fact for now, then it is possible to equalise rank-deficient system and still retain the benefits of FSE. If the system in Figure 6.7 were sampled at $T/4$ then two of the DOF could be used make the system full-rank while a further two can be used to perform FSE and hence may be equalised using FIR filters. It is feasible that such a method could be used for applications other than radio communications where the channel bandwidth is not subject to the same limitations. Given this potential problem in inverting rank-deficient fractionally-sampled channels we will continue to assume that $P \geq M$.

6.6 Subband Fractionally-Spaced Equalisation

In this section we apply fractional-sampling to the subband approach which was the topic of Chapter 5 to create a subband FSE. We aim to create a system that performs better than a subband SSE due to the fractional-spacing, exploits the advantages of subband processing to reduce the computational cost of inverting the fractionally-sampled MIMO channel and improves the convergence speed of adaptive inversion and tracking over that of fullband FSE.

There are two possible approaches when combining subband processing with fractional-sampling– (i) applying the subband processing inside the upsampled system which results in the analysis and synthesis filtering banks being decomposed into polyphase components, or (ii) using the polyphase representation and decomposing the phases into subbands. We discuss each in turn.

For simplicity we consider a subband SISO system where the channel, equaliser and subband analysis and synthesis filter banks function at a sampling period which is double the symbol period, i.e. $T/2$. This is shown in Figure 6.8(a). Figure 6.8(b) shows the same system but with the subband analysis and synthesis expressed in polyphase form, as explained in Chapter 5, with the subband decimation and expansion explicitly shown. The re-sampling operations of the fractional-sampling can be combined with the re-sampling operations of the subband system, which is shown in Figure 6.8(c). We can see that the inputs and outputs to half the analysis and synthesis filtering bank respectively are guaranteed to be zero, hence they may be excluded thus halving the number of operations.

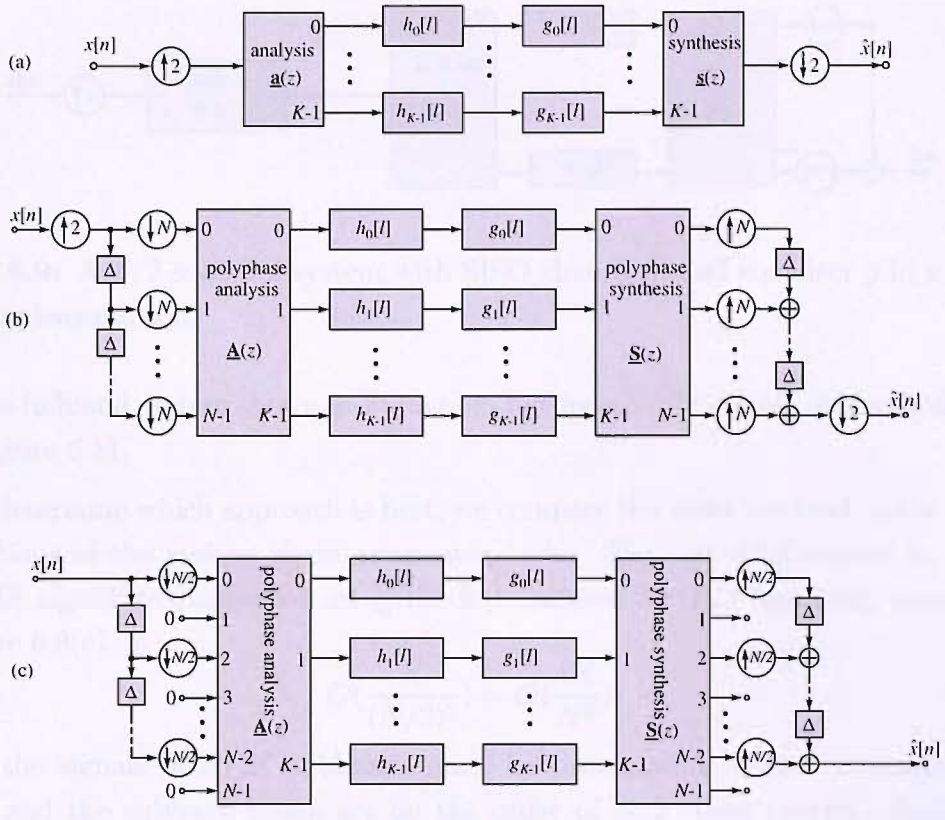

Fig. 6.8: A $T/2$ subband system with SISO channel h and equaliser g expressed in (a) basic form, (b) polyphase form, and (c) combined polyphase form.

However, relative to a normal GDFT filter bank the downsampling ratio is halved to $N/2$, and this must be taken into account when considering overall complexity. Further, the system shown in Figure 6.8(c) expresses both channel and equaliser in subbands, hence the analysis filtering occurs directly after the upsampling. In an implementation however, this would not be the case- the channel would be between the upsampler and analysis filter bank, as shown in Figure 6.9, and hence the analysis filter would have non-zero input to *all* its phases, and would still have to function at the upsampled rate.

The second approach involves the subband decomposition of the symbol-spaced polyphase representation of the system, which was shown for a $T/2$ 2×2 MIMO system in Figure 6.3. For the purposes of this discussion we show the polyphase representation of a $T/2$ SISO system with the phases being processed in subbands in Figure 6.10(a). As before we draw the distinction between this system, which is used for calculating the subband equaliser filter coefficients, and the manner in which such a system would actually be implemented, which is shown in Figure 6.10(b). To identify the phases of the channel in subbands we use an extension

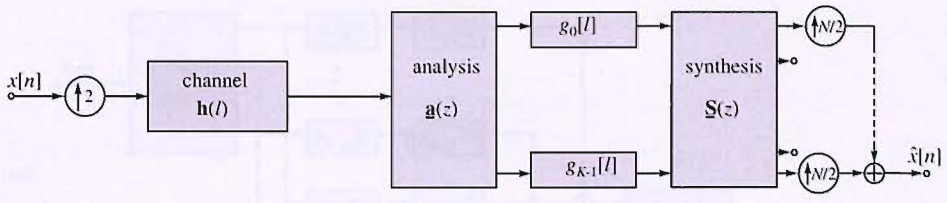

Fig. 6.9: A $T/2$ subband system with SISO channel h and equaliser g in a form for implementation.

of the fullband system shown in Figure 6.5 but for a SISO system, which is shown in Figure 6.11.

To determine which approach is best, we compare the costs involved in the computations of the various signal processing tasks. The cost with respect to N of NLMS algorithm performed using the first method for $T/2$ sampling, shown in Figure 6.8(c), is

$$\mathcal{O}(\frac{K}{(N/2)^2}) = \mathcal{O}(\frac{4K}{N^2}), \tag{6.35}$$

i.e. the signals in all K subbands must be processed at a rate decimated by $N/2$ and the subband filters are on the order of $N/2$ times shorter relative to the fullband case. For algorithms such as the RLS, the computational complexity in terms of multiply-accumulate operations depends quadratically on the filter length, such that the coefficient of K in the cost would also be even greater than it is with the NLMS algorithm. The cost of the NLMS algorithm using the second method for $T/2$ sampling, in Figure 6.10(b), however is

$$\mathcal{O}(\frac{\text{Num}_{\text{analysis banks}}\ K}{N^2}) = \mathcal{O}(\frac{2K}{N^2}), \tag{6.36}$$

i.e. there are two subband blocks, each running at symbol rate decimated by N. As the order of the algorithm increases, the coefficient of K will be unaffected since this only depends on the fractional-sampling factor (two in our case). Hence it is clear that the second method is more desirable and we shall proceed using this. This method was also used in [72, 163, 171, 172].

Although we have only considered a SISO system so far, creating fractionally-spaced subband MIMO system is a fairly straight-forward extension of the system shown in Figure 6.4 by processing the paths between the symbol-sampled phases of the received signals and equaliser output in subbands using the method discussed in this section.

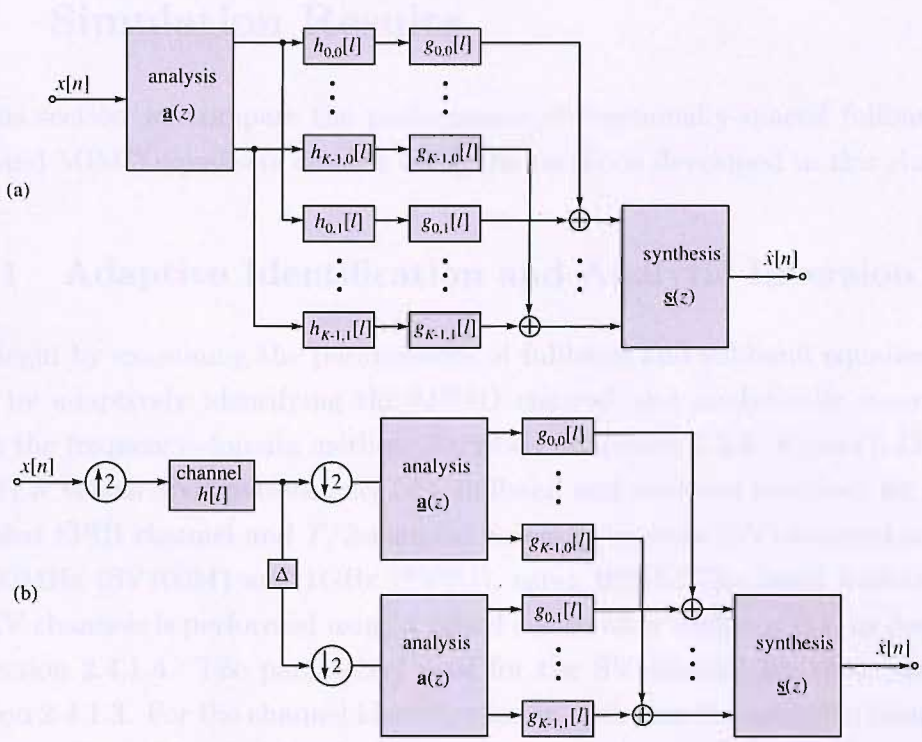

Fig. 6.10: Subband decomposition performed on polyphase representation of fractionally-sampled system used for (a) analysis, and (b) implementation.

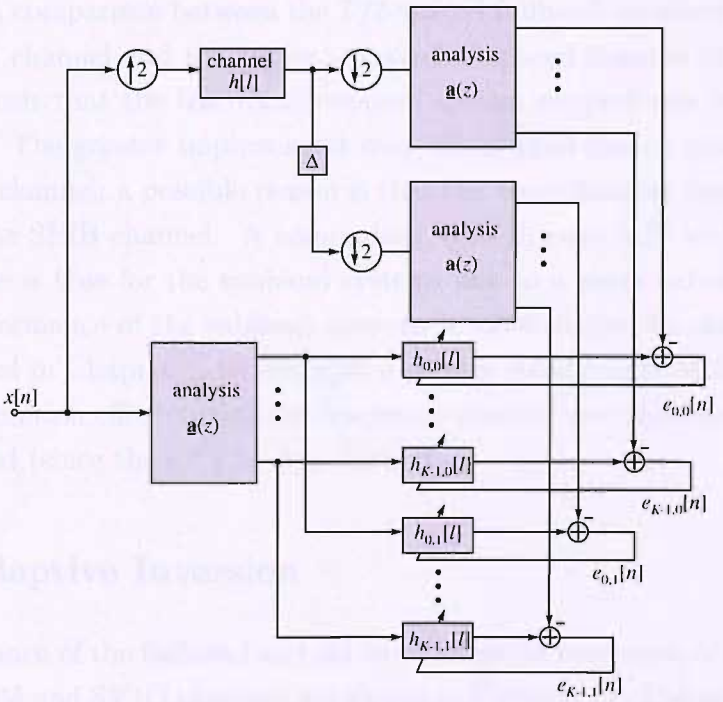

Fig. 6.11: Adaptive identification two phase in subbands of $T/2$ fractionally-spaced channel.

6.7 Simulation Results

In this section we compare the performance of fractionally-spaced fullband and subband MIMO equalisers created using the methods developed in this chapter.

6.7.1 Adaptive Identification and Analytic Inversion

We begin by examining the performance of fullband and subband equalisers created by adaptively identifying the MIMO channel and analytically inverting it using the frequency-domain method described in Section 4.2.3. Figure 6.12 shows the BER versus SNR performance of a fullband and subband equaliser for a $T/2$-sampled SPIB channel and $T/2$-sampled Saleh-Valenzuela (SV) channel sampled at 100MHz (SV100M) and 1GHz (SV1G), using BPSK. The band limitation on the SV channels is performed using a raised cosine filter with $r = 0.1$, as described in Section 2.4.1.4. The parameters used for the SV channel are those stated in Section 2.4.1.3. For the channel identification in each case the adaptive filters were chosen in line with previous chapters and were adapted long enough to reach a steady-state using the M-NLMS algorithm with $\tilde{\mu} = 0.18$. The subband parameters are the same as those in Chapter 5 for consistency, i.e. $K = 16$, $N = 14$ and $L_p = 448$. The per-phase equaliser filter lengths used in Figure 6.12 are shown in the legend. A comparison between the $T/2$-spaced fullband equaliser for the SPIB and SV100M channel and the equivalent symbol-spaced channel in Figures 4.21 and 4.22 reveals that the fractionally-spaced system outperforms by a considerable margin. The greater improvement over the symbol-spaced system is shown by the SPIB channel; a possible reason is that the band-limiting attenuation may be less for the SPIB channel. A comparison with Figures 5.27 and 5.28 reveals that the same is true for the subband systems but to a lesser extent. It is likely that the performance of the subband systems is more limited by other sources of error discussed in Chapter 5, for example a greater steady-state MSE and greater circular convolution effect during the frequency-domain inversion due to the short filters required (since the FFT is also shorter).

6.7.2 Adaptive Inversion

The performance of the fullband and subband adaptive inversions of a $T/2$-spaced SPIB, SV100M and SV1G channels are shown in Figure 6.13. The adaptation and subband parameters are the same as previously. Although for the SPIB channel the subband inversion converges slightly faster than for the fullband case the difference is minimal. This is since the channel is only mildly frequency-selective so

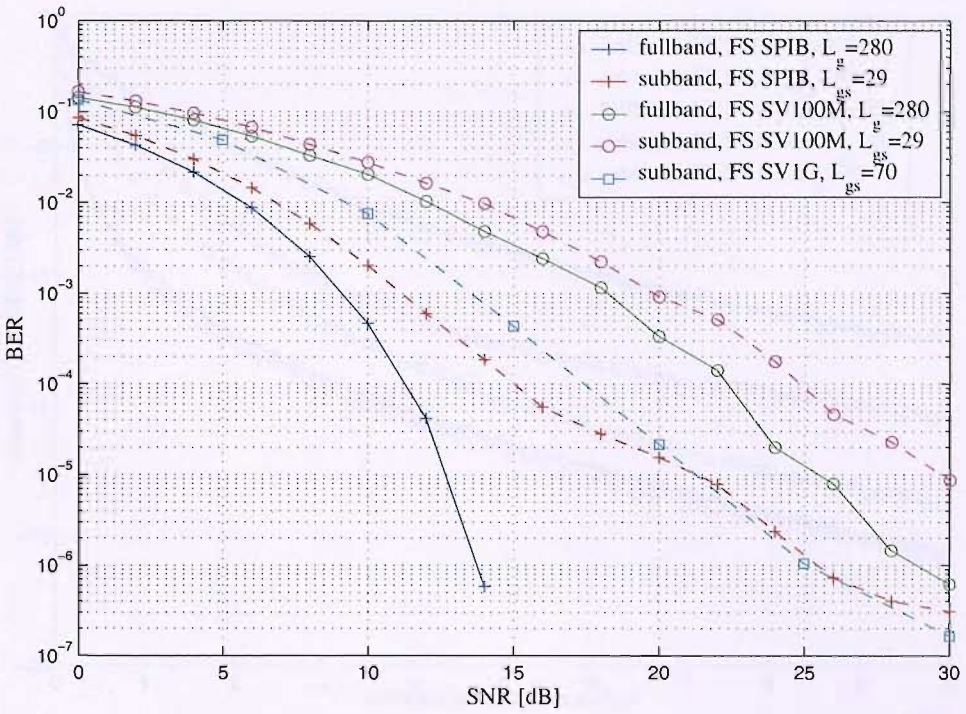

Fig. 6.12: Fullband and subband ($K = 16$) BER vs SNR for $T/2$-spaced 2×2 MIMO channels using an equaliser calculated with the frequency-domain method, and applying the best regularisation factor at each SNR.

we would not expect the subband system to outperform even using fractionally-spaced equalisation. The improvement for the SV100M channel is much more significant, with the subband system showing an improvement of about 6 dB over the fullband system by 10,000 fullband symbol periods. Comparing these results with Figures 4.17 and 5.22 shows the effect of fractional spacing on the adaptive inversion. The fractionally-spaced fullband inversion of the SPIB channel shows approximately a 4 dB improvement over the symbol-spaced system after 80,000 fullband sampling periods. For the SV100M channel the improvement is only about 2 dB giving further credibility to the previous hypothesis that the SPIB channel has a lesser band-limiting attenuation than the SV100M channel. A similar conclusion follows from a comparison of the subband adaptation profiles; the fractionally-spaced SPIB channel shows an improvement of about 3 dB by 80,000 fullband sampling periods whereas only a 1 dB difference is achieved for the SV100M channel. Finally the improvement for the SV1G channel is about 2 dB. Nevertheless the system still benefits from the potential computational savings from the subband approach even if in some cases the adaptation improvement is small.

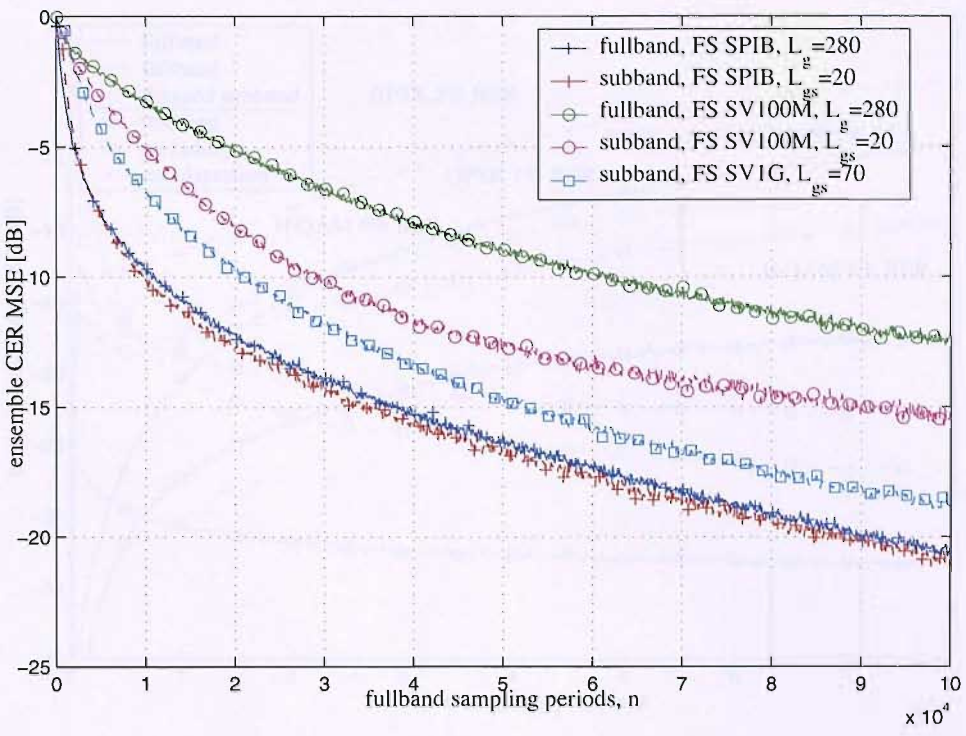

Fig. 6.13: Fullband and subband ($K = 16$) adaptive inversion MSE for $T/2$-spaced 2×2 MIMO channels. For no adaptation, the subband and delayed subband curves are identical.

6.7.3 Adaptive Equaliser Tracking

In this section the tracking ability of subband and fullband $T/2$-spaced equalisers is examined. Figures 6.14 and 6.15 show the tracking MSEs for a $T/2$ SPIB and SV100M 2×2 MIMO channel, respectively, starting from a near MMSE equaliser found using the frequency-domain inversion method described in Section 4.2.3. MSE profiles are shown for each combination of a fullband, subband and delayed subband system with tracking in a fading environment, tracking in a non-fading environment and fading with no adaptation (i.e. no tracking). The delayed subband tracking shows a realistic error-free blind tracking performance since it accounts for the delay in the subband filter banks, as explained in Section 5.3.4. The curve with fading and no adaptation shows the worst-case performance where an adaptive system would be completely incapable of tracking— although of course a poor adaptive system could exhibit an even worse performance. The curve where there is no fading shows a best-case performance which would be achieved if the adaptive system were able to track the fading channel equaliser perfectly. Hence we expect the actual tracking performance to be somewhere in between these two extremes and this curve's position between the extremes gives an idea of the ef-

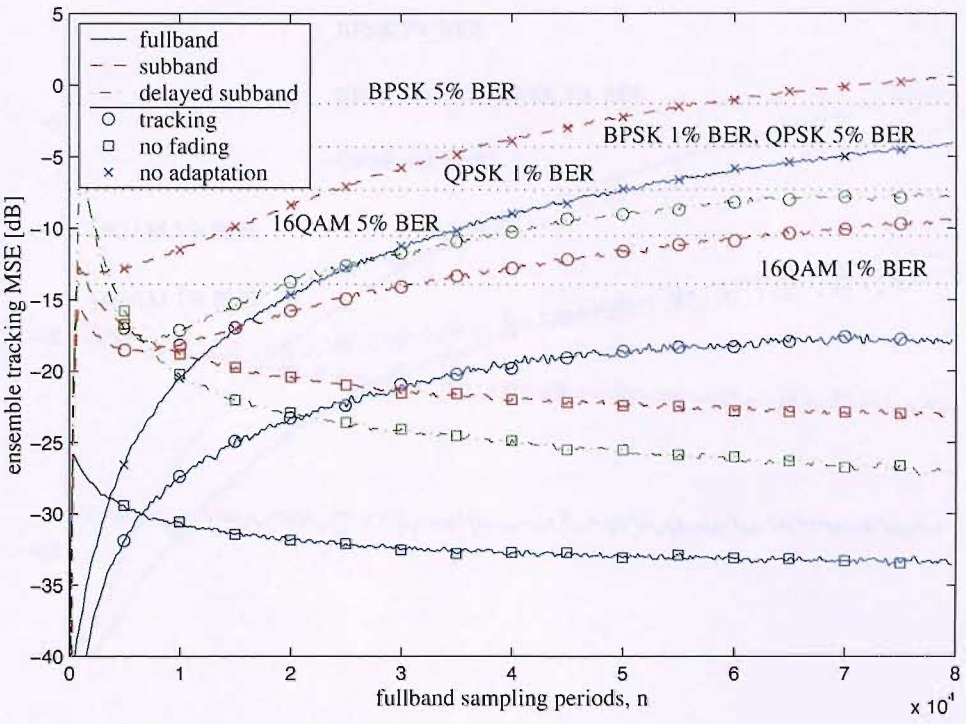

Fig. 6.14: Channel-Equaliser Tracking MSE of a FS $T/2$ SPIB 2×2 MIMO channel.

fectiveness of the adaptive system in tracking the equaliser. The performance of the fullband system for the SPIB channel in Figur 6.14 is approximately half way between the best and worst cases and is able to maintain an MSE that would result in a BER of well below 1% using 16-QAM modulation. Here the equaliser has 280 taps per fractional phase. The subband tracking MSE is a little better than for the delayed-subband system but both are worse than for the fullband system. The equaliser lengths for both subband systems are $L_{g,s} = L_{g,f}/N = 20$ per fractional phase. Evidently the relatively small range of the spectral dynamics of the SPIB channel means that the subband systems are unable to improve the tracking ability. Further, since the fullband MMSE equaliser response is relatively long, the subband equalisers are too short to be able to model well the MMSE equaliser, hence the performance is worsened still. Finally, we may compare the performance of these systems using $T/2$-spaced equalisation to that of a symbol spaced equaliser in Figure 5.24. Although the fullband tracking performance is better by about 6 dB, the subband performance is comparable for the $T/2$ and T-spaced cases.

Figure 6.15 shows tracking results from the $T/2$ SV100M MIMO channel. The equaliser lengths for each system are the same as for the SPIB channel above. Immediately the benefit of the subband approach for this channel can be seen.

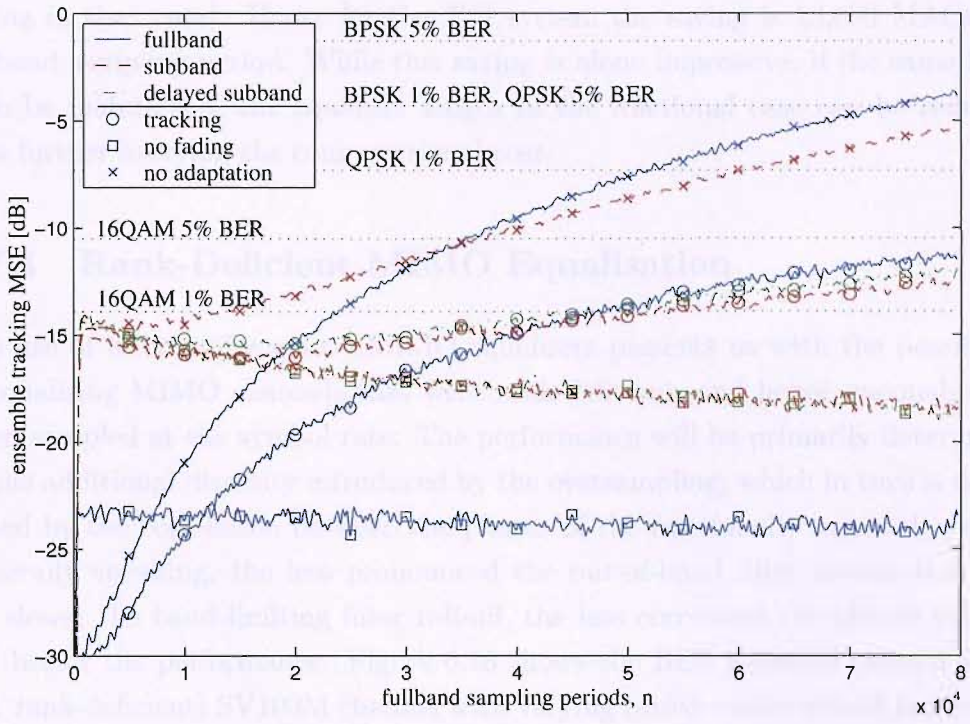

Fig. 6.15: Channel-Equaliser Tracking MSE of a FS $T/2$ SV100M 2×2 MIMO channel.

Though starting at a higher MSE, the subband systems are able to maintain a lower MSE than the fullband system by the end of the simulation. The SV100M channel has greater spectral dynamics than the SPIB channel, hence the greater benefit in using the subband system. Comparing the tracking curves to the best and worst case extremes we see that that while the subband curves are approximately in the middle of the range, the fullband curves are closer than the worst-case of no adaptation. From this we may again conclude that the subband system tracks better in both absolute and relative natures (i.e. relative position between the best and worst extremes). Comparing these results to the equivalent symbol-spaced equaliser curves in Figure 5.25 we see that the fractionally-spaced approach produces an improvement in MSE of about 6dB for fullband adaptation and similarly for the subband and delayed subband methods by the end of the simulation.

Finally, we briefly consider the computational cost benefit of the fractionally-spaced subband technique. Assuming the equaliser length per fractional phase is the same as the fullband equaliser length then the savings are multiplied by the fractional sampling factor. In this case the up-sampling factor is two, hence the savings are double. Referring the computational cost plot in Figure 5.14 and using $L_{g,s} = L_{g,f}/N$, where $L_{g,f} = 280$, the cost saving over the fullband method per fractional phase is about 6,500 MACs per fullband sampling period (a 72% cost

saving in that case). Hence for the $T/2$ system the saving is 13,000 MACs per fullband sampling period. While this saving is alone impressive, if the same BER is to be maintained, the equaliser length in the fractional case can be reduced, thus further lowering the computational cost.

6.7.4 Rank-Deficient MIMO Equalisation

The use of fractionally-spaced MIMO equalisers presents us with the possibility of equalising MIMO channels that were rank-deficient, and hence unequalisable, when sampled at the symbol rate. The performance will be primarily determined by the additional diversity introduced by the oversampling, which in turn is determined by the correlation between the phases of the fractionally sampled system. Generally speaking, the less pronounced the out-of-band filter attenuation and the slower the band-limiting filter roll-off, the less correlated the phases will be, and better the performance. Figure 6.16 shows the BER achieved using a 2×1 (i.e. rank-deficient) SV100M channel with varying raised cosine roll-off factors, as explained in Section 2.4.1.4, and a 2×1 SPIB channel, using BPSK modulation. Firstly, we see that the performance with the SPIB channel is better than any of the SV100M channels, suggesting that the out-of-band filter attenuation is lower for the SPIB channel. This reinforces the hypothesis made in Section 6.7.1 as to the reason that the SPIB channel performed better. For the SV100M channels the greater the roll-off factor, the gentler the roll-off and hence the lower the out-of-band attenuation immediately adjacent to the pass-band, as is shown in Figure 2.15. Hence the best performance is shown for the higher roll-off factors. As the roll-off factor decreases the difference between the performance becomes increasingly less up until the point where $r = 0.1$ and $r = 0.3$. In fact, here the performance are very similar is for higher SNRs the performance for $r = 0.1$ becomes slightly better than for $r = 0.3$. A possible reason is that for $r = 0.1$ although the roll-off is steeper the out-of-band attenuation is less than for $r = 0.3$ potentially making the sub-channel correlation less.

These results effectively show the power of fractionally-spaced equalisation for MIMO channels. In a real system the sub-channels may be highly correlated due to potential close proximity of the antennas especially on a physically small mobile station (MS). In the extreme where the sub-channels to and from the MS antennas are completely correlated when sampled at symbol-spacing, the MIMO system becomes unequalisable and the capacity collapses back down to that of a single channel system, meaning MIMO communication is impossible. However, with fractional-sampling MIMO communication is possible albeit generally with a poor BER.

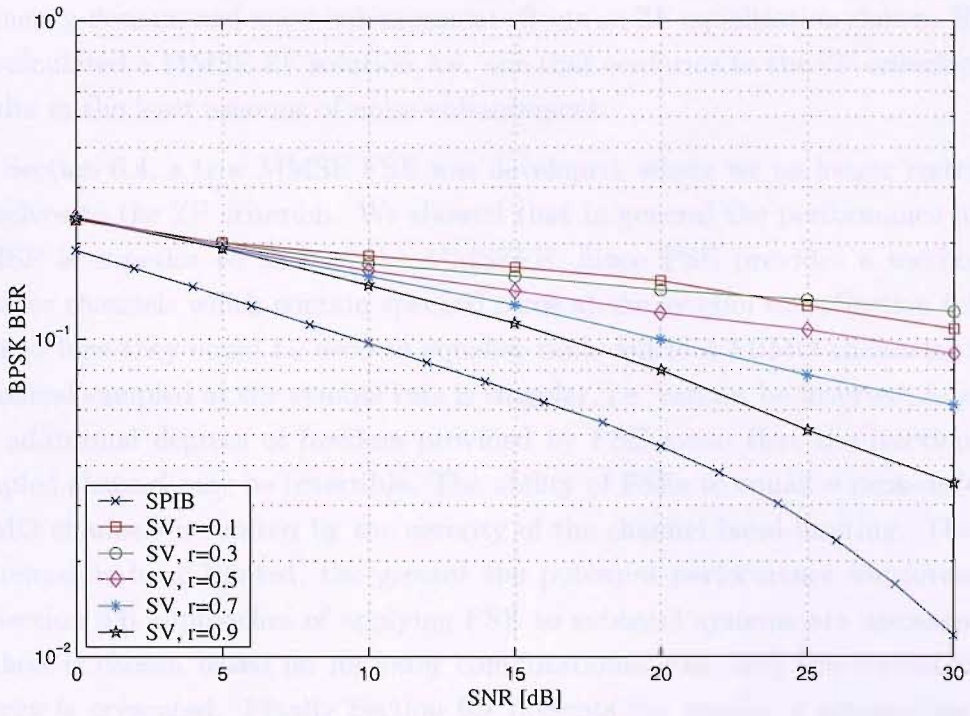

Fig. 6.16: SNR vs BER for a SPIB channel and SV100M channels with a range of raised-cosine roll-off factors, using a BPSK modulation scheme.

6.8 Summary

Single channel fractionally-spaced equalisation (FSE) is known to improve performance in terms of MSE and BER over symbol-spaced systems. It can also enable shorter equaliser filters and the capability of equalising channels that contain spectral zeros. This chapter has covered the application of fractionally-spaced equalisers to fullband and subband MIMO systems.

In Section 6.1, we explained the principle behind why FSE can perform at least as well as symbol-spaced equalisers (SSE), and often better. The optimum receiver is a serial concatenation of a matched filter and a SSE, however FSEs can perform both these tasks. Further, whereas receiver symbol timing offset can have a great impact of the performance of a SSE-based system, FSEs are relatively immune. Section 6.2 developed a polyphase representation of FSE, which is not only more convenient for further analysis, but also puts the system into a form where the MIMO equalisation concepts developed in previous chapters are directly applicable. Zero-forcing equalisation (ZFE) of MIMO FSE was covered in Section 6.3. ZF FSE is significantly different to ZF SSE; not only can perfect ZF FSE be performed using FIR filters (unlike SSE) but there are an infinite number of ZF solutions, one of which provides the MMSE solution. Equalisability was calculated in the

frequency-domain and noise-enhancement effects on ZF equalisation shown. Hence we calculated a MMSE ZF solution, i.e. one that conforms to the ZF criterion but results in the least amount of noise-enhancement.

In Section 6.4, a true MMSE FSE was developed, where we no longer restricted ourselves to the ZF criterion. We showed that in general the performance of the MMSE is superior to that of the MMSZFE. Since FSE provides a method to equalise channels which contain spectral zeros at the symbol rate, Section 6.5 explained how they could be used to equalise rank-deficient MIMO channels. Such a channel sampled at the symbol rate is singular, i.e. cannot be inverted, however the additional degrees of freedom provided by FSE mean that the fractionally-sampled channel may be invertible. The ability of FSEs to equalise rank-deficient MIMO channels is limited by the severity of the channel band-limiting. The less a channel is band-limited, the greater the potential performance improvement. In Section 6.6 approaches of applying FSE to subband systems are discussed. A method is chosen based on its lower computational cost, and the system architecture is presented. Finally Section 6.7 presents the results of simulations and examines the performance compared to symbol-spaced systems. When performing adaptive identification followed by analytic inversion the fractionally-spaced systems generally outperform the symbol-spaced system by a considerable margin. The same is true for the adaptive system inversion and tracking. When using FSE to invert a rank-deficient channel we see that the performance depends on the severity of the band-limiting. Although the performance never falls below a BER of 10^{-2} for any type of channel considered here, it is still an improvement over the symbol-spaced system, where inversion is impossible. This effectively demonstrates the power of FSE for MIMO systems with highly correlated sub-channels, which is likely when the MIMO antennas are closely located.

Chapter 7

Conclusions

7.1 Summary

This thesis has been concerned with computationally efficient methods of inversion and equalisation for a broadband MIMO channel with the best possible performance and tracking the equaliser for fading channels. As is true with many aspects of communications we have found that there is a trade-off between obtaining the best possible performance in terms of CER MSE and BER and implementing algorithms with the lowest possible computationally cost. Which method to use for finding and tracking the equaliser is inevitably a function of many variables such as the channel impulse response and related spectral behaviour, the dimensions of the MIMO channel, the speed of the MS, the modulation scheme used, the desired BER and others. This thesis has covered many of these points, examining the relationships between these factors in an effort to determine a set of "rules" that can be used when designing a real system.

In **Chapter 2** MIMO channels were formally introduced and some of the background topics that have formed the basis of past relevant research were reviewed. Further research into broadband MIMO equalisation algorithms was motivated. Next, the chapter covered the channel capacity increases which are promised by MIMO channels, and indeed this is the main motivation for the method. Finally, channel models were developed that have been used throughout this thesis to demonstrate algorithms and they were characterised in terms of their spectral, temporal and spatial dynamic behaviour.

In **Chapter 3** an introduction to multi-channel adaptive filtering was given. This has been the basis of many of the techniques used to equalise and track the channels, which we assume are unknown at either the transmitter or receiver. The chapter gave an in depth coverage of the performance characteristics of the

main developed algorithm, namely M-NLMS. Finally, the existence of some other potential adaptive algorithms was briefly mentioned, before presenting simulation results that showed the performance of the M-LMS algorithm, identifying various broadband MIMO channels. We saw that for multi-channel adaptive identification, convergence was slowed by a factor approximately equal to the number of channels involved in the adaptation. In the tracking simulations we found that the MSE performance is be described in terms of a steady-state misadjustment and lag due to the non-stationarity of the channel. Finally, we saw that for MSs moving at a constant velocity, the steady-state tracking MSE is worse for a MIMO system than a SISO due to the additional paths that must be tracked. For example, for a 100 MHz sampled symbol-sampled SV channel and a MS moving at 120 km/h, the tracking MSE is 10 dB worse for the 2×2 MIMO channel than for the SISO.

In **Chapter 4** inversion criteria for a broadband MIMO equaliser were stated, and some mathematical tools were introduced which were used during the development and can be used for the equaliser calculation, such as the pseudo-inverse and method of regularisation. An alternative possibility of using pre-distortion at the transmitter was highlighted. Fractionally-spaced equalisation was briefly introduced. The chapter continued to a coverage of three techniques for analytically inverting the broadband MIMO channel, namely in the z, time and frequency-domain. The choice of equaliser filter lengths and also the effects of channel estimation errors and noisy adaptation on the calculated channel inversion were explained. An alterative fully adaptive method of finding the equaliser was covered and its advantages and disadvantages were covered. Finally, simulation results were presented showing the performance of systems created using the techniques developed in this chapter. Whilst the z-domain inversion method was capable of outperforming the others at high SNR it could not always be used and was prone to stability problems. The time-domain method results in a MMSE FIR equaliser but calculation was computationally intense. The frequency-domain method resulted in MSE performance approaching MMSE at low SNRs but worsened at higher SNRs when the circular convolution errors became significant relative to the noise. However the computational cost involved in calculation is much less than the time-domain method and the circular convolution effect could be partly alleviated using the method of regularisation, meaning that in general the frequency-domain method gave the best compromise in terms of MSE performance and computational cost. Channel estimation errors had the potential to affect derived equalisers, but by applying temporal averaging to the channel taps during an ergodic portion of the adaptation, performance could be improved. Direct adaptive inversion was generally far too slow to be useful starting with no channel state information. Finally, tracking simulations for an MSs moving at 120

km/h showed that an acceptable MSE hence BER could be maintained, albeit in some cases this was borderline.

In **Chapter 5** the method of subband signal processing was introduced, where a signal or system is split into many frequency-bands, and any signal processing task is performed in these subbands independently. Subband systems have emerged as a way to potentially reduce the computational cost of signal processing algorithms, something which is needed for large and complicated broadband MIMO systems, while in some cases improving associated performance. The chapter continued by covering the basis of multi-rate operations, modulated filter banks and oversampling to solve the problem of interdependence between adjacent subbands. The properties of subband systems were then briefly described, before implementing the fullband inversion techniques of Chapter 4 in subbands. Finally, the performance of systems implemented using subbands in terms of computational cost, adaptation, CER MSE and BER was shown. For subband adaptive identification the adaptation was always slower and reached a worse final MSE than fullband identification. The relative complexity between subband and fullband identification depends on the relationship used between the equaliser lengths, but the simulations show that the subband method is often capable of delivering computational savings. Despite the worsened MSE performance, subband adaptive identification is a necessary step if subsequent subband analytic inversion and subband adaptive tracking are to be performed. The simulations showed that subband analytic inversion is capable of delivering comparable MSE performance as the fullband system, but at significantly lower computational cost. Apart from cost reduction, the other benefit arises from potentially improved convergence and tracking when spectrally coloured inputs are used, such as is the case when the equaliser itself to a frequency-selective channel is to be obtained or tracked. The simulations showed that for highly frequency-selective channels, the subband system was often able to achieve an improved steady-state MSE for time-varying channels when compared to the fullband system. Overall we found that subband systems are most suited to highly frequency-selective channels, channels with an impulse response comparable or relatively long compared to the subband prototype filters length and time-varying channels where tracking is required.

In **Chapter 6** the principle behind fractionally-spaced equalisation (FSE) was shown. The chapter explained that FSE can perform both the task of matched filtering and symbol-spaced equalisation (SSE). It then developed a polyphase representation of FSE, before developing zero-forcing FSE. Equalisability was calculated in the frequency domain and noise-enhancement effects were shown. Next, the minimum mean squared error (MMSE) FSE was calculated, and we saw that MMSE FSE outperforms MMSE zero-forcing FSE– with FSE there are an infi-

nite number of zero-forcing equalisers, one of which gives the MMSZFE solution. The chapter explained how FSE can be used to equalise MIMO systems that are rank-deficient, and hence unequalisable, when sampled at the symbol rate. It also showed that the FSE performance of rank-deficient MIMO systems depends on the band-limiting of the channel. Next the chapter covered how FSE may be applied to subband systems, creating a subband adaptive MIMO FSE, before finally showing and explaining the results of numerous simulations. When the equaliser is obtained by adaptive identification followed by analytic inversion, the fullband fractionally-spaced system outperformed the symbol-spaced system by a considerable margin. The same performance improvements arose for the subband system comparison but to a lesser extent. Though the fullband fractionally-spaced equaliser showed better MSE performance than the subband version, the cost was again less for the latter to the extent that for the 1 GHz-sampled SV channel only the subband version was practicable. For adaptive inversion however, the subband method exhibited markedly better convergence performance for the SV channels. This translated to an improved steady-state MSE of the order of 1 or 2 dB for time-varying SV channels. Lastly of the simulations, results are shown for the MSE performance of FSE equalisers for MISO channels that are rank-deficient when sampled at the symbol rate. For the SPIB channel, for example, the MSE performance at high SNRs is quite reasonable, meaning that in the extreme case of a MIMO channel where the sub-channels are so correlated that the system collapses to a MISO, FSE can be used to recover some of the MIMO benefits.

Early in this treatise, MIMO channel capacities were discussed. The capacities of the two channels used throughout this discourse— namely the symbol-spaced SPIB and a symbol-spaced channel based on the Saleh-Valenzuela model sampled at 100 MHz (SV100M)— were shown in Chapter 2. A fitting way to conclude this thesis is to compare the capacities of channel-equaliser systems for various equalisers calculated using the many methods examined in this work. Figure 7.1 and Figure 7.2 show the capacities for equalised SPIB and SV100M channels, respectively. The upper lines in both figures represent the bound of the isolated channels, and the closer the post-equalised systems reach this bound the greater their information-bearing capacity. In both cases we see that, as expected, the fullband inversion achieves the greatest capacity, irrespective of whether the initial adaptive identifications were performed in the fullband or subband domain. However, as was demonstrated in Chapters 5 and 6 the subband approach potentially benefits from improved equaliser tracking and lower computational complexity.

It would be interesting to see a framework of all the various methods and processes we have considered in this thesis in graphical form. Clearly the many different techniques considered in this thesis afford us many different ways of inverting a

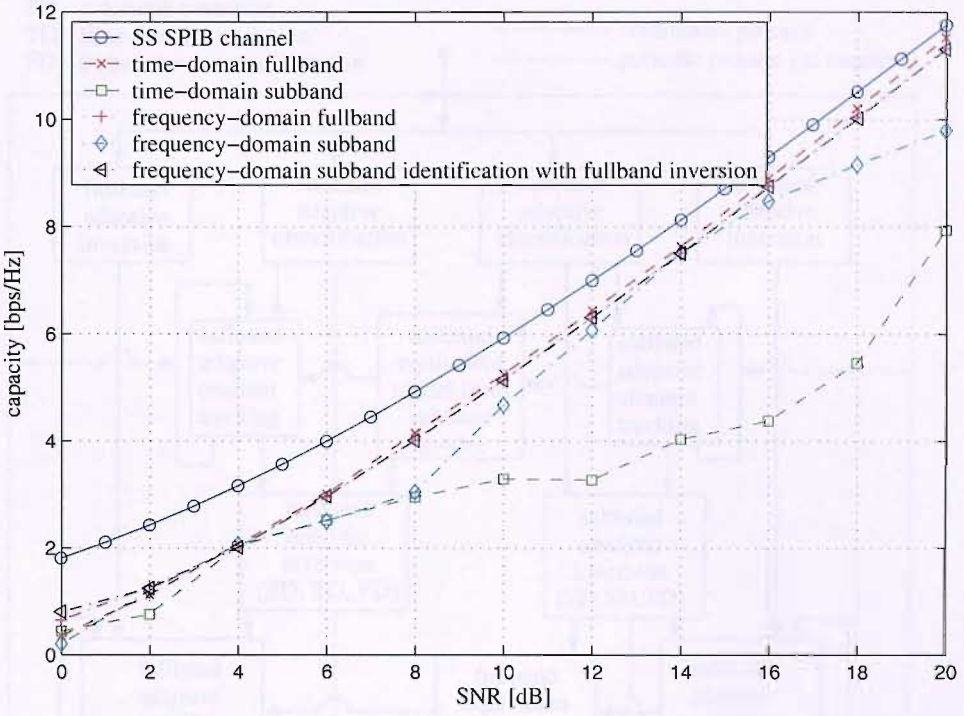

Fig. 7.1: Capacity of SS SPIB channel, and Channel-Equaliser systems using the various methods covered in this thesis.

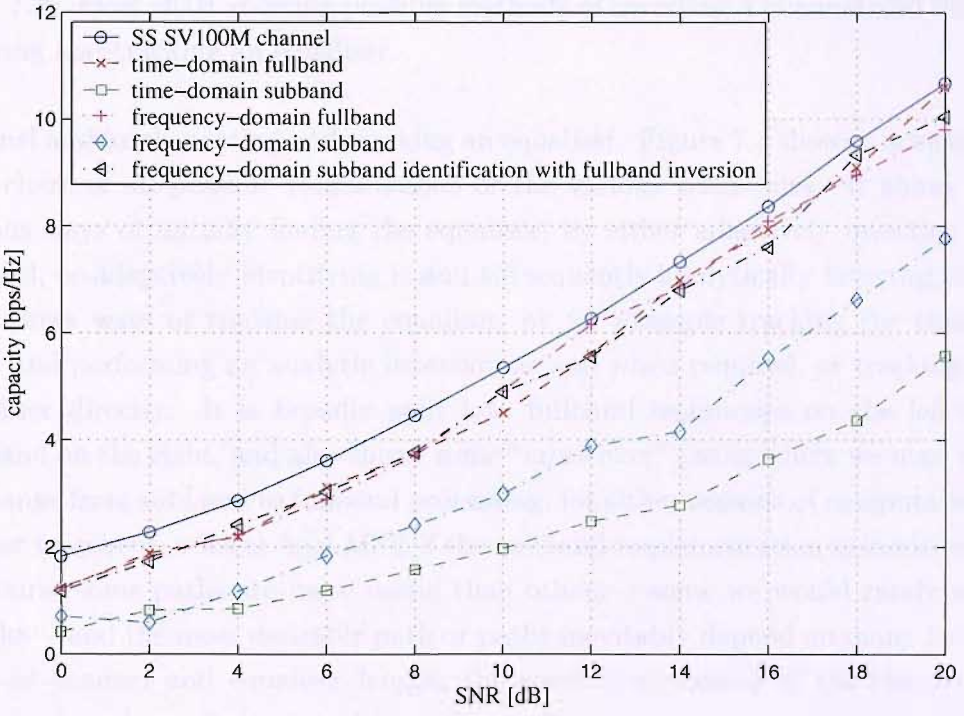

Fig. 7.2: Capacity of SS SV100M channel, and Channel-Equaliser systems using the various methods covered in this thesis.

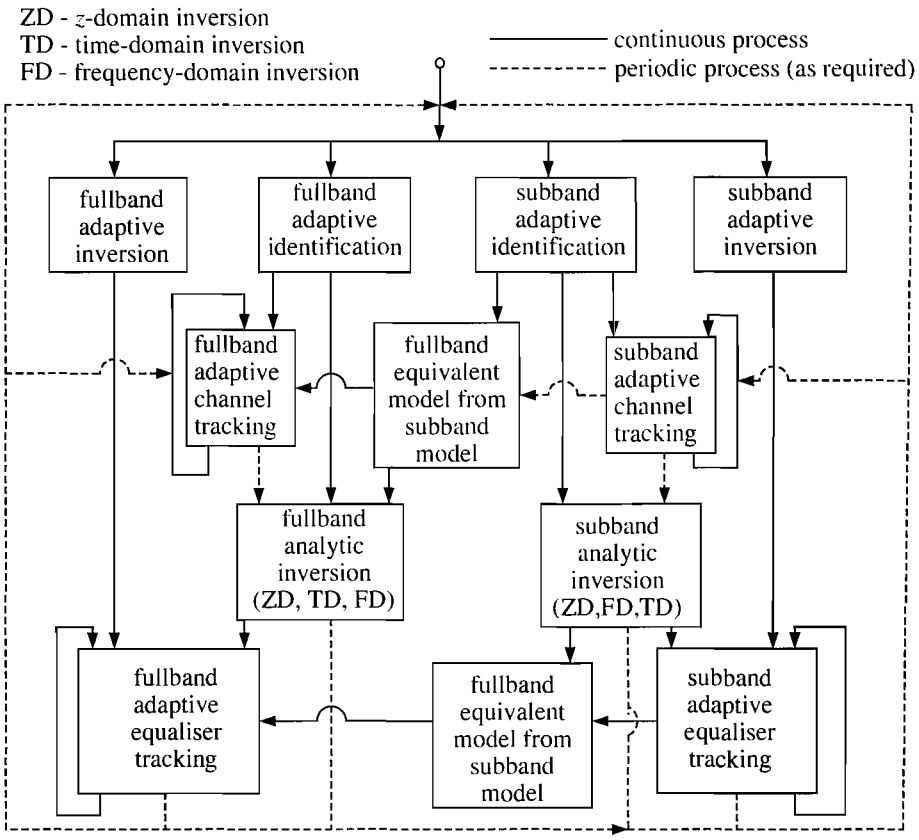

Fig. 7.3: Flow chart showing possible methods of inverting a channel and implementing and tracking an equaliser.

channel and implementing and tracking an equaliser. Figure 7.3 shows a schematic flow chart of all possible combinations of the various techniques. It shows the various ways of initially finding the equaliser, by either adaptively inverting the channel, or adaptively identifying it and subsequently analytically inverting it. It also shows ways of tracking the equaliser, by for example tracking the channel itself and performing an analytic inversion as and when required, or tracking the equaliser directly. It is broadly split into fullband techniques on the left and subband on the right, and also shows some "cross-over" paths where we may wish to change from subband to fullband processing, for either reasons of computational cost or to achieve a lower final MSE if the subband implementation is inadequate. Of course some paths are more useful than others— some we would rarely want to take— and the most desirable path or paths inevitably depend on many factors such as channel and equaliser length, the spectral dynamics of the channel as well as what the optimisation objectives are. Fractionally-spaced systems are not included in the diagram since in general these always perform better than symbol-spaced systems, hence they should always be used.

The overall conclusions that we may draw from this work is that the subband technique has demonstrated itself to be a powerful method for reducing the computational cost involved in tracking highly frequency-selective channels where the channel impulse response and required equaliser length are both long relative to the subband prototype filter length. For shorter channels the advantages diminish and in some cases the subband solution is clearly undesirable. Another powerful feature demonstrated by the subband method is its improved ability to track the equaliser of a fading broadband MIMO channel at a lower computational cost. We have seen that generally time-domain analytic inversion will result in the best MSE and BER performance, but frequency-domain inversion has a much lower associated computational cost. Finally, we have seen that fractionally-spaced subband adaptive MIMO equalisers are capable of providing the best MSE performance for highly broadband and hence frequency-selective channels at a reduced computational cost.

7.2 Outlook

A potentially interesting extension to this work would be the development of a direct projection method from the subband time domain to the fullband frequency domain. Presently two steps are necessary in this conversion– i) converting the subband time representation into the fullband time representation using the equivalent fullband method outlined in Section 5.3.2.1, and ii) converting to fullband frequency domain through use of a FFT. By recognising that the subband representation is already part of the way towards a fullband frequency domain representation, since the signals are represented in the time domain but in a number of discrete frequency bands, it becomes clear that it should be possible to convert these directly into the frequency domain within each subband and combine the resulting responses so that the fullband frequency representation results.

Other fields of research that remain open to further investigation are areas such as the effects of spatial dynamics mentioned in Chapter 2, using the RLS adaptation algorithm in place of the NLMS which has been used through-out this thesis, and performing adaptation and/or signal processing in the frequency-domain.

Much of this work used idealised channels or channels that are not specifically MIMO, but have been used as MIMO by implementing multiple SISO models. Whilst this was adequate for our purposes, it does not take into account any spatial effects that would arise from antennas that are physically located in close proximity to one another, and hence the sub-channels would display some correlation. It

would be interesting to model these spatial dynamics and observe their effect on the systems developed in this thesis.

The adaptation algorithm used through-out this thesis has been based on the NLMS. Another algorithm that was touched upon was the RLS. It was considered in Chapter 3 but discounted due its greater potential for stability problems and computational cost. It would interesting, however, to further investigate the use of this or other algorithms and try to overcome their problems, since the RLS algorithm has a much greater potential adaptation rate and could potentially display far superior performance than has been shown in this thesis using just the NLMS algorithm.

All the equalisation techniques in this thesis have been performed in the time-domain or subband-domain, though even in the subband domain, signals are still represented as time sequences within each subband. In Chapter 4, a method of calculating an equaliser in the frequency-domain was shown, but it was only the calculation itself that was performed in the frequency-domain; the resultant equaliser was still implemented in the time or subband domain. There is a large field of work however where any adaptations and the processing of the signals themselves are all performed entirely in the frequency domain. A possible avenue of investigation would be to study where there is an overlap between these techniques and those that have been studied in this thesis, and by taking the best or most promising parts of all these methods, to create more superior still wideband MIMO equalisers.

Appendix A

Fading Channel Model

A.1 Rayleigh Faded Doppler Fading Channel

The fading caused by movement through space is Rayleigh, and by taking the speed of the MS into account we apply a smoothing or Doppler filter, because at normal speeds the MS is unlikely to move far enough in one symbol period for the fading coefficient to be un-correlated to previous ones. To understand this we must consider the Doppler spread of a signal transmitted from a moving MS to a base station (BS), shown in Figure A.1.

It is well-known that if the transmitter moves towards to receiver and the signal travels along the direct path the signal will experience a shift in frequency upward. The opposite is true if the transmitter moves away from the receiver. This shift is known as the Doppler shift. However in the multi-path environment shown in Figure A.1 there are several paths from the MS to the BS. Note that although all environments are almost always multi-path to some extent they may still be flat in the frequency domain, as the coherence bandwidth may be greater than the signal bandwidth. In this case, whatever the direction of movement it is likely that some of the signal paths may shorten by varying amounts, and so the signal will experience an upwards Doppler shift, but some will lengthen by varying amounts and so will experience a downwards Doppler shift. The effect of this is that if a carrier frequency, f_c, is transmitted from the moving MS it will be spread by the Doppler effects, and a spread version will be received at the BS. The amount of spreading can be characterised in the frequency domain by an amount known as the Doppler spread, f_d. The relationship between the Doppler spread and the symbol bandwidth determines whether the channel is termed slow-fading or fast-fading. If the Doppler frequency is much less than the symbol bandwidth the channel is slow-fading, and vice versa. In reality, most real channels used for

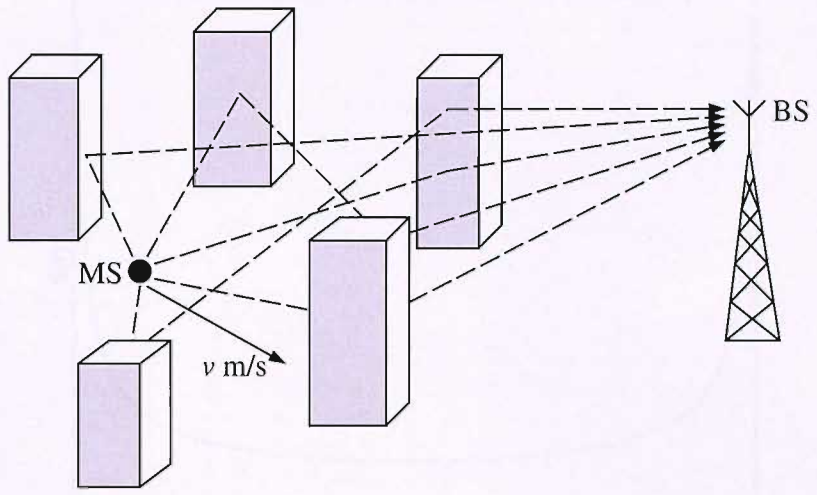

Fig. A.1: A MS moving through a multi-path environment.

mobile radio communication are slow-fading, and a fast-fading channel would be very difficult if not impossible to adaptively track. The Doppler spread is directly related to the speed of the MS, v, and the signal's carrier frequency,f_c,

$$f_d = \frac{v f_c}{c}, \tag{A.1}$$

where $c = 3 \times 10^8$ m/s, the speed of light. For example a MS transmitting at 1800 MHz and moving at 120 km/h will have a Doppler spread of

$$f_d = \frac{120 \text{ km/h} \times 1000 \text{ m/km} \times 1800 \text{ MHz} \times 10^6 \text{ Hz/MHz}}{3600 \text{ s/h} \times 3 \times 10^8 \text{ m/s}} = 200 \text{ Hz}, \tag{A.2}$$

which means that if the symbol bandwidth is much greater than 200 Hz the channel will be slow-fading. From this it is possible to use the Doppler filter, through which a Rayleigh signal is passed, to create a Doppler Rayleigh faded channel envelope appropriate for the speed of the MS [23, 173, 174]. The power spectral density (PSD) of the Doppler filter depends on the azimuthal gain pattern of the antennas and the signal distribution as a function of the azimuthal angle of departure, but if we assume a vertical $\lambda/4$ antenna, where the azimuthal gain is uniformly 1.5, and a uniform signal distribution then the PSD of the Doppler filter is given by [23]

$$S(f) = \frac{1.5}{\pi f_d \sqrt{1 - \left(\frac{f - f_c}{f_d}\right)^2}}, \tag{A.3}$$

and zero elsewhere. Note that as $f_d \to \infty$ then the channel becomes that of the unfiltered Rayleigh-fading model in Section 2.4.2.2. This PSD is shown graphically in Figure A.2. We may also perform Doppler filtering in the baseband, in which case we set $f_c = 0$.

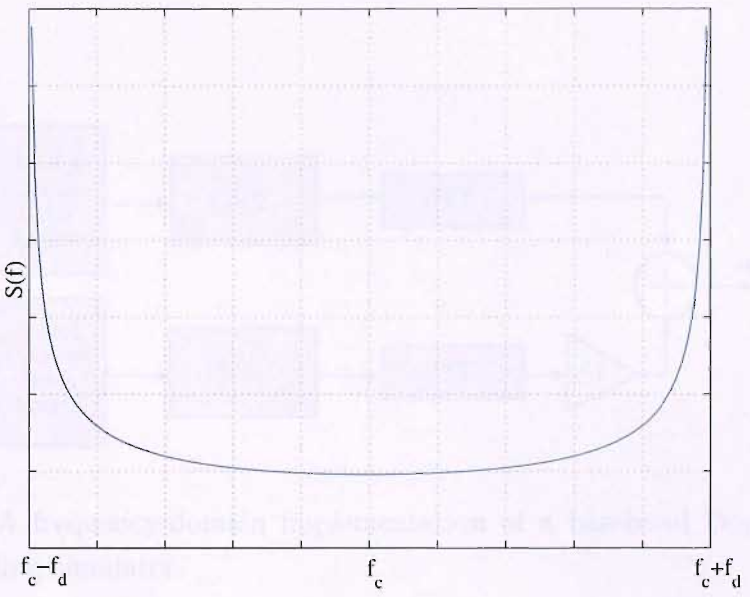

Fig. A.2: Doppler power spectral density.

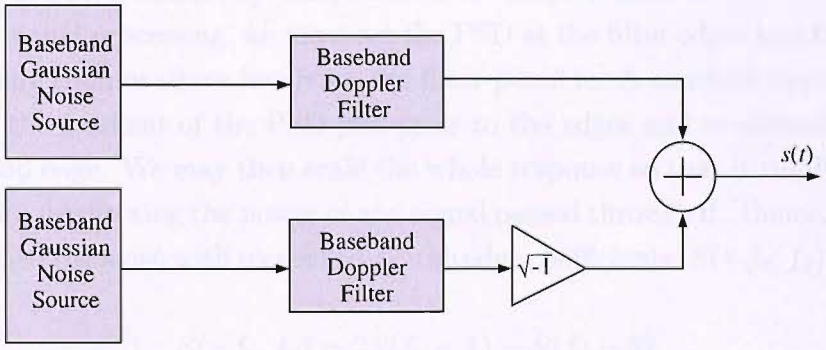

Fig. A.3: A baseband Doppler-filtered Rayleigh fading simulator.

To create the Doppler-filtered Rayleigh fading envelope, we use the approach shown in Figure A.3. The most computationally efficient way to perform the simulation to create the Doppler-filtered Rayleigh fading envelope is to multiply the spectrum of the Gaussian noise sources by the square root of Doppler filter PSD and then perform an IFFT to obtain the time-domain representation. The in-phase and quadrature are then vectorially combined. A further opportunity to reduce the computational load now arises as the spectrum of a Gaussian process is also Gaussian. Therefore rather than generating the Gaussian noise in the time-domain and then performing an FFT to transform this into the frequency-domain we may simply use a scaled Gaussian signal directly as the spectrum. The Gaussian must first be multiplied by a factor of $1/\sqrt{2f_s}$, to maintain a signal power of unity in the time-domain. This frequency-domain implementation is shown in Figure A.4.

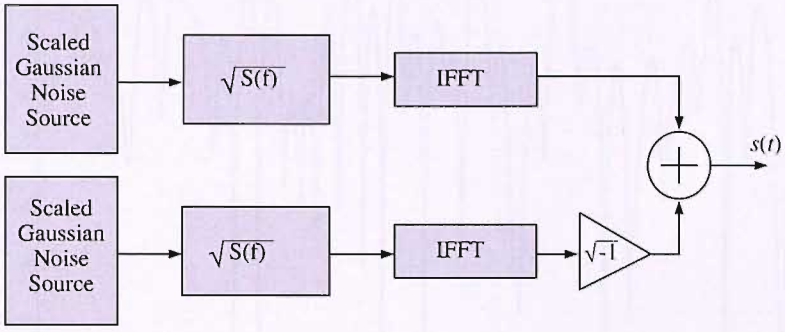

Fig. A.4: A frequency-domain implementation of a baseband Doppler-filtered Rayleigh fading simulator.

A problem with the PSD is that at the filter edges the PSD tends to infinity. When we are performing any computations is discrete time, as is always the case in digital signal processing, we must set the PSD at the filter edges to a finite value to make any computations involving the filter possible. A common approach is to calculate the gradient of the PSD just prior to the edges and to extend the slope to the band edge. We may then scale the whole response so that it results in unity power gain, unaffecting the power of any signal passed through it. Hence, assuming a normalised response with respect to f_d, the edge coefficients, $S(-f_d, f_d)$, are given by

$$S(-f_d, f_d) = 2S(f_d - 1) - S(f_d - 2). \tag{A.4}$$

Using the previous example of an MS moving at 120 km/h and with $f_c = 1800$ MHz, resulting in $f_d = 200$ Hz, we can now simulate using the frequency-domain simulator implementation a typical Doppler-filtered Rayleigh fading envelope for this MS, and this is shown in Figure A.5.

If we have a time-dispersive channel we may use several Doppler-filtered Rayleigh fading simulators in conjunction with the corresponding time-delays as shown in Figure A.6, to produce frequency-selective fading effects. Each Rayleigh simulator must be independent of all others. The gains a_0 to a_N are determined by the impulse response discussed in Section 2.4.1. One of these channels would be needed for each element in $\mathbf{H}$.

Finally, other models exist that in some cases may prove more suited to the environment we are attempting to characterise. For example, instead of the Rayleigh model we may use a Rician model [23] which is similar except that it also contains a single line of sight component. However, in this thesis we will only use

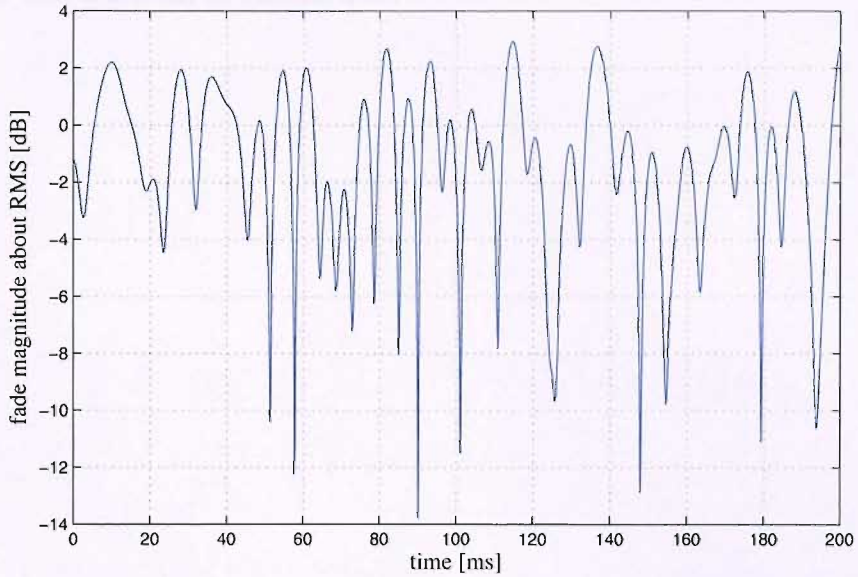

Fig. A.5: A typical Doppler-filtered Rayleigh fading envelope at 1800 MHz for an MS travelling at 120 km/h.

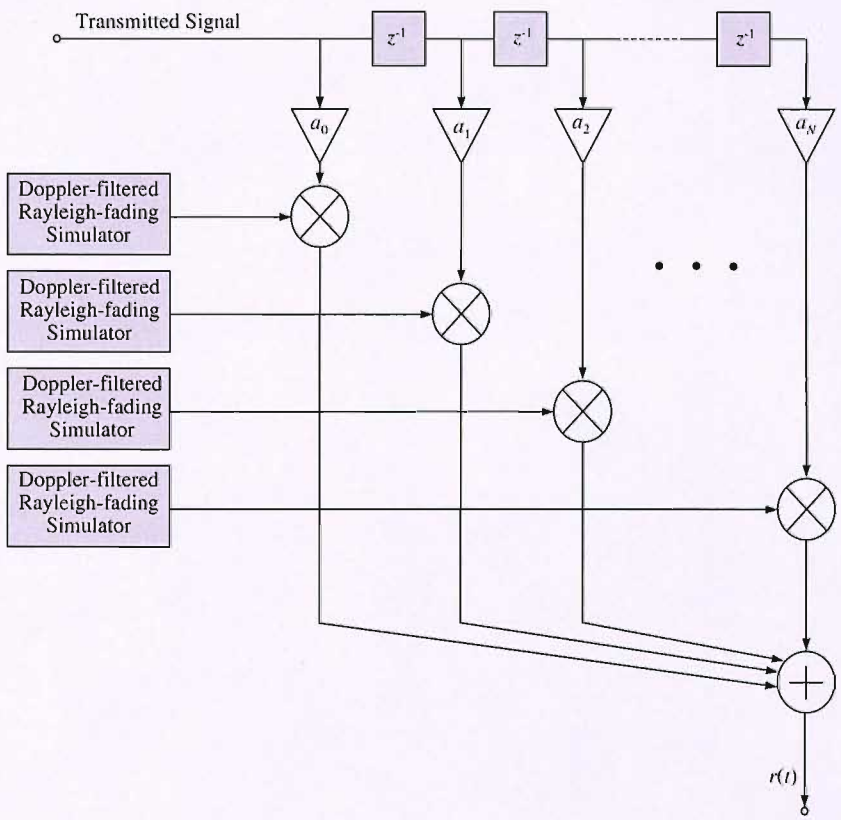

Fig. A.6: A Doppler-filtered Rayleigh fading frequency-selective channel simulator.

Rayleigh-based models in simulations.

Appendix B

MIMO Capacity Derivations

B.1 Linear MIMO Capacity Increase

Derivation to shown that the MIMO capacity, C, increases approximately linearly with the number of transmitters, M, assuming that $P > M$ where P is the number of receivers.

$$C = \log_2 \det\left(\mathbf{I}_M + \frac{\rho}{M}\mathbf{H}\mathbf{H}^H\right),$$

where $\mathbf{I}_M$ is an $M \times M$ identity matrix. Continuing, we have

$$\mathcal{E}\{C\} = \log_2 \det\left(\mathbf{I}_M + \frac{\rho}{M}\mathcal{E}\{\mathbf{H}\mathbf{H}^H\}\right).$$

Assuming the element of H are all complex Gaussian i.i.d. we have

$$\mathcal{E}\{C\} = \log_2 \det\left(\mathbf{I}_M + \frac{\rho}{M}\sigma^2\mathbf{I}_M\right),$$

and assuming $\sigma^2 = 1$, so

$$\begin{aligned}
\mathcal{E}\{C\} &= \log_2 \det\left(\mathbf{I}_M + \tfrac{\rho}{M}\mathbf{I}_M\right) \\
&= \log_2 \left(1 + \tfrac{\rho}{M}\right)^M \\
&= M \log_2 \left(1 + \tfrac{\rho}{M}\right) \\
&\approx M \log_2 \left(\tfrac{\rho}{M}\right) \qquad \text{for } \tfrac{\rho}{M} \gg 1 \\
&\approx M \left[\log_2 \rho - \log_2 M\right] \\
&\approx M \log_2 \rho \qquad \text{for } \rho \gg M.
\end{aligned}$$

Notice that the condition $\rho >> M$ is the same as the previous condition $\frac{\rho}{M} >> 1$, so this the necessary and sufficient condition for this to be a good approximation.

B.2 Limiting MIMO Capacity

Derivation to find the limiting capacity of a MIMO system as M tends to infinity.

$$\begin{aligned}\lim_{M\to\infty}\mathcal{E}\{C\} &= \lim_{M\to\infty} M\log_2\left(1+\tfrac{\rho}{M}\right)\\ &= \lim_{M\to\infty}\frac{M\ln\left(1+\frac{\rho}{M}\right)}{\ln 2}\\ &= \tfrac{1}{\ln 2}\lim_{M\to\infty}\frac{\ln\left(1+\frac{\rho}{M}\right)}{M^{-1}}.\end{aligned}$$

Both numerator and denominator tends to zero so we invoke *l'Hopital's rule* yielding

$$\begin{aligned}\lim_{M\to\infty}\mathcal{E}\{C\} &= \tfrac{1}{\ln 2}\lim_{M\to\infty}\frac{d/dM\left(\ln\left(1+\frac{\rho}{M}\right)\right)}{d/dM(M^{-1})}\\ &= \tfrac{1}{\ln 2}\lim_{M\to\infty}\frac{1/(1+\rho/M)\cdot-\rho M^{-2}}{-M^{-2}}\\ &= \tfrac{1}{\ln 2}\lim_{M\to\infty}\rho/(1+\rho/M)\\ &= \tfrac{\rho}{\ln 2}.\end{aligned}$$

Appendix C

Multi-channel MMSE Solution

C.1 Multi-Channel MMSE Equaliser - Regularised Pseudo-Inverse Equivalence

The regularised pseudo-inverse takes the form $(\mathbf{H}_c^H\mathbf{H}_c + \beta\mathbf{I})^{-1}\mathbf{H}_c^H$, where $\mathbf{H}_c$ is the convolutional matrix of the channel. We would like to show that the Wiener-Hopf solution is equivalent to this and find an expression for β. The following derivation is is valid for the time-domain representation described in Section 4.2.2. We simplify the derivation considerably is we assume $\mathbf{R}_x = \mathbf{I}$, i.e. unity power random white Gaussian inputs. Notice that the Wiener-Hopf solution places the inverses of the MIMO channel into columns, however we require the inverse to be in the rows therefore we must work with $\mathbf{g}_m^H$.

Hence performing the calculation of the columns of $\mathbf{G}$ one at a time, and exploit-

ing the Singular Value Decomposition, $\mathbf{H}_c = \mathbf{U}\mathbf{S}\mathbf{V}^H$ we have

$$\begin{aligned}
\mathbf{g}_m^H &= \left((\mathbf{H}_c\mathbf{R}_x\mathbf{H}_c^H + \mathbf{R}_\nu)^\dagger \mathbf{H}_c\mathbf{d}_m\right)^H && \text{(C.1)}\\
&= \mathbf{d}_m^H\mathbf{H}_c^H \left((\mathbf{H}_c\mathbf{I}\mathbf{H}_c^H + \mathbf{R}_\nu\right)^\dagger && \text{(C.2)}\\
&= \mathbf{d}_m^H\mathbf{H}_c^H \left(\mathbf{U}\mathbf{S}\mathbf{V}^H\mathbf{V}\mathbf{S}^H\mathbf{U}^H + \mathbf{R}_\nu\right)^\dagger && \text{(C.3)}\\
&= \mathbf{d}_m^H\mathbf{H}_c^H \left(\mathbf{U}\mathbf{S}\mathbf{S}^H\mathbf{U}^H + \mathbf{R}_\nu\right)^\dagger && \text{(C.4)}\\
&= \mathbf{d}_m^H\mathbf{H}_c^H \left(\mathbf{U}(\mathbf{S}\mathbf{S}^H + \mathbf{U}^H\mathbf{R}_\nu\mathbf{U})\mathbf{U}^H\right)^\dagger && \text{(C.5)}\\
&= \mathbf{d}_m^H\mathbf{V}\mathbf{S}^H\mathbf{U}^H\mathbf{U}(\mathbf{S}\mathbf{S}^H + \mathbf{U}^H\mathbf{R}_\nu\mathbf{U})^{-1}\mathbf{U}^H && \text{(C.6)}\\
&= \mathbf{d}_m^H\mathbf{V}\mathbf{S}^H(\mathbf{S}\mathbf{S}^H + \mathbf{U}^H\mathbf{R}_\nu\mathbf{U})^{-1}\mathbf{S}^{-1}\mathbf{V}^H\mathbf{V}\mathbf{S}^H\mathbf{U}^H && \text{(C.7)}\\
&= \mathbf{d}_m^H \left(\mathbf{V}\mathbf{S}^H(\mathbf{S}\mathbf{S}^H + \mathbf{U}^H\mathbf{R}_\nu\mathbf{U})\mathbf{S}^{-1}\mathbf{V}^H\right)^{-1}\mathbf{H}_c^H && \text{(C.8)}\\
&= \mathbf{d}_m^H \left(\mathbf{V}\mathbf{S}^H\mathbf{U}^H\mathbf{U}(\mathbf{S}\mathbf{S}^H + \mathbf{U}^H\mathbf{R}_\nu\mathbf{U})\mathbf{S}^{-1}\mathbf{V}^H\right)^{-1}\mathbf{H}_c^H && \text{(C.9)}\\
&= \mathbf{d}_m^H \left(\mathbf{H}_c^H\mathbf{U}(\mathbf{S}\mathbf{S}^H + \mathbf{U}^H\mathbf{R}_\nu\mathbf{U})\mathbf{S}^{-1}\mathbf{V}^H\right)^{-1}\mathbf{H}_c^H && \text{(C.10)}\\
&= \mathbf{d}_m^H \left(\mathbf{H}_c^H\mathbf{U}\mathbf{S}\mathbf{V}^H\mathbf{V}\mathbf{S}^{-1}(\mathbf{S}\mathbf{S}^H + \mathbf{U}^H\mathbf{R}_\nu\mathbf{U})\mathbf{S}^{-1}\mathbf{V}^H\right)^{-1}\mathbf{H}_c^H && \text{(C.11)}\\
&= \mathbf{d}_m^H \left(\mathbf{H}_c^H\mathbf{H}_c\mathbf{V}\mathbf{S}^{-1}(\mathbf{S}\mathbf{S}^H + \mathbf{U}^H\mathbf{R}_\nu\mathbf{U})\mathbf{S}^{-1}\mathbf{V}^H\right)^{-1}\mathbf{H}_c^H && \text{(C.12)}\\
&= \mathbf{d}_m^H \left(\mathbf{H}_c^H\mathbf{H}_c(\mathbf{V}\mathbf{S}^{-1}\mathbf{S}\mathbf{S}^H\mathbf{S}^{-1}\mathbf{V}^H + \mathbf{V}\mathbf{S}^{-1}\mathbf{U}^H\mathbf{R}_\nu\mathbf{U}\mathbf{S}^{-1}\mathbf{V}^H\right)^{-1}\mathbf{H}_c^H && \text{(C.13)}\\
&= \mathbf{d}_m^H \left(\mathbf{H}_c^H\mathbf{H}_c(\mathbf{I} + \mathbf{H}_c^\dagger\mathbf{R}_\nu(\mathbf{H}_c^H)^\dagger)^{-1}\right)\mathbf{H}_c^H && \text{(C.14)}\\
&= \mathbf{d}_m^H \left(\mathbf{H}_c^H\mathbf{H}_c + \mathbf{H}_c^H\mathbf{H}_c\mathbf{H}_c^\dagger\mathbf{R}_\nu(\mathbf{H}_c^H)^\dagger)^{-1}\right)\mathbf{H}_c^H && \text{(C.15)}\\
&= \mathbf{d}_m^H \left(\mathbf{H}_c^H\mathbf{H}_c + \mathbf{H}_c^H\mathbf{R}_\nu(\mathbf{H}_c^H)^\dagger)^{-1}\right)\mathbf{H}_c^H && \text{(C.16)}
\end{aligned}$$

We have assumed that $\mathbf{R}_x = \mathbf{I}$. In several steps we have exploited the fact that $\mathbf{S}^{-1}\mathbf{S}^H = \mathbf{I}$. In (C.1) we have used that $(\mathbf{H}_c\mathbf{R}_x\mathbf{H}_c^H + \mathbf{R}_\nu)^\dagger$ is Hermitian. In step from (C.5) to (C.6) we have used $(\mathbf{U}(\mathbf{S}\mathbf{S}^H + \mathbf{U}^H\mathbf{R}_\nu\mathbf{U})\mathbf{U}^H)^\dagger = \mathbf{U}(\mathbf{S}\mathbf{S}^H + \mathbf{U}^H\mathbf{R}_\nu\mathbf{U})^{-1}\mathbf{U}^H$. In the step from (C.7) to (C.8) we have used $\mathbf{V}\mathbf{S}^H(\mathbf{S}\mathbf{S}^H + \mathbf{U}^H\mathbf{R}_\nu\mathbf{U})^{-1}\mathbf{S}^{-1}\mathbf{V}^H = \left(\mathbf{V}\mathbf{S}^H(\mathbf{S}\mathbf{S}^H + \mathbf{U}^H\mathbf{R}_\nu\mathbf{U})\mathbf{S}^{-1}\mathbf{V}^H\right)^{-1}$. Finally, in (C.14), (C.15) and (C.16) $(\mathbf{H}_c^H)^\dagger$ is the zero-forcing pseudo-inverse of the Hermitian of the channel, which is quite easy to calculate.

Hence we have proved the theorem with $\beta = \mathbf{H}_c^H\mathbf{R}_\nu(\mathbf{H}_c^H)^\dagger$. Further if all the noise powers are the same, σ_ν^2 we have

$$\mathbf{g}_m^H = \mathbf{d}_m^H \left(\mathbf{H}_c^H\mathbf{H}_c + \sigma_\nu^2\mathbf{I}\right)^{-1}\mathbf{H}_c^H \qquad \text{(C.17)}$$

Mathematical Notation

General Notation

h	scalar quantity
$\mathbf{h}$	vector quantity
$\mathbf{H}$	matrix quantity
$h(t)$	function of a continuous variable t
$h[n]$	function of a discrete variable n

Relations and Operators

$(\cdot)^F$	fractional representation
$(\cdot)^H$	hermitian (conjugate transpose)
$(\cdot)^T$	transpose
$(\cdot)^*$	complex conjugate
$(\cdot)^\phi$	polyphase representation
$(\tilde{\cdot})$	para-hermitian (time-reversed conjugate transpose)
$(\cdot)^\dagger$	pseudo-inverse
$\mathcal{E}\{\cdot\}$	expectation operator
$(\hat{\cdot})$	estimate
∇	gradient operator
rank$\{\mathbf{A}\}$	rank of $\mathbf{A}$ (number of linearly independent rows)
tr$\{\mathbf{A}\}$	trace of $\mathbf{A}$

Symbols and Variables

Δ	delay
λ	eigenvalue
μ	step-size parameter, LMS algorithm
$\tilde{\mu}$	normalized step-size parameter, NLMS algorithm
ρ	signal-to-noise ratio

σ^2	variance
τ	delay / lag
ξ	cost function
ω	(angular) frequency
Ω	normalized (angular) frequency $\Omega = \omega T_s$, with sampling period T_s
$\underline{\mathbf{a}}(z)$	analysis filter bank
$\underline{\mathbf{A}}(z)$	analysis filter polyphase matrix
$\mathbf{B}$	Channel-equaliser response
$\mathbf{c}[n]$	weight error vector
c	samples from a Gaussian random variate
C	capacity, computational complexity
$d[n]$	desired signal
$e[n]$	adaptive filter error signal
h	SISO flat channel gain
$h_{mp}[n]$	channel response between transmitter m and receiver p
$\mathbf{H}$	MIMO channel matrix
$\mathbf{G}$	MIMO equaliser matrix
$\mathbf{I}$	identity matrix
K	number of subbands
L	adaptive filter length
M	number of transmitters
N	decimation factor
P	number of receivers
r	correction co-efficient
$r_{xd}[n]$	cross-correction between x and d
$\mathbf{R}$	auto-correlation matrix
R	up/downsamping factor for fractionally-spaced equalisation
$\underline{\mathbf{s}}(z)$	synthesis filter bank
$\underline{\mathbf{S}}(z)$	synthesis filter polyphase matrix
S	number of multi-channel adaptive filter inputs
T	number of multi-channel adaptive filter outputs
$u_s[n]$	multi-channel adaptive filter input
$\mathbf{u}[n]$	adaptive filter state vector
$v_t[n]$	multi-channel adaptive filter output
$\mathbf{w}$	adaptive filter coefficients vector
$\mathbf{w}_{opt}$	optimum coefficient vector
$x[n]$	MIMO channel output
$y[n]$	MIMO channel output

References

[1] G. J. Foschini and M. J. Gans, "On Limits of Wireless Communications in a Fading Environment when Using Multiple Antennas," *Wireless Personal Communcations*, , no. 6, pp. 315–335, 1998.

[2] E. Telatar, "Capacity of Multi-antenna Gaussian Channels," *European Transactions on Telecommunications*, vol. 10, no. 6, pp. 585–595, November-Decemeber 1999.

[3] G.D. Golden, G.J. Foschini, R.A. Valenzuela, and P.W. Wolniansky, "Detection algorithm and initial laboratory results using V-BLAST space-time communication architecture," *IEE Electronics Letters*, vol. 35, no. 1, pp. 11–14, January 1999.

[4] P.W. Wolniansky, G.J. Foschini, G.D. Golden, and R.A. Valenzuela, "V-BLAST: An architecture for achieving very high data rates over rich-scattering wireless channels," in *Proc. URSI International Symposium on Signals, Systems and Electronics*, September 1998, pp. 295–300.

[5] R. M. Fano, *Transmission of Information*, pp. 168–178, John Wiley and Sons, New York, 1961.

[6] G. J. Foschini, "Layered Space-Time Architecture for Wireless Communication in a Fading Environment When Using Multi-Element Antennas," *Bell System Technical Journal*, pp. 41–59, Autumn 1996.

[7] G. G. Raleigh and J. M. Cioffi, "Spatio-Temporal Coding for Wireless Communications," in *Proc. IEEE GLOBECOM*, November 1996, vol. 3, pp. 1809–1814.

[8] S. Weiss, G. W. Rice, and R. W. Stewart, "Multichannel Equalization in Subbands," in *Proc. IEEE Workshop on Applications of Signal Processing to Audio and Acoustics*, New Paltz, NY, October 1999, pp. 203–206.

[9] S. M. Alamouti, "A Simple Transmit Diversity Technique for Wireless Communications," *IEEE Journal on Selected Areas of Communications*, vol. 16, no. 8, pp. 1451–1458, October 1998.

[10] V. Tarokh and T. K. Y. Lo, "Principle Ratio Combining for Fixed Wireless Applications When Transmitter Diversity Is Employed," *IEEE Communications Letters*, vol. 2, no. 8, pp. 223–225, August 1998.

[11] V. Tarokh, N. Seshadri, and A. R. Calderbank, "Space-Time Codes for High Data Rate Wireless Communication: Performance Criterion and Code Construction," *IEEE Transactions on Information Theory*, vol. 44, no. 2, pp. 744–765, March 1998.

[12] S. Weiss and R. W. Stewart, *On Adaptive Filtering in Oversampled Subbands*, Shaker Verlag, Aachen, Germany, 1998.

[13] V. Bale and S. Weiss, "Comparison of Analytic Inversion Techniques for Equalisation of Highly Frequency-Selective MIMO Systems," in *Proceedings of Workshop on Signal Processing for Wireless Communications*, King College, London, UK, June 2004, pp. 150–155.

[14] V. Bale and S. Weiss, "An Optimum Linear Frequency-Selective MIMO Equaliser using Time-Domain Analytic Inversion," in *PREP Postgraduate Research Conference*, University of Hertfordshire, UK, April 2004, vol. Oral Presentations, pp. 24–25.

[15] V. Bale and S. Weiss, "A Low-Complexity Subband Adaptive MIMO Equaliser for Highly Frequency-Selective Channels," in *Spectral Methods and Multi-rate Signal Processing*, Vienna, Austria, September 2004, pp. 61 68.

[16] V. Bale and S. Weiss, "Equalisation of Broadband MIMO Channels by Subband Adaptive Identification and Analytic Inversion," in *Proceedings of International ITG/IEEE Workshop on Smart Antennas*, Duisburg, Germany, April 2005, vol. CD.

[17] V. Bale and S. Weiss, "Subband Adaptive Equaliser Tracking for Fractionally-Sampled Fading Broadband MIMO Channels," in *Proceedings of European Signal Processing Conference (EUSIPCO) 2005*, Antalya, Turkey, 2005, vol. CD.

[18] H. E. Nichols, A. A. Giordano, and J. G. Proakis, "MLD and mse Algorithms for Adaptive Detection of Digital Signals in the Presence of Interchannel

Interference," *IEEE Transactions on Information Theory*, vol. 23, no. 5, pp. 563–575, September 1977.

[19] J. Salz, "Digital Transmission Over Cross-Coupled Channels," *AT&T Technical Journal*, vol. 64, no. 6, pp. 1147–1159, July-August 1985.

[20] S.J. Elliot and P.A. Nelson, "Algorithm for Multichannel LMS Adaptive Filtering," *IEE Electronics Letters*, vol. 21, no. 21, pp. 979–981, 10^{th} October 1985.

[21] P. A. Nelson, H. Hamada, and S. J. Elliot, "Adaptive Inverse Filters for Stereophonic Sound Reproduction," *IEEE Transactions on Signal Processing*, vol. 40, no. 7, pp. 1621–1632, July 1992.

[22] T. Gänsler and J. Benesty, "Stereophonic acoustic echo cancellation and two-channel adaptive filtering: an overview," *International Journal of Adaptive Control and Signal Processing*, vol. 14, no. 6, pp. 565–586, September 2000.

[23] T. Rappaport, *Wireless Communications, Principles and Practice*, Communications Engineering and Emerging Technologies. Prentice-Hall, 1996.

[24] S. Verdú, *Multiuser Detection*, Cambridge University Press, 1998.

[25] G. J. Foschini, G. D. Golden, R. A. Valenzuela, and P. W. Wolniansky, "Simplified Processing for High Spectral Efficiency Wireless Communication Employing Multi-Element Arrays," *IEEE Journal on Selected Areas of Communications*, vol. 17, no. 11, pp. 1841–1852, November 1999.

[26] B. Bjerke and Proakis.J. G., "Multiple-Antenna Diversity Techniques for Tranmission over Fading Channels," in *Proc. IEEE Wireless Communications and Networking Conference*, September 1999, vol. 3, pp. 1038–1042.

[27] B. A. Bjerke and J. G. Proakis, "Equalization and Decoding for Multiple-Input Multiple-Output Wireless Channels," *EURASIP Journal on Applied Signal Processing*, , no. 3, pp. 249–266, 2002.

[28] A. Bhargave, R. J. P. de Figueiredo, and T. Eltoft, "A Detection Algorithm for the V-BLAST System," in *Proc. IEEE GLOBECOM*, 2001, vol. 1, pp. 494–498.

[29] C. Z. W. Hassell Sweatman, J. S. Thompson, B. Mulgrew, and P. M. Grant, "A Comparison of Detection Algorithms including BLAST for Wireless Communication using Multiple Antennas," in *Proc. International Symposium on Personal, Indoor and Mobile Radio Communications*, September 2000, pp. 698–703.

[30] C. Z. W. Hassell Sweatman, J. S. Thompson, B. Mulgrew, and P. M. Grant, "A Comparison of the MMSE Detector and its BLAST Versions for MIMO Channels," in *Proc. IEE Seminar on MIMO: Communications Systems from Concepts to Implementations*, December 2001, pp. 19/1–19/6.

[31] N. Boubaker, K. B. Letaief, and R. D. Murch, "A Low Complexity Multicarrier BLAST Architecture for Realizing Data Rates Over Dispersive Fading Channels," in *Proc. IEEE Vehicular Technology Conference*, Spring 2001, pp. 800–804.

[32] L. Hanzo, M. Muenster, B.J. Choi, and T. Keller, *OFDM and MC-CDMA for Broadband Multi-user Communications, WLANs and Broadcasting*, John Wiley and Sons Ltd, July 2003.

[33] N. Boubaker, K. B. Letaief, and D. M. Ross, "Performance of BLAST Over Frequency Selective Wireless Communication Channels," *IEEE Transactions on Communications*, vol. 50, no. 2, pp. 196–199, February 2002.

[34] ETSI, "Rec. ETSI GSM 05.02," Tech. Rep., European Telecommunications Standards Institution (ETSI), 1990.

[35] S.L. Ariyavisitakul, J. Winters, and N.R Sollenberger, "Joint equalization and iterference suppression for high data wireless systems," *IEEE Journal on Selected Areas of Communications*, vol. 18, no. 7, pp. 1214–1220, July 2000.

[36] A. Lozano and C. Papadias, "Layered Space-Time Receivers for Frequency-Selective Wireless Channels," *IEEE Transactions on Communications*, vol. 50, no. 1, pp. 65–73, January 2002.

[37] D. K. C. So and R. S. Cheng, "Detection Techniques for V-BLAST in Frequency Selective Fading Channels," in *Proc. IEEE Wireless Communications and Networking Conference*, March 2002, vol. 1, pp. 487–491.

[38] D. K. C. So and R. S. Cheng, "Layered Maximum Likelihood Detection for V-BLAST in Frequency Selective Fading Channels," in *Proc. IEEE Vehicular Technology Conference*, Spring 2002, vol. 1, pp. 135–139.

[39] A. J. Paulraj and C. B. Papadias, "Space-Time Processing for Wireless Communications," *IEEE Signal Processing Magazine*, vol. 14, no. 6, pp. 49–83, November 1997.

[40] V. Tarokh and H. Jafarkhani, "A Differential Detection Scheme for Transmit Diversity," in *Proc. IEEE Wireless Communications and Networking Conference*, September 1999, vol. 3, pp. 1043–1047.

[41] D. Gesbert, M. Shafi, D. Shiu, P. J. Smith, and A. Naguib, "From Theory to Practice: An Overview of MIMO Space-Time Coded Wireless Systems," *IEEE Journal on Selected Areas of Communications*, vol. 21, no. 3, pp. 281 302, April 2003.

[42] B. Hassibi and M. Hochwald, "High-Rate Codes That Are Linear in Space and Time," *IEEE Transactions on Information Theory*, vol. 48, no. 7, pp. 1804–1824, July 2002.

[43] S. Catreux, L. J. Greenstein, and V. Erceg, "Some Results and Insights on the Performance Gains of MIMO Systems," *IEEE Journal on Selected Areas of Communications*, vol. 21, no. 5, pp. 839–847, June 2003.

[44] L. Zheng and D. N. C. Tse, "Diversity and Multiplexing: A Fundamental Tradeoff in Multiple-Antena Channels," *IEEE Transactions on Information Theory*, vol. 49, no. 5, pp. 1073–1096, May 2003.

[45] C. C. Martin, J. H. Winters, and N. R. Sollenberger, "Multiple-Input Multiple-Output (MIMO) Radio Channel Measurements," in *Proc. IEEE International Symposium of the Antennas and Propagation Society*, July 2001, vol. 1, pp. 418–421.

[46] A. Adjoudani, E. C. Beck, M. Burg, A. P. Djuknic, T. G. Gvoth, D. Haessig, S. Manji, M. A. Milbrodt, M. Rupp, D. Samardzija, A. B. Siegel, T. Sizer, C. Tran, S. Walker, A. Wilkus, and P. W. Wolniansky, "Prototype Experience for MIMO BLAST Over Third-Generation Wireless System," *IEEE Journal on Selected Areas of Communications*, vol. 21, no. 3, pp. 440 451, April 2003.

[47] D. P. McNamara, M. A. Beach, P. Karlsson, and P. N. Fletcher, "Initial Characterisation of Multiple-Input Multiple-Output (MIMO) Channels for Space-Time Communication," in *Proc. IEEE Vehicular Technology Conference*, September 2000, vol. 3, pp. 1193–1197.

[48] V. Jungnickel, V. Pohl, and C. von Helmolt, "Capacity of MIMO Systems with Closely Spaced Antennas," *IEEE Communications Letters*, vol. 7, no. 8, pp. 361–363, August 2003.

[49] G. G. Raleigh and J. M. Cioffi, "Spatio-Temporal Coding for Wireless Communication," *IEEE Transactions on Communications*, vol. 46, no. 3, pp. 357–366, March 1998.

[50] P. Stoica, Y. Jiang, and J. Li, "On MIMO Channel Capacity: An Intuitive Discussion," *IEEE Signal Processing Magazine*, pp. 83–84, May 2005.

[51] P.J. Smith and M. Shafi, "An Approximate Capacity Distribution for MIMO Systems," *IEEE Transactions on Communications*, vol. 52, no. 6, pp. 887–890, June 2004.

[52] A. F. Molisch, M. Steinbauer, M. Toeltsch, E. Bonek, and R. S. Thomä, "Capacity of MIMO Systems Based on Measured Wirelss Channels," *IEEE Journal on Selected Areas of Communications*, vol. 20, no. 3, pp. 561–569, April 2002.

[53] D. Gesbert, H. Bölcskei, D. Gore, and A. Paulraj, "MIMO Wireless Channels: Capacity and Performance Prediction," in *Proc. IEEE GLOBECOM*, 2000, vol. 2, pp. 1083–1088.

[54] D. Gesbert, H. Bölcskei, D. A. Gore, and A. J. Paulraj, "Performance Evaluation for Scattering MIMO Channel Models," in *Proc. Asilomar Conference on Signals, Systems, and Computers*, November 2000, vol. 1, pp. 748–752.

[55] A. Burr, "Capacity of Adaptive MIMO Systems in a Finite Scattering Channel," in *Proc. IEE Seminar on MIMO: Communications Systems from Concept to Implementation*, Decmeber 2001, pp. 24/1–24/6.

[56] A. Burr, "Capacity Bounds and Estimates for the Finite Scatterers MIMO Wireless Channel," *IEEE Journal on Selected Areas of Communications*, vol. 21, no. 5, pp. 812–818, June 2003.

[57] G.J. Byers and F. Takawira, "Spatially and Temporally Correlated MIMO Channels: Modeling and Capacity Analysis," *IEEE Transactions on Vehicular Technology*, vol. 53, no. 3, pp. 634–643, 2004.

[58] S. Loyka and J. Mosig, "Channel capacity of n-antenna BLAST architecture," *IEE Electronics Letters*, vol. 36, no. 7, pp. 660–661, March 2000.

[59] S. Loyka, "Channel capacity of two-antenna BLAST architecture," *IEE Electronics Letters*, vol. 35, no. 17, pp. 1421–1422, August 1999.

[60] D. Shiu, G. J. Foschini, M. J. Gans, and J. M. Kahn, "Fading Correlation and Its Effect on the Capacity of Multielement Antenna Systems," *IEEE Transactions on Communications*, vol. 48, no. 3, pp. 502–513, March 2000.

[61] A. Goldsmith, S.A. Jafar, N. Jindal, and S. Vishwanath, "Capacity Limits of MIMO Channels," *IEEE Journal on Selected Areas of Communications*, vol. 21, no. 5, pp. 684–702, June 2003.

[62] M. Chiani, M.Z. Win, and A. Zanella, "On the Capacity of Spatially Correlated MIMO Rayleigh-fading Channels," *IEEE Transactions on Information Theory*, vol. 49, no. 10, pp. 2363–2371, 2003.

[63] L. Hanlen and A. Grant, "Capacity Analysis of Correlated MIMO Channels," in *IEEE Symposium on Information Theory*, July 2003, p. 263.

[64] J.H. Kotecha and A.M. Sayeed, "On the Capacity of Correlated MIMO Channels," in *IEEE Symposium on Information Theory*, June 2003, p. 355.

[65] T. Ratnarajah and R. Vaillancourt, "Correlated MIMO Channel Capacity," in *Proc. Asilomar Conference on Signals, Systems, and Computers*, 2003, vol. 1, pp. 1100–1104.

[66] P.J. Smith, R. Sunit, and M. Shafi, "Capacity of MIMO Systems with Semicorrelated Flat Fading," *IEEE Transactions on Information Theory*, vol. 49, no. 10, pp. 2781–2788, October 2003.

[67] H.H. Dam, S. Nordholm, and H.J. Zepernick, "Frequnecy-Domain Adaptive Equalization for MIMO Systems," in *Proc. IEEE Vehicular Technology Conference*, Autumn 2003, vol. 1, pp. 443–446.

[68] M. Failli, "Digital land mobile radio communications, COST 207," Tech. Rep., European Commission, 1989.

[69] B. Sklar, *Digital Communications: Fundamentals and Applications*, Prentice Hall, Englewood Cliffs, 1988.

[70] "Signal Processing Information Base: Micro-wave Channel Data," Rice University, http://spib.rice.edu.

[71] A. A. M. Saleh and R. A. Valenzuela, "A Statistical Model for Indoor Multipath Propagation," *IEEE Journal on Selected Areas of Communications*, vol. 5, no. 2, pp. 128–137, February 1987.

[72] H. Mohamad, *Subband Adaptive Equalisation for Communication Transceivers*, Ph.D. thesis, University of Southampton, UK, 2003.

[73] S.K. Jayaweera and H.V. Poor, "MIMO Capacity Results for Ricean Fading Channels," in *Proc. IEEE GLOBECOM*, 2003, vol. 4, pp. 1806–1810.

[74] G. Lebrun, M. Faulkner, M. Shafi, and P.J. Smith, "MIMO Ricean Channel Capacity," in *Proc. IEEE International Conference on Communications*, 2004, vol. 5, pp. 2939–2943.

[75] W.C. Lee, "Effects of Correlation Between Two Mobile Radio Base-Station Antenna," *IEEE Transactions on Communications*, vol. 21, no. 11, pp. 1214–1224, November 1973.

[76] P. Kyritsi, R. A. Valenzuela, and D. C. Cox, "Effect of the Channel Estimation on the Accuracy of the Capacity Estimation," in *Proc. IEEE Vehicular Technology Conference*, Spring 2001, vol. 1, pp. 293–297.

[77] M. Rupp, "On the influence of uncertainties in MIMO decoding algorithms," in *Proc. Asilomar Conference on Signals, Systems, and Computers*, Monterey, CA, 2002, vol. 1, pp. 570–574.

[78] S. Haykin, *Adaptive Filter Theory*, Prentice Hall, Englewood Cliffs, 3rd edition, 1996.

[79] B. Widrow and S. D. Stearns, *Adaptive Signal Processing*, Prentice Hall, Englewood Cliffs, New York, 1985.

[80] T. K. Moon and W. C. Stirling, *Mathematical Methods and Algorithms*, Prentice Hall, Upper Saddle River, NJ, 2000.

[81] B. Widrow, J. McCool, and M. Ball, "The Complex LMS Algorithm," *Proceedings of the IEEE*, vol. 63, pp. 719–720, August 1975.

[82] B. Widrow, J. M. McCool, M.G. Larimore, and C. R. Johnson, "Stationary and Nonstationary Learning Characteristics of the LMS Adaptive Filter," *Proceedings of the IEEE*, vol. 64, no. 8, pp. 1151–1162, August 1976.

[83] O. M. Macchi, *Adaptive Processing: The LMS Approach with Applications in Transmission*, Wiley, New York, 1995.

[84] N.J. Bershad and O.M. Macchi, "Comparison of LMS and RLS Algorithms for Tracking a Chirped Signal," in *Proc. IEEE International Conference on Acoustics, Speech and Signal Processing*, Glasgow, Scotland, May 1989, vol. 2, pp. 896–899.

[85] N.J Bershad and O.M. Macchi, "Adaptive Recovery of a Chirped Sinusoid in Noise, Part 1: Performance of the RLS Algorithm," *IEEE Transactions on Signal Processing*, vol. 39, no. 3, pp. 583–594, March 1991.

[86] O.M. Macchi, "A General Methodology for Comparison of Adaptive Filtering Algorithms in a Non-stationary Context," in *Proc. European Signal Processing Conference*, Barcelona, Spain, September 1990, vol. 1, pp. 189–192.

[87] O.M. Macchi and N.J. Bershad, "Adaptive Recovery of Chirped Sinusoid in Noise, Part 2: Performance of the LMS Algorithm," *IEEE Transactions on Signal Processing*, vol. 39, no. 3, pp. 595–602, March 1991.

[88] T. Walzman and M. Schwartz, "Automatic Equalization using the Discrete Frequency Domain," *IEEE Transactions on Information Theory*, vol. 19, pp. 59–68, 1973.

[89] E. R. Ferrara, "Fast Implementation of LMS Adaptive Filters," *IEEE Transactions on Acoustics, Speech, and Signal Processing*, vol. 28, no. 4, pp. 474–475, August 1980.

[90] G. Clark, S. Mitra, and S. Parker, "Block Implementation of Adaptive Digital Filters," *IEEE Transactions on Acoustics, Speech, and Signal Processing*, vol. 29, no. 3, pp. 744–752, June 1981.

[91] G. Clark, S. Mitra, and S. Parker, "Block Implementation of Adaptive Digital Filters," *IEEE Transactions on Circuits and Systems*, vol. 28, no. 6, pp. 584–592, June 1981.

[92] J. J. Shynk, "Frequency-Domain and Multirate Adaptive Filtering," *IEEE Signal Processing Magazine*, vol. 9, no. 1, pp. 14–37, January 1992.

[93] D. Mansour and A.H. Gray, Jr., "Unconstrained Frequency-Domain Adaptive Filters," *IEEE Transactions on Acoustics, Speech, and Signal Processing*, vol. 30, pp. 729–734, 1982.

[94] J.C. Lee and C.K. Un, "Performance of Transform-Domain LMS Adaptive Algorithms," *IEEE Transactions on Acoustics, Speech, and Signal Processing*, vol. 34, pp. 499–510, 1986.

[95] M. V. Clark, "Adaptive Frequency-Domain Equalization and Diversity Combining for Broadband Wireless Communications," *IEEE Journal on Selected Areas of Communications*, vol. 16, no. 8, pp. 1385–1395, October 1998.

[96] D. Falconer, S. L. Ariyavisitakul, A. Benyamin-Seeyar, and B. Eidson, "Frequency Domain Equalization for Single-Carrier Broadband Wireless Systems," *IEEE Communications Magazine*, vol. 40, no. 4, pp. 58–66, April 2002.

[97] J. Benesty and D.R. Morgan, "Frequency-Domain Adaptive Filtering Revisited, Generalization to the Multi-channel Case, and Applications to Acoustic Echo Cancellation," in *Proc. IEEE International Conference on Acoustics, Speech and Signal Processing*, June 2000, vol. 2, pp. 789–792.

[98] R. Dinis, R. Kalbasi, D. Falconer, and A. Banihashemi, "Channel Estimation for MIMO Systems Employing Single-Carrier Modulations with Iterative Frequency-Domain Equalization," in *Proc. IEEE Vehicular Technology Conference*, Autumn 2004, vol. 7, pp. 4942–4946.

[99] J. Coon, S. Armour, M. Beach, and J. McGeehan, "Adaptive Frequency-Domain Equalization for Single-Carrier Multiple-Input Multiple-Output Wireless Transmissions," *IEEE Transactions on Signal Processing*, vol. 53, no. 8, pp. 3247–3256, August 2005.

[100] G. Strang, *Linear Algebra and Its Applications*, Academic Press, New York, 2nd edition, 1980.

[101] G. H. Golub and C. F. Van Loan, *Matrix Computations*, John Hopkins University Press, Baltimore, Maryland, 3rd edition, 1996.

[102] P. P. Vaidyanathan, *Multirate Systems and Filter Banks*, Prentice Hall, Englewood Cliffs, 1993.

[103] A.N. Tihonov, "Solution of Incorrectly Formulated Problems and the Regularization Method," *Soviet Mathematics Doklady*, vol. 4, pp. 1035–1038, 1963.

[104] W. H. Press, S. A. Teukolsky, W. T. Vetterling, and B. P. Flannery, *Numerical Recipes in C*, Cambridge University Press, Cambridge, 2nd edition, 1992.

[105] A.N. Tikhonov and V.Y. Arsenin, *Solutions of Ill-Posed Problems*, New York: Wiley, 1977.

[106] O. Kirkeby, P. A. Nelson, F. Orduna-Bustamante, and H. Hamada, "Local Sound Field Reproduction Using Digital Signal Processing," *Journal of the Acoustical Society of America*, vol. Vol.100, no. No.3, pp. 1584–1593, March 1996.

[107] T. Haustein, C. von Helmolt, E. Jorswieck, and V. Pohl, "Performance of MIMO Systems with Channel Inversion," in *Proc. IEEE Vehicular Technology Conference*, 2002, vol. 1, pp. 35–39.

[108] Q.H. Spencer, A.L. Swindlehurst, and M. Haart, "Zero-forcing methods for downlink spatial multiplexing in multiuser MIMO channels," *tsp*, vol. 52, no. 2, pp. 461–471, February 2004.

[109] R. Ramesh, D. Hui, A.R. Hafeez, and H. Arslan, "Prefilter design for low complexity equalization of MIMO systems," in *Proc. IEEE Vehicular Technology Conference*, Spring 2004, vol. 2, pp. 871–875.

[110] J.R. Treichler, I. Fijalkow, and C. R. Johnson Jr, "Fractionally Spaced Equalizers: How Long Should They Really Be?," *IEEE Signal Processing Magazine*, vol. 13, pp. 65–81, May 1996.

[111] S.U.H. Qureshi and G.D. Forney Jr, "Performance and Properties of a T/2 Equalizer," in *National Telecommunication Conference Record*, Los Angeles, USA, December 1977, pp. 11.1.1–11.1.14.

[112] R.D. Gitlin and S.B. Weinstein, "Fractionally Spaced Equalization: An Improved Digital Transversal Equalizer," *Bell System Technical Journal*, vol. 60, pp. 275–296, February 1981.

[113] S. Qureshi, "Adaptive Equalization," *IEEE Communications Magazine*, vol. 20, no. 2, pp. 9–16, 1982.

[114] S.U.H. Qureshi, "Adaptive Equalization," *Proceedings of the IEEE*, vol. 73, no. 9, pp. 1349–1387, September 1985.

[115] C.B. Papadias and D.T.M. Slock, "Fractionally Spaced Equalization of Linear Polyphase Channels and Related Blind Techniques based on Multichannel Linear Prediction," *IEEE Transactions on Signal Processing*, vol. 47, pp. 641–654, March 1999.

[116] A. Ahlén and M. Sternad, "Optimal Deconvolution based on Polynomial Methods," *IEEE Transactions on Acoustics, Speech, and Signal Processing*, vol. 37, no. 2, pp. 217–226, February 1989.

[117] A. Ahlén and M. Sternad, "Wiener Filter Design Using Polynomial Equations," *IEEE Transactions on Signal Processing*, vol. 39, no. 11, pp. 2387 2399, November 1991.

[118] S.T. Neely and J.B. Allen, "Invertibility of a room impulse response," *Journal of the Acoustical Society of America*, vol. 66, no. 1, pp. 165–169, July 1979.

[119] M. Miyoshi and Y. Kaneda, "Inverse Filtering of Room Acoustics," *IEEE Transactions on Acoustics, Speech and Signal Processing*, vol. 36, no. 2, pp. 145–151, February 1988.

[120] G. Davis, "A fast algorithm for the inversion of block toeplitz matrices," *IEEE Transactions on Signal Processing*, vol. 43, no. 12, pp. 3022–3025, 1995.

[121] F. de Hoog, "A new algorithm for solving Toeplitz systems of equations," *Elsevier Science:Linear Algebra and Its Applications*, vol. 88/89, pp. 123–138, April 1987.

[122] A. González and J. J. López, "Time Domain Recursive Deconvoution in Sound Reproduction," in *Proc. IEEE International Conference on Acoustics, Speech and Signal Processing*, 2000, vol. 2, pp. 833–836.

[123] J. J. López and A. Gónzalez, "Two-step Levinson algorithm for time domain multichannel deconvolution," *IEE Electronics Letters*, vol. 36, no. 7, pp. 686–688, 30th March 2000.

[124] O. Kirkeby, P. A. Nelson, H. Hamada, and F. Orduna-Bustamante, "Fast Deconvolution of Multichannel Systems Using Regularization," *IEEE Transactions on Speech and Audio Processing*, vol. 6, no. 2, pp. 189–194, March 1998.

[125] R. W. Lucky, "Automatic Equalization for Digital Communication," *Bell System Technical Journal*, vol. 44, pp. 547–588, April 1965.

[126] O. Kirkeby, P.A. Nelson, H. Hamada, and F. Orduna-Bustamante, "Fast deconvolution of multi-channel systems using regularisation," Tech. Rep. 255, ISVR, University of Southampton, UK, 1996.

[127] Y. Huang, J. Benesty, and C. Jingdong, "Seperating ISI and CCI in a Two-step FIR Bezout Equalizer for MIMO Systems of Frequency-Selective Channels," in *Proc. IEEE International Conference on Acoustics, Speech and Signal Processing*, 2004, vol. 4, pp. 797–800.

[128] J. Zheng and B.D. Rao, "Capacity Analysis of MIMO Systems with Unknown Channel State Information," in *IEEE Information Theory Workshop*, San Antonio, Texas, USA, October 2004, pp. 413–417.

[129] M. Vu and A. Paulraj, "Some Asymptotic Capacity Results for MIMO Wireless with and without Channel Knowledge at the Transmitter," in *Proc. Asilomar Conference on Signals, Systems, and Computers*, 2003, vol. 1, pp. 258–262.

[130] A. Tulino, A. Lozano, and S. Verdu, "MIMO Capacity with Channel State Information at the Transmitter," in *IEEE Eighth International Symposium*

on Spread Spectrum Techniques and Applications, Sydney, Australia, August 2004, pp. 22–26.

[131] T. Yoo and A. Goldsmith, "Capacity of Fading MIMO Channels with Channel Estimation Error," in *Proc. IEEE International Conference on Communications*, 2004, vol. 2, pp. 808–813.

[132] T. Yoo, Y. Eunchul, and A. Goldsmith, "MIMO Capacity with Channel Uncertainty: Does Feedback Help?," in *Proc. IEEE GLOBECOM*, 2004, vol. 1, pp. 96–100.

[133] A. Maleki-Tehrani, B. Hassibi, and J. M. Cioffi, "Adaptive Equalization of Multiple-Input Multiple-Output (MIMO) Frequency Selective Channels," in *Proc. Asilomar Conference on Signals, Systems, and Computers*, November 1999, vol. 1, pp. 547–551.

[134] A. Maleki-Tehrani, B. Hassibi, and J. M. Cioffi, "Adaptive Equalization of Multiple-Input Multiple-Output (MIMO) Channels," in *Proc. IEEE International Conference on Communications*, June 2000, vol. 3, pp. 1670–1674.

[135] A. Sayed and T. Kailath, "A state-space approach to RLS adaptive filtering," *IEEE Signal Processing Magazine*, vol. 11, pp. 502–511, July 1994.

[136] A. González and J. J. López, "Fast Transversal Filters for Deconvolution in Multichannel Sounds Reproduction," *IEEE Transactions on Speech and Audio Processing*, vol. 9, no. 4, pp. 429–440, May 2001.

[137] Y. Li and K.J.R Liu, "On Blind Equalization of MIMO Channels," in *Proc. IEEE International Conference on Communications*, 1996, vol. 2, pp. 1000–1004.

[138] S. Ohno, H. Sakai, and H. Yoshida, "Adaptive Blind Equalization of Multichannel FIR Systems," in *Proc. IEEE International Symposium on Circuits and Systems*, 1999, vol. 3, pp. 66–69.

[139] W. Kellermann, "Analysis and Design of Multirate Systems for Cancellation of Acoustical Echoes," in *Proc. IEEE International Conference on Acoustics, Speech and Signal Processing*, New York, USA, 1988, vol. 5, pp. 2570–2573.

[140] A. Gilloire and M. Vetterli, "Adaptive Filtering in Subbands with Critical Sampling: Analysis, Experiments and Applications to Acoustic Echo Cancelation," *IEEE Transactions on Signal Processing*, vol. SP-40, no. 8, pp. 1862–1875, August 1992.

[141] A. Gilloire, "Experiments with Subband Acoustic Echo Cancelers for Teleconferencing," in *Proc. IEEE International Conference on Acoustics, Speech and Signal Processing*, Dallas, April 1987, pp. 2141–2144.

[142] A. Gilloire and M. Vetterli, "Adaptive Filtering in Subbands," in *Proc. IEEE International Conference on Acoustics, Speech and Signal Processing*, New York, April 1988, pp. 1572–1575.

[143] S. Weiss, *On Adaptive Filtering in Oversampled Subbands*, Ph.D. thesis, Signal Processing Division, University of Strathclyde, Glasgow, May 1998.

[144] S. Weiss, S. R. Dooley, R. W. Stewart, and A. K. Nandi, "Adaptive Equalization in Oversampled Subbands," in *Proc. Asilomar Conference on Signals, Systems, and Computers*, November 1998, vol. 1, pp. 389–393.

[145] H. Yamada, H. Wang, and F. Itakura, "Recovering of Broadband Reverberant Speech Signal by Subband MINT Method," in *Proc. IEEE International Conference on Acoustics, Speech and Signal Processing*, April 1991, vol. 2, pp. 969–972.

[146] A. J. Coulson, "A Generalization of Nonuniform Bandpass Sampling," *IEEE Transactions on Signal Processing*, vol. 43, no. 3, pp. 694–704, March 1995.

[147] R.E. Crochiere and L.S. Rabiner, "Interpolation and Decimation of Digital Signals: A Tutorial Review," in *Proceedings of the IEEE*, March 1981, vol. 69, pp. 300–331.

[148] R.E. Crochiere and L.S. Rabiner, *Multi-Rate Digital Signal Processing*, Prentice Hall, Englewood Cliffs, NY, USA, 1983.

[149] P. P. Vaidyanathan, "Multi-Rate Digital Filters, Filter Banks, Polyphase Networks and Applications: A Tutorial," in *Proceedings of the IEEE*, January 1990, vol. 78, pp. 56–93.

[150] C. E. Shannon, "A Mathematical Theory of Communications (Part I)," *Bell System Technical Journal*, vol. Vol.27, pp. 379–423, 1948.

[151] C. E. Shannon, "A Mathematical Theory of Communications (Part II)," *Bell System Technical Journal*, vol. Vol.27, pp. 623–656, 1948.

[152] A. Stenger, R. Rabenstein, S. Weiss, and R. W. Stewart, "Measuring Performance Limits of Subband Adaptive Systems," in *Proc. Asilomar Conference on Signals, Systems, and Computers*, Monterey, CA, November 1998.

[153] H. Yasukawa, S. Shimada, and I. Furukawa, "Acoustic Echo Canceller with High Speech Quality," in *Proc. IEEE International Conference on Acoustics, Speech and Signal Processing*, Dallas, April 1987, vol. IV, pp. 2125–2128.

[154] H. Yasukawa, I. Furukawa, and Y. Ishiyama, "Characteristics of Acoustic Echo Cancellers Using Sub-Band Sampling and Decorrelation Methods," *IEE Electronics Letters*, vol. 24, no. 16, pp. 1039–1040, August 1988.

[155] H. Yasukawa and S. Shimada, "An Acoustic Echo Canceller Using Subband Sampling and Decorrelation Methods," *IEEE Transactions on Signal Processing*, vol. 41, no. 2, pp. 926–930, February 1993.

[156] H. Yasukawa, "Performance Degradation of a Subband Adaptive Digital Filter with Critical Sampling," *IEICE Transactions on Fundamentals of Electronics, Communications, and Computer Science*, vol. E77A, no. 9, pp. 1497–1501, September 1994.

[157] S. Weiß, L. Lampe, and R. W. Stewart, "Efficient Implementations of Complex and Real Valued Filter Banks for Comparative Subband Processing with an Application to Adaptive Filtering," in *Proc. International Symposium on Communication Systems and Digital Signal Processing*, Sheffield, UK, April 1998, pp. 32–35.

[158] S. Weiß, R. W. Stewart, A. Stenger, and R. Rabenstein, "Performance Limitations of Subband Adaptive Filters," in *Proc. European Signal Processing Conference*, Rodos, Greece, September 1998, vol. III, pp. 1245–1248.

[159] S. Weiss, A. Stenger, R.W. Stewart, and R. Rabenstein, "Steady-state performance limitations of Subband Adaptive Filters," *IEEE Transactions on Signal Processing*, vol. 49, no. 9, pp. 1982–1991, September 2001.

[160] S. Weiss, "Analysis and Fast Implementation of Oversampled Modulated Filter Banks," in *Mathematics in Signal Processing V*, J. G. McWhirter and I. K. Proudler, Eds., chapter 23, pp. 263–274. Oxford University Press, March 2002.

[161] S. Weiss and R.W. Stewart, "Fast Implementation of Oversampled Modulated Filter Banks," *IEE Electronics Letters*, vol. 36, pp. 1502–1503, August 2000.

[162] D. R. Morgan, "Slow Asymptotic Convergence of LMS Acoustic Echo Cancelers," *IEEE Transactions on Speech and Audio Processing*, vol. 3, no. 2, pp. 126–136, March 1995.

[163] H. Mohamad, S. Weiss, and M. Rupp, "MMSE Limitations for Subband Adaptive Equalisers," in *Proc. Asilomar Conference on Signals, Systems, and Computers*, Monterey, California, USA, November 2002, vol. 2, pp. 1233–1237.

[164] S. Weiss and R. W. Stewart, "On the Optimality of Subband Adaptive Filters," in *Proc. IEEE Workshop on Applications of Signal Processing to Audio and Acoustics*, New Paltz, New York, October 1999, pp. 59–62.

[165] M. Rupp and R. Frenzel, "Analysis of LMS and NLMS Algorithms with Delayed Co-efficient update under the Presence of Spherically Invariant Processes," *IEEE Transactions on Signal Processing*, vol. 42, pp. 668–672, March 1994.

[166] G.D. Forney, Jr., "Maximum-likelihood sequence estimation of digital sequences in the presence of intersymbol interference.," *IEEE Transactions on Information Theory*, vol. IT-18, pp. 363–378, May 1972.

[167] D.T.M. Slock and C.B. Papadias, "Blind fractionally-spaced equalization based on cyclostationarity," in *Proc. IEEE Vehicular Technology Conference*, Stockholm, Sweden, June 1994, pp. 1286–1290.

[168] L. Tong, G. Xu, and T. Kailath, "Blind identification and equalization of multiple channels: A time domain approach," *IEEE Transactions on Information Theory*, vol. 40, pp. 340–349, March 1994.

[169] J.K. Tugnait, "On blind identifiability of multipath channels using fractional sampling and second-order cyclostationary statistics," *IEEE Transactions on Information Theory*, vol. 41, pp. 308–311, January 1995.

[170] T. Kailath, *Linear Systems*, Prentice-Hall, Englewood Cliffs, NJ, 1980.

[171] Mohamad.H., S. Weiss, Rupp.M, and L. Hanzo, "A Fast Converging Fractionally Spaced Equaliser," in *Proc. Asilomar Conference on Signals, Systems, and Computers*, Monterey, California, USA, November 2001, vol. 2, p. 1460=1464.

[172] H. Mohamad, S. Weiss, M. Rupp, and L. Hanzo, "Fast Adapation of Fractionally Spaced Equalisers," *IEE Electronics Letters*, vol. 38, no. 2, pp. 96–98, January 2002.

[173] R.H. Clarke, "A Statistical Theory of Mobile-Radio Reception," *Bell System Technical Journal*, vol. 47, pp. 957–1000, 1968.

[174] M.J. Gans, "A Power Spectral Theory of Propagation in the Mobile Radio Environment," *IEEE Transactions on Vehicular Technology*, vol. 21, pp. 27–38, February 1972.